

The University of Nottingham

UNITED KINGDOM · CHINA · MALAYSIA

THE ROLE OF MINIATURE SPECIMEN CREEP TESTS IN POWER PLANT LIFE MANAGEMENT

BIANCA CACCIAPUOTI

B.Eng, M.Sc. (Aerospace Engineering)
Università degli Studi di Napoli Federico II

Thesis submitted to the University of Nottingham for the degree of Doctor of Philosophy

January 2018

CONTENTS

Abstract ..... **v**

List of Publications ..... **vi**

Acknowledgments ..... **vii**

1 Introduction **1**

2 Literature review **4**

2.1 Creep 4

2.1.1 Creep under constant uniaxial stress 4

2.1.2 Time hardening and strain hardening formulations 7

2.1.3 Creep deformation under a multi-axial stress condition 8

2.1.4 Creep continuum damage models 8

2.1.5 Creep modelling and FE analyses 11

2.2 Creep of power plant components and life management 13

2.2.1 Service conditions 13

2.2.2 Typical failure 14

2.2.3 Life management and lifing 16

2.2.4 Inspection planning 18

2.2.5 Condition assessment 26

2.3 Surface hardness testing technique for ductile material characterization 27

2.3.1 Historical background 27

2.3.2 Standard hardness tests 29

2.3.3 Empirical relations between hardness and yield strength 30

2.3.4 Current status of application 31

2.3.5 Hardness based lifing models 32

2.4 Miniature specimen creep testing techniques 34

2.4.1 Overview 34

2.4.2 Scoop sampling 35

2.4.3 Impression creep test 38

2.4.4 Small punch creep test 40

2.4.5 Small ring creep test 42

2.4.6 Small two-bar creep test 44

2.4.7 Data conversion techniques 47

2.5 Evaluation of Current Miniature Testing Methods 58

2.6 Application of small specimen creep testing techniques 61
2.6.1 Strength ranking 61
2.6.2 Decision on improved inspection, replacement and repair strategy 62
2.6.3 Small specimen creep data correlated with hardness data for life assessment 64
2.6.4 Application for irradiated materials 65
2.6.5 Fracture 69
2.6.6 Other applications 70
2.7 Challenges and research gaps 72
3 Development of a new approach through miniature specimen creep testing techniques and hardness tests for life assessment of power plant materials 75
3.1 Introduction 75
3.2 Plant assessment model adopting small specimen creep testing in a condition based monitoring framework 76
3.2.1 Novel holistic condition assessment 76
3.2.2 Novel empirical relations between hardness and minimum creep strain rate 80
3.3 Current practice 86
3.3.1 Ageing main steam pipework 86
3.3.2 Hardness and surface replica data 94
3.3.3 Risk management 100
3.4 Conclusions 102
4 Investigation on the capability of impression creep test 104
4.1 Introduction 104
4.2 Comparison of uniaxial creep and impression creep test data output 104
4.3 Effect of misalignment of the ICT indenter 106
4.4 General comments on ICT conversion parameters 109
4.5 Conclusions 111
5 Investigation on the creep damage evolution of an ex-service CrMoV pipe section through impression creep test and metallurgical inspection data 112
5.1 Introduction 112
5.2 Experimental work 114
5.2.1 Tested material 114
5.2.2 Operating history and prior examinations 116
5.2.3 Test program 120

5.2.4 Microstructure 121
5.2.5 Hardness and replica 122
5.2.6 Impression creep test 123
5.3 Characterisation of the pipe section material 124
5.3.1 Microstructure investigation 124
5.4 Hardness and replica investigation 128
5.5 Impression creep test results 131
5.6 General comments on the through thickness behaviour 132
5.7 Other ex-service material through section examinations 134
5.7.1 Station A: Unit 1: 2014 134
5.7.2 Station A: Unit 2: 2015 136
5.7.3 Station B: Unit 1: 2015 137
5.7.4 Station A: Unit 1: 2009 139
5.8 Summary of through section creep cavity counts 143
5.9 Discussion 144
5.9.1 Implications 145
6 Investigation on possible improvements of the CEN Code of Practice 147
6.1 Introduction 147
6.2 Chakrabarty's membrane stretching theory 148
6.2.1 Problem description 148
6.2.2 Membrane stress solutions 149
6.2.3 Strain solution and correlation of the contact boundary angle 151
6.2.4 Applicability of the Membrane Stretching Theory to the SPCT Specimen Behaviour 151
6.2.5 Finite element model definition 152
6.2.6 Meshing and Contact Modelling 153
6.2.7 Constitutive material models 154
6.2.8 Elastic-Plastic Constitutive Models 155
6.3 Tested Material and Test rig 156
6.4 Calculation of the contact angle 157
6.5 Results and discussion 158
6.5.1 Experimental results 158
6.5.2 Preliminary FE Results 162
6.5.3 Effects of Load Magnitudes 164
6.5.4 Effects of Friction Coefficient 164
6.5.5 Effects of Punch/Specimen Dimensions 165

6.5.6 FE and analytical solutions 166
6.5.7 Comparison with the Experimental Findings 170
6.5.8 Evolution of the Contact Angle under Different Material Constitutive Models 173
7 Concluding discussion and future work 175
7.1 The role of small specimens in power plant life management 175
7.1.1 A novel approach based on hardness and impression creep tests for condition monitoring 177
7.1.2 Considerations on impression creep test 179
7.1.3 Through thickness examination of an ex-service CrMoV pipe section 179
7.1.4 A step forward for the realization of an improved Code of Practice for small punch creep test 180
7.2 Concluding remarks 181
7.3 Future Work 183
8 References 184

ABSTRACT

The current Thesis describes for the first time based on extensive industrial data how small specimen creep testing techniques can be applied within a practical and deployable life assessment framework and in conjunction with other assessment techniques. The current state of the art for small specimen creep testing is critically reviewed; a review of traditional techniques used on site for the metallurgical assessment of material condition is also included, with examples from site investigations and assessment campaigns in both conventional and nuclear plant applications. The work describes how small specimen creep testing methods and other complementary tools can be used in a new and structured approach to life management. This specifically refers to the potential to develop and implement novel life assessment models that take advantage of the significant amount of site data currently routinely acquired during plant outage overhauls.

A novel predictive lifing model for the use of hardness data is developed. In fact, a novel, phenomenological, relationship between room temperature hardness and creep data, obtained by uniaxial creep and impression creep tests, has been found and used for an innovative lifing approach that includes hardness data in a modified Liu and Murakami creep damage model. The latter is discussed with a description of how it could be practically implemented and validated in-service.

The capability of impression creep testing method in determining the minimum creep strain rate data by use of conversion relationships that relates uniaxial creep test data and impression creep test data is demonstrated. Consequences of possible geometry inaccuracies in the position of the indenter were investigated and some general comments on the conversion relationships are also provided.

The creep damage evolution of an ex-service CrMoV pipe section is investigated in order to demonstrate how normally acquired industry data and data obtained by small specimen creep tests could be used in a real situation. The study emphasises the importance of correlating the operating conditions (temperature and stress) of power plant components with the results from metallurgical examinations and small specimen creep tests.

The current research also reports a novel investigation of the applicability of Chakrabarty's theory, for membrane stretching of a circular blank over a rigid punch, to small punch creep test and determines new ranges of applicability of the CEN Code of Practice CWA 15627.

LIST OF PUBLICATIONS

1) Cacciapuoti, B., W. Sun, and D.G. McCartney, *A study on the evolution of the contact angle of small punch creep test of ductile materials*. International Journal of Pressure Vessels and Piping, 2016. 145: p. 60-74.

2) Cacciapuoti, B., W. Sun, D.G. McCartney, A. Morris, S. Lockyer, N.A. Razak, C.M. Davies, and J. Hulance, *An Evaluation of the Capability of Data Conversion of Impression Creep Test.* Materials at High Temperatures, 2017. **34**(5-6): p. 415–424.

3) Morris, A., B. Cacciapuoti, and W. Sun, *The Role of Small Specimen Creep Testing within a Life Assessment Framework for High Temperature Power Plant.* International Materials Reviews, 2018. 63(2): p. 102-137.

4) Cortellino, F., J.P. Rouse, B. Cacciapuoti, W. Sun, and T.H. Hyde, *Experimental and Numerical Analysis of Initial Plasticity in P91 Steel Small Punch Creep Samples.* Experimental Mechanics, 2017. 57: p. 1193–1212.

5) Cacciapuoti, B., A. Morris, W. Sun, D.G. McCartney, J. Hulance, *Correlation and Capability of using Site Inspection Data and Small Specimen Creep Testing for a Service-Exposed CrMoV Pipe Section*, Materials at High Temperatures, 2017. Under revision.

6) Morris, A., B. Cacciapuoti, and W. Sun, *The Role of Hardness on Condition Monitoring and Lifing for High Temperature Power Plant Structural Risk Management.* Measurement, 2017. Under revision.

ACKNOWLEDGMENTS

First of all, I would like to acknowledge my supervisors, Prof Wei Sun and Prof Graham McCartney from the University of Nottingham, and Prof Andy Morris from EDF Energy (West Burton Power) Limited. Their expert advice, guidance and support during my studies were fundamental for this research to be completed and for six papers I am co-author of to be submitted for publication in international journals.

The financial support provided by the Engineering and Physical Sciences Research Council (EPSRC) through the Flexible and Efficient Power Plant project (Flex-E-Plant, Grant number: EP/K021095/1), that sponsored the research, is also acknowledged. I also thank the following partners for their valuable contributions: GE Power, Doosan Babcock Limited, Centrica plc., EDF Energy (West Burton Power) Limited, Uniper Technologies Limited, Goodwin Steel Castings Limited, NPL Management Limited, R-MC Power Recovery Limited, RWE Generation UK plc., Scottish and Southern Energy (SSE) plc., Siemens Industrial Turbomachinery and TWI Limited.

I would also like to thank EDF Energy (West Burton Power) Limited for granting permission to publish industrial data.

Acknowledges also go to Mr Shane Maskill and Dr Tom Hoey from the University of Nottingham for their expert assistance in experimental testing. I would also like to thank Mr Mike Goodbun (RWE Generation UK plc), Mr Bin Azahari Ahmad (the University of Nottingham) and Dr Xu Xu (the University of Loughborough) for their help and support on material characterization, which led to the submission of the paper on the creep damage evolution of an ex-service CrMoV pipe section to an international journal.

I need to express my highest gratitude to Dr Francesco Cortellino, who guided and supported me during the very first months of both my new life in the UK and my PhD project. His precious technical advice led to the publication of the paper on the evolution of the contact angle for small punch creep test. His friendship, honesty and decency helped me in becoming a better person and a better engineer and, hopefully, a good wife.

A big thank you also goes to all of the PhD students and post-docs of the Structural and Dynamics Group, who have been my companions during the last three years and have shared with me all of the pain and the joys of this long journey. I also need to thank Miss Lorelei Gherman for her precious friendships.

My gratitude also goes to my Mom, Dad and Sister who always sustained me during my studies and gave me a huge help in organising my wedding with Francesco, when I needed to complete my research with appropriate calm and concentration.

1 INTRODUCTION

It is common that high temperature power plant components are now working far beyond their original designed life. Therefore, establishing their in-service material properties has become a matter of significant concern for power generation companies. In particular, repair ranking and replacement strategies require acquisition of creep data of in-service components (both static and rotating) operating at high temperatures and pressures. One of the main aims of power generation companies is to maximise plant availability and profitability, whilst maintaining safety. In order to achieve these objectives they must be able to understand, with good certainty, the remaining life of the assets at any time during their operation so that it can cost-effectively plan future inspections, refurbishments and replacements as required. It is a standard practice to use different approaches and diverse data sets, such as off-load and on-load monitoring to evaluate component conditions.

Although the characterisation of the full creep curve of materials for power plant applications can be accomplished by use of standard size uniaxial creep tests, shortage of materials to be tested has led to the development of unconventional creep testing techniques, which include miniature creep testing specimens. The latter can also be very useful to investigate material creep behaviour of critical regions of power plant components, including, for example, welds with heat affected zones and pipe bends. Nonetheless, there is the need of a new holistic condition assessment approach that integrates small specimen testing data with data acquired from existing inspection procedures, e.g. hardness measurements, along with material or component behaviour models that utilise in-service operational data, such as steam temperature and pressure, which are routinely acquired.

The aim of the research reported in the present thesis is to develop the aforementioned new holistic condition assessment approach and to improve the understanding of the capabilities of small specimen creep tests.

Thus, Chapter 2 presents a Literature Review that describes creep phenomenon and its implications for power plant components. The current condition assessment of those components is also briefly illustrated. Moreover, in view of the need of developing a new holistic condition assessment approach, hardness techniques and

miniature specimen creep testing techniques are reviewed. Creep fatigue and creep buckling are also recognised failure modes for components operating at high temperature and pressure, but are reviewed elsewhere [1-4]. In view of the findings arising from the Literature Review, challenges and research gaps were identified and they are addressed in the subsequent Chapters of this work.

Chapter 3 describes the development of a new approach for life assessment of power plant materials through miniature specimen creep testing techniques and hardness tests. A novel empirical relationship between hardness and minimum creep strain rate has been identified and used to develop an innovative method for monitoring of power plant components. Case studies are also reported.

Chapter 4 investigates the capabilities of impression creep testing techniques by correlating converted minimum creep strain rates obtained by impression creep test of disparate power plant steels with the corresponding uniaxial data. The Chapter also includes some comments on the conversion parameters and explores the consequences on their determination when the indenter is not perfectly aligned with the specimen.

Chapter 5 investigates the creep damage evolution of an ex-service 0.5CrMoV pipe section through impression creep test and metallurgical inspection data. The study emphasises the importance of correlating the operating conditions (temperature and stress) of power plant components with the results from metallurgical examinations and small specimen creep tests. The research seeks for a correlation among micro- and macro-hardness measurements, surface replicas data and minimum creep strain rates (obtained by impression creep tests) of the parent material of the pipe section. Also, optical and SEM micrographs have been used to assess possible metallurgical differences through the thickness of the pipe section. This investigation shows how impression creep testing data could be practically used in the holistic approach, developed in Chapter 3, for the evaluation of life consumption of power plant components.

Chapter 6 proposes an improvement of the CEN Code of Practice [5] for small punch creep test, which allows for the full characterisation of materials' creep deformation curve. In fact, increasing the understanding of the small punch specimen during the

creep test is of high importance in order for this technique to be practically used in the novel the holistic approach developed in Chapter 3.

Chapter 7 discusses the challenges and research gaps addressed in the former Chapters, draws some conclusions on the presented research and proposes some future work that could lead to possible improvements of the methods presented in this thesis.

2 LITERATURE REVIEW

2.1 CREEP

Creep is a phenomenon that occurs when a component is subjected to a stress at a temperature above 0.30 of the absolute material melting temperature, T_m [2]. The material creep strain, ε^c, depends on the applied stress, σ, and temperature, T, and on the exposure time, t [1]. Creep deformation is unrecoverable and generally occurs at stress levels far below the material yield stress [1, 6]. Abe [4] defines creep as a slow and continuous permanent deformation of materials over extended periods under load. The operating temperature, expressed as a fraction of T_m, determines the mechanisms that govern the creep deformation of metals at a microstructural level [2]. In particular, in metals when $0.30T_m \leq T \leq 0.35T_m$ creep deformation is due to the motion of defects, e.g. dislocations, prevented by solutes, precipitate, grain boundaries and/or by other dislocations [2, 7]. Temperatures between $0.35T_m$ and $0.4T_m$ allow the atoms energy level to be high enough for the dislocations to move away from the encountered obstacles [2, 7]. When $0.4T_m < T \leq 0.6T_m$ the so-called creep recovery process take place. In such situations, dislocations "climb" over the obstacles because atoms in the vicinity of the obstacles can diffuse away from them [2, 7]. At temperatures up to 0.8 T_m and above creep occurs by pure diffusion [2]. Such temperatures are outside the range of engineering interest [2].

2.1.1 Creep under constant uniaxial stress

Typical creep tests are carried out by statically loading in tension a uniaxial specimen at constant stress and constant temperature [6]. The test output is the characteristic strain versus time sigmoid curve presented in Figure 1. The uniaxial sample is initially instantaneously deformed with either elastic or elastic-plastic strain, depending on the stress level; then its deformation undergoes the classical three regions of the creep curve: primary, secondary and tertiary creep state. In the primary creep region the strain rate decreases with time: the dislocation density increases, making the strain hardening to be the governing mechanism, while diffusion governs creep recovery that generates dislocation motion [2, 6-8]. In the secondary region, the strain rate is constant with time due to the balance between the rate of generation of dislocations (hardening) and the rate of recovering (softening) [2, 4, 6-8]. As

illustrated in Figure 1, isolated cavities start to nucleate on grain boundaries towards the end of the secondary creep region [9]. In the tertiary creep region, the strain rate increases with time because more cavities nucleate at the grain boundaries together with micro-cracks that propagates as macro-cracks and lead the specimen to fail at the so-called rupture time (t_R in Figure 1).

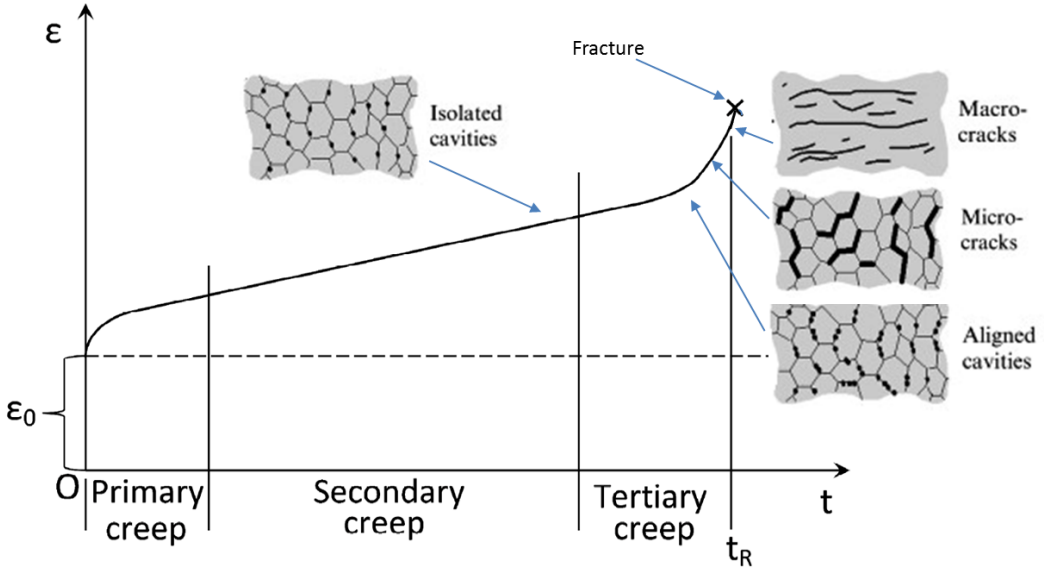


Figure 1. Typical uniaxial creep test output in terms of creep strain versus time. ε_0 is the instantaneous strain. The creep degradation through life is also presented. Adapted from Ref. [1, 9].

The secondary creep region has been also known as "steady state creep" and this notation has now been overcome for engineering creep resistant steels and alloys [10]. In fact, the material microstructure always evolves during creep, suggesting that there is no dynamic microstructural equilibrium for those materials, that, on the contrary, characterizes the secondary region of simple metals and alloys, and therefore the steady state may never be reached [4, 11]. Some advanced materials, for example those used for gas turbines, do not have a recognised steady state phase and the creep curve is completely non-linear. However, power plant components are designed to operate in the secondary region of the creep curve in order to avoid sudden failures that may happen in the tertiary region due to a quick increase of the creep strain rate [12].

Although the above clarification was necessary for completeness of the present dissertation, it is also worth to mention that the so-called "steady state approximation"

is an essential hypothesis for the following mathematical treatments, such as the *reference stress method* described in section 2.4.7.1.

A generally accepted approximation relates the creep deformation to stress, temperature and time by separating the three effects as in equation (1), where σ indicates the stress, *T* the temperature and *t* the time [1, 2].

$$\varepsilon^c = f_1(\sigma) f_2(T) f_3(t) \tag{1}$$

The temperature dependency is well represented by an Arrhenius-type relation, as shown in equation (2), where *R* is the gas constant and Q_c is the creep activation energy [2].

$$f_2(T) = exp\left[-\frac{Q_c}{RT}\right] \tag{2}$$

The Bailey-Norton law is able to describe primary and secondary creep stages in a condition of constant temperature and constant stress, as expressed in equation (3), where *B*, *m* and *n* are material constants depending on the operating temperature.

$$\varepsilon^c = B\sigma^n t^m \tag{3}$$

Figure 2-a shows the effects of temperature on typical creep curve. In this case, the instantaneous deformation does not depend on increasing temperature, while the secondary creep rate increases and, consequently, the time to failure decreases [1]. Figure 2-b shows the effects of stress on typical creep curve; the secondary creep rate and the instantaneous deformation increase and the time to failure decreases [1].

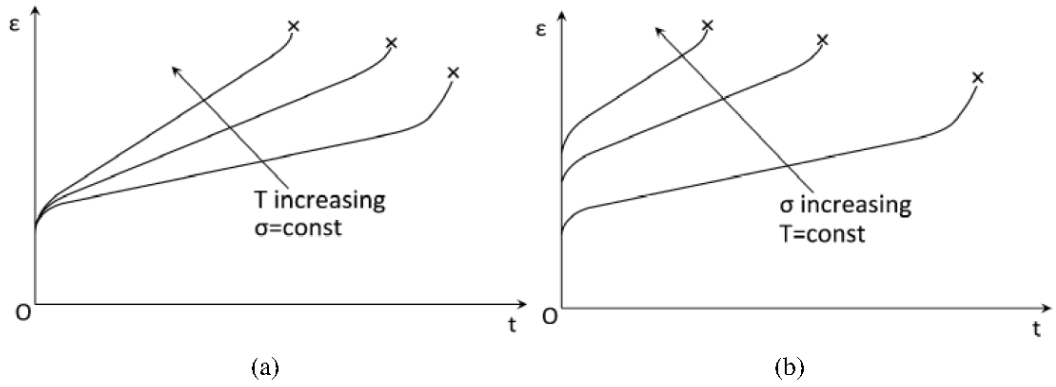


Figure 2. Effects of **(a)** temperature and of **(b)** stress on typical creep curve, from Ref. [1].

2.1.2 Time hardening and strain hardening formulations

When the uniaxial creep test is carried out at constant tensile load, the stress continuously increases with time and the necking of the specimen cross-section significantly concur to stress increment during creep [4]. Many theories have been developed to describe the creep behaviour of the uniaxial specimen under variable stress, but none of them is completely satisfactory because they were obtained from hypothetical generalizations of creep equations for constant stress [2]. In fact, the creep behaviour of the specimen depends on both the current state and its past history [1, 2]. Two of the most accepted theories are the *time hardening* and the *strain hardening* formulations [2]. Time hardening theory is derived from the differentiation of equation (3) with respect to time, by assuming constant stress or step variations of the stress field with long duration, and it is here reported in equation (4), where $\dot{\varepsilon}^c$ is the strain rate [1, 7].

$$\dot{\varepsilon}^c = Bm\sigma^n t^{m-1} \tag{4}$$

The strain hardening formulation is obtained by deriving the time variable from Bailey-Norton's law, as in equation (5), and then by substituting that in equation (4). Finally, equation (6) expresses the strain hardening formulation, which is generally more accurate than the time hardening approximation [1].

$$t = \left[\frac{\varepsilon^c}{B\sigma^n}\right]^{\frac{1}{m}} \tag{5}$$

$$\dot{\varepsilon}^c = B^{\left(\frac{1}{m}\right)} m \sigma^{\left(\frac{n}{m}\right)} [\varepsilon^c]^{\left(\frac{m-1}{m}\right)} \tag{6}$$

For several applications, e.g. power plant components designed to operate in the secondary region of the creep curve, the secondary state approximation can be adopted and the creep strain rate is that of steady state creep, $\dot{\varepsilon}_{\mathrm{ss}}^{\mathrm{c}}$, that can be expressed through the well-known Norton law, as in equation (7) [1]. In such hypothesis, the creep strain rate is assumed to not be time-dependent; therefore the time exponent (*m – 1)* of equation (4) is equal to 0 [1].

$$\dot{\varepsilon}_{\mathrm{ss}}^{\mathrm{c}} = B\sigma^{n} \tag{7}$$

2.1.3 Creep deformation under a multi-axial stress condition

In the secondary creep region, creep deformation under a multi-axial stress condition can be modelled as in equation (8), where $\dot{\varepsilon}_{ij}^{c}$ is the multi-axial creep strain rate, S_{ij} is the deviatoric stress tensor, $\dot{\varepsilon}_{\mathrm{EQ}}^{\mathrm{c}}$ is the von Mises equivalent creep strain rate and σ_{EQ} is the von Mises equivalent stress.

$$\dot{\varepsilon}_{ij}^{c} = \frac{3}{2}\frac{\dot{\varepsilon}_{\mathrm{EQ}}^{\mathrm{c}}}{\sigma_{EQ}}S_{ij} = \frac{3}{2}B\sigma_{EQ}^{n}\frac{S_{ij}}{\sigma_{EQ}} \tag{8}$$

Equation (8) is one of the possible relationships available for modelling creep deformation under a multi-axial stress condition [2]. From experimental observations, Kraus [1] reports that equation (8) reduces to Norton's law when a uniaxial stress field occurs in the material, the volume of solid body is considered constant during creep, the principal directions are the same for creep strain and stress, and the hydrostatic part of the stress tensor does not concur in creep deformation.

2.1.4 Creep continuum damage models

In order to assess creep remaining life of components, accurate knowledge of secondary and tertiary regions of the creep curve is necessary and the secondary state approximation is not acceptable [4]. In the tertiary creep region, modelling of creep deformation (under a uniaxial or a multi-axial stress condition) requires the introduction of a number of internal variables, ω_i, that take into account damage accumulation in the material and its evolution during creep, and that concur in creep

deformation together with stress, temperature and time, as specified in equations (9) and (10) [2, 13].

$$\dot{\varepsilon}^c = \dot{\varepsilon}^c(\sigma, T, \varepsilon^c, \omega_i) \tag{9}$$

$$\dot{\omega}_i = \dot{\omega}_i(\sigma, T, \varepsilon^c, \omega_i) \tag{10}$$

As mentioned in section 2.1.1, in the tertiary creep region, the strain rate increases with time due to creep cavitation, which strongly depends on material and loading conditions [11]. When this phenomenon takes place, the sample starts losing its load carrying capability [7]. Cavities are an evident feature of the transition through to tertiary creep for ferritic steels. In some materials, such as for example P91 steels, the evidence of creep cavities seems to be less pronounced; hence, those materials are more difficult to assess just using discrete models based on cavity count; therefore, a continuum damage model must be used. Some, generally accepted, discrete models are described in [11].

Kachanov (1958) and Rabotnov (1969) have been the firsts to propose, in a uniaxial form, a creep continuous damage mechanics model that describes the cavitation damage and it is able to predict the sample failure [2, 13, 14]. In the conventional continuum damage mechanics, the damage parameter, ω, is intended as the ratio between the damaged area, due to material deterioration, and the initial undamaged area, A_0, and therefore it ranges from 0, for an undamaged material, to 1, for a failed/fractured material element. Damage can thus be expressed by equation (11), where A' is the undamaged area.

$$\omega = \frac{A_0 - A'}{A_0}, \quad with \;\; 0 \leq \omega \leq 1 \tag{11}$$

The multi-axial form of Kachanov-Rabotnov's model [2, 13] is due to Leckie and Hayhrust and is here given in equations (12) and (13), where $\dot{\omega}$ is the damage rate, σ_1 is the maximum principal stress, σ_{RUP} is the rupture stress defined in equation (14), ϕ and A are material constant, and α is a material constant taking into account the multi-axiality of the stress field.

$$\dot{\varepsilon}_{ij}^{c} = \frac{3}{2} B \left(\frac{\sigma_{EQ}}{1-\omega}\right)^{n} \frac{S_{ij}}{\sigma_{EQ}} \tag{12}$$

$$\dot{\omega} = A \frac{\sigma_{RUP}^{\chi}}{(1-\omega)^{\phi}} \tag{13}$$

$$\sigma_{RUP} = \alpha\sigma_1 + (1-\alpha)\sigma_{EQ} \tag{14}$$

It should be noted that the rupture stress is a composition of the maximum principal stress and of the von Mises equivalent stress, summarising the multi-axiality of the stress state in a single variable [13]. If the stress field is uniaxial, α = 1 and σ_{RUP} reduces to σ_1.

During creep, as the damage accumulates and evolves in the material, the stress is redistributed on those undamaged ligaments that can still carry some load [7]. The effective stress, σ_{EFF}, which acts on the undamaged material, is related to nominal uniaxial stress, σ_{nom}, and to damage through equation (15) [7].

$$\sigma_{EFF} = \frac{\sigma_{nom}}{1-\omega} \tag{15}$$

Another creep damage model that takes into account the multi-axiality of the stress state is the Liu and Murakami creep constitutive damage model [13]. Liu and Murakami based their model on those by Hutchinson and Riedel for materials undergoing creep-constrained grain boundaries cavitation [15, 16]. The former stated that a damaged material contains a dilute concentration of micro-cracks and, as a consequence, the creep strain rate has a linear dependence on the micro-crack damage parameter [15]. Riedel extended Hutchinson's model to non-dilute micro-cracks assumption, demonstrating the existing of an exponential relationship between the micro-crack damage parameter and the creep strain rate for the uniaxial stress state [16]. In the Hutchinson model, the creep strain rate is expressed as the sum of the dilatational creep components and the deviatoric creep components. According to Liu and Murakami, the former components are negligible when the material constant *n* is higher than 3 [13]. By assuming the continuum damage mechanics definition for ω and by considering a cylindrical material cell, with the diameter and the height having the same size, containing a penny shaped micro-crack, or, equivalently, a cavitated

grain boundary facet, Liu and Murakami proved that the damage parameter, ω, is a function of the length and the density of the micro-cracks and does not depend on the material constant n [13]. Instead the micro-crack parameter, ρ, is also a function of n, as showed in equation (16) [13].

$$\rho = \frac{2(n+1)}{\pi\sqrt{1+\frac{3}{n}}}\omega^{3/2} \tag{16}$$

Liu and Murakami's constitutive model, here reported in equations (9) and (18), where D, q_2 and χ are material constants, relates the creep strain rate, $\dot{\varepsilon}_{ij}^{c}$, to stress and damage fields. The material constant D is defined in equation (19). It should be noted that the hydrostatic part of the tensor stress does not concur to creep damage.

$$\dot{\varepsilon}_{ij}^{c} = \frac{3}{2}B\sigma_{EQ}^{n}\frac{S_{ij}}{\sigma_{EQ}}exp\left[\frac{2(n+1)}{\pi\sqrt{1+\frac{3}{n}}}\left(\frac{\sigma_1}{\sigma_{EQ}}\right)^2\omega^{3/2}\right] \tag{17}$$

$$\dot{\omega} = D\frac{1-exp[-q_2]}{q_2}\sigma_{RUP}^{\chi}exp[q_2\omega] \tag{18}$$

$$D = A(\phi+1) \tag{19}$$

The rupture stress is defined as in equation (14). It is easy to demonstrate that the material constants B, n, χ, ϕ and α are the same for both Kachanov-Rabotonv's and Liu-Murakami's damage models [6, 7].

2.1.5 Creep modelling and FE analyses

Norton-Bailey's law is included in finite element software, e.g. ABAQUS [17], but it can be integrated only to obtain primary and secondary creep regions of the creep curve. Kachanov-Rabotonv's and Liu-Murakami's damage models have been successfully used for component assessment and material characterization by means of finite element (FE) analyses, but, when Kachanov-Rabotonv's model is used, convergence problems arise as ω approaches its maximum value because of the singularity in equations (12) and (13) [13, 18, 19]. Both the damage models can be implemented in ABAQUS through the use of a CREEP User Subroutine [7]. In

particular, equation (13) can be integrated as in equation (20) in order for the failure time, t_r, to be obtained as in equation (21); and equation (18) can be integrated as in equation (22) in order for the failure time to be calculated as in equation (23) [6, 7].

$$\int_0^1 (1-\omega)^{\phi} d\omega = A\sigma_{RUP}^{\chi} \int_0^{t_r} dt \tag{20}$$

$$t_r = \frac{1}{A(\phi+1)\sigma_{RUP}^{\chi}} \tag{21}$$

$$\int_0^1 ex\,p[-q_2]\,d\omega = \frac{D\sigma_{RUP}}{q_2}[1-ex\,p(-q_2)] \int_0^{t_r} dt \tag{22}$$

$$t_r = \frac{1}{D\sigma_{RUP}^{\chi}} \tag{23}$$

2.1.5.1 Determination of the material constants

In order to implement Kachanov-Rabotonv's and Liu-Murakami's damages model into an FE code, the involved material constants (e.g. *n*, *B*, *D*, χ, ϕ, q_2) have to be determined. With this aim, at least three uniaxial creep tests have to be carried out at different stresses and at the same temperature [6]. By representing equation (7) in an alternative form, such as equation (24), a plot of $log(\dot{\varepsilon}^c)$ versus $log(\sigma)$ will produce a straight line [6]. The slope of the best linear fitting is the material constant *n*, and the intercept is *log(B)*.

$$log(\dot{\varepsilon}^c) = nlog(\sigma) + log(B) \tag{24}$$

The constants *D* and χ can be determined from the same tests by plotting (from equation (23)) $log(t_r)$ versus $log(\sigma)$, equation (25), that will produce a straight line; χ and *D* values can be obtained from the slope and the intercept, respectively [6].

$$\log(t_r) = -\chi log(\sigma) + log\left(\frac{1}{D}\right) \tag{25}$$

The material constant ϕ can be obtained by an optimization process that gives the best fit of the experimental creep test curves.

In order to determine the material constant q_2, a curve of creep strain versus t, such that given in equation (26), must be obtained for each stress level [6].

$$\dot{\varepsilon}^c = B\sigma^n exp\left[\frac{2(n+1)}{\pi\sqrt{1+\frac{3}{n}}}\left(-\frac{\ln(1-D(1-e^{-q_2})\sigma^{\chi}t}{q_2}\right)^{3/2}\right] \quad (26)$$

Equation (26) does not have a close-form solution, therefore a time-marching procedure is needed and it can be carried out by calculating the creep strain increment, $\Delta\varepsilon_i^c$, at the current time step, i, as in equation (27), where Δt is a small (constant) time interval and $\dot{\varepsilon}_i^c$ is the minimum creep strain rate at the current time step, i [6].

$$\Delta\varepsilon_i^c = \dot{\varepsilon}_i^c \cdot \Delta t \quad (27)$$

These creep strain increments are then accumulated to give the value of the total creep strain at the i time step, as showed in equation (28) [6].

$$\varepsilon_i^c = \varepsilon_{i-1}^c + \Delta\varepsilon_i^c \quad (28)$$

This procedure must be carried out up to time to failure, t_r, by using the initial values of n, B, D and χ calculated so far and an initial, attempting, value of q_2; an optimization process can be used to obtain the material constants that give the best fit to all of the experimental ε_c versus t curves [6].

2.2 CREEP OF POWER PLANT COMPONENTS AND LIFE MANAGEMENT

2.2.1 Service conditions

Power plant components often operate at elevated temperatures and pressures. The main steam boilers can operate at maximum 565 °C if made of conventional low-alloy ferritic steels, up to 650 °C if made of high-strength 9–12% chromium steels (ultra super critical temperatures) and up to 675-700 °C if made of high chromium or high nickel austenitic steels [11, 20]. High-pressure steam turbine rotors can operate at pressures up to 170 bar, for very long periods, up to several years, depending on the safety regulations for inspections [11, 20]. High-chromium and high nickel steels have

been developed in the last century in order to increase the creep strength of materials for power plant applications with the aim of reducing the cost of fuel and the use of fuel resources by improving the thermal efficiency of power plant steam [4, 11].

2.2.2 Typical failure

Viswanathan and Stringer define a component "industrially failed" when it can no longer serve its intended function safely, reliably and economically [3]. Failure of power plant components is mostly due to creep damage, corrosion damage, and creep fatigue damage. The former can cause dimensional changes in the components such as, for example, swells and leaks in headers, steam pipes and reheater tubes [3]. Failure due to creep damage mainly occurs in weldments. Figure 3 shows the classification of cracking in weldments, which depends on the position of the crack as per follow [3, 21]:

- Type I: the damage is longitudinal or transverse in the weld metal and remains entirely within the weld metal.
- Type II: the damage is longitudinal or transverse in the weld metal, but grows into the surround of the heat affected zone (HAZ).
- Type III: the damage spreads in the coarse-grained region.
- Type IV: the damage initiates or grows in the inter-critical area (the transition region between the fully-transformed, fine-grained HAZ, and the partially-transformed parent base metal) of the HAZ.

Usually, premature failure of the component occurs in the Type IV region of the weld because of the creep voids that develops in the fine grained and inter-critically annealed heat-affected zones of the weld [21]. A typical catastrophic failure in a seam welded hot reheat pipe is shown in Figure 4. Generally, axial cracks in pipes are attributed to the internal pressure loading and to geometry imperfections or distortions of seam welded pipe systems, while, circumferential cracks are associated with combined pressure and piping system loads [21].

Corrosion damage is typical of pipelines that operates in dense-phase CO_2 environments. This subject is fully reviewed in [22, 23].

Creep fatigue damage is typically caused by thermal stresses induced by constraint to thermal expansion during transient conditions and it may implicate large plastic strains whereby localised stress concentrations [3]. Constraints to thermal expansion can be internal or external. Any heavy section component, such as rotors, headers, drums, casings, can be seen as an internal constraint, as thermal gradients arise between the surface and the interior or vice versa [3]; joining of thick sections to thin sections, and materials of different coefficients of thermal expansion, like dissimilar metal welds, can be seen as external constraints [3].

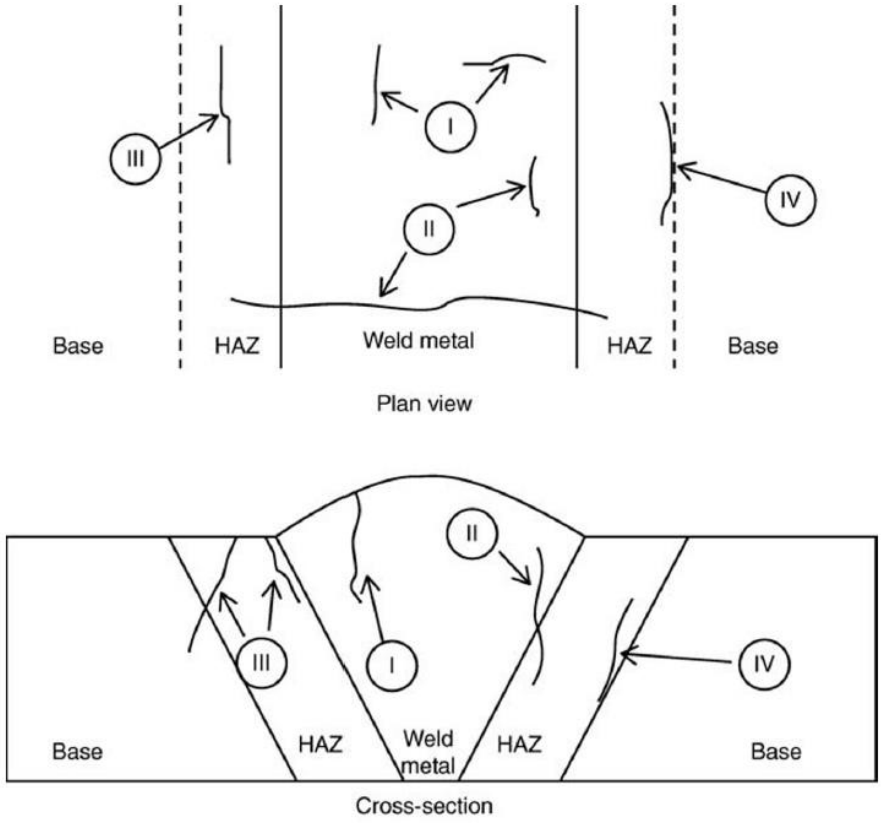


Figure 3. Classification of cracking in weldments, from Ref. [24].



Figure 4. Typical, catastrophic, failure in a seam welded hot reheat pipe [21].

2.2.3 Life management and lifing

Components for power plant applications can fail catastrophically, costing human lives in addition to expenses of repairs, replacements, and legal process costs [3]. This is the reason why inspection planning, life assessment and lifing models are mandatory for power plant utilities.

A range of non-destructive inspection based assessment techniques and surveys are used during a statutory plant shutdown to support an evaluation of the condition of components operating at high temperature and pressure. These techniques do not provide a direct measure of accumulated creep damage (life consumption); however they support the subsequent residual life assessment by reference to similar components and systems on sister plant. The current assessment approach requires extensive data mining and review of large quantities of site metallurgical data, from a number of different power stations and at different times in their lifecycle [20].

The techniques routinely used to assess the condition of components during a plant

outage include surface replication, surface hardness, ultrasonic inspection, magnetic particle inspection and physical dimension measurements using callipers and micrometers. The selection and use of these techniques is influenced by a host of considerations such as cost, perceived risk, familiarity and confidence with the techniques, plant access, accuracy, reliability, regulator preference and tradition. In addition, on-load monitoring of pressure and temperature conditions can be used to provide a generally conservative estimate of the residual creep life. This involves using sampled operational steam or metal temperature data coupled with steam pressure data, with an appropriate creep rupture expression to determine the residual creep life [20].

It is standard practice to use different approaches and diverse data sets, such as outage overhaul inspection data and on-load monitoring to evaluate component condition. This is necessary because of the intrinsic scatter in the material creep properties and uncertainty in some of the load components, such as fixed support loads and reaction loads from adjacent components and systems, which can also vary as the plant is cycled on and off load. It should be noted that modern plant design can limit the ability to deploy some of these traditional techniques due to restricted access for inspection [20].

For example, heat recovery steam generators (HRSGs) are designed so that it is not possible to use traditional diametral strain measurements on the steam headers. Hence, this provides a requirement to consider the use of the novel techniques to assess creep life consumption such as optical strain gauges [25], alternating current potential drop [26] and small specimen testing techniques such as impression creep, small punch and ring specimens [27, 28].

With respect to the use of the non-destructive techniques, on-line strain rate measurement offers great potential to the utility, from the perspective of being able to use the information to pro-actively manage the integrity throughout the whole life cycle of the station and to prompt beneficial changes in operation, in good time. The ultimate aim is to use the strain rate data iteratively in pipework or component specific computational models, where the system or component model response would be calibrated against component specific strain rate information, and compared against other relevant condition assessment data obtained during the plant outage. This would

demonstrate a truly holistic approach and is considered to be the ultimate aim for optimal plant integrity management [20].

2.2.4 Inspection planning

The inspection planning process is driven by the need for the utility to demonstrate compliance with pressure systems safety regulations (PSSR) requirements [29] and is applicable to both conventional and civil nuclear advanced gas cooled reactor (AGR) pressure systems [20].

2.2.4.1 Off-load: Outage Works

The following outage inspection techniques are applicable to both conventional and AGR high temperature and pressure systems. These techniques cannot be used as systematic input into a predictive creep life assessment model of the piping system or other high temperature components because of the uncertainty of the data collected through them [20].

Pipe movement

Pipe movement is obtained via hot and cold surveys of pipework hanger positions, an example of one type of pipe hanger set-up is shown in Figure 5. In this arrangement there are two spring loaded pipe hanger supports either side of the main steam pipe, with connections to structural steelwork above and connections to the main steam pipe via a ring (trunnion) clamp below (out of the image) [20]. This arrangement is designed to ensure that a constant load is imposed on the pipe as it moves up or down with normal plant operational transients. The hot and cold surveys provide information on pipework operational loads (between cold condition and full load hot operation), which can be compared against the design basis and prompting readjustment of hangers as required [20].

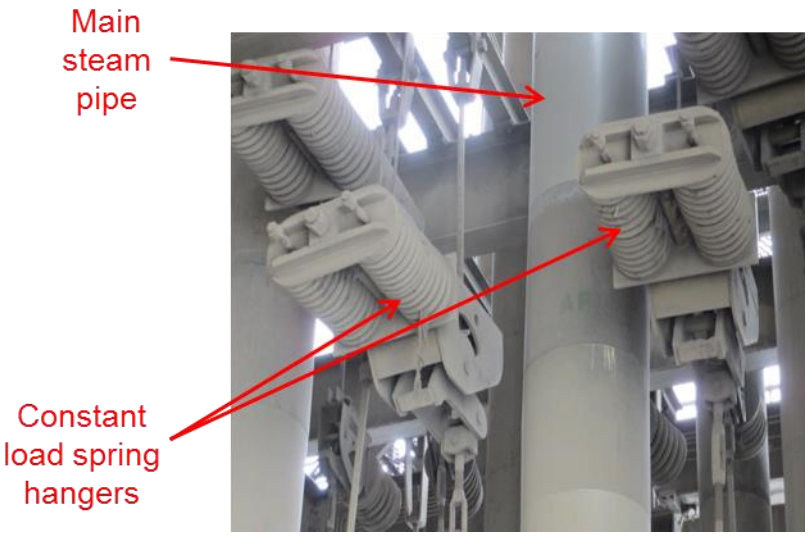


Figure 5. Typical pipe hanger arrangement, from Ref. [20].

Passive strain measurement

Bow gauge micro-meters shown in Figure 6 are typically used for headers and pipework for diameters up to about 600 mm with a precision of 0.01 mm, especially when used with a more accurate locating method such as non-oxidising creep pips [20]. It has been shown [30] that safe management of plant can be achieved with well controlled and managed diametral surveys, coupled with interrogation of other outage and operational plant data. However, a review of large datasets from periodic conventional fossil-fired plant diametral surveys show much greater than expected variability and emphasises the need for good procedural control on site if such methods are to be relied on [20].

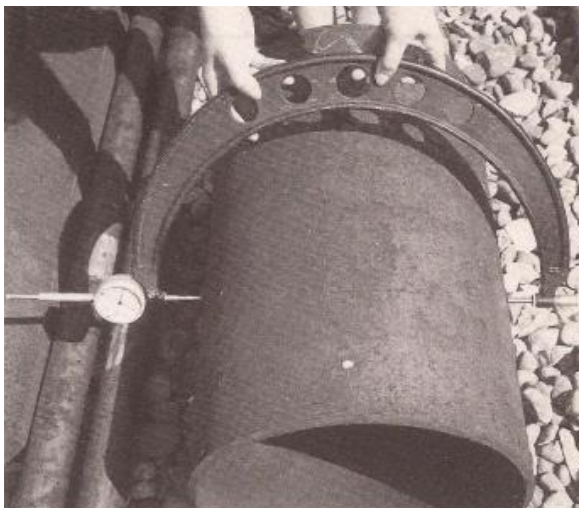


Figure 6. Bow gauge micrometer with dial gauge, from Ref. [20].

More recent developments to improve the accuracy and reliability of passive strain measurement include the ARCMAC high temperature optical strain measurement system [31, 32]. The ARCMAC system uses stud-welded optical targets attached to the component in a bi-axial arrangement, which is illuminated from a light source within a purpose designed camera system with a telecentric lens and beam splitter arrangement [20]. The attachment of the stud-welded optical gauge is facilitated by the use of a purpose designed gauge carrier that allows consistent gauge installation, along with the installation of a suitable protective cover. The optical arrangement and illumination ensures that accurate measurements of strain can be captured even if the camera system is not located precisely normal to the target gauge. The strain measurement resolution is ~ 60 micro-strain with an error of <10%. Gauge images captured during subsequent shutdown periods enables the creep strain rate to be deduced. Further extensions to these optical strain measurement techniques have been developed using surface speckle coatings and digital image correlation techniques to provide a non-contact surface strain distribution (across a weldment), with reference images from an adjacent ARCMAC gauge to provide a calibrated strain reference [33, 34].

Surface creep replicas

Surface creep replicas are targeted at regions considered to be more prone to creep damage accumulation, such as weldments, pipe penetrations (fillet welds), attachment welds, pipe bends and pipe terminal positions [20]. The requirement for creep replicas is dependent on the age of the plant and the perceived risk, which may be influenced for example by adverse readings from routine passive strain measurement campaigns or known periods of mal-operation evident from reviews of operational data [20]. It is not unusual for several hundred replicas to be taken during an outage on a single unit.

The surface replica technique involves capturing the surface features on a film that can subsequently be examined under a microscope. This involves careful surface preparation by grinding the surface with progressively finer abrasive papers, with final polishing. This process should be undertaken with great care to avoid removing the creep damaged surface and also to ensure that any surface oxidation and decarburised layers are removed. The prepared surface for replica assessment typically covers a surface area of 25x50 mm, and it is then etched with a dilute acid such as Nital to

reveal the microstructure. A soft cellulose acetate strip is then pressed onto the surface and allowed to dry before spraying with a matt black paint. This provides a contrast under white light when the replica is removed and examined under the microscope. Carefully applied this process should reveal creep cavities that can subsequently be counted per mm^2 and classified. It should be noted that different types of steel may require a modified process to the above in order to obtain the best quality surface replica [20].

Figure 7 illustrates a surface replica of a 0.5CrMoV steel main steam line weld, taken after grinding to a depth of 5 mm from the outside surface. In this example, a high creep cavity count was assessed at 842 cavities/mm^2 (dark features in Figure 7). In this case the material had been in operation on one of the EDF Energy's conventional fossil-fired power stations for circa 260 khr before retirement and subsequent examination [20].

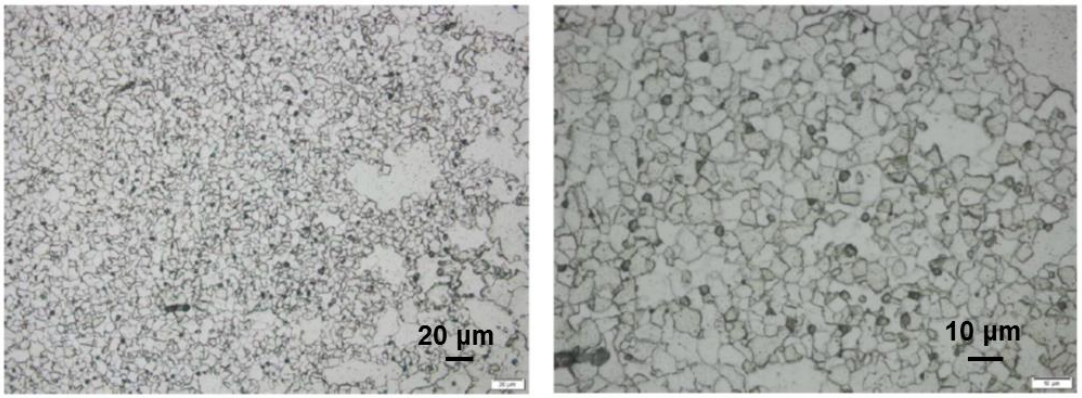


Figure 7. Weld Type IV region of a main steam pipework weld, surface replica taken 5 mm below the outer surface at (a) x200 magnification and (b) x500 magnification, from Ref. [20].

Surface Hardness

Surface hardness are outage measurements targeted at regions considered to be more susceptible to creep damage accumulation. It is custom and practice to cross-check these results against periodic trends from surface creep replicas obtained from an adjacent location [20].

Surface hardness technique is frequently used during an outage to provide a large amount of data, with the key feature of the subsequent assessment being the change in surface hardness at a repeat location between periodic inspection intervals. There are

a range of portable site hardness test tools available, either using ultrasonic contact impedance, direct measurement or dynamic rebound, which uses the impact and rebound velocities to determine the surface hardness value. It is necessary to prepare the surface before testing (to remove hard scale), and these methods are frequently used on site during the outage.

Decisions on repair or return to service options that use hardness data is typically based on rate of change in hardness and experiential knowledge from hardness trends associated with other similar components, material, service age and duty [20].

Material composition checks

Checking of material composition by means of portable x-ray fluorescence analysers is a standard practice for confirming that the correct materials have been installed on plant [20].

2.2.4.2 On-load: use of operational data

The station routinely records steam temperature and pressure data at selected key points in the process system. The decision on the sampling interval is influenced by the stability of operation; if the unit is prone to temperature instability then the sampling interval should be reduced. These techniques are applicable to both conventional and AGR high temperature pressure systems [20].

In addition, most stations will invariably have installed additional surface mounted or deep drilled thermocouples on key components or on components being monitored as part of a safety case. This data is stored in the plant historian and various data sampling frequencies can be defined. Typically if a plant transient is being monitored the thermocouple sampling interval may be as frequent as every 15-30 seconds. For longer term creep temperature monitoring the sampling interval could be increased to several minutes. With respect to creep temperature monitoring, the decision on the sampling interval is influenced by the stability of operation; if the unit being monitored is prone to temperature instability then the sampling interval should be reduced. Hence, some judgement and experience is needed to define the required sampling interval prior to any computation being undertaken [20].

Once this data is collected the station evaluates what is termed as the creep

effective temperature (CET), defined as the average temperature at which all of the creep damage (over the monitored period) can be equated to [20]. This approach typically uses the design pressure in the computation, although it is possible to use the measured operational pressure. However, for the purposes of the CET calculation, the design pressure is usually sufficient.

The creep rupture life calculation, using CET, gives a value of creep rupture life, which is dependent upon stress and temperature. Equation (29) is used to estimate the creep rupture life of CMV material and is based on the Manson-Brown 4th degree polynomial formula, where t_r is the predicted time to creep rupture in hours, T is the temperature in Kelvin, $\sigma = 1.25\ \sigma_{ref}$ and $p_0, p_1, \ldots p_7$ are constants, which values for the 0.5%Cr0.5%Mo0.25%V (CMV) steels are collated in Table 1 [20].

$$\frac{\log t_r - p_5}{(T - p_6)^{p_7}} = p_0 + p_1 \log\sigma + p_2(\log\sigma)^2 + p_3(\log\sigma)^3 + p_4(\log\sigma)^4 \qquad (29)$$

Table 1. Constants for equation (29).

p_0	p_1	p_2	p_3	p_4	p_5	p_6	p_7
-0.10086133	0.2521769	-0.27441233	0.12751693	-0.02218978	8.659	650	0.95

For a main steam line the creep reference stress, σ_{ref}, is equivalent to the mean diameter hoop stress in equation (30), where p is the operating pressure, D_0 is the pipe outside diameter and t_w is the wall thickness.

$$Mean\ Diameter\ Hoop\ Stress\ = p(D_0 - t_w)/2t_w \qquad (30)$$

Figure 8 shows the effect of changes in operating temperature from 568 °C to 578 °C against the minimum creep rupture life, for two operating stress levels of 42 and 47 MPa of a typical main steam line based on nominal dimensions of 360 mm outside diameter, 60 mm wall thickness with an operating pressure of 168 bar. The subsequent mean diameter hoop stress is 42 MPa and it can be observed that an increase in operating temperature of ~5 °C or an increase in stress of ~ 10% results in a reduction in creep rupture life of ~ 20 khr.

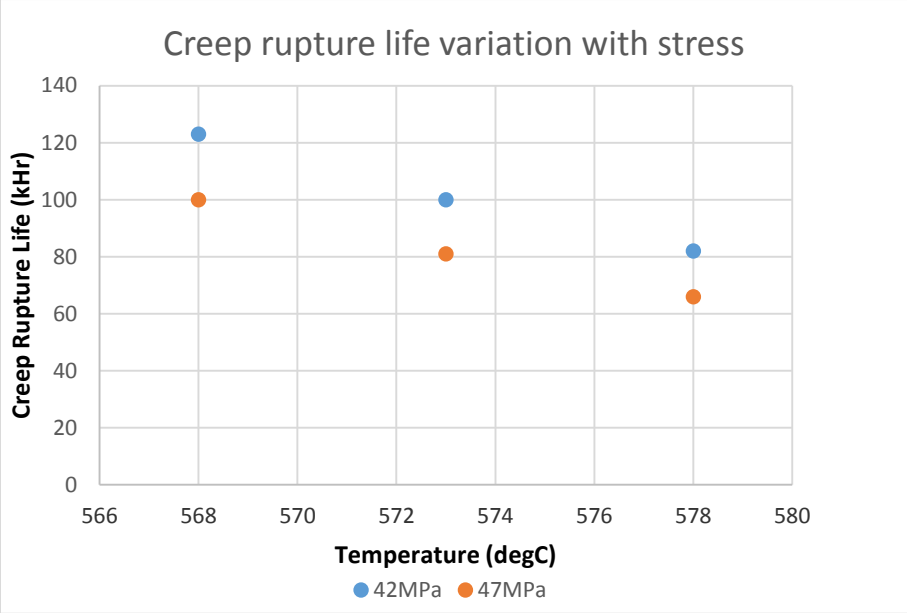


Figure 8. Sensitivity of creep rupture life, from Ref. [20].

The above example is significant for the following reasons [20]:

1. Relatively modest increases in operating conditions (temperature and stress) result in a significant reduction in creep rupture life;

2. The reduction in creep rupture life of ~ 20 khr, due to variation in temperature or stress is approximately equivalent to a typical 4-year operating period for a large conventional fossil-fired power station;

3. Stations would prefer to be able to plan future outage scope and replacement strategies with more certainty for budgetary purposes; the example presented shows the dilemma that stations face as unit operation nears the end of practical commercial life.

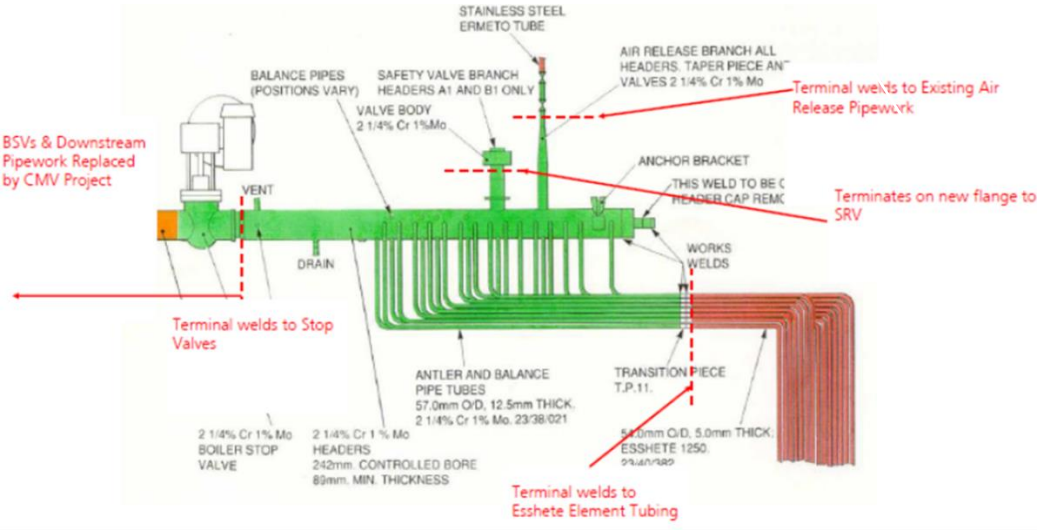
From the perspective of the station the sensitivity to modest increases in operating conditions makes planning the scope of subsequent outages or replacement exercises fraught with uncertainty. This uncertainty triggers a natural response to conduct more sampling inspections at subsequent outages and may result in premature replacement of large sections of pipework or components [20].

The primary use of the CET computation is to provide a systematic process to identify operational issues and to prompt a correction. In addition, historical CET computations on units and across steam systems and components are used to support

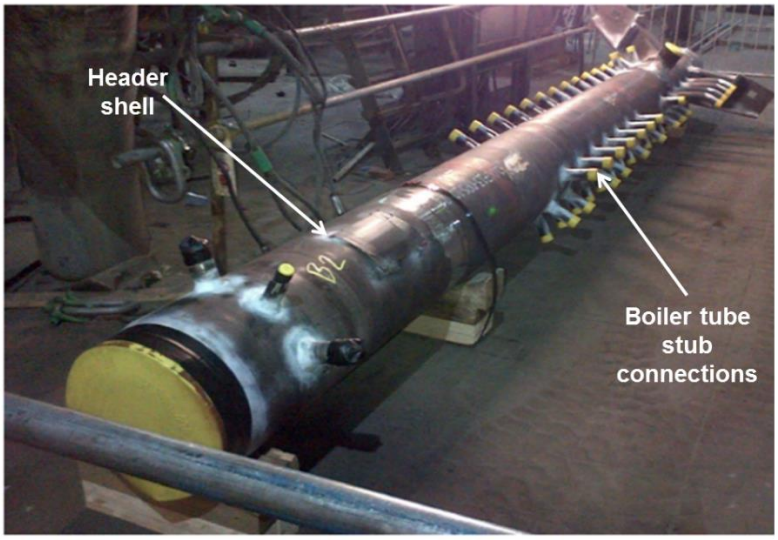
the definition of the inspection scope prior to the next statutory outage[20].

It should be noted that on current UK conventional fossil-fired stations the steam outlet design conditions are nominally 568 °C and 168 bar. However, from experience it is not unusual for steam temperatures to cycle beyond 600 °C, which is the limit of the CMV creep rupture models, in equation (29). In such cases, the use of the CET data is problematical and a consequence of such adverse operation is that more 'inspection sampling' during an outage is usually stipulated in order to determine if the operational instability has manifested itself as an unexpected accumulation of creep damage or the initiation of damage (metallurgical or physical macro-cracks) at weldments. Hence, unstable temperature excursions should be minimised. Unstable operation can also result in severe (rapid) thermal transients occurring on plant, which can result in the initiation of fatigue cracks in weldments and for high temperature systems subsequent propagation via creep crack growth through wall [35] under steady load conditions [20].

Figure 9 (a) shows the design of a large steam header, which is a significant class of high temperature thick sectioned component installed in a boiler. These components are subject to very similar outage inspections and on-line CET assessments as described for main steam pipes, however these are considered to be more complex to assess due to the numerous penetrations in the header shell and difference in stiffness between the relatively rigid header shell and the thin interconnecting boiler tubes. Steam headers ensure proper distribution of steam across the boiler space, with the boiler tubes providing the heat transfer surface within the furnace of a conventional fossil-fired boiler. There are many different designs of steam header (material and geometry) within a typical conventional fossil-fired boiler. The photograph in Figure 9 (b) shows the limited access available associated at the inter-ligament positions on this particular design for material extraction. For this design the approach would be to take a reference small specimen material sample [5, 27, 36] from the adjacent and accessible header shell [20].



(a)



(b)

Figure 9. 6th Stage superheater outlet header (a) schematic component and (b) replacement component, from Ref. [20].

2.2.5 Condition assessment

The requirement to understand with certainty the remaining life of power plant components becomes ever more acute in commercial electricity generation where the profitability may be marginal, whether caused by government or environmental policy, market prices, taxation or other factors. From a technical perspective, the current approach to define a 'holistic' view of the condition of the generating assets is achieved by the assimilation and deductive assessment of information gleaned from the activities described in Sections 2.2.4.1 and 2.2.4.2. The current approach is

considered to be ‘inspection based’ and does not [20]:

- Provide a predictive life assessment beyond the next major statutory outage;
- Actively integrate the various disparate data sets obtained from the plant outage or on-load monitoring.

Therefore, the development of a new high temperature plant condition assessment, that also includes miniature specimen testing techniques, is needed. As aforementioned, miniature specimen testing techniques could be very useful in testing material from critical areas (see Figure 9), while hardness measurements are of great interest for power plant companies because of the simplicity of the technique and of the large amount of data collected so far. For these reasons hardness and miniature specimen testing techniques are delved deepen in sections 2.3 and 2.4 of this Literature Review.

2.3 SURFACE HARDNESS TESTING TECHNIQUE FOR DUCTILE MATERIAL CHARACTERIZATION

Surface hardness is a non-destructive technique, often used during plant outages or other offload periods to acquire broad intelligence on the condition of the material in-service at high temperature. One of the attractions of the technique is that it can be deployed relatively easily and widespread across a power plant. Invariably the capture of hardness data is accompanied with other procedures such as surface replicas. Often the hardness and surface replica data is assessed together in order to direct a suitable course of action to ensure that the plant is safe to operate over the next period. As materials age in service at high temperatures the expectation is that the hardness will reduce and in addition the surface replica will also show a change in condition, usually interpreted as a measurement or count of the amount of creep cavities per unit area.

2.3.1 Historical background

The idea of hardness dates back between 460 BC and 370 BC, when the philosopher Democritus defined the atoms “hard” because of their lacking of voids. He divided the materials into hard or soft, depending on the location and arrangement of the voids among the atoms [37]. However, the very first who defined hardness, by

basing his theory on Democritus' intuition, was Aristotele (384-322 BC) in his *Meterology*: "Of the qualities of bodies hardness and softness are those which must primarily belong to a determined thing, for anything made up of the dry and the moist is necessarily either hard or soft. Hard is that the surface of which does not yield into itself" [38, 39]. A modern definition of hardness is due to Ashby (1951): "Hardness is a measure of the resistance to permanent deformation or damage" [40]. In the last century, at least four groups of hardness testing techniques have been developed, measuring the resistance of the material to permanent deformation when it is subjected to static load, to deformation when it is subjected to an impacting load or to wear by abrasion or to scratching [41]. However those tests measure different properties of the material, thus hardness has not a unique definition [41].

As reported by Tabor, Brinell was the first, in 1900, to establish a modern method to measure the static indentation hardness of ductile materials [37]. As Technical Manager of a company, the Fagersta Bruks, which used to produce steel, Brinell was asked to deal with a new lot of steel considered "poor" by customers [37]. Thus, he conceived the ground-breaking of the standard Brinell test, which consisted in compressing a ball of hard steel between two plates of steels, one from the "poor" lot and the other from the suitable set. Brinell determined whether one plate was harder than the other by measuring the size of the impression left by the ball on the plates [37, 42]. Although only a small range of materials can be tested with the spherical indenter of steel, Brinell's test showed to be of great interest for both industries and researchers, therefore hardness techniques have been developed and improved in terms of accuracy and applicability to different materials from 1900 to now on.

This limit of the Brinell test has been overcome in 1925, when Smith and Sandland elaborated the Vickers test, characterised by a diamond indenter with a pyramidal shape with a square base [43]. Indenters with disparate shapes have also been adopted from 1925 to the present time [44-47].

Hardness testers have also been used since 1905 to measure hardness at high temperatures (up to 0.8 of the material melting temperature), with the aim of finding a relationship between the hardness variation and the variation with temperature and time of the material properties [39, 48].

A hardness tester was also used for measurements at very low loads (<1 kgf), for the first time, by Lips and Sack in 1936 [49]. This method of measurement allows the investigation of very small variation in hardness and it is known as micro-

indentation hardness testing, due to the load and impression size, which are small with respect to bulk tests [50].

Portable hardness machines are popularly used for on-site sampling for power plant high temperature components. Currently, micro-hardness mapping can be used to obtain detailed hardness variation within a small, critical region, such as the various metallurgical zones in a fusion weld.

Hardness is scale dependent when the indentation size is similar to or smaller than the grain size of the tested material.

2.3.2 Standard hardness tests

The standard Brinell test is carried out at room temperature by applying a static load, *P*, in kgf, for 30s on a spherical indenter made of hard steel, which compresses a sample in its normal direction. The Brinell hardness number (*HB*) has the dimensions of a pressure and, in the absence of friction between the specimen and the punch, is expressed by equation (31), where *A* is the curved area of indentation, in mm^2 [42]. In defining the HB, Brinell first included in equation (31) the projected area of indentation, but this caused variations in the hardness measurements due to indentation size effects [42].

$$HB = \frac{P}{A} \tag{31}$$

Standard Brinell test cannot evaluate the hardness for those materials which present hardness higher than about 400 HB, therefore Smith and Sandland proposed the Vickers test in 1925, which makes use of a square based diamond as indenter, and gives the same hardness number as the Brinell test [37, 50]. As expressed in equation (32), Vickers number, *HV*, is given by the ratio of the applied load in grams-force, and the pyramidal area of indentation, where *d* is the length of diagonal in μm. The angle between two diagonals of the pyramid is 136°, whilst *HV* is generally expressed in kgf/mm^2 [50]. Vickers test has the essential advantage of being able to assess the hardness of any material and to locate it on one continuous scale [50]. Figure 10 shows (a) the standard Vickers indenter, (b) the indentation produced, and (c) the plastic flow in the indentation area.

$$HV = 1854.4\frac{P}{d^2} \tag{32}$$

In 1939 Knoop et al. developed a test similar to Vickers, particularly helpful in the evaluation of very thin materials and in the estimation of the effects of the orientation of crystals on hardness [37, 46, 50]. In Knoop test the indenter has the shape of an elongated pyramid and its number, *HK*, is given by equation (33).

$$HK = 14229\frac{P}{d^2} \tag{33}$$

The fastest hardness test, that also has the advantage of involving depth measurements instead of optical measurements, is the Rockwell test, but a worldwide unified hardness scale still does not exist, even if a step forward has been done by Song et al. in order to overcome this problem [37, 50, 51].

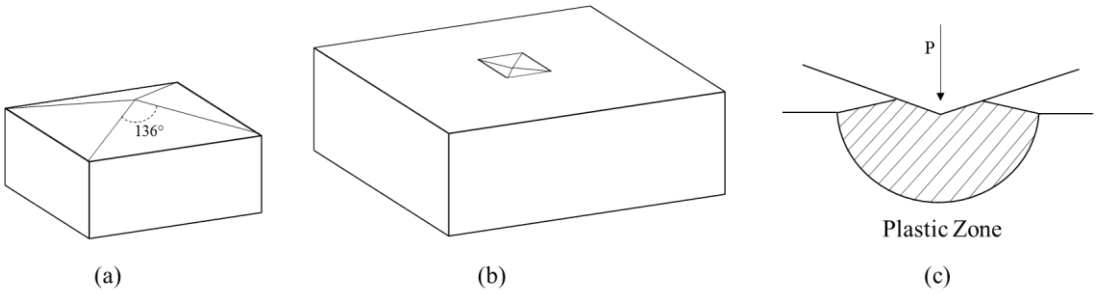


Figure 10. (a) Standard Vickers diamond pyramid indenter, (b) the indentation it produces, and (c) the plastic flow around the indentation, adapted from ref. [37].

As a general rule for obtaining a successful hardness value among the described ones, the specimen must be much larger than the indentation and every indentation must be carried out at a distance of at least 3*d* or 4*d* [37, 50]. Friction should also be considered, as it has been proved to affect the test, especially at very low loads [50].

2.3.3 Empirical relations between hardness and yield strength

By considering the hypotheses of isotropic material, fully work-hardened behaviour, constant yield stress, σ_y, and negligible elastic deformation, and keeping into account that the hydrostatic part of the stress tensor does not concur to plastic flow, it has been demonstrated that the mean contact pressure, *p*, between the specimen

and the indenter is given by equation (34) [50, 52-54].

$$p \cong 3\sigma_y \tag{34}$$

The uniaxial flow strength, *S*, is related to hardness by equation (35), where *c* is an elastic constraint factor equal to 3 for metals that do not significantly strain harden when HV is measured in kg_f/mm^2 and *S* in MPa [53, 55-57].

$$HV = cS \tag{35}$$

The plastic strain related to *S* only depends on the geometry of the indenter tip and is 0.08 for a diamond pyramid hardness test [55, 58].

The ultimate tensile stress, σ_{UTS}, and the yield stress are related to hardness through the Cahoon et al. relationships (equations (36) and (37)), where *N* is the strain-hardening exponent [59, 60].

$$\sigma_{UTS} = \frac{HV}{2.9}\left(\frac{N}{0.217}\right)^N \tag{36}$$

$$\sigma_y = \frac{HV}{3}(0.1)^N \tag{37}$$

The tensile properties of ferritic steels can be accurately calculated by equations (36) and (37) at temperatures up to 400 °C if the strain-hardening exponent is known by previous uniaxial tensile tests [61].

2.3.4 Current status of application

Surface hardness measurements take place during off-load monitoring of power plant components, together with pipe movement checks, passive strain measurements, surface creep replicas and material composition checks, but, nowadays, they cannot be routinely used as an input into a predictive creep life assessment of the piping system [20], especially because the scatter in the measured data can be large. Furthermore, hardness measurements are highly affected by microstructural variations, which cause concerns during condition monitoring of welds [62-65]. Currently, utilities adopt hardness technique as part of the quality assurance tests in order to evaluate microstructural quality of components and in-service trends, while the Electric Power Research Institute (EPRI) provides guidelines and perspectives on the use of hardness testing [66-69]. However, hardness and micro-hardness tests application is not limited to power plant issues. In fact, in 2009, Infante

et al. used those two techniques to investigate the possible causes of the failure of aero-engine compressor blades [70].

2.3.5 Hardness based lifing models

The research of a correlation between hardness data and time temperature parameters has been ongoing since 1943 [71, 72]. A modified Kachanov's damage model that includes hardness and the effects of structural degradation and creep cavitation was developed by Cane et al. in 1985 [73, 74]. Their method is able to predict upper and lower boundaries for the time to rupture, but many material constants and parameters, including hardness due to solid solution strengthening, need to be determined or measured, making this approach of little practical use.

In 2006, Masuyama found the following relationship, equation (38), between the remaining life, t_r, for 9Cr-Mo-V-Nb steel and the changes in hardness, expressed as the ratio of the hardness of the crept specimens, H, and the initial hardness, H_0 [63].

$$\frac{H}{H_0} = 0.98 - 0.15\frac{t}{t_r} \Rightarrow \frac{t}{t_r} = \frac{1}{0.15}\left(0.98 - \frac{H}{H_0}\right) \tag{38}$$

By assuming the initial drop in hardness to be zero, Masuyama also established a relationship between the drop in hardness and the Larson-Miller parameter (LMP), as shown in equation (39), where K_s is a fitting constant, t the time in hours and T the absolute temperature [75, 76].

$$\ln(H_0 - H) = K_s(LMP) = K_s T(20 + \log t) \tag{39}$$

From equation (39) Masuyama expressed H_0 and the remaining life as a function of the Larson-Miller parameter, as reported in equations (40) and (41) [75].

$$H_0 = H + \exp[K_s T(20 + \log t)] \tag{40}$$

$$\frac{t}{t_r} = \frac{1}{0.15}\left(0.98 - \frac{H}{H + \exp[K_s T(20 + \log t)]}\right) \tag{41}$$

Many researchers base their models for creep life evaluation on hardness as a function of the Larson-Miller parameter [64, 77, 78]. In particular, Furtado et al. have correlated the Larson-Miller parameter and the changes in hardness for a particular material, but their method only provides a first evaluation of damage if the initial hardness of the material is known at time t=0 hours, and cannot be used for establishing the damage and the remaining life of welds [76, 79-81]. Mukhopadhyay et al. also emphasised the necessity of considering a different non-linear correlation between hardness and LMP, based on experimental observations [78].

For ductile materials, equation (42) relates the failure time, t_r, to the applied stress [82].

In 2007, Allen and Fenton, starting from equation (42), derived a practical normalised hardness-based stress model to predict the failure life of new and service aged P91 steel [82]. Their method is here given in equations (43) and (44), where G and q are a material and a fitting constant respectively, and s is a normalising parameter defined as the ratio between the applied stress and the flow stress. The latter is in turn defined as the average of the 0.2% proof stress and the ultimate tensile stress.

$$t_r = B\sigma^{-n}\exp\left(\frac{Q_c}{RT}\right) \tag{42}$$

$$B\sigma^{-n} = G(s/HV^{-qn}),\ \ with\ q > 1 \tag{43}$$

$$\ln(t_r) - \left(\frac{Q_c}{RT}\right) = \ln(G) - n\ ln(S) + qn\ ln(HV) \tag{44}$$

The fitting constant q has been introduced by Allen and Fenton to take into account the possible non-linear correlation between creep strength and high temperature tensile strength or the possible non-linear relationships between high temperature tensile properties and room temperature tensile and hardness properties [82]. This method is of practical use, but underestimates the failure life and overestimates Q_c and n, therefore it should be improved by considering the flow stress as temperature dependent [82].

2.4 MINIATURE SPECIMEN CREEP TESTING TECHNIQUES

2.4.1 Overview

Establishing the remaining life of components operating at high temperatures is a major concern for power plant utilities. In particular, repair ranking and replacement strategies require acquisition of creep data of in-service components. Although the characterisation of the full creep curve of these materials can be accomplished by use of standard size uniaxial creep tests, shortage of materials to be tested has led to the development of unconventional creep testing techniques, which include miniature specimen creep testing techniques.

These techniques can be very useful to investigate material creep behaviour of critical regions of power plant components, such as welds with heat affected zones, and pipe bends. Moreover, miniature creep testing techniques can be treated as quasi-non-invasive methods and do not require weld repair when samples are carefully removed, "scooped", from in-service components as long as, for example, the maximum excavation depth does not exceed 10% of the wall thickness of the main steam pipe [83-85].

In the last two decades, researchers all over the world (USA, UK, Europe, Japan and China) have developed and investigated these non-traditional methods, also trying to assess relevant Standards and Codes of Practice [5, 28, 86, 87].

Miniature specimen testing techniques developed for power plant applications and, in particular for material creep properties characterisation include: sub-size conventional uniaxial creep specimens, with typical diameters of 1.5 to 3 mm; impression creep test specimens, with typical dimensions of 10x10x2.5 mm for a rectangular sample; small punch creep test specimens, with recommended disk radius of 8 mm and thickness of 0.3 to 0.5 mm; small ring creep test specimens, with typical radius of 6 mm; and two-bars creep specimen, with typical gauge length of 26 mm [5, 27, 36]. Typical test temperatures for the miniature specimens are up to 700 °C. Among miniature specimen creep testing techniques only small punch creep test (SPCT) and small two-bar creep test allow the full creep curve to be characterised, because the specimens are taken to rupture [27, 88]. Despite this advantage, during small punch creep test, interaction of several non-linearities, such as large

deformations, large strains, non-linear material behaviour and non-linear contact interactions between the specimen and the punch, induces a complex multi-axial stress field in the specimen that also evolves in time [7, 89]. This affects the SPCT fracture mechanism and introduces several challenges into the development of a robust correlation to convert SPCT data into respective standard uniaxial creep test data [90]. Another major concern is the non-repeatability of the testing method, since the experimental results depend on the set up geometry [5]. With two-bar creep testing technique, the pins must be made of a material with much higher (depending on the size of the sample, the pin diameter and thickness of uniform section) creep strength than that of the specimen, therefore a limitation resides in the range of materials that can be potentially tested. Accurate secondary creep properties are provided by small ring creep testing technique, but time-dependent geometric correction functions to compensate for the effects of geometry changes during the deformation process are needed [27, 91]. Impression creep testing method is easy to perform and it has shown to be able to provide reliable secondary creep properties, particularly at relatively high stresses and in the heat affected zones of welds [92]. Although specimens are not taken to rupture, the technique has shown to be very suitable in power plant component life assessment [93].

A requirement all of the miniature creep testing techniques have in common is the need to convert small specimen creep testing data to the corresponding uniaxial data. Conversion relationships exist, except for the small punch creep test, for which a procedure to interpret the experimental output is still under research [5, 94].

2.4.2 Scoop sampling

In order to manufacture miniature specimens from in-service components, scoop sampling techniques are currently used for industrial procedures [83, 95]. Rolls-Royce produced the SSamTM-2 sampler for the extraction of material samples, shown in Figure 11; the machine has a length of 420 mm and presents a hemispherical shell cutter of 50 mm in diameter, which can remove a “button” shaped sample of material, that is, typically, 25 mm in diameter and 4 mm thick [83]. Rolls-Royce has also designed two other smaller samplers, one able to fit within a 38 mm diameter tube bore and the second within a 30 mm annulus [83]. Scoop sampling techniques are such that the wall thickness of the component does not become smaller than the design wall

thickness after some material has been removed [96]. Nevertheless, an increase of the creep strain rate in the sample area has been observed by finite element (FE) analyses of drum, steam pipes and turbine rotor bores. This is due to the increase in stress at the bottom of the of the excavation, which is up to 1.2-1.5 times greater than the stresses in the intact wall in the same depth from the external surface of the component [85, 97]. In order to assess the creep damage due to this stress increment caused by the scoop sampling, Klevtsov and Dedov carried out FE analyses of a steam pipe with an outer diameter, D_0, of 325 mm and a wall thickness, t_w, of 30 mm, and creep cavity count on three bends steam pipes of 12Ch1MF and 15Ch1M1F [85]. Two important conclusions can be deducted from their research; firstly, after 23-27 khr of service, the analysed components presented the same creep damage in the region under the scooping area and at a distance of 10 mm from that. Secondly, tensile properties of the materials remained the same during service and were independent of the excavation location and of the specimen typology [85].

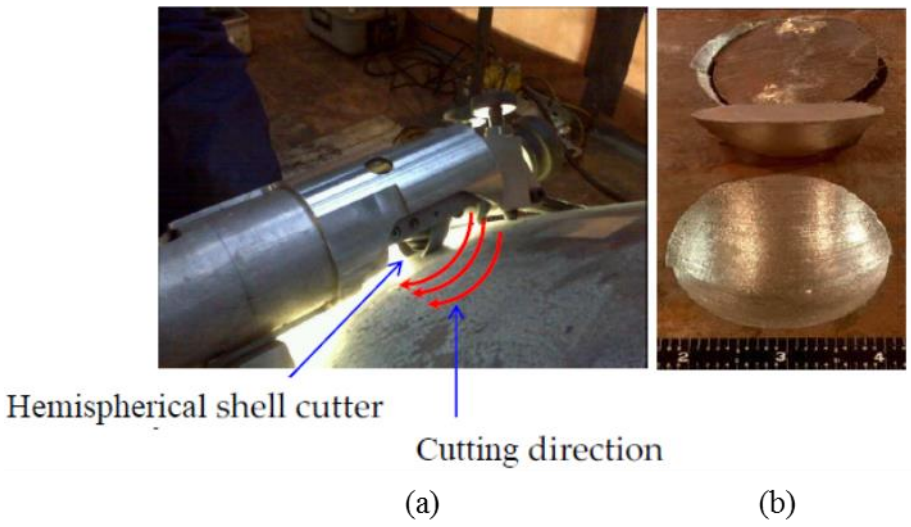


Figure 11. Photographs of (a) scoop sampling in process on pipework, and (b) a typical scoop sample, from Ref. [98].

Brett carried out 170 impression creep tests, scoop sampled by using the SSamTM-2 on CrMoV main steam and hot reheat pipes, which had a wall thickness of 60-65 mm and 30-35 mm respectively [84, 99-101]. He found that the scoop technique can be considered to be ‘quasi non-destructive’ since it does not require the repair stage as long as the maximum excavation depth does not exceed 10% of the wall thickness of the main steam pipe. For the hot reheat pipe a depth larger than 10% of the wall thickness is acceptable only over a restricted area in the centre of the

excavation [84].

Rouse et al. investigated the effects of scoop sampling on the creep response of straight pipe sections with different geometries, for a range of cut depths from 1 to 5 mm and for different load conditions, for the material 0.5Cr0.5Mo0.25V at 640 °C [102]. They found that the presence of the excavation generates a localized stress around the base of the excavated notch. In the case of a static application of the load to the pipe, the condition is considered safe if the stress at the base of the excavation does not exceed the magnitude of the stress at the inner surface. This condition is achieved only when the depth of the excavation, *h'*, is 1 mm for a pipe section with D_0 = 360 mm and t_w = 60 mm. Rouse at al. also propose a parametric equation which can estimate the scoop sample riser effect for a wide range of materials and pipe geometries, here given in equation (45), where *A, B, C, …, I* are fitting constants [102]. Future study is needed on the effects of scoop sampling on the sampled component under the effects of cyclic load conditions.

$$\frac{\sigma_R}{\sigma_{MDH}}\left(\frac{D_0}{t_w}, h'\right) = A\frac{{D_0}^4}{t_w} + B\frac{{D_0}^3}{t_w} + C\frac{{D_0}^2}{t_w} + Dh'^2 + E\left(\frac{{D_0}^2}{t_w} + h'^2\right) + F\frac{D_0}{t_w} + Gh' + H\left(\frac{D_0}{t_w} + h'\right) + I \tag{45}$$

These studies on the effect of the scoop excavation suggest that a degree of prior assessment is required before a sampling exercise is undertaken to consider the excavation depth, component geometry, material type, material condition and the operational duty of the plant. The study by Rouse et al. [102] considers operating temperatures at 640 °C, which is much higher than the typical plant operating temperatures (~ 570 °C) that Brett's study alludes to. This emphasises the need to measure on plant or estimate by analysis, the operating temperature related to a proposed sampling location.

For practical purposes a scoop sample location would be identified as a location on a future inspection schedule, noting that the additional cost and effort for the inspection of scoop sample locations typically is insignificant when compared to the full inspection scope during an outage. Ideally, all scoop sample locations would be accessible for repair should the need be foreseen.

2.4.3 Impression creep test

Impression creep testing technique consists of applying a steady load to a material by means of a flat-ended rectangular indenter. Figure 12 (a) and Figure 12 (b) show the typical specimen geometry and a schematic diagram of load arrangement, respectively, where d is the indenter width, w, b and h are the width, the length and the thickness of the sample, respectively. The recommended geometry dimensions are $w = b = 10$mm, $d = 1$mm, $h = 2.5$mm [103]. Dimension ratio and size effects that can affect the test output can be avoided if the recommended specimen dimensions are chosen for the test [104, 105]. Also, bulk creep properties are obtained because the contact area between the specimen and the indenter is large enough to cover more than 6-10 grains [92]. Generally, Nimonic 115 indenter is used for the test. Although further research is needed, reliable results can also be obtained by means of a ceramic indenter (used at Forschungszentrum Jülich GmbH, Institute for Energy and Climate Research) and of Nimonic tools with a cylindrical part allowing the indenter to rotate and settle parallel to the specimen surface (used at VTT Technical Research Centre of Finland) [106]. The test is generally isothermal and the load is constant with time. During the test, the indenter displacement is measured, e.g. through a linear variable differential transducer (LVDT), and the output is represented by creep displacement against time curve, which includes the primary and secondary stages. Since the specimen is not taken to rupture, this test does not allow for the tertiary stage data of the creep behaviour to be acquired. The technique has been proved reliable in determining secondary creep properties of the tested material and Monkman-Grant's relationship can be used to evaluate the component time to failure [107].

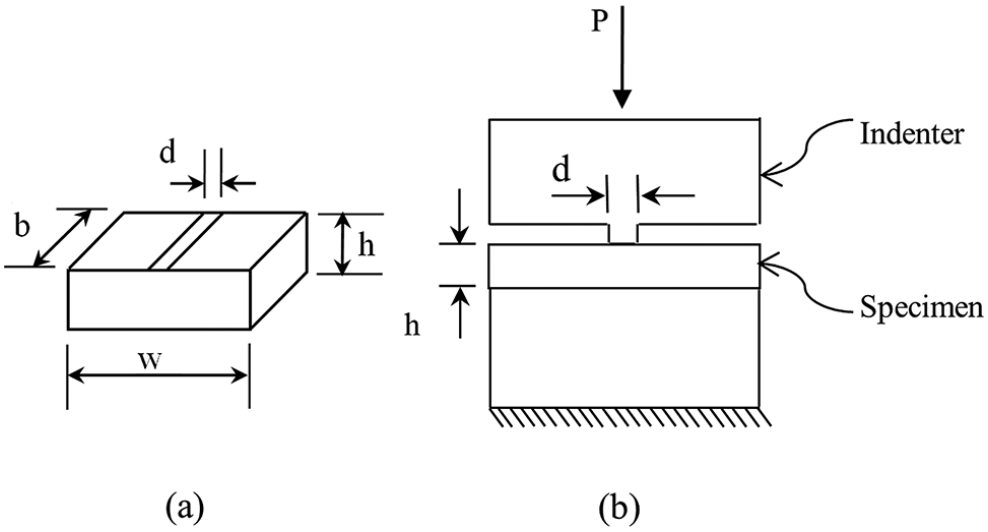


Figure 12. (a) Impression creep test specimen adapted from ref. [103] and **(b)** schematic diagram showing the specimen loading arrangement, adapted from ref. [108].

During an impression creep test the deformation of the specimen is strongly localised in the immediate vicinity of the indenter. Figure 13 shows a typical tested specimen of a cast 1/2CrMoV (CMV).

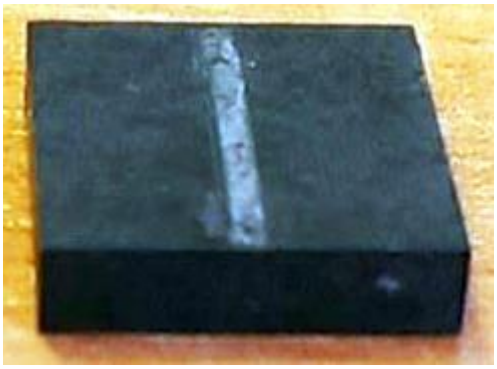


Figure 13. Typical tested specimen of a cast 1/2CrMoV.

Figure 14 (a) shows impression deformations with time at 90 MPa and 600 °C, obtained from three different ex-service 1/2CrMoV steam pipe samples (TLB93, TLB94, TLB97) [105]. Figure 14 (b) presents impression deformations of the heat affected zone (HAZ) of a P91 weld at 650 ^{o}C, subjected to steady loading from the parent material side. The plots are typical deformation creep curves from an impression creep test, where primary and secondary deformation regions can be identified. The two regions should not be confused with those of a typical creep curve obtained from a uniaxial testing, as the load and deformation mechanisms that govern the two of testing techniques are different. Also, during an impression creep test, the

specimen is subjected to global compression, while small deformations take place and there is no crack development. During a uniaxial creep test, the necking of the specimen leads to an increase in stress and strain. When the uniaxial creep test is carried out at constant stress, by means of load feedback, the stress does not increase with the increasing necking and the uniaxial specimen experiences an acceleration in the creep rate due to the propagation of micro-cracks (e.g. inter-granular cavitation damage), which actually characterize the tertiary creep regime of the uniaxial specimen.

The slight fluctuations in the observed data of an impression test are mainly caused by temperature variations within the furnace and laboratory. However, it can be seen that these variations are typically well within about ± 1 μm [105].

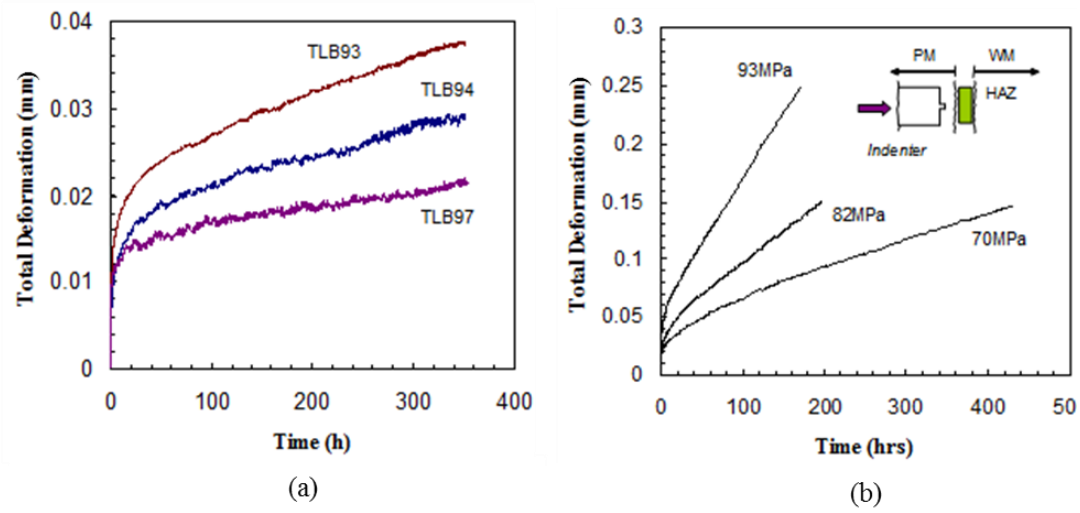


Figure 14. (a) Impression deformations with time at 90 MPa and 600 °C obtained from three different ex-service 1/2CrMoV steam pipe samples (TLB93, TLB94, TLB97), from ref. [105], and **(b)** impression deformations of the HAZ of a P91 weld at 650 ºC, subjected to steady loading from the parent material side, from ref. [105].

2.4.4 Small punch creep test

Small punch creep test (SPCT) consists in pushing a hemispherical indenter into a disc specimen clamped between an upper and lower die containing the receiving hole. A schematic cross section of the test rig is given in Figure 15-a. The CEN Code of Practice CWA 15627 [5] recommends a disc thickness, t_0, of 0.3-0.5 mm, an indenter radius, R_s, of 1.0-1.5 mm and a specimen diameter of 3-10 mm.

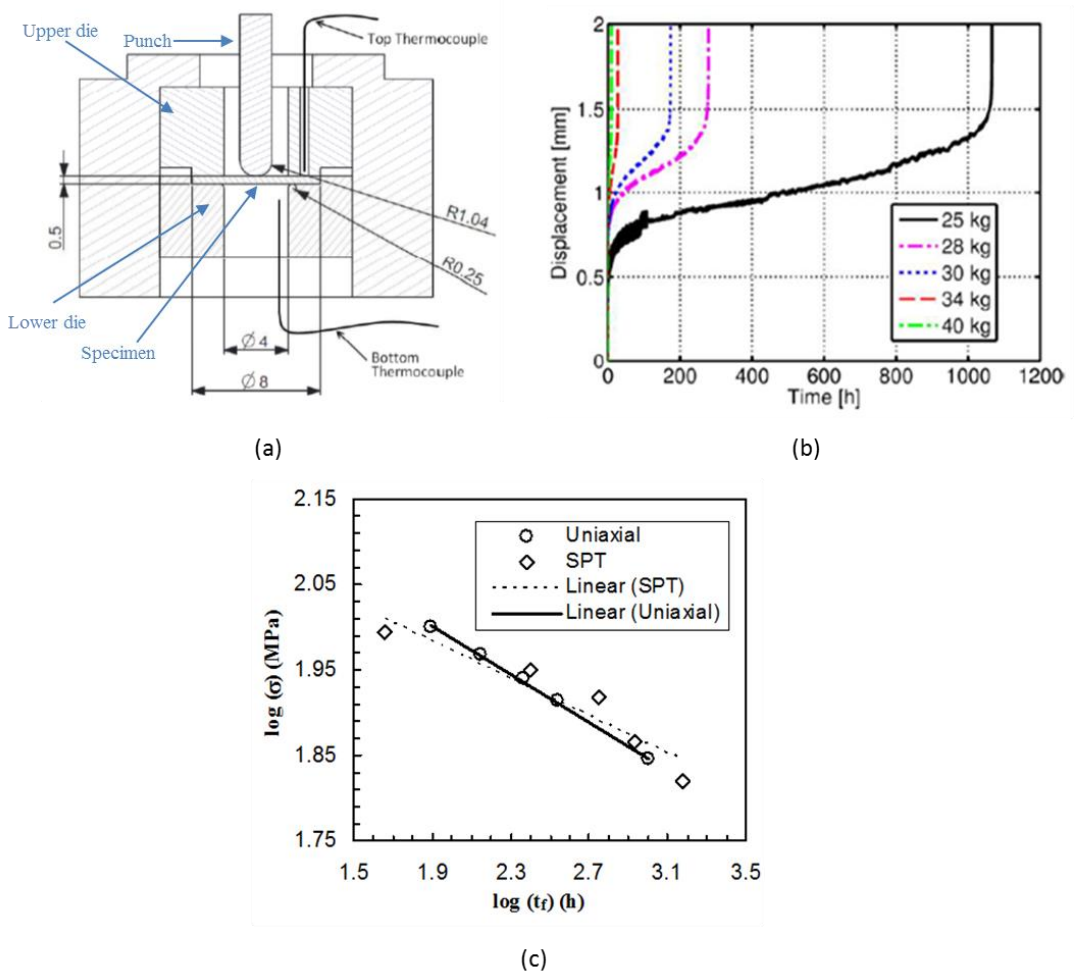


Figure 15. (a) Cross section of a typical experimental set-up used for small punch creep tests with dimensions in [mm], adapted from Ref. [7]; (b) typical small punch creep test data output for a P91 steel at 600 °C, from Ref. [109]; (c) creep rupture data obtained from a SPCT (SPT in the graph) on a P91 steel at 650 °C, compared with corresponding uniaxial data, from Ref. [110].

Typical small punch test consists of applying a constant load to the punch. A displacement versus time curve is obtained by means of a LVDT, as shown in Figure 15-b, and creep rupture data can be collected and compared to corresponding uniaxial data, as presented in Figure 15-c [89]. The test can also be carried out by keeping the deflection rate constant. In this case, a punch load versus punch displacement curve is acquired and material properties of the specimen can be obtained by an inverse method [111, 112].

Figure 16 shows that three regions (indicated by I, II and III in figure) can be identified on the typical displacement, Δ, versus time, *t*, curve of a small punch creep test. The first region, I, is characterized by a decreasing deflection rate; high stresses (even higher than the material yield stress) and strains occur in the specimen in the small area in contact with the punch due to the highly localised contact loading [7,

113]. Thus, the early stage of the test is characterised by local plasticity and initial large deformation of the specimen, which structural behaviour is mainly governed by bending [7, 114]. The transition from the primary to the secondary stage (region II in Figure 16) is due to a change in the specimen shape from a flat disc to a conical sample, and therefore, the governing deformation mode changes from bending to membrane stretching and the deformation rate is approximately at its minimum value [7, 28]. Nucleation of circumferential cracks take place during both primary and secondary stage of the test, meaning that strain hardening and creep recovery are not the only mechanisms involved [7, 115]. Geometric stiffening, dislocation creep, material degradation and crack nucleation and propagation are all involved during these two stages making the small punch specimen behaviour different from the uniaxial creep sample [7].

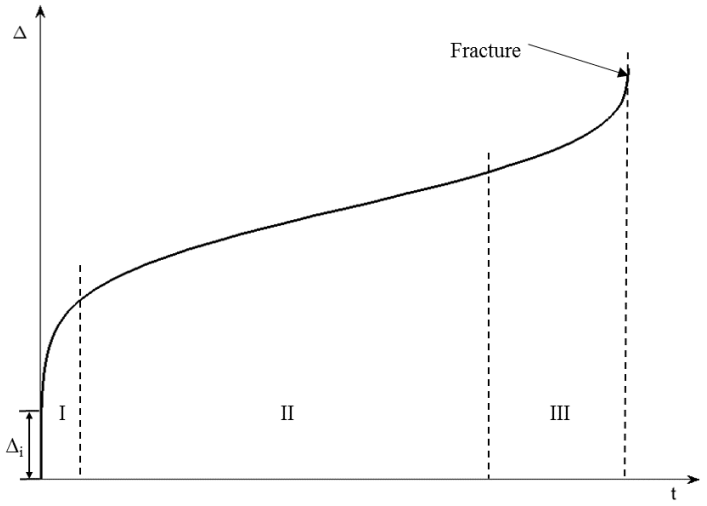


Figure 16. Typical small punch creep test output, adapted from Ref. [90].

The displacement rate increases in the last region (III in Figure 16) of the deformation curve and material deterioration, inter-granular cavitation, macro-cracks propagation in the through-thickness direction, and specimen necking occur until the sample fails [112].

2.4.5 Small ring creep test

The small ring creep test method was designed at the University of Nottingham in 2009. The technique involves diametrically loading in tension of a circular or elliptical ring, as shown in Figure 17-a.

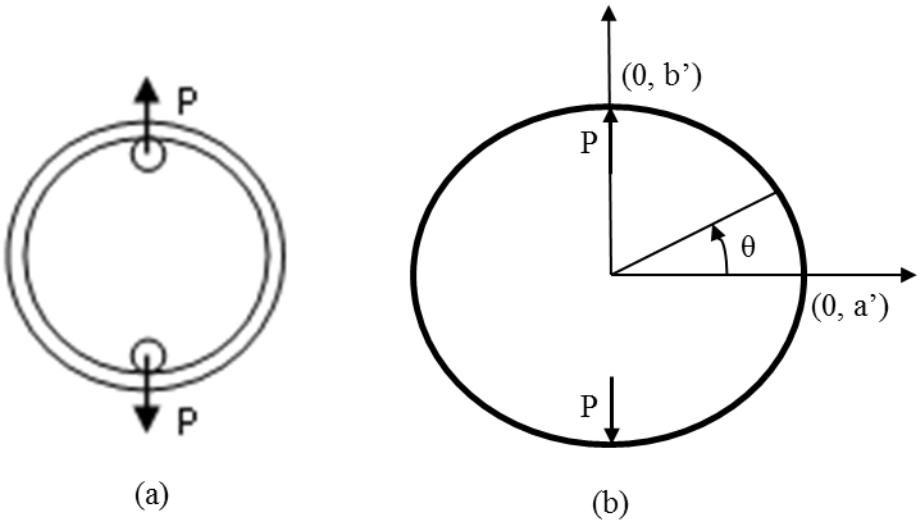


Figure 17. (a) Small ring creep test specimen, adapted from Ref. [103] and **(b)** reference frame of the small ring, adapted from Ref. [27].

The test output is the deformation versus time curve. An analytical solution for the load-line displacement rate of the elliptical ring in the secondary region of the creep curve has been developed at the University of Nottingham by assuming as the main hypotheses the effects of the shear stresses to be negligible, bending as the governing deformation mode, and material obeying Norton's creep law [27]. The solution is given in equation (46), where *a'* and *b'* are the ellipse half-axes and b_0 and *d'* are the thicknesses in the radial and axis directions, respectively, *P* is the applied load, while Int_2 is defined in equation (47), where θ is the angular coordinate of the small ring system, as shown in Figure 17-b, and θ' the value of θ for null bending moment, *M*. If the ring is circular *a'=b'=R,* where *R* is the radius of the ring.

$$\dot{\Delta} = \left(\frac{2n+1}{n}\right)^n Int_2(n, a'/b') \frac{4a'b'}{d'} A' \left(\frac{Pa'}{b_0 d'^2}\right)^2 \tag{46}$$

$$Int_2\left(n,\frac{a'}{b'}\right) = -\int_0^{\theta'}\left\{(cos\theta - cos\theta')^n(1 - cos\theta)\sqrt{\left[\left(\frac{a}{b}\right)^2 sin^2\theta + cos^2\theta\right]}\right\}d\theta + \int_0^{\theta'}\left\{(cos\theta' - cos\theta)^n(1 - cos\theta)\sqrt{\left[\left(\frac{a}{b}\right)^2 sin^2\theta + cos^2\theta\right]}\right\}d\theta \quad (47)$$

The test results for circular (*a'/b'* = 1) and elliptical (*a'/b'*= 2) rings, with *R/d'* = 5, for a P91 steel at 650°C, with a range of equivalent uniaxial stresses, are shown in Figure 18 in terms of displacement, Δ, versus time.

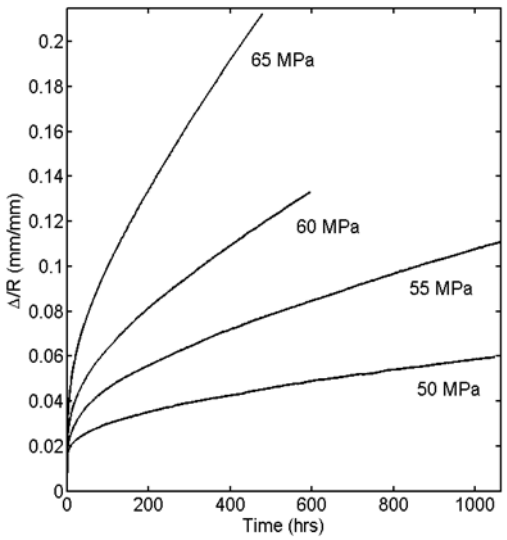


Figure 18. Deformation (Δ/R) versus time curves obtained from circular rings for a P91 steel at 650 °C from Ref. [27].

2.4.6 Small two-bar creep test

Another small specimen experimental technique which has been recently developed at the University of Nottingham by Hyde et al. is the two-bar specimen (TBS) test [36]. Figure 19-a shows the typical test rig, while Figure 19-b shows the typical two-bar specimen, which consists of two relatively slim bars connected by supporting ends. The sample is creep tested by applying a constant load to the

supporting ends by the use of two pins (Figure 19-a). The specimen geometry consists of the initial bar length, L_T, which is the distance between the centres of the loading pins, the length of the loading pins supporting end, k, the specimen thickness, d_T, the diameter of the loading pins, D_T, and the bar width, b_T [36]. Hyde et al. recommended $L_T/b_T = 4.5$, $D_T/(2b_T) = 1.25$, $k/D_T = 1.3$ [36] and a bar length, L_T, of 26 mm, which is larger than the diameter of the small punch creep test specimen recommended in the CEN Code of Practice [5], i.e. 8 mm, and of the impression creep test specimen recommended in ref. [104]. The two-bar creep test allows for the characterisation of the entire creep displacement versus time curve. During the test, the applied stress and temperature do not vary with time. The test output is the displacement versus time curve, characterised by the three typical creep stage regions, as shown in Figure 20-a. A comparison between rupture data of two-bar creep test and uniaxial test is given in Figure 20-b in terms of stress versus time to rupture, t_f.

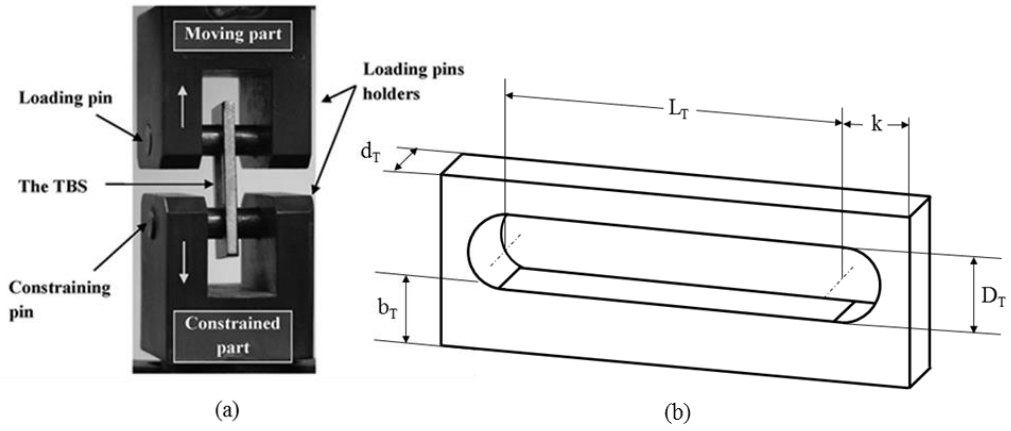


Figure 19. (a) Two-Bar experiment setup and loading application; (b) schematic representation of the Two-Bar specimen, adapted from Ref. [116].

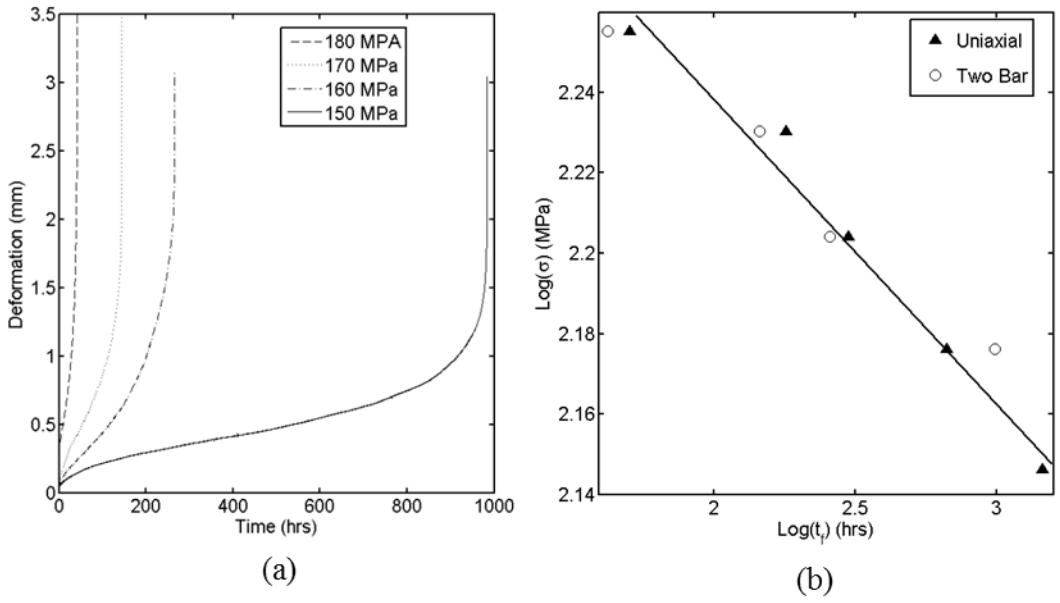


Figure 20. (a) Deformation versus time curves obtained from two bar specimens for a P91 steel at 600 °C and **(b)** creep rupture data from Ref. [117].

During the test, the creep deformation of the specimen is essentially due to stretching under uniaxial stress, as well as the rupture of the bars. Bending occurs in the area of the contact between the sample and the pins, but it has be proven not to have a significant effect on the failure mode and on creep deformation [116]. This behaviour of the specimen is also observed by FE analysis results, as shown in the contour plot presented in Figure 21, where the specimen failure of P91 steel at 600 °C and applied stress of 170 MPa is achieved when the damage variable, ω, approaches unity. Two-bars creep test output is very close to uniaxial creep test output because most of the uniform section is predominantly under a uniaxial state of stress.

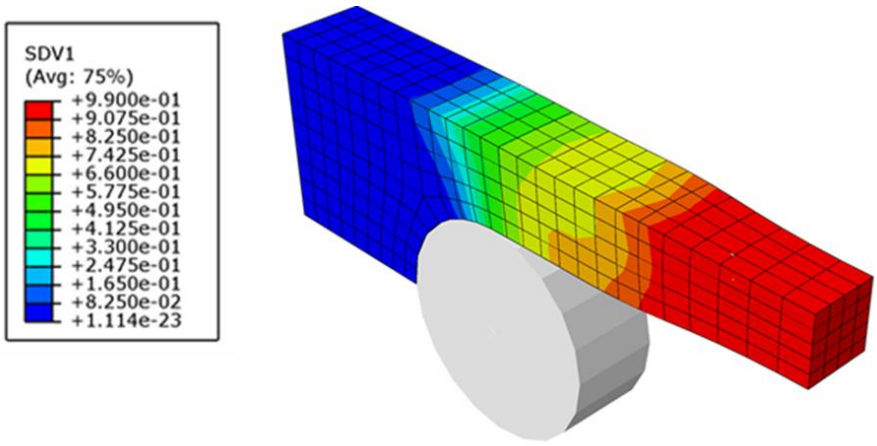


Figure 21. Contour plot of damage parameter, ω, in the TBS for P91 at 600ºC, (σ = 170 MPa, t_f = 169h), from Ref. [36]. Only a quarter of the specimen is modelled due to symmetry.

2.4.7 Data conversion techniques

2.4.7.1 Reference stress method

A major concern in the evaluation of test data of small specimen creep testing techniques is their correlation with uniaxial creep data. The approach currently used for data conversion is the *reference stress method* [2, 10]. For materials obeying the Norton creep law, equation (7) the reference stress method involves calculating two reference parameters, η and β, such that a relationship between the equivalent uniaxial stress, σ_{ref}, and the applied stress, σ, and a relationship between the creep strain rate in the steady-state, $\dot{\varepsilon}^c_{ss}$, and the creep displacement rate obtained by small specimen creep testing techniques, $\dot{\Delta}^c_{ss}$, are established.

$\dot{\Delta}^c_{ss}$ can be expressed as a function of the creep material properties, the dimensions of the specimen and the nominal stress, σ_{nom}, as reported in equation (48).

$$\dot{\Delta}^c_{ss} = f_1(n) f_2(dimensions) B \sigma^n_{nom} \tag{48}$$

The reference parameter η is defined as a material independent, non-dimensional constant such that the ratio $f_1(n)/\eta^n$ is also constant with n. Thus, the equivalent gauge length (EGL) of the structure can be defined as in equation (49). It should be noted that the EGL does not vary with n since none of the terms in equation (49) does.

$$EGL = \frac{f_1(n)}{\eta^n} f_2(dimensions) \tag{49}$$

If l is a characteristic dimension of the sample, for example a length, the reference parameter β can be expressed as in equation (50) and again it should be noted that this constant is independent of n.

$$\beta = \frac{EGL}{l} \tag{50}$$

Finally, equations (51) and (52) represent the sought relationships for $\dot{\Delta}_{ss}^{c}$ and $\dot{\varepsilon}_{ss}^{c}$.

$$\dot{\Delta}_{ss}^{c} = EGL\, B\sigma^{n} = \beta l B\sigma_{nom}^{n} = \beta l B\sigma_{nom}^{n} = \beta l\, \dot{\varepsilon}_{ss}^{c}(\sigma_{ref}) \tag{51}$$

$$\dot{\varepsilon}_{ss}^{c}(\sigma_{ref}) = B\sigma_{ref}^{n}, \qquad \sigma_{ref} = \eta\sigma_{nom} \tag{52}$$

2.4.7.2 Conversion relationships for impression creep test

For the specific case of impression creep testing technique with a rectangular indenter, the nominal stress is the mean indenter pressure, $\bar{p}$ given by the ratio between the applied load, *P*, and the contact area, A_c, as expressed in equation (53), where *b* is the length of the specimen and *d* the width of the indenter. Thus, the reference stress is expressed as in equation (54).

$$\bar{p} = \frac{P}{A_c} = \frac{P}{bd} \tag{53}$$

$$\sigma_{ref} = \eta\bar{p} \tag{54}$$

If the load-line impression displacement in the steady state, Δ_{ss}^{c}, is relatively small, compared to the specimen thickness, the reference stress parameters, η and β, are assumed to be not dependent on the impression depth and the minimum creep strain rate in the steady state is given by equation (55) [104]. The reference parameter β' can be determined by equation (56), where the stress multiplier, α, is chosen arbitrarily (as η is the parameter which is set by minimizing the variation of β' with *n*). η is the value of α such that β' is constant with *n*, thus $\beta'(\eta) = \beta$, as expressed in equation (57) [104]. Hence, the creep displacement rate, $\dot{\Delta}_{ss}^{c}$, needs to be known for different *n* values, e.g. by means of numerical analysis, in order for β to be calculated [104].

$$\dot{\varepsilon}_{ss}^{c} = \frac{\dot{\Delta}_{ss}^{c}}{\beta d} \tag{55}$$

$$\beta' = \frac{\dot{\Delta}_{ss}^{c}}{dB(\alpha\bar{p})^{n}} \tag{56}$$

$$\beta'(\eta) = \beta = \frac{\dot{\Delta}_{ss}^{c}}{dB(\eta\bar{p})^{n}} \tag{57}$$

The conversion parameters, η and β, for an impression creep test can be determined by finite element (FE) analyses for different *n* values. Solutions have been provided by Hyde et al. for a number of *w/d* and *h/d* values by performing several elastic-creep FE analyses [104]. By 2D plane strain FE analysis, for the recommended geometry, "standard size", *w/d* = 10 and *h/d* = 2.5, β has been assessed to be practically constant and equal to 2.051 if $\alpha = \eta = 0.418$, as shown in Figure 22, where $\log(\beta')$ is plotted against *n* [92]. By 3D FE analysis and for the same geometry, β is practically constant and equal to 2.18 if $\alpha = \eta = 0.430$ [104]. The latter are the recommended results in order to avoid errors of up 3% when converting the displacement rate of an impression creep test to the equivalent uniaxial minimum creep strain rate [104].

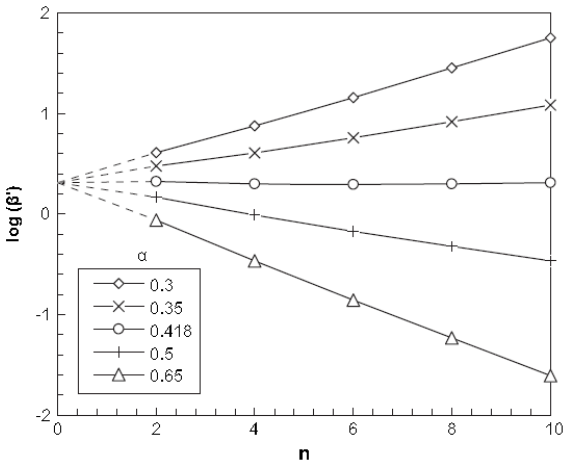


Figure 22. Variation of $\log(\beta')$ with *n*, obtained by 2D FE analysis, adapted from ref. [92].

FE analysis also showed that, for a particular value of *h/d*, above a certain *w/d* value η and β are practically independent of *w/d*. Also, the values of *w/d* over which η is independent of *w/d* vary as *h/d* is varied, as it can be seen from Figure 23 (a) and Figure 23 (b), where η and β are plotted against *w/d* for different values of *h/d*, respectively [104]. Generally, η decreases when *h/d* increases, while β increases when *h/d* increases. When there is shortage of material and lower *w/d* and *h/d* ratios must be used for impression creep test specimens (sub-sized specimens), it is recommended, in order to achieve the highest accuracy, to use the η and β-values for actual *w/d* and *h/d* values [104].

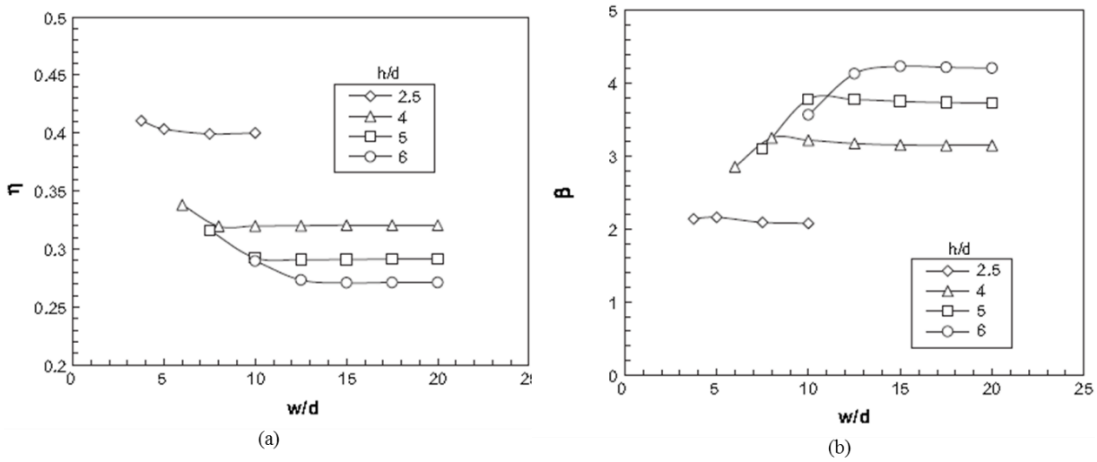


Figure 23. (a) Variation of η with w/d *and* h/d, and **(b)** variation of β with w/d *and* h/d from ref. [104].

Figure 24 presents a comparison between minimum creep strain data obtained by uniaxial creep tests and converted minimum creep strain rate (MSR) data obtained by impression creep tests for 316 stainless steel at 600 °C and 2¼Cr1Mo weld metal at 640 °C samples [105]. Typically, minimum creep strain rates data from impression and unixial creep tests of a given materal lie on the same straigth line, on a log-log scale.

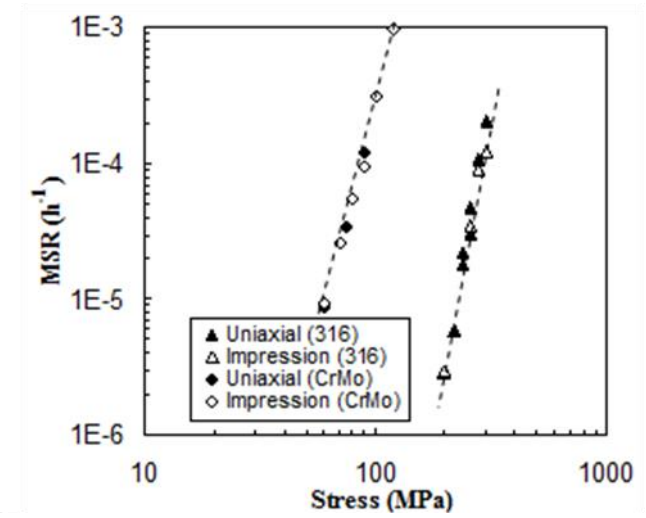


Figure 24. Minimum creep strain rate data for 316 stainless steel at 600 °C and 2¼Cr1Mo weld metal at 640 °C, obtained from uniaxial and impression creep tests, from ref. [105].

A study on sub-sized specimen case has been carried out at the University of Nottingham [105] in order to assess the consistency of data acquired during "sub-sized" impression creep tests with respect to those collected during "standard size" impression creep tests. In particular, the total deformations of the sub-sized specimens

and of the "standard size" specimens have been compared, as well as the minimum creep strain rates obtained by the two set of tests. Figure 25 (a) shows the deformation versus time curves obtained from 10×10×2.5 mm specimens for a P91 steel at 650 ºC, while Figure 25 (b) shows the deformation versus time curves obtained from 6×6×1.5 mm specimens for a P91 steel at 650 ºC [105]. Although a difference in the deformation magnitudes occurs, the minimum creep strain rates obtained by the "sub-sized" impression creep tests by using $\eta = 0.43$ and $\beta = 2.18$, are systematically higher but close to those obtained by "standard" impression creep tests [105]. This can be noted from Figure 26, that plotted the minimum creep strain rates against stress obtained by uniaxial creep tests of the same material at the same test temperature and stresses [105].

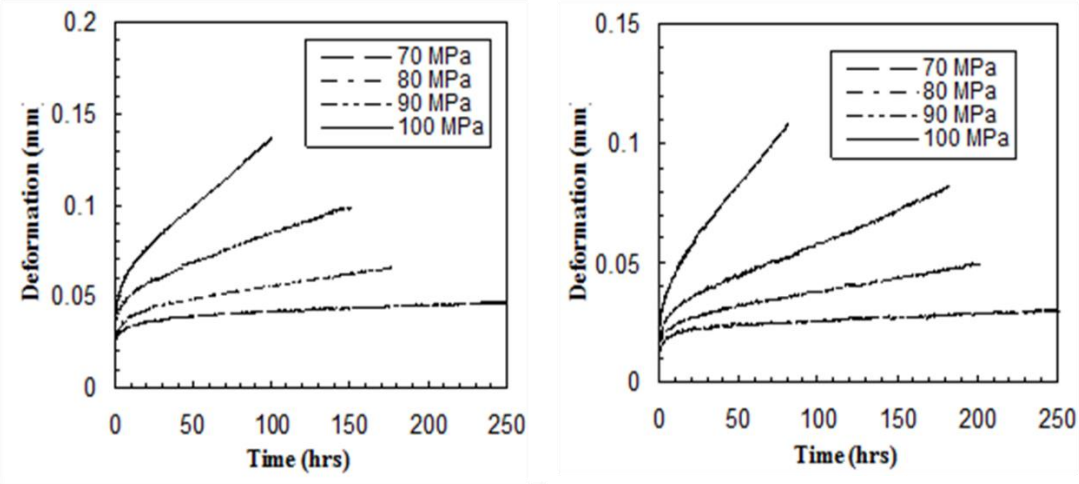


Figure 25. (a) Deformation versus time curves obtained from 10×10×2.5 mm specimens for a P91 steel at 650 °C, and (b) deformation versus time curves obtained from 6×6×1.5 mm specimens for a P91 steel at 650 °C, from ref. [105].

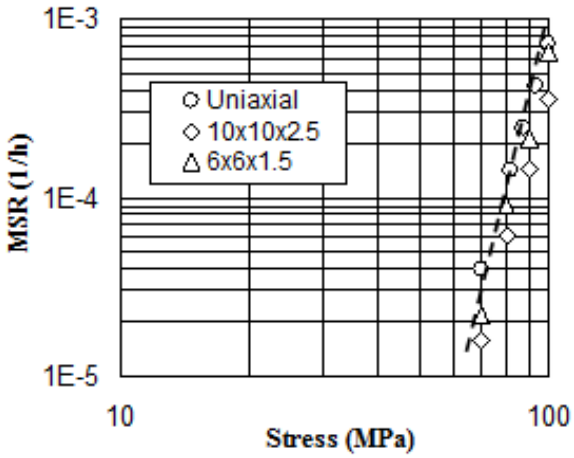


Figure 26. Minimum creep strain rate data for the P91 steel at 650 °C, obtained from impression tests with two sets of specimen dimensions, compared with those obtained from uniaxial creep tests, from ref. [105].

Another work carried out at the University of Nottingham [105] has shown the reliability of impression creep testing technique in determining secondary creep properties when non isothermal and non iso-stress tests are performed. In particular, the results of minimum creep deformation rate corresponding to a number of stress and temperature levels, from a single impression creep test sample, can be obtained by stepped-load and stepped-temperature tests. The former consists of applying an increasing or reducing load when a section of deformation curve has been obtained from the previous step, while the temperature is held constant. The stepped-temperature test, on the other hand, consists in applying a constant load, while the temperature increases or decreases at suitable time intervals.

Figure 27 (a) shows the deformation curves for a 1/2Cr1/2Mo1/4V steel at 565 ^{o}C, obtained from stepped-load impression creep tests [118]. The loading history is important in terms of primary creep component. In fact, when the previous load level is lower, there is primary creep under the new loading; while, when the previous load level is higher, there is no primary creep under the new loading [105]. This does not affect the minimum creep strain rate associated with each region of the presented creep deformation curves. As shown in Figure 27 (b), the minimum creep strain rate data, obtained by stepped-load tests, with η = 0.4003 and β = 2.079 (from earlier 2D FE analysis [92, 119]), and plotted against the applied stress, are in good agreement with the MSRs resultant by uniaxial tests and practically the same as those obtained by impression creep tests with no-loading histories [118]. It should be noted that the tests carried out with previous lower loading histories leads to more accurate MSR data, with respect to tests with previous higher loading histories, when compared to the

corresponding single load tests [105].

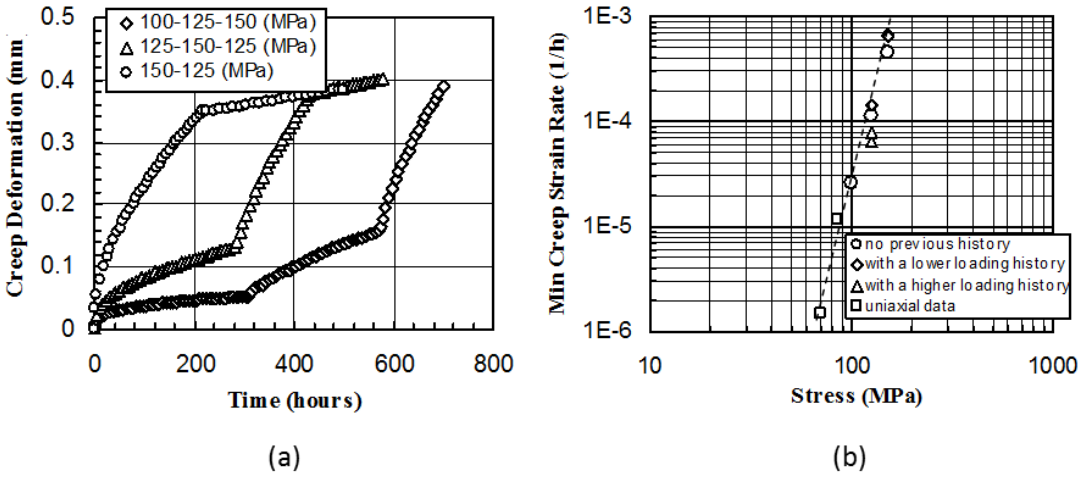


Figure 27. (a) Deformation curves for a 1/2Cr1/2Mo1/4V steel at 565 °C, obtained from stepped-load impression creep tests, from ref. [105], and (b) minimum creep strain rate data for the 1/2Cr1/Mo1/4V steel at 565 °C, obtained from stepped-load impression tests and uniaxial creep tests, from ref. [118].

Figure 28 (a) shows the variation of total impression deformation with time for an ex-service ½CrMoV steam pipe material (MSC9/MT572), subjected to stepped-temperatures, at 40 MPa, while Figure 28 (b) shows the corresponding, converted, MSR data [105]. A comparison with individual temperature test data is needed and, at this stage, only the activation energies can be calculated by using a temperature-dependent Norton's law [105]. The latter is expressed by equation (58), where A' and n' are material constants, T is the temperature in K, R is the gas constant, equal to 2 in this case, and Q_c is the activation energy. The Q_c values in the temperature ranges of 630-655 °C and 655-680 °C are 20082 and 30259 cal/mole, respectively [105].

$$\dot{\varepsilon}_{ss}^{c} = A'\sigma^{n'}\exp[-Q_c/RT] \qquad (58)$$

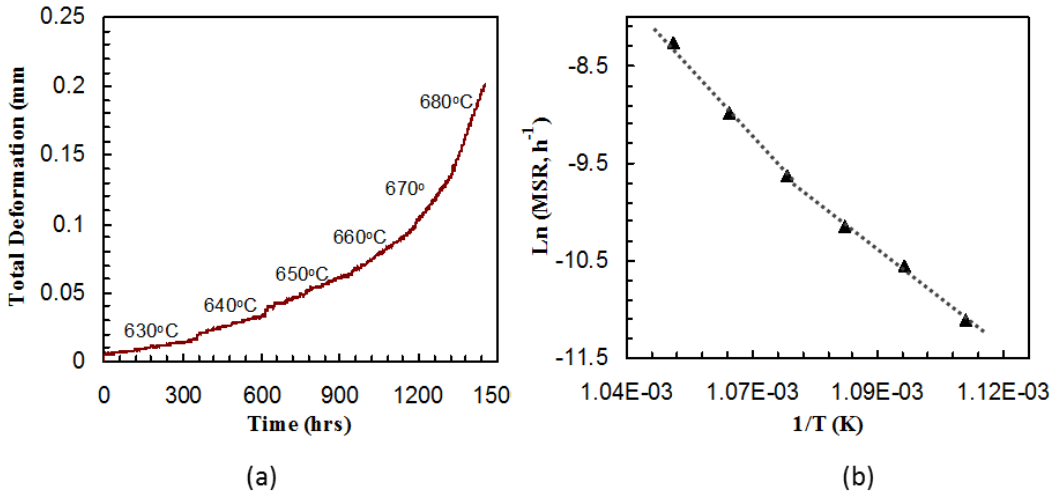


Figure 28. (a) Variation of total impression deformation with time and **(b)** minimum creep strain rates versus 1/T for an ex-service ½CrMoV steam pipe material (MSC9/MT572), subjected to stepped-temperatures, at 40 MPa, from ref. [105].

2.4.7.3 CEN data interpretation technique for small punch creep test

Agreed standards for small specimen creep testing techniques still do not exist, but two codes of practice have been released for small punch creep test by the European committee for standardisation in 2006 [5] and by the standardisation administration of China in 2012 [86, 87]. Efforts in developing a standard draft for the small punch creep test are also ongoing in Japan [120]. In the USA, an ASTM standard test method for small punch testing of ultra-high molecular weight polyethylene used in surgical implants has been released, but does not concern creep testing [121].

The European CEN CWA 15627 Code of Practice [5], last updated in 2007, has been accepted as a first iteration for industrial applications all through the world, even if it is far away from being a recognised standard and certainly needs to be improved [122]. The CEN Code of Practice consists of two parts, Part A is related to specifications for the test rig, test procedure and interpretation of results for small punch test designed for material characterisation [5]. Part B is focused on the test rig, test procedure, test specimen preparation, interpretation of results and methods for deriving the yield strength, the ductile-to-brittle transition temperature (DBTT) and the fracture toughness [5, 122]. Hurst and Matocha published a critical review on the CEN CWA 15627 also suggesting some potential improvements of the code [122]. One of their concerns is related to the shear punch test, which is not included in the code, even if it has been proven to be a reliable technique for the evaluation of tensile

properties [122, 123].

An open problem regarding small punch creep testing is the correlation between the load level applied to the small disc specimen and the stress induced in a conventional uniaxial creep test that exhibits the same time to rupture. Some equations for data interpretation have been proposed in the CEN CWA 15627, but the procedure is still not totally accepted for industrial applications and further investigation on the complex behaviour of the specimen during testing is ongoing [124].

Li and Sturm [5, 125] found a third order polynomial based on Chakrabarty's membrane theory [126] and valid for R_s=1.25 mm and a_p=2 mm (receiving hole radius), which correlates the strain, ε, at the contact boundary between the punch and the disc and the central displacement of the punch, Δ, as shown in equation (59). An empirical relationship between the applied load and the membrane stress, σ_m, is also given in the CEN Code of Practice and is here reported in equation (60) [5]. Equation (59) allows to convert small punch creep data in the corresponding uniaxial data and thus allows the correlation of the two set of data, as shown in Figure 15-c.

$$\varepsilon = 0.17959\Delta + 0.09357\Delta^2 + 0.0044\Delta^3 \quad (59)$$

$$P/\sigma_m = 1.72476\Delta + 0.05638\Delta^2 + 0.17688\Delta^3 \quad (60)$$

These relationships are only valid when bending deformation of the specimen is negligible and thus the deformation mode can be assumed to be governed by membrane stretching. This happens when large deformations are exhibited by the specimen during the test, that is, from an engineering estimation, when Δ>0.8 mm [5]. However, according to many researchers, during small punch creep test the specimen deformation is caused by bending prior to membrane stretching [88, 127, 128].

Another empirical relationship, again derived by Chakrabarty's membrane theory, is reported in an annex of the Code of Practice [5], and can be used to derive the load to be applied for the SPCT, here given in equation (61), where K_{SP} is a correction factor depending on the tested material.

$$P/\sigma_m = 3.33 K_{SP} R_s^{-0.2} a_p^{1.2} t_0 \quad (61)$$

In order to find K_{SP}, at least five small punch creep tests are necessary as well

as a comparison with a conventional creep test [5, 112]. This parameter generally ranges between 1 and 1.5 [129]. An additional difficulty in SPCT data interpretation is the notable variation of the reference parameters due to large deformations involved in the test [112] and, although it is still possible to define η, as in equation (62), in virtue of equation (59) a constant EGL, and thus a constant β, cannot be determined [27].

$$\eta = \frac{0.6\pi}{K_{SP}}\left(\frac{a_p}{R_s}\right)^{0.2} \tag{62}$$

2.4.7.4 Conversion relationships for small ring creep test

By virtue of the reference stress method, the equivalent uniaxial creep stress and the equivalent uniaxial creep strain rate for the load-line deformation rate, $\dot{\Delta}$, of a small ring creep test are given in equations (63) and (64) [27, 91]. For the full mathematical treatment refer to Ref. [27].

$$\sigma_{ref} = \eta \frac{Pa\prime}{b_0 d\prime^2} \tag{63}$$

$$\dot{\varepsilon}^c(\sigma_{ref}) = \frac{d'}{4a'b'\beta}\dot{\Delta} \tag{64}$$

Large deformations involved during the test do not significantly affect the conversion parameter η, the thickness in the radial direction, b_0, and the thickness axis direction, d'; while they affect a', which decreases during the test as well as σ_{ref}; the conversion parameter β also varies with the ratio a'/b' at each instant of time [27, 91]. As a consequence, the creep curve still shows primary and secondary regions, but the latter is characterised by a finite curvature rather than a constant rate [91]. In other words, with this test, a constant strain rate is not quite achieved, but it is still possible to calculate the equivalent uniaxial data by using the method proposed by Hyde et al. [91], which involves calculating the instantaneous values of a'/b', η, β, σref and $\dot{\varepsilon}^c$ at many intervals in the secondary region. The average of the calculated values of σ_{ref} and $\dot{\varepsilon}^c$ can be then assumed to be the equivalent uniaxial data [91]. Converted minimum creep strain rates versus the applied stress are presented in Figure 29.

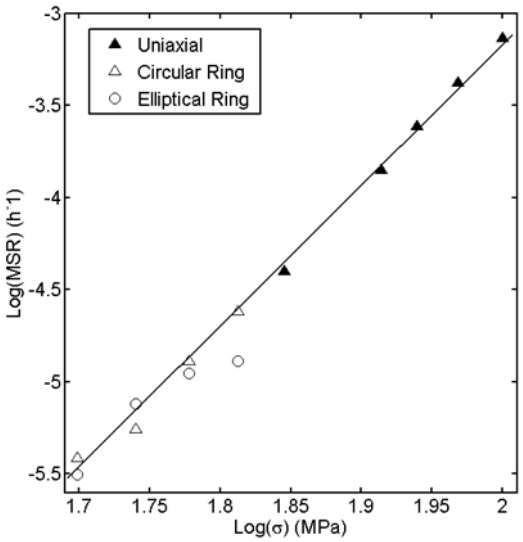


Figure 29. Minimum creep strain rate data for a P91 steel at 650°C obtained from uniaxial and ring tests, from Ref. [27].

It can be observed that the method proposed by Hyde et al. in ref. [91] allows highly accurate secondary creep properties to be obtained, since the small ring data are on the same straight line as the uniaxial data. In order to obtain a better defined steady-state, Hyde et al. are developing a software capable of varying the load during the test according to equation (63) as the specimen shape changes [91].

2.4.7.5 Conversion relationships for small two-bar creep test

The equivalent uniaxial creep stress and the equivalent uniaxial creep strain rate of small two-bar creep test are again defined through the reference stress method and here given in equations (65) and (66), where η and β are determined by FE analyses, as for impression creep test, and their values are 0.9866 and 1.456, respectively [36]. The η value approaches unity because most of the uniform section of the two-bar specimen is predominantly under a uniaxial state of stress. However, those values were obtained by the use of Norton's law, thus the FE analyses could well predict the primary and secondary region of the creep curve, but not the tertiary region. Consequently, further investigation in determination of the reference stress parameters is ongoing [116].

$$\sigma_{ref} = \eta \frac{P}{2b_T d_T} \tag{65}$$

$$\dot{\varepsilon}^c_{ss}(\sigma_{ref}) = \frac{\dot{\Delta}^c_{ss}}{L_T \beta} \tag{66}$$

Converted minimum creep strain rate data from two-bar tests are in good agreement with uniaxial data, as shown in Figure 30-a. Good correlation between uniaxial and two-bar creep test data has also been proved in Ref. [117] and here shown in Figure 30-b.

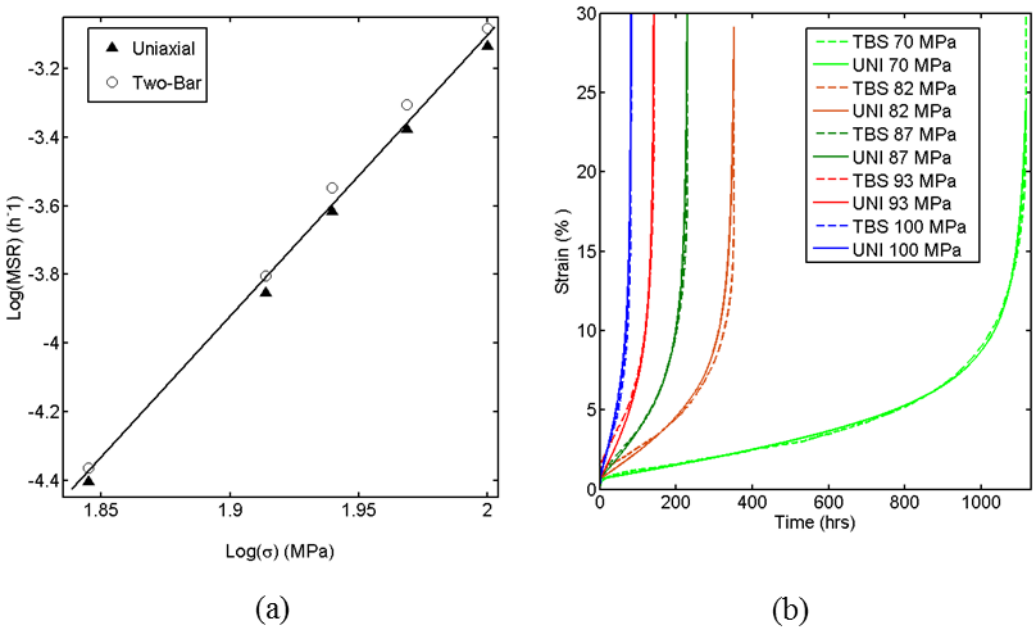


Figure 30. (a) Creep strain rate data obtained from two-bar and uniaxial specimens for a P91 steel at 600 °C, from Ref. [103], and **(b)** fitted uniaxial and converted (by using equation (66)) two-bar strain versus time curves for a P91 steel at 650 °C, from Ref. [117].

2.5 Evaluation of Current Miniature Testing Methods

The selection of a small specimen creep test technique is dictated by factors such as, economics, the type of data required, e.g. creep rupture data or creep strain rate data, material to be tested and the test conditions [110].

In practice, the impression creep test method is easy to perform and it gives accurate output in terms of minimum creep strain rate, particularly at relatively high stresses and in the heat affected zones of welds. This technique appears to be useful in power plant component life assessment [93], and has been deployed in-service to support decisions to continue operation as opposed to undertaking immediate repairs. Despite these advantages, the test has some limitations, e.g. the indenter creep resistance needs to be two or three order higher in magnitude than that of the specimen. Also, tertiary creep behaviour cannot be obtained, because of the compressive stress field in the specimen which does not allow the material to exhibit creep damage [92].

The deformations involved during the test are very small, of the order of μm, requiring very accurate data acquisition and temperature control systems. Furthermore, FE analyses of this test are complicated by the contact interaction between the indenter and the specimen. The same problem is observed in numerical simulations of small punch creep test, where the contact is also non-linear.

The small punch creep test potentially allows the entire characterisation of material behaviour up to failure, because the specimen is taken to rupture; the test can also be used to perform focused analyses on critical locations of operating components. Despite these advantages the interaction of several non-linearities, such as large deformations, large strains, non-linear material behaviour and non-linear contact interactions between the specimen and the punch, induces a complex multi-axial stress field in the specimen which also evolves in time [8, 89, 130, 131]. This affects the SPCT fracture mechanism and introduces several challenges for the identification of a robust correlation to convert SPCT data into respective standard uniaxial creep test data [90, 112]. Another major concern is the non-repeatability of the testing method, since the experimental results depend on the set up geometry [5]. For this reason, a well-established and universally accepted method for data interpretation still does not exist. Difficulties in obtaining good agreement between FE analysis and small punch creep test, in terms of time to failure, are due to the effects of punch load misalignments, to initial plasticity and to approximation of the friction formulation between the specimen and the test machine components used in the FE analyses [90, 94, 127, 132, 133]. FE investigations have shown an increase of the failure life up to 10 times when initial plastic deformation is included in the model [127]; the time to failure can also increase up to 8 times when the friction coefficient between the specimen and the punch varies from 0 to 0.5 [7, 134, 135]. Punch load misalignments can also increase the time to failure by up to 1.49 times, in the worst possible situations [133].

The small ring creep test method is able to provide accurate minimum creep strain rates, especially at relatively low equivalent uniaxial stresses with a unique application of this test type being for creep resistant materials. During the creep test, the small ring specimen is subjected to relatively large deformations, from which relatively small strains are obtained with a lower equivalent stress than that applied to

other miniature specimens. As shown in Figure 18-b, the minimum creep strain rate data obtained from circular and elliptical ring creep test at stresses between 50 and 65 MPa lie on the same straight line as the uniaxial data obtained at higher stresses, between 70 and 100 MPa. The deviation of the elliptical ring data from the straight line is in the range of the typical scatter of creep tests, which is about of 8%. Future development involves the establishment of time-dependent geometric correction functions to compensate for the effects of geometry changes during the deformation process [27, 91].

The small two-bar creep test allows production of full uniaxial creep curves, but further experimental data and validation are necessary. With this technique, the pins must be made of a material characterised by higher creep strength than that of the specimen, therefore there is a limitation in the range of materials which can be potentially tested. In the case of testing high creep strength materials, e.g. Nickel based super-alloys for turbine blades, using the two-bar specimen, careful consideration of the specimen design should be given. Relatively larger diameter pins and smaller cross-sectional areas of the test sections of the two-bar specimen should be adopted to reduce the mean contact stresses between the pins and the specimen. In such a case, the material for the pins can be chosen to have a similar creep strength as that of the test material. The contact between the pins and the specimen induces a bending deformation in the extreme regions of the specimen, while the stress distribution in the bars is almost constant [116]. In view of this feature, the reference stress parameters for this specimen type are almost one, as the stress field in the effective section of the structure is considerably similar to that found in conventional uniaxial creep test specimen. Furthermore, the specimen is taken to failure, therefore contrary to the impression creep and the small ring creep tests, the tertiary creep region of the material can be characterised and the failure behaviour identified.

In conclusion, good agreement between small specimen creep data and uniaxial creep data have been obtained with all of the techniques described so far, particularly with good correlation against minimum creep strain rates. Both small punch and small two-bar creep tests are able to predict the specimen failure life, but difficulties in data interpretation of small punch data have not been overcome yet, while, methods for data interpretation of the two-bar test are still under investigation,

even though this test has already been validated for steel materials and a nickel-based super-alloy material. Impression and small ring creep tests are both suitable for the determination of the steady-state creep properties. The noise in the impression creep test output can be of the same order of the output itself, since very small deformation occurs during the test. An opposite problem has been observed for the small ring creep test, during which the specimen shape varies, causing the reference stress to change as well. As a final consideration, small specimen creep testing techniques look very promising for determining creep properties and providing information about failure, even though further experimental and numerical investigations are needed.

2.6 APPLICATION OF SMALL SPECIMEN CREEP TESTING TECHNIQUES

Small specimen creep testing techniques are currently applied for ranking the strength of power plant components, in order to establish repair strategies and supporting life assessment. They are also used in nuclear applications and for fatigue life evaluation [20].

2.6.1 Strength ranking

Power plant materials age during high temperature service and periodic structural integrity assessments are needed to quantify their permissible service life. Implementing an inspection priority for welds that are subject to in-service creep damage and fatigue cracking is standard practice, with suitable inspection and repair methods being readily available to the utility [20].

However, identifying a suitable and cost-effective inspection priority for ageing parent material is of concern due to the extensive amount of material that may be affected, and the difficulty in identifying the optimum locations and inspection sampling regime required [20]. In fact, in order to take out enough material for uniaxial creep testing, power plant components have to be removed from service and large sections have to be cut out, requiring weld repair to return to service. This not only implies large costs for the utilities, but also introduces more weak regions in the components, such as Type IV regions (see section 2.2.2). However, weld locations are always known, allowing for inspections, repairs or replacements as required, while it is generally unknown what part of the parent material has accumulated more creep damage. For this reason, inspection usually starts from critical zones of the parent

material, like for example pipe bending, where stress concentrates.

2.6.2 Decision on improved inspection, replacement and repair strategy

In the open literature, many examples of plant component strength ranking have been considered in case studies [84, 100, 101]. In the 1990's, RWE npower carried out impression creep and small punch tests on scoop samples from two Grade 91 headers which were considered close to premature Type IV weld failures. As a reference material, a weak Grade 91 bar section was creep tested by using both small specimen and standard testing methods. By plotting the impression creep strain rates obtained from the headers samples against the strain rate of the reference material, it was found that the creep strength was similar for both materials, as shown in Figure 31. In the same plot were also reported the strain rates for a prematurely failed endplate and two other samples taken from plant items with no known problems. Cross-weld specimens were also creep tested from the reference material, specifically welded, in order to acquire Type IV data. The test results led to an early inspection of the headers, one of which was found to be widely cracked, while the other header cracked a few years later. Hence, deployment of the non-conventional small specimen creep testing methods avoided costly failure in service and associated unplanned outage time and allowed life extension of the headers [101, 136].

Other tests were carried out by RWE npower by sampling main steam pipework components with the intention to identify the damage at an early stage, the results of which are plotted in Figure 32 that shows impression creep strength ranking for CMV. The ISO lower bound line intersects a sample which parallel conventional uniaxial testing has shown possesses a strength equivalent to the lower bound (mean-20%) ISO value for this material in the as-received condition [84, 136]. By testing a significant number of ex-service CMV samples an empirical correction factor was found as well, in order to compare components of very different plant ages. The histogram in Figure 33, shows the CMV data corrected for operating hours at the time of sampling to reflect strength at the start of life, is helpful in placing any other CMV sample within the creep strength scatter band [136]. Although small specimen testing techniques have been proved to be extremely useful in the creep strength ranking, their standardization is still required and the effects of the scoop sampling on the creep response of components still needs to be investigated [136].

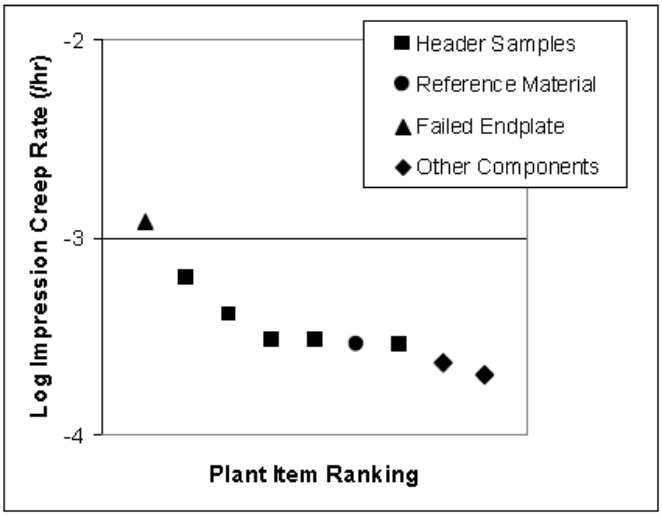


Figure 31. Impression creep strain rates of plant items ranked in order of decreasing MSR, obtained from samples from the suspect header compared to a sample from a weak failed endplate and samples from other components, from Ref. [136].

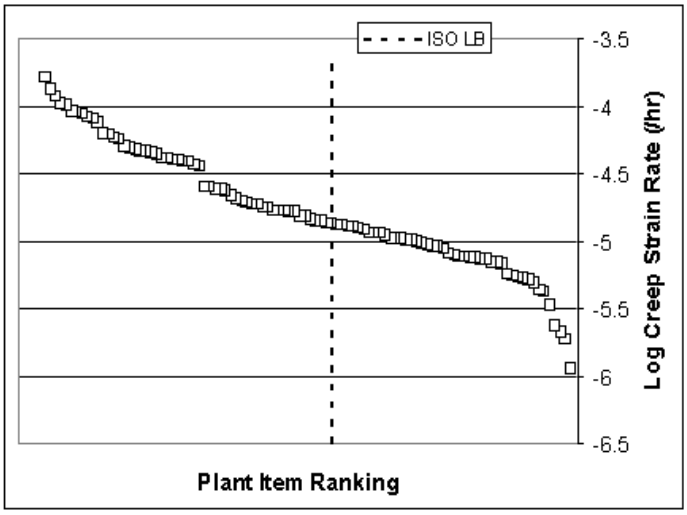


Figure 32. Impression creep strength ranking plot for CMV as-sampled, from Ref. [136].

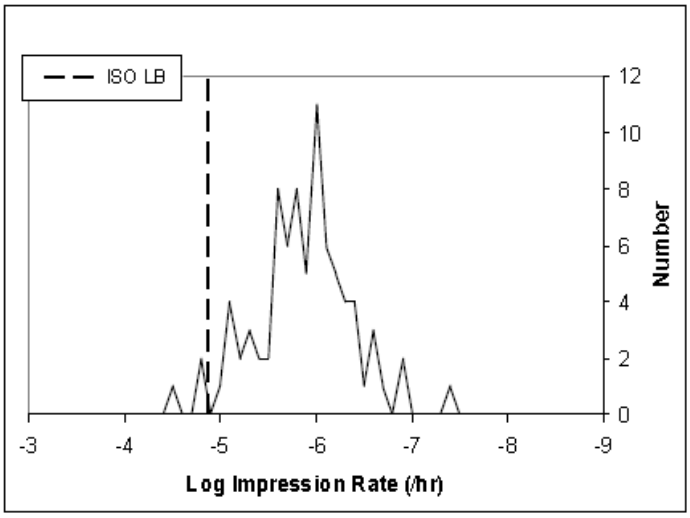


Figure 33. Histogram showing the CMV data, corrected for operating hours at the time of sampling to reflect strength at the start of life, from Ref. [136].

2.6.3 Small specimen creep data correlated with hardness data for life assessment

The research into the correlation between room temperature hardness data and time temperature parameters has been ongoing since 1943 [71, 72], but no physical link nor any explicit relationship between them has been found. Many researchers have related creep life evaluation and hardness data through the Larson-Miller parameter, but this approach only allows a first assessment of the damage if the initial hardness, at a time of 0 hours of creep, is known [63, 64, 76-81]. Unfortunately, it is very rare for a station to have record of this initial hardness data and as a consequence, the method is suitable only to provide an initial idea of the component damage. Currently, hardness data continues to be routinely collected during plant outages because of the simplicity of the test method and the potential to provide an indication of the condition of the material in contrast to the evaluation of the minimum creep strain rate, but more research is needed to evaluate the benefits.

Creep and hardness data are not correlated by any mechanical model because of the different parameters they are related to, since creep life is a function of the operating temperature and stress, while hardness, after prolonged service, is mostly related to the thermal aging at the operating temperature [93]. Nevertheless, Brett [99] found that by plotting the variations of minimum creep strain rates obtained by both uniaxial and impression creep tests at 600 °C and at a stress of 155 MPa, against room temperature hardness for Grade P91 steels (with different service histories) the

samples with the lowest minimum creep strain rates have the highest hardness (Figure 34-a). Brett [99] also plotted the time to failure against the hardness (Figure 34-b), and found that the samples with the highest hardness have the longest time to failure as well, where the time to failure for the impression test samples were calculated by using the Monkman–Grant relationship [79, 93]. Hence material hardness data, which is routinely captured on ageing materials during statutory outages, is a characterising parameter that should be further researched in order to establish if it could be more deeply integrated into a life prediction model [20]. The variability associated with site acquired hardness data should be considered in such research [20].

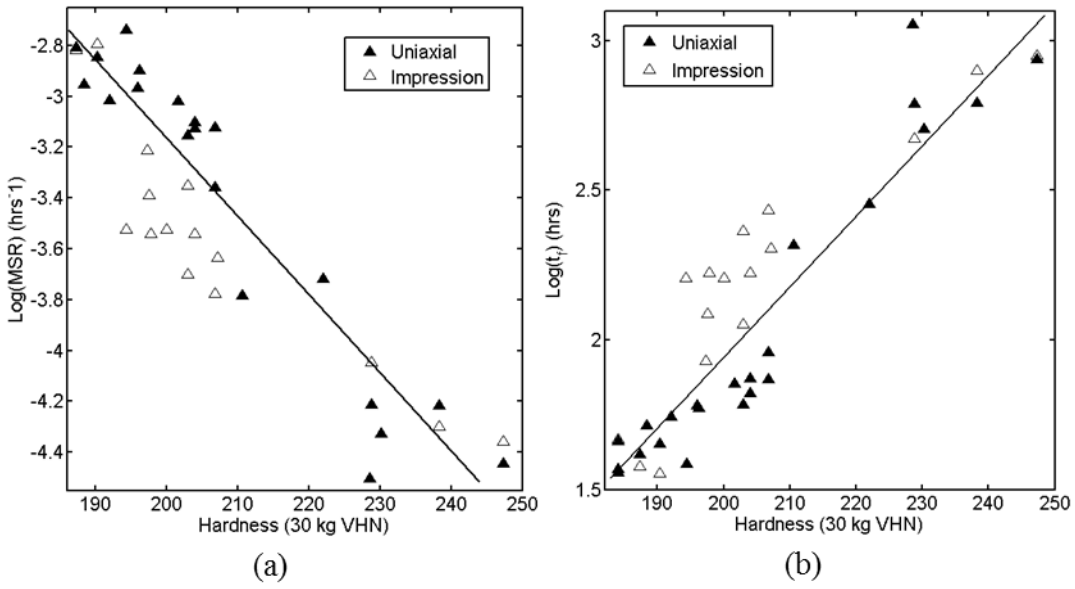


Figure 34. (a) Variations of minimum creep strain rates at 600°C and at a stress of 155MPa, with room temperature hardness for Grade P91 steels (with different service histories) from ref. [99], and (b) variations of uniaxial rupture life, t_f, at 600 °C and at a stress of 155MPa, with room temperature hardness for Grade P91 steels (with different service histories), from ref. [99].

2.6.4 Application for irradiated materials

Understanding the effects of neutron irradiation on the performance of materials used in the construction of nuclear power stations is a challenge when considering the requirements for life extension of existing reactor designs and future advanced fusion reactor technologies [20]. The use of small specimen testing to characterise materials behaviour has many advantages in this respect due to the small volumes of irradiated material required. The ASTM symposium [137] in 1983 provided an initial milestone for the development of these methods for irradiated specimens. This highlighted some of the important considerations that have influenced

the development of the testing methods, such as limited space in hot test cells, the effect of neutron fluence gradients across the reactor components, personnel dose levels in post-irradiation testing and the development of materials suitable for use in high energy (~ 14 MeV) nuclear fusion reactors [20].

Currently the small punch (SP) testing technique has gained an important role for monitoring nuclear power plant operation and critical areas, such as the heat affect zone of welds. In particular, the material state of all Slovak reactor pressure vessels is monitored through SP testing (several thousand material samples) as part of the advanced surveillance specimen programs, which aims to extend the reactor pressure vessels life in the WWER-440 pressurised light water reactors by at least 20 years [138, 139], with typical operating conditions at 297°C and 123bar [140]. The focus of this surveillance program is to provide a through life assessment of the tensile strength and ductile-brittle transition temperature at various locations within the reactor, with material extracted using the Rolls-Royce SSamTM-2 device with comparison against reference material blocks [20]. Sampling locations are defined with care so that there is no requirement for subsequent repair or monitoring [20].

Some of the small specimens have been irradiated in the Halden research reactor at a fluence of 4.02 x 1023 n/m2 [138], which showed an expected increase in the tensile and yield stress properties. Comparisons between the fracture appearance transition temperature (FATT) values obtained from the SP tests and standard charpy tests provided good agreement between material in the initial state and the irradiated condition. This application of SP testing provides the Slovak regulatory authorities with contemporary information on the change in material properties due to in-service operation and irradiation levels [20].

This application of SP testing is similar to the use of impression creep testing applied to ageing conventional power plant materials subject to thermal creep by Brett et al. [84, 99-101]. Importantly the examples provided by these investigators show practical examples of the techniques use to assess the condition of operating plant, driven by regulatory and safety requirements [20].

Hyde at al. [28] produced a comprehensive review of the use of miniature specimen testing for mechanical and creep material properties. This importantly

concluded that viable test methods exist; however there is no single specimen design that can cater for all data requirements. It is evident that commercial objectives have driven the development of some of these techniques, such as SP and impression creep and on specific materials of interest on operating plant, such as CMV and P91 steels on conventional stations [20]. Hyde's [28] review provided a perspective on future requirements and emphasised the need for greater standardisation of experimental test methods [20].

Small specimen testing is perceived as a key approach for obtaining critical information on the mechanical properties, deformation and fracture behaviour of candidate materials in support of the ongoing design and development of fusion reactors. The challenges associated with the development of the international fusion materials irradiation facility (IFMIF) to test reactor materials at high fluxes of 14MeV and temperatures in the range 250-550 °C, is described by Knaster et al. [141]. This test facility is expected to be ready and available to use within 10 years from project approval and is constrained for test volumes of up to 500 cm^3. A range of small specimens have been irradiated as part of the engineering validation and engineering design activities (EVEDA) phase, with subsequent tests related to tensile data, fracture toughness, creep and fatigue crack growth, thereby demonstrating the practical set-up of the irradiation capsules. However, one of the major challenges cited by Knaster et al. to overcome is ensuring adequate validation of the derived irradiated properties to the regulatory bodies. This again emphasises the need for accepted standards and codes of practice for all the deployed small specimen test methods and in readiness for the high flux IFMIF facility once constructed. The further validation of these test methods on ageing materials on operational nuclear or conventional stations will certainly support this objective.

Lucas et al. [142] provides some examples of the developments required related to improve understanding of the fracture, fatigue and deformation behaviour. Fracture toughness tests on a range of specimen sizes on candidate reduced activation ferritic-martensitic EUROFER97 steel are described, with the use of correction factors derived with finite element simulations of crack tip stress fields to address specimen size effects. These tests show the requirement for close scrutiny of the mechanics of the testing process coupled to the observed material behaviour. Knaster et al. [141]

emphasised the ultimate requirement for validation of material properties derived from small specimen tests in support of the design of fusion reactors. The challenge is to establish material behaviour models that use the measured parameters and observed behaviour of the materials tested; a mechanistic modelling approach. These material behaviour models must be demonstrably scalable to account for the size of the reactor components and expected in-service loading due to neutron fluence gradients, thermal gradients and environmental factors such as the presence of helium produced by the fusion process, which will influence the fracture behaviour [142].

Reduced activation ferritic martensitic steels such as F82H are candidates for use in fusion reactors [143] and have been developed from modified 9Cr-1Mo steels (by replacing Mo and Nb with W and Ta), which are used extensively in modern conventional power stations. In 2014, Bruchhausen et al. [144] assessed the behaviour of ferritic-martensitic oxide dispersion steels by use of SP testing at 650°C complemented by uniaxial creep tests. Importantly the SP tests were conducted in accordance with the current CEN SPCT Code of Practice [5]. The SP failed specimens were extracted from a material block in the transverse and longitudinal directions and the micrographs of the failed specimens exhibited very different crack patterns, which are indicative of the anisotropic alloy microstructure.

The evident strong anisotropy is considered due to scatter in the steady state creep response and influenced by the biaxial stress field active in the SP test and variability in the alloy's microstructure, which was also evident from other uniaxial creep tests on conventional specimens. These results illustrate again the requirement for comprehensive modelling-simulation studies of the SP and other small specimen tests in order to inform the relevant Code of Practice. It is important to adapt this integrated test-modelling approach to the situation of in-service components and the inevitable regulatory requirement to demonstrate fitness-for-service in a production reactor. The requirement for integrated small specimen experimental designs to provide fundamental material behaviour models is reiterated in Odette et al.'s review on innovations in small specimen testing [145].

One of the challenges of demonstrating the validity of selected materials used in a production fusion reactor is to account for the effects of the neutron fluence and thermal gradients in the structural components. Gilbert et al. [146] have reviewed

some of the factors influencing material behaviour such as neutron flux gradients, component size and helium production on the design of a proposed demonstration fusion power plant (DEMO). The study shows an expected spatial variation of the neutron flux across various structural components, which is also evident in other reactor designs associated with naval pressurised water reactors. For these naval reactor designs the through life effects on material behaviour due to the spatial variation in irradiation creep and swelling is accounted for by measuring the deformation of representative fuel coupons irradiated in research reactors, supplemented by measurements of end of life fuel deformation of spent reactor fuel modules. These experiences with the effects of spatial variation of neutron flux in naval reactors, coupled with the very high energy levels expected in production fusion reactors only further emphasise the need for standardised small specimen test codes of practice.

On conventional power plant an analogy can be made with the change to flexible operation in the 1990's [20]. This resulted in large periodic thermal stress gradients acting across thick-sectioned components, resulting in critical integrity problems [35]. The older conventional stations are still suffering from the effects of this type of operation, which coupled with the long running hours has driven the development and field application of small specimen testing methods [20].

2.6.5 Fracture

Understanding the long-term fracture behaviour is critical to ensure the integrity of irradiated structures. The SP testing technique has undeniable advantages due to the small irradiated specimen volume and availability of a recognised Code of Practice [5]. Material properties of the heat affected zone of welds, and the ductile-to-brittle transition temperature (DBTT) can be determined by the use of the SP testing technique [138, 147].

SP testing technique was first used by Baik et al. in 1983, who evaluated the DBTT of a Ni-Cr steel and established a linear relationship between small punch and standard Charpy V-Notch test results in terms of DBTT [148, 149]. Mao and Kameda, by observing SP test data, found that neutron irradiation significantly increases the DBTT in Fe based alloys doped with Cu [150], while Wakai et al. proved that the

production of helium can cause the shift of DBTT in F82H steels [151].

According to Kasada et al. [152], the master curve (MC) methodology, developed by the American Society for Testing and Materials [153], has been successfully used by employing small specimens in the assessment of the drop in fracture toughness caused by neutron irradiation. More recently, Martínez-Pañeda et al. have proposed a novel methodology which involves a notched small punch specimen for the evaluation of the fracture toughness [154]. In particular, they determined a linear relationship between the notch mouth opening displacement and the vertical displacement of the SP, and a critical value of the notch mouth opening displacement of the SP, that can be compared with the corresponding parameter in conventional fracture tests [154].

2.6.6 Other applications

There are a variety of other applications to note such as, screening of materials, assessment of hydrogen embrittlement, supporting fatigue studies and investigating very high temperature performance of materials such as single crystal alloys used in gas turbine applications. These are all derivatives of the methods discussed previously and are discussed briefly in this section.

One of the other aspects to note in this review is that many of these small specimen tests require the development of novel measurement techniques due to factors such as specimen size and geometry, requirements for hot cells in nuclear applications or for testing in combustion atmospheres for conventional plant applications. These may present requirements for the use of full-field optical based non-contact measurement systems such as digital image correlation, infra-red thermography, laser extensometry etc [20].

In 2013, Methew et al. [155] demonstrated the benefits of using the SP techniques to rapidly investigate the creep performance of 316LN stainless steel with different nitrogen content levels, using the technique as a means of differentiating the creep rupture performance between alloy heats. Although the SP technique provides the ability to undertake multiple tests quickly the study emphasised the potential for shortfalls due to the short duration of the tests, typically < 1000 hours and the inability to assess effects due to longer-term thermal ageing and environmental factors.

Hydrogen embrittlement of steels is a particular concern for materials employed in hydrogen-powered vehicles and offshore platforms, as well as in power plant components [156, 157]. Furthermore, hydrogen can be added to materials during the manufacturing process [158]. Therefore, investigating the effects of hydrogen embrittlement is of great interest. One of the latest studies on this matter has been conducted by García et al., who investigated the effects of hydrogen embrittlement on the tensile properties of three different CMV steels (parent material, welding, and heat treated welding) through small punch tests [159]. They found that the yield strength of the steels can be assessed by the SP test yield load and that the technique is able to evaluate the degradation of the material tensile properties due to the hydrogen environment.

Fatigue studies are crucial in many engineering fields and especially in the design of nuclear reactors because of the temperature and neutron flux cycles they are subjected to [160, 161].

Hirose et al. [160] and Nogami et al. [161] for example describes the development of small-scale fatigue specimens, with a specimen gauge diameter of 1.25 mm for testing reduced activation ferritic-martensitic steels in nuclear applications. These cyclic load test present challenges for test machine alignment, load control and measurement of extension, especially for applications to irradiated specimens in a hot cell. Validation of these small-scale fatigue tests for full-size components is a challenge, due regard to the potential in-service load cycles (strain range and hold periods) and operating environment is required as well as the impact of thermal or environmental ageing that might be expected to occur in an operating reactor. It is envisaged that such small-scale tests will be invaluable as a means of assessing for example the performance not only of the base material but also the welding fabrication process and therefore reducing the overall time and cost to develop a material that is fit for purpose. Therefore the development of new testing methods using small specimens is of great interest in current research [160-163].

Roebuck et al. [164] have developed a novel miniature specimen testing facility use for assessing the high temperature properties of Ni-base superalloys such as CMSX-4 used in the manufacture of gas turbine hot gas path components. This facility operates at temperatures above 1000°C, includes water cooled grips and has

been used to investigate flow stress dependence on strain and temperature, resistivity measurements, oxidation, pyrometry measurements and recrystallisation kinetics. The test facility also comprises an environmental chamber and is equipped to apply high heating and cooling rates and variable thermo-mechanical loads. Single crystal superalloys such as CMSX-4 are subject to very arduous operating conditions in an operational gas turbine engine and often manufactured in relatively thin sections, hence the need for miniature specimens and suitable test facilities to determine properties and characterise their behaviour.

2.7 CHALLENGES AND RESEARCH GAPS

As aforementioned in section 2.2.5, developing an integrated model for conventional plant applications is an open problem. A new assessment framework will need to illustrate how small specimen testing should be used in conjunction with data acquired from existing inspection procedures, such as hardness measurements, along with material or component behaviour models that utilise in-service operational data, such as hardness measurements.

Hardness data is routinely acquired during periodic inspections of ageing conventional plant and is usually interpreted in conjunction with metallurgical evaluation by creep replicas. There are some material models in use on conventional plant that couple surface hardness data with the Von Mises stress to evaluate time to creep rupture. These models typically are used to supplement safety case assessments on operating plant and hence are necessarily used in conjunction with several other methods, e.g. those described in section 2.2.4. Nonetheless, it is evident that such hardness models may be able to be further developed to a position where a practical forward-looking lifing model can be routinely implemented on operational plant. Therefore, one of the goals of the present thesis is the development of an integrated lifing model that takes into account both creep data from impression creep tests and hardness data.

It is clear that the current approach for the evaluation of life consumption is based on experimental knowledge and on a limited use of analytical methods. This holistic condition assessment process is based on the described off-load and on-load condition monitoring, but does not undertake predictive life assessments beyond the

next major statutory outage, and does not seek to integrate the various disparate data sets obtained from the plant outage and/or on-load monitoring. Miniature specimen creep testing techniques could be successfully used together with the currently used condition assessment methods in order to provide a more predictive life assessment approach. Thus, part of this thesis is dedicated to the investigation of the through thickness behaviour of a 31-year-aged 0.5CrMoV (CMV) pipe section carried out by means of hardness data collection, optical and SEM micrographs, impression creep tests and surface replicas for creep cavity count in order to seek for a possible correlation between disparate methods and gathered data.

In order to include small specimen testing techniques in a new holistic approach, the reliability of these methods becomes of major concern. Therefore, one of the aim of the present work is to assess the consistency of impression creep testing technique, with particular attention to the conversion parameters established so far. Also, many researchers [88, 127, 128] stated, but did not demonstrate, that during small punch creep test the specimen deformation is caused by bending prior to membrane stretching even when large deformations take place, making Chakrabarty's membrane stretching theory not always applicable for interpretation of small punch creep test data. Therefore, demonstration of that hypothesis and establishment of new ranges of applicability of Chakrabarty's theory are open problems covered by this thesis. Another major concern is the non-repeatability of the small punch creep testing method, since the experimental results depend on the set up geometry [5]. For this reason, a well-established and universally accepted method for data interpretation still does not exist.

In conclusion, the aims of this work are as per follow:

- to develop a new holistic condition assessment that includes miniature specimen creep testing data;
- to develop a novel lifing method based on hardness and impression creep testing data;
- to assess the reliability of impression creep test;
- to seek for a possible correlation between data obtained by well-established

methods, e.g. replica creep cavity count, hardness measurements, micrographs, etc., and data obtained by miniature specimen creep testing data;

- to investigate small punch specimen behaviour for possible improvements of the CEN Code of Practice.

3 DEVELOPMENT OF A NEW APPROACH THROUGH MINIATURE SPECIMEN CREEP TESTING TECHNIQUES AND HARDNESS TESTS FOR LIFE ASSESSMENT OF POWER PLANT MATERIALS

3.1 INTRODUCTION

The main objective of the power station is to maximise plant availability and profitability, whilst maintaining safety. In order to achieve this objective the station must be able to understand, with good certainty, the remaining life of the assets at any time during the operation of the asset so that it can cost-effectively plan future inspections, refurbishments and replacements as required. This requirement to understand with certainty the remaining life becomes ever more acute in commercial electricity generation where the profitability may be marginal, whether caused by government or environmental policy, market prices, taxation or other factors. From a technical perspective the current approach to define a 'holistic' view of the condition of the generating assets is achieved by the assimilation and deductive assessment of information gleaned from the activities described in the previous Chapter (see section 2.2.4). The process is strongly dependent on the experience of the assessment engineers, who ideally will also have conducted similar investigations on other generating plant (likely of different age and condition).

Hence, the current approach is considered to be 'inspection based' and usually results in an incremental increase to future inspection sample size to contain a perceived emerging threat. The current approach is captured in Figure 35. However, the current 'holistic' condition assessment process does not provide a predictive life assessment beyond the next major statutory outage, neither does it actively integrate the various disparate data sets obtained from the plant outage or from on-load monitoring. Figure 35 seeks to illustrate two significant missing activities, namely 1) miniature specimen testing and 2) on-load condition assessment, which could be exploited to embed a more predictive life assessment approach and thereby satisfy the main objectives of the plant owner.

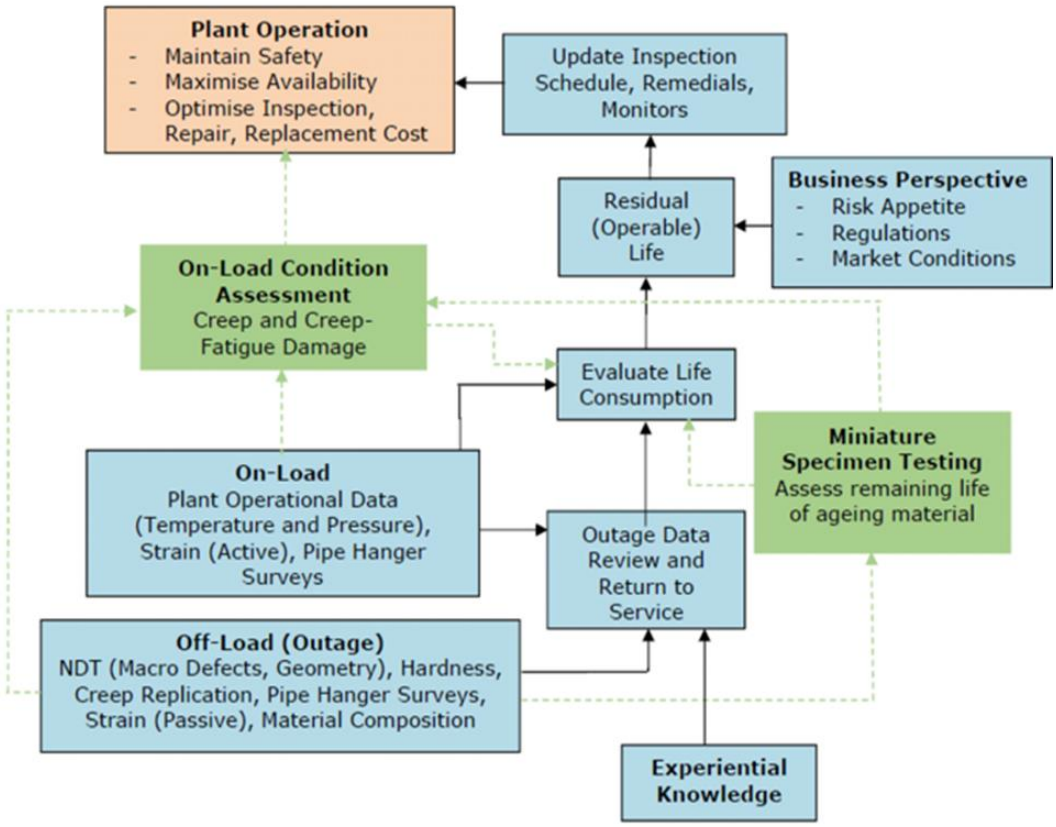


Figure 35. High temperature plant conditon assessment (dotted line represent aspects of data analysis/methods that are not fully utilised. Solid lines represent the current and well established IBA approach).

3.2 PLANT ASSESSMENT MODEL ADOPTING SMALL SPECIMEN CREEP TESTING IN A CONDITION BASED MONITORING FRAMEWORK

3.2.1 Novel holistic condition assessment

The current approach results in an increasing inspection and assessment scope as the plant ages, until a point at which the economic life is reached and replacement is advised. The development of this staged approach to life management has been heavily influenced by the periodic inspection, condition assessment and remediation of defects and damage in welds, with the assessment of the condition of parent material following later in life and primarily influenced by the utilities desire to manage their requirements for large capital spend on plant refurbishment. As an example, for high temperature CMV main steam pipes on conventional plant this staged approach is typically applied as follows:

- Stage 1: includes first weld inspections after 50 khr of operation;
- Stage 2: first parent material checks (bends) initiated at circa 130 khr;

- Stage 3: initiation of planned inspection of straight pipe sections (parent material) at circa 190 khr, with first pass of bend inspections completed;

- Stage 4: Economic replacement scheduled at around 260 khr.

The case study presented later in section 3.3.1 will show that considerable effort from inspection bodies is required throughout the life of the plant to understand the rate at which the material deteriorates until component replacement is required. This has shown the uncertainty that the plant owner is faced with, due to the lack of consistency in inspection data trends. In broad terms the generating plant operates on a 3 to 4-year ahead operating ticket, whereas ideally the plant operator would prefer a longer-term 8-10 year forward prediction of the rate of life consumption to facilitate economic decisions related to capital investment and optimisation of periodic statutory inspections. In addition, a more predictive assessment of life consumption would provide the plant operator with the opportunity to optimise operation such that the economic lifetime of the assets can be safely and cost-effectively extended. The optimisation of life consumption to minimise outage inspection scope and prolong asset life is worth multi-million pounds over the life of a station.

Figure 35 illustrates the current inspection based assessment (IBA) procedures, with the inclusion of small specimen testing and on-load condition assessment highlighted as areas that warrant further development and implementation. Small specimen creep testing provides the opportunity to remove some of the uncertainty associated with the site outage inspection and assessment processes currently used. Based on the current maturity level of miniature specimen testing techniques, it is proposed that one of the most practical approach to consider at the moment is the further development and deployment of the impression creep method, particularly since it has been exploited on ageing plant by Brett [84, 100, 101, 165] for purposes of component risk ranking and condition assessment. The extensive programme of sampling undertaken on Slovakian reactors [138, 139, 166] is also noteworthy and is another example of the pro-active and systematic use of these small specimen testing techniques. The key point to note is that more precise information is required on the in-service rate of material ageing and any subsequent acceleration of the ageing rate that might indicate that repairs or replacements are required. The intention is to provide more reliable and periodic measurements of material properties throughout

the operating life of the asset. This approach can be applied to both conventional and nuclear generating assets and will allow the plant operator sufficient time to implement positive corrections to operation that maximise the useful life of the asset. Data obtained from these small specimen tests can be used to:

- Amend and update relevant pipeline system and component life prediction models;
- Advise plant operators on creep strain rates and changes in material behaviour, hence allow operating conditions to be optimised with respect to the plant owner's requirements for economic asset life;
- Influence and optimise the inspection scope at subsequent statutory outages;
- Provide a more informed view on the loads acting on complex regions such as welds, complemented by expert review of outage findings from weld inspections and metallography, thereby improving the management of weld integrity;
- Enable some current non-productive site examination methods to be gradually phased out or improved.

In order to provide useful information to the plant operator, results from small specimen testing must be acquired at a suitable time in life to enable appropriate modifications to plant operation to be implemented.

The following modification to the current approach is proposed for high temperature pipework. This essentially provides an earlier baseline condition assessment from targeted sample locations, supplemented by interrogation of online monitoring data. Subsequent statutory inspections provide periodic updates on the condition of the in-service ageing materials. Importantly, this modified approach gives the operator more opportunity to optimise how they can effectively manage the plant. The proposed modified approach is as follows (weld inspections would start initially as per normal practice at 50 khr):

- **Stage 1**: Develop full pipeline model(s) of a lead system, which allows estimates of creep strain rate, based on design values for material creep models,

hanger survey data, plant temperature and pressure monitored data. Ideally, pipeline model(s) developed by ~ 75 khr and used to proactively support future outage inspection planning. This essentially provides the baseline or reference model(s) for the plant.

- **Stage 2**: Start to acquire small specimen samples from lead pipeline(s). Specimens should be obtained from straight pipe sections that are adjacent to bends proposed to be first inspected at ~ 100 khr and from positions that will not require subsequent repair or additional monitoring. Update pipeline model(s) accordingly and compare predictions against outage inspection findings. Review and update future periodic inspection plans (including weld inspection plans).

- **Stage 3**: Select additional targeted small specimen samples to further assess and optimise pipeline model(s), thereby supporting continued safe operation towards end of life. The selection of suitable locations for additional material sampling would be informed by assessment of previous inspection findings. Review and update periodic inspection plans.

- **Stage 4**: At an economic point, plan to implement replacements.

It is important to recognise that there is a cost to implement small specimen testing, however it is anticipated that this will be offset by cost reductions elsewhere, such as:

- Reduction in the use of diametral strain measurements;

- Optimisation of outage site creep replica and hardness sampling and analysis campaigns;

- Optimisation of outage weld inspections.

In view of developing the new holistic condition assessment, correlation between small specimen data and currently used inspection techniques data, e.g. hardness measurements, must be found.

3.2.2 Novel empirical relations between hardness and minimum creep strain rate

Creep life is a function of the operating temperature and stress, while hardness change, after prolonged service, is mostly related to the thermal aging at the operating temperature [93]. Although creep and hardness data are not correlated by any mathematical model because of the different parameters they are related to, which represent different deformation mechanism [93], it is possible to find a fitting equation that relates the minimum creep strain rate (MSR), $\dot{\varepsilon}^c$, to hardness. Figure 36 shows minimum creep strain rate obtained by impression creep and uniaxial creep tests at 600°C at a reference stress of 155MPa plotted against Vickers hardness at room temperature, for Grade P91 steels with different service histories.

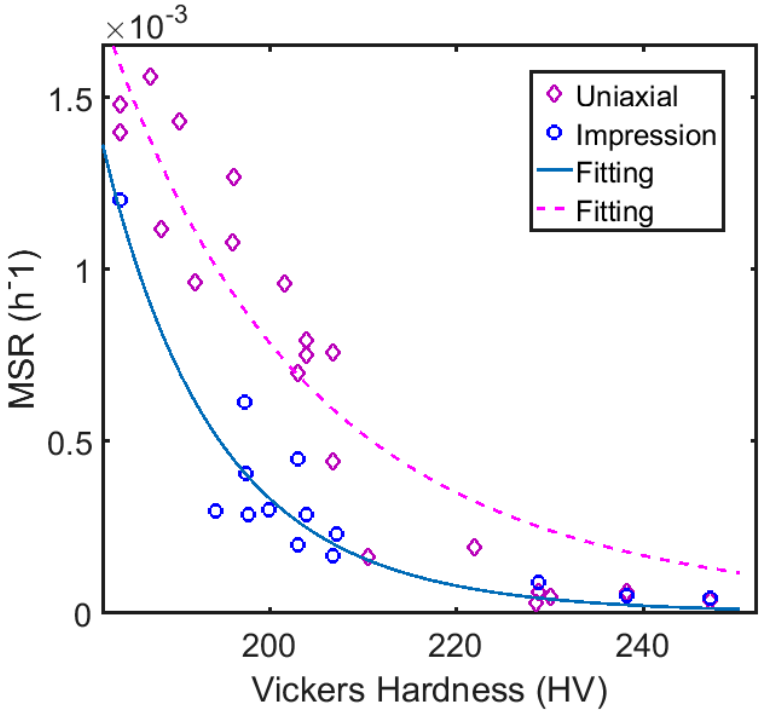


Figure 36. Minimum creep strain rate obtained by impression creep and uniaxial creep tests versus Vickers Hardness at room temperature at 600°C at a reference stress of 155 MPa, for Grade P91 steels with different service histories.

The phenomenological relationship between MSR and hardness is given in equation (67), where *a* and *b* are fitting constants, listed in Table 2.

$$\dot{\varepsilon}^c = aHV^b \tag{67}$$

Table 2. Fitting constants for equation (67) (for $\dot{\varepsilon}_c$ in h^{-1}).

Creep Test	a	b
Uniaxial	$2.34x10^{16}$	*-8.463*
Impression	$1.75x10^{23}$	*-11.53*

For ductile materials, the relationship between MSR and stress, σ, at a given temperature is generally expressed by Norton's power-law (see equation (7) in Chapter 2). By substituting the second term of equation (67) in equation (7), a relationship between Vickers hardness and stress, can be obtained as in equations (68) and (69).

$$HV = \left(\frac{B}{a}\sigma^n\right)^{1/b} \tag{68}$$

$$\sigma = \left(HV^b \frac{a}{B}\right)^{1/n} \tag{69}$$

Equation (68) has many limitations due to its phenomenological nature, but can give some information about the decrease of hardness with stress during creep exposure time, stating $b<n$. Furthermore, equation (69) can be used to relate hardness with damage, ω, defined as the ratio between the damaged area and the initial area, A_0. Damage can thus be expressed by equation (11), where A' is the undamaged area.

$$\omega = \frac{A_0 - A'}{A_0}, \quad with \;\; 0 \leq \omega \leq 1 \tag{70}$$

Cavitation damage is well described by Liu and Murakami's constitutive model, which allows the entire creep curve to be obtained and which degenerates to Norton's law when ω=0 [13]. The uniaxial form of Liu and Murakami's model is given again for the reader convenience in equations (71) and (72), where D, q_2 and χ are material constants, values of which, for Grade P91 at 600°C, are collated in Table 3.

$$\dot{\varepsilon}^c = B\sigma^n exp\left[\frac{2(n+1)}{\pi\sqrt{1+\frac{3}{n}}}\omega^{3/2}\right] \tag{71}$$

$$\dot{\omega} = D\frac{1-\exp[-q_2]}{q_2}\sigma^{\chi}\exp[q_2\omega] \tag{72}$$

By substituting the second term of equation (69) in equations (71) and (72), a modified Liu and Murakami's damage model including hardness can be obtained and it is expressed by equations (73) and (74).

$$\dot{\varepsilon}^c = aHV^b exp\left[\frac{2(n+1)}{\pi\sqrt{1+\frac{3}{n}}}\omega^{3/2}\right] \tag{73}$$

$$\dot{\omega} = D\frac{1-\exp[-q_2]}{q_2}\left(HV^b\frac{a}{B}\right)^{\chi/n}\exp[q_2\omega] \tag{74}$$

If all of the constants involved are known, damage calculation is possible by placing in equations (73) and (74) the hardness value measured at room temperature during inspections of the components, every two or four years according to the system safety regulations. The component failure can be assumed to happen when ω approaches its maximum value, 1. Although caution is necessary in using the modified Liu and Murakami creep damage model, since further investigation is needed, this novel approach could give an indication about material remaining life. In fact, although the applied stress could remain constant during service, the component hardness generally drops due to aging. Through the modified Liu and Murakami creep damage model, such drop in the hardness value will result in a reduction of the time to failure, giving the utility some useful information about the current component conditions.

Figure 37 shows the variation with time of the creep strain for the same material and temperature obtained by using Liu and Murakami's method with a reference stress of 155MPa and by using the modified Liu and Murakami method with different hardness values and fitting constants from both uniaxial and impression creep test data. For the same hardness value, equation (69) used with *a* and *b* from uniaxial creep test data overestimates the value of the reference stress with respect to equation (69) used with *a* and *b* from impression creep test data. Consequently, the value of the time to failure obtained through the modified Liu and Murakami method is overestimated.

Table 3. Constants of Liu and Murakami's damage model for a Grade P91 steel at 600°C (for σ in MPa and *t* in hrs) from ref. [109].

B	n	D	χ	q_2
$1.51\text{x}10^{-30}$	11.795	$2.12\text{x}10^{-27}$	10.953	5.3

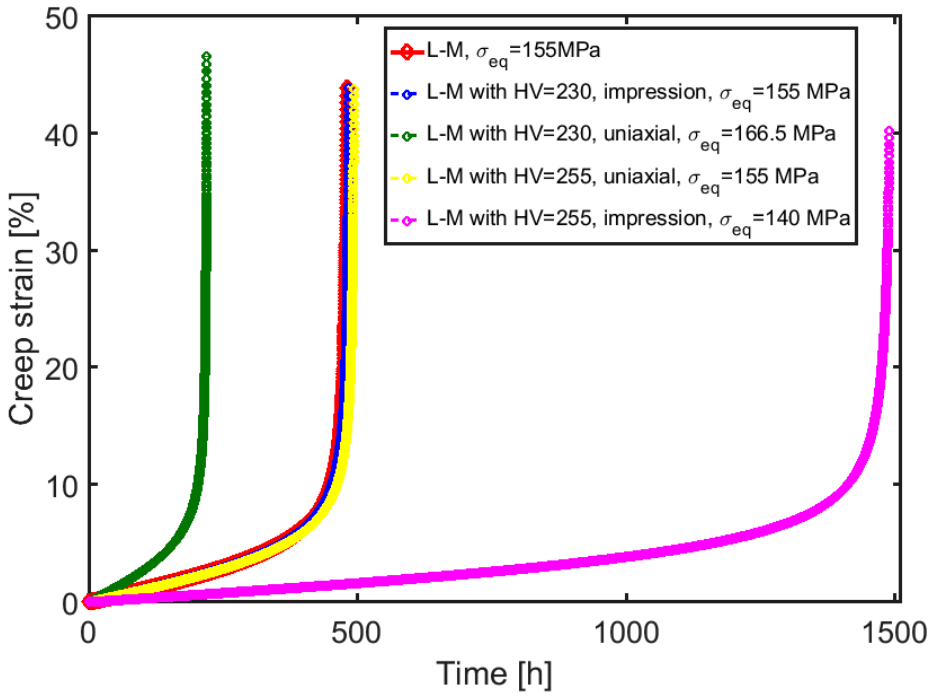


Figure 37. Creep strain versus time by using Liu and Murakami's and the modified Liu and Murakami methods.

An estimation of the failure life from impression creep test data is also possible via the Monkman-Grant relationship, equation (75), where m and C are material constants [107]. By substituting $\dot{\varepsilon}^c$ with the second term of equation (67) in equation (75), a relationship between hardness and the failure life is obtained and expressed in equation (76). Because of the less number of material constants involved in the calculation, this method for assessing the remaining life is convenient for practical use by the plant. Furthermore, the constant C can be determined by only one uniaxial test, and, for ferritic steels, m is roughly equal to 1. Monkman-Grant's relationship is intended as only a guide for remaining life assessment [107] as well as equation (76).

$$\log(t_r) + m\log(\dot{\varepsilon}^c) = C \tag{75}$$

$$\log(t_r) + m\log(aHV^b) = C \tag{76}$$

However, when HV > 190, the modified Liu and Murakami model is generally able to provide failure time from impression creep test results closer to the corresponding uniaxial creep test data than Monkman-Grant's relationship (equation (75)), as shown in Figure 38, which presents the variation of the time to failure with hardness value. It is worth to note that the proposed method does not need an initial hardness value at t = 0 h for the failure life to be established, contrary to other approaches established so far [63, 75, 79-81] and described in Chapter 2 (see section 2.3.5).

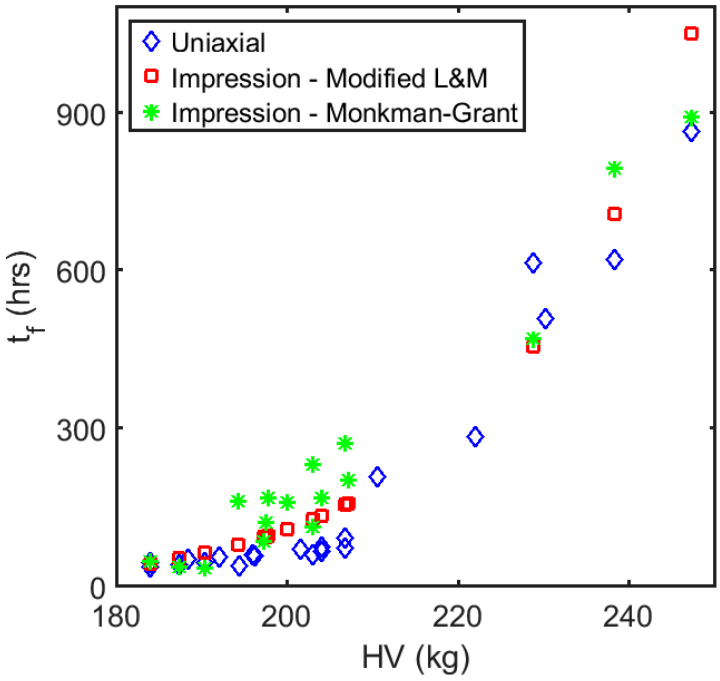


Figure 38. Variation of the time to failure with hardness for a Grade P91 steel at 600°C and 155MPa, obtained by uniaxial, impression creep with modified Liu and Murakami's method, and impression creep with Monkman-Grant's relationship.

3.2.2.1 Model implementation and validation

Implementation and validation of the hardness modified Liu and Murakami model for in-service operational conditions would be approached with the following considerations. Over an extended period of service from initial commissioning it is feasible to consider acquiring hardness data, but with the following guidance.

- If possible, secure some extra lengths of pipe during the construction phase so that parent and welded test specimens can be manufactured at a suitable time in order to quantify initial material lifing parameters. Other opportunities to

acquire materials will almost certainly arise during service, for example it may be necessary to replace a defective weld or valve.

- In the ideal case, baseline hardness measurements would be acquired during the initial construction phase of the plant. For example, this data could be acquired on selected locations at the same time as original construction welds are inspected.

- Identify a small number of reference locations on the pipe system, ideally adjacent to accessible fixed walkways and platforms to negate any requirement for installation of temporary scaffolding. For a typical main steam line on a conventional unit this could be circa 4-5 locations, one adjacent to the boiler stop valve located at the boiler outlet, one towards the high pressure stop/control valve and the remainder at intermediate positions.

- As the station enters service there will be opportunities to acquire hardness data at times other than during the main statutory outages; typically this would be during short planned maintenance outages. In this event, having accessible reference locations identified is essential in order to minimise access costs.

- Periodic statutory outages provide the ideal opportunity to acquire hardness data at targeted locations. The question then arises, how is this data subsequently used in a practical way to predict the life consumption rate and importantly advise the station on, a) any modifications to operating duty, b) optimising the inspection schedule for the next statutory outage.

- A whole pipe work system interface framework model has been developed [167] as part of the Flex-E-plant consortium. This model provides a readily available method whereby the hardness modified Liu and Murakami creep damage model discussed in this Chapter could be implemented.

- Iteration is a necessary step to challenge, improve and ultimately validate the proposed damage model; this must be facilitated by scrutiny of other plant condition assessment data routinely obtained during plant outages and likely supplemented using targeted small specimen extraction and testing [1]. The available whole pipe system interface framework [167] enables the

implementation of this hardness modified Liu and Murakami creep damage model.

The above outlines an approach to model validation that is essentially based on periodic re-calibration in order to optimise operation and the scope of through life plant inspections. There are many other high temperature systems and components in operation on a typical large conventional thermal power station. The general approach described above is equally applicable to these, however these may present different challenges. For example, the complex geometry encountered in steam headers and large forgings and castings requires the development of novel analytical approaches to assess the impact of operational temperature and pressure cycles via online monitoring [168].

3.3 CURRENT PRACTICE

3.3.1 Ageing main steam pipework

The data presented in this case study is based on conventional plant operation and focused on information and techniques currently used to assess the remaining creep life and hence decide on replacement.

The through life integrity of main steam CMV butt welded pipework systems has been dominated by the condition of the weldments, which have typically been addressed by means of periodic inspection, weld repair or pipe spool replacement. Most of the integrity issues associated with the weldments have manifested as circumferentially distributed creep cavitation or subsequent circumferential cracking. This damage is affected by pipework system loads and it is not uncommon to find the observed weld damage biased (creep cavitation or depth of cracking) around the circumference of the pipe weld. Invariably at the latter stages of a stations life the location and condition of all the major welds has been established and procedures are in place to implement any needed repair and replacement activities.

However, the failure of parent material is more likely to occur due to the acting pipe hoop stress, which can potentially initiate longitudinal cracking. It is very difficult to comprehensively identify those parent material regions close to creep life expiry, noting the large volume of parent material in typical steam pipe systems. As the pipe system enters the later stages of life, conducting piecemeal butt weld replacement by

the insertion of new pipe spools becomes more difficult due to the aged condition of the cut faces of the original pipe section, which is typically assessed by on-site surface replication and hardness testing. This ‘test’ of the parent material condition, when conducting pipe spool replacements, is often used as an opportunistic indicator of parent material condition, due to the opportunity to undertake some metallurgical examination through thickness.

Firstly some background related specifically to the case study pipework example. During the 2005 outage on a unit on Station ‘A’, Figure 39 (Unit operating history 221.8 khr and 2846 starts), high levels of surface creep damage were identified in a number of main steam bends and straight pipe sections, most significantly on steam leg B2. Subsequently, creep rupture and creep crack growth tests were conducted on material extracted from straight pipework sections removed from service, which indicated a minimum creep life of between 250-275 khr. Consequently, in 2009, some partial replacement of main steam CMV pipework was undertaken and at the time of the replacement the unit had accumulated 242.5 khr and 3552 Unit starts.

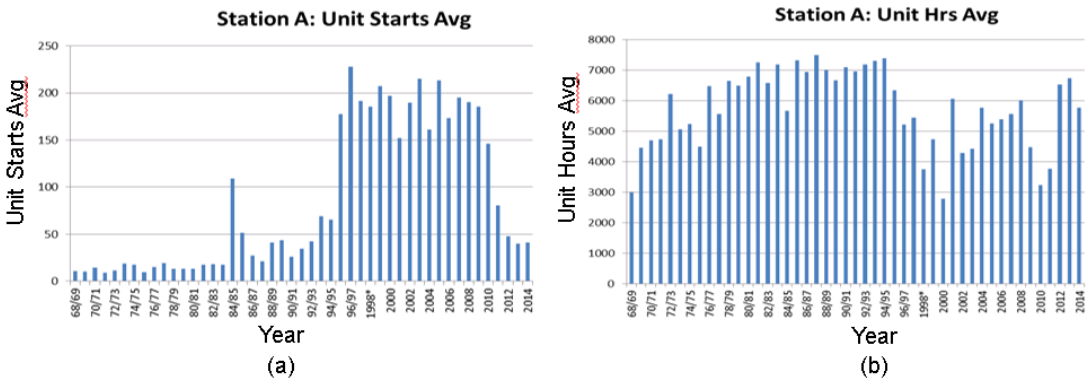


Figure 39. (a) Unit average operating starts for station A and **(b)** unit average operating hours for station A.

This case study considers one of the straight pipework sections removed from steam leg B1 and the subsequent laboratory examination to investigate the distribution of creep cavitation damage on the surface and through wall. This pipe sections (and others) were removed to reduce operational risk, having been sanctioned as life expired based on surface replication results during the 2009 outage, which showed moderate to high levels of creep damage. The nominal design information for this main steam pipework is;

- Outside Diameter 342 mm
- Wall Thickness 60 mm
- Design Pressure 173.8 bar
- Design Temperature 568 °C.

3.3.1.1 In-service inspection history

During service the CMV pipework system had been subjected to the standard outage examinations and periodic in-service creep effective temperature (CET) analyses. These analyses had been undertaken regularly since 1993, typically based on a 6-month block of steam temperature data from the monitored steam leg. Table 4 shows a sample of this CET data for all four steam legs (A1, A2, B1, B2) on the unit. The data presented in Table 4 is determined using the approach described in section 2.2.4.2. Data blocks of more or less than 6-months could be used to expedite the calculation. The noted step in CET values between the monitored dates is quite normal for a large conventional fossil-fired units and is driven by changes in operation, such as the move from base load to flexible operation, and other factors such as a drive to extract more MW from each unit. This just reflects the very real commercial pressures affecting operation.

Table 4. Steam leg CET values.

Year	A1 (°C)	A2 (°C)	B1 (°C)	B2 (°C)
2009	565.2	562.6	562.7	560.3
2005	567.4	565.8	563.7	563.2
2003	567.3	568.0	564.7	561.2
2001	566.0	568.0	563.2	561.5
1999	554.4	565.4	560.7	561.1
1997	567.8	566.4	566.3	566.5
1995	566.1	564.3	565.7	565.3
1993	568.5	567.2	568.0	568.7

The CET data collated over a number of years of service shows that each steam leg operates at creep effective temperatures that can be as much as 5 °C different (omitting the suspiciously low 1999 CET data for leg A1). Such relatively modest differences in creep effective temperature can result, if sustained for a long enough period of time, in significant differences in creep rupture life from leg-to-leg on a unit. Figure 40 shows this leg-to-leg variation with temperature, noting that practical plant

control is further complicated when the units are subjected to a high number of starts, as illustrated by past station operation in Figure 39-a.

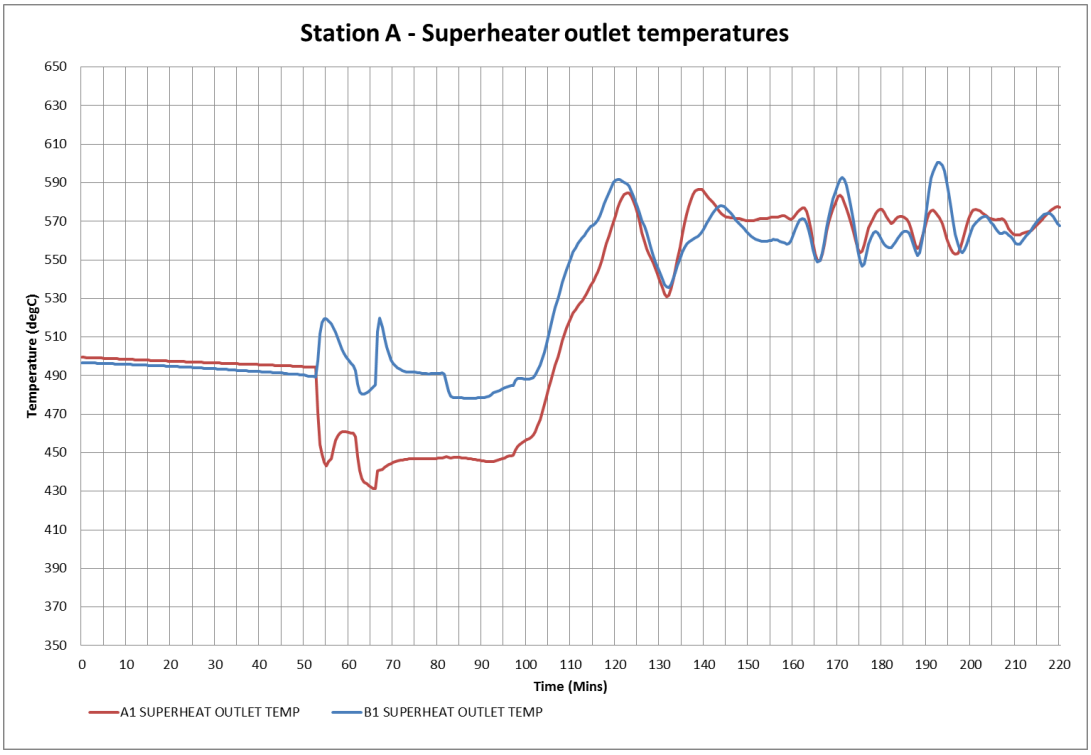


Figure 40. Typical steam temperature trace for two boiler outlet steam legs (A1 and B1).

Another standard approach taken during the outage is to take diametral strain measurements. Typically, these are taken over installed stellite grade 6 creep pips, as reference measurement locations, on the outer diameter. For the case of the unit on Station 'A' the pipework creep pip locations were towards the boiler stop valve at the 160 ft level in the boiler, as well as at the 100 ft and 60 ft levels. Various diametral strain measurements had been taken over installed creep pips during successive outages dating back to 1993 (unit operation at 161 khr and 321 starts) and including the 2009 outage. Table 5 shows the pipe diametral measurements taken at the 160 ft level on legs B1 and B2 between 1993 and 2005 for comparison. Four diametral measurements are taken across the eight installed creep pips around the pipe circumference.

Table 5. Diametral measurements, main steam legs B1 and B2.

Measurement Location			Measurement over creep pips corrected to 20°C (mm)				
Leg	Boiler Level	Axis	1993 (161,643 h)	1997 (187,116 h)	1999 (196,583 h)	2001 (203,010 h)	2005 (221,799 h)
B1	160 ft	N-S	364.31	364.62	364.77	364.82	364.98
		E-W	364.03	364.46	364.64	364.69	365.03
		NE-SW	364.44	364.79	364.97	365.02	365.27
		SE-NW	365.23	365.61	365.79	365.81	366.11
		Average	364.50	364.87	365.04	365.09	365.35
B2	160 ft	N-S	368.27	368.58	368.71	368.73	368.89
		E-W	365.61	366.04	366.24	366.27	366.64
		NE-SW	367.11	368.02	367.64	367.69	368.83
		SE-NW	368.07	368.38	368.53	368.50	368.77
		Average	367.26	367.75	367.78	367.80	368.28

The pipe diametral measurements show a generally steady increase in pipe outside diameter, with only a small number of measurement anomalies evident. Hence, the average strain rate over the period 1993 to 2005 (60,000 h) is ~ $4x10^{-8}$ h^{-1}, which equates to a minimum operational creep life of ~ 300,000 h. The strain rate is determined by evaluating the diametral strain between periods and correcting for the temperature at which the measurement was taken and any micrometer zero (offset) errors recorded. Pipe diametral measurements can sometimes be taken directly across the pipe outer diameter, if this is the case additional corrections would be required to account for oxide film growth over the time period between successive measurements. The subsequent site diametral measurements are assessed using conservative residual life formulae, which are derived from strain measurements taken from a series of internally pressurised creep rupture tests undertaken by the UK's former central electricity generating board.

When comparing the CET and diametral data for legs B1 and B2, leg B1 shows a lower average strain rate, but a higher CET trend when compared with leg B2. It might have been expected that the higher CET trend on leg B1 over the extended period of measurements would have led to a higher diametral strain rate. This shows the current difficulty interpreting such measurement data in isolation and the reason why other more invasive methods, such as surface replication, is used to assess material condition.

During the 2009 outage the original CMV straight pipe section, identified as SM14, was removed from leg B1 for further laboratory examination; based on observed 'High Orientated' creep replica results. The adjacent pipe section immediately upstream from this removed section was left in service, with only a 'Very Isolated' replica assessment level assigned to the parent material.

3.3.1.2 Post-service laboratory examination

Both surface creep cavity and through section creep cavity mapping was carried out to industry procedures described in GENSIP guidance [169]. GENSIP refers to the UK 'Generators Safety and Integrity Programme', which is a member self-funded utility collaboration tasked with ensuring best practice is shared across the industry. The creep cavity damage levels indicated are classified in accordance with the definitions in Table 6. These classifications are provided by the technical service provider and enable them to compare observed creep damage and hence recommend a suitable course of action. The surface creep cavity mapping was taken at various axial and circumferential positions on the examined specimen (SM14 from leg B1), and is illustrated in Table 7.

Table 6. Creep cavity damage level (technical service provider classification).

Level	Description	Abbreviation
0	Clear	C
1	Isolated	I
2	Isolated/low orientated	I / LO
3	Low orientated	LO
4	Low orientated/mid orientated	LO / MO
5	Mid orientated	MO
6	High orientated	HO
7	High orientated/grouped	HO / G
8	Grouped	G
9	Aligned	A
10	Micro cracking	MC
11	Cracking	Crack

With reference to the pictorial representation and definitions in Figure 1, the technical service provider classification in Table 6 is more generally interpreted as follows: Isolated (Level 2-3), Aligned (Level 8-9), Micro-cracking (level 10). In addition, Figure 7 (Chapter 2) shows a photomicrograph from a section of retired CMV pipework, with a creep cavity count of 842 cavities/mm^2, in this case the

classification would be judged at level 5-6 mid to high orientated. This exhibits quite a high creep cavity count per unit area and would be expected to progress to grouped and aligned in the short term if left in service.

Table 7. Creep cavity surface damage levels: CMV straight section SM14, leg B (technical service provider classification).

Angular Position Around Ring	Distance along pipe (m)										
	0.5	0.75	0.8	0.85	0.9	0.95	1	1.4	1.5	1.6	2
0°					1						
45°		3	7	4	5	7	6		1		
90°					3						
135°	2	3	3	6	7	6	1	6	5	6	3
180°			6	5	5		4		3		
225°		7		5	3	7		3	6	7	
270°					1				7		
315°		3		6	3	2		3	7	7	

The German VGB guideline [170] provides a revision of the Neubauer-Wedel creep cavity classification [171] and is reproduced in Table 8.

Table 8. VGB guideline classification [170].

Assessment Class	Structural and Damage Conditions
0	As received, without thermal service load
1	Creep exposed, without cavities
2a	Advanced creep exposure, isolated cavities
2b	More advanced creep exposure, numerous cavities without preferred orientation
3a	Creep damage, numerous orientated cavities
3b	Advanced creep damage, chains of cavities and, or grain boundary separations
4	Advanced creep damage, micro-cracks
5	Large creep damage, macro-cracks

ECCC recommendations [172] on residual life and microstructure references investigations undertaken to correlate the VGB damage classification [170] against residual life for low alloy steels in the heat-affected zone of a weld. In this particular investigation VGB damage level 3 correlates to an expended life fraction of 0.691.

With reference to the ex-service SM14 straight specimen surface replication (Table 7), three angular positions (135°, 225° and 315°) at distance 1500mm along the

pipe were selected for through section creep void mapping. Table 9 shows an example for the 315° position. Each of the through section samples was carefully aligned with the corresponding surface replica position (Table 7). A series of replicas were taken at through section depth increments of approximately every 4mm until the bore was reached. At each 'depth' position surface replicas were taken horizontally across the width of the extracted through wall specimen, resulting in a sample of approximately 15 per 'depth' position. These replicas were commenced at a distance of 2 mm from the cut face to avoid any damage from specimen preparation.

Table 9. Through section creep cavity count distribution (1500 mm and Circ/315° Position) **(**technical service provider classification).

% Through Wall (from outside surface)	Cavity Count (Cavities/mm2)	Category	Classification number
0.00		G	8
9.23	115	LO	3
18.46	75	LO	3
27.69	50	LO	3
36.92	60	LO	3
46.15	55	LO	3
55.38	45	LO	3
64.62	25	I	1
73.85	13	I	1
83.08	10	I	1
100.00	0	C	0

The results show a trend of reducing cavity count through the section, peaking at the outer surface position. It is possible to further summarise and compare the through wall cavity count distributions in Table 9 as follows, based on the classifications in Table 6 (Technical service provider) and Table 8 (VGB):

- Outer 10% of the wall section: Classification ≥ 5: (VGB 3)
- Intermediate 60% of the wall section: Classification 2-3: (VGB 2)
- Inner 30% of the wall section: Classification ≤ 1: (VGB 1)

This illustrates the somewhat subjective nature of the cavity count classifications and the importance, of where possible, having a clear understanding of the origin of the cavity count classification used during an in-service inspection and the subsequent impact on residual life.

3.3.1.3 Comments

The following points are evident considering the site inspection history and subsequent examination of the ex-service life expired CMV straight pipe section SM14:

- Leg B1 shows a lower average strain rate based on diametral measurements compared to leg B2, but operates at a higher temperature (CET),
- There are significant operational temperature differences between the main steam legs exiting a 500MW conventional boiler,
- Through section creep cavity mapping on straight pipe section SM14 (Table 9) shows a wide range of damage levels, peaking at the outer surface, which infers a significant residual life for the bulk of the parent material.

These results emphasise why the current inspection and sentencing approach requires expert deduction and elicitation of various data sets in order to provide advice on future inspection plans, monitoring schemes and eventual repair and replacement options.

The case study illustrates some of the more subjective aspects of the current approach to life assessment of ageing components at high temperature. The importance of the experts view on the condition of the component under examination should not be underestimated, as well as the need for comparison against other similar components elsewhere (possibly older with respect to service duty) is evident. The case study shows that the current life assessment process would benefit from more synergistic use of the data routinely collected during an outage. In addition, life assessment would greatly benefit from the more pro-active use of in-service monitoring data along with the use of more predictive models for assessing residual life, which would subsequently allow optimisation of future plant operation.

3.3.2 Hardness and surface replica data

Despite some hardness lifing models have been developed so far, as described in Chapter 2 (see section 2.3.5), there is no universally applied and accepted hardness based material life model currently in use. Various plant service organisations routinely capture hardness data as part of periodic plant outage campaigns and usually

in conjunction with data obtained from other examination techniques such as surface replicas. The use of hardness in a lifing model can be contemplated for scenarios such as supporting safety case assessments [82], but noting that such safety cases are invariably complemented by data acquired from several other examination techniques and periodic measurements [20]. Currently, hardness testing on operational plant is undertaken to provide general surveillance data, essentially to track trends over time and with limiting values defined based on practical experience. The benefits of this approach are that a relatively large number of plant locations can be cost-effectively sampled during a plant outage. However, a key aspect of this approach is the identification of the rate of change in hardness over time. Hardness testing is complemented by interrogation of other plant data such as operating temperatures, surface replicas, non-destructive testing results, etc.

The following case study will discuss the hardness data trends, correlation with surface replicas and provides an overview on how subsequent operational risk is managed throughout life on parent CMV main steam lines in-service on a conventional fossil-fired power station.

3.3.2.1 Plant conditions

Data from the four main steam and four hot reheat lines on one 500MW boiler are considered in this case study. The main steam lines transport steam from the boiler outlet header to the high pressure steam turbine, with nominal design operating conditions of 568°C and 165.5bar. The main steam lines are approximately 350mm outer diameter with a nominal wall thickness of 65mm, which equates to a mean diameter hoop stress of 36MPa at the nominal design pressure. The hot reheat lines transport steam from the boiler reheater to the intermediate pressure turbine, with nominal design operating conditions of 568°C and 41bar. The hot reheat lines are approximately 500mm outer diameter with a wall thickness of 27mm, which equates to a mean diameter hoop stress of 36MPa at the nominal design pressure. It is worth noting that typical operation involves multiple plant starts with some overshoot of the nominal design operating temperature.

For this case study on CMV main steam and hot reheat lines hardness data has been collated over two successive outages, separated by 4 years, as outlined in Table 10.

Table 10. Unit hours and unit starts for two successive outages.

	Outage 1	Outage 2
Unit hours	239.649×10^3	259.733×10^3
Unit starts	3425	3971

3.3.2.2 Hardness and creep replica data

The number of pipework locations examined during both outage 1 and outage 2 is summarised in Table 11. For each of these locations both surface creep replicas and hardness measurements were obtained; noting that this just covers the examination of parent material.

Table 11. Number of hardness and creep replica data points of the parent material.

	Outage 1	Outage 2
Main steam	146	408
Hot reheat	79	663

It should be emphasised that the above only represents parent material hardness and creep replica data from one of the four 500MW boilers operating at the station. There are at least as many hardness and creep replica data points for the weldments covering both the weld metal and heat affected zones. The corresponding creep replicas are classified in this particular study based on the assessment levels defined in Table 12.

Table 12. Creep replica assessment levels.

Creep replica assessment level	Definition	Creep cavities per mm^2
1	Clear	0
2	Very isolated	1-10
3	Isolated	10-50
4	Low orientated	50-250
5	Orientated (Including high orientated)	250-500
6	Grouped	500-1000
7	Aligned	1000-1500

Figure 41 (a) and (b) show the sample variation in hardness for parent main steam for outage 1 and 2, respectively, and Figure 41 (c) and (d) show the sample variation in hardness for parent hot reheat pipework material for outage 1 and 2,

respectively. Typically, a start of life hardness HV value for CMV is ~ 170HV, hence extended service life results in a significant reduction in hardness. Table 13 gives the sample means and standard deviations for the two outage populations, a general reduction in hardness level is evident between these two outage samples.

Table 13. Hardness sample statistics (in HV).

	Main Steam		**Hot Reheat**	
	Mean	Standard Deviation	Mean	Standard Deviation
Outage 1	132.91	9.95	139.73	10.42
Outage 2	125.05	7.69	132.87	8.33

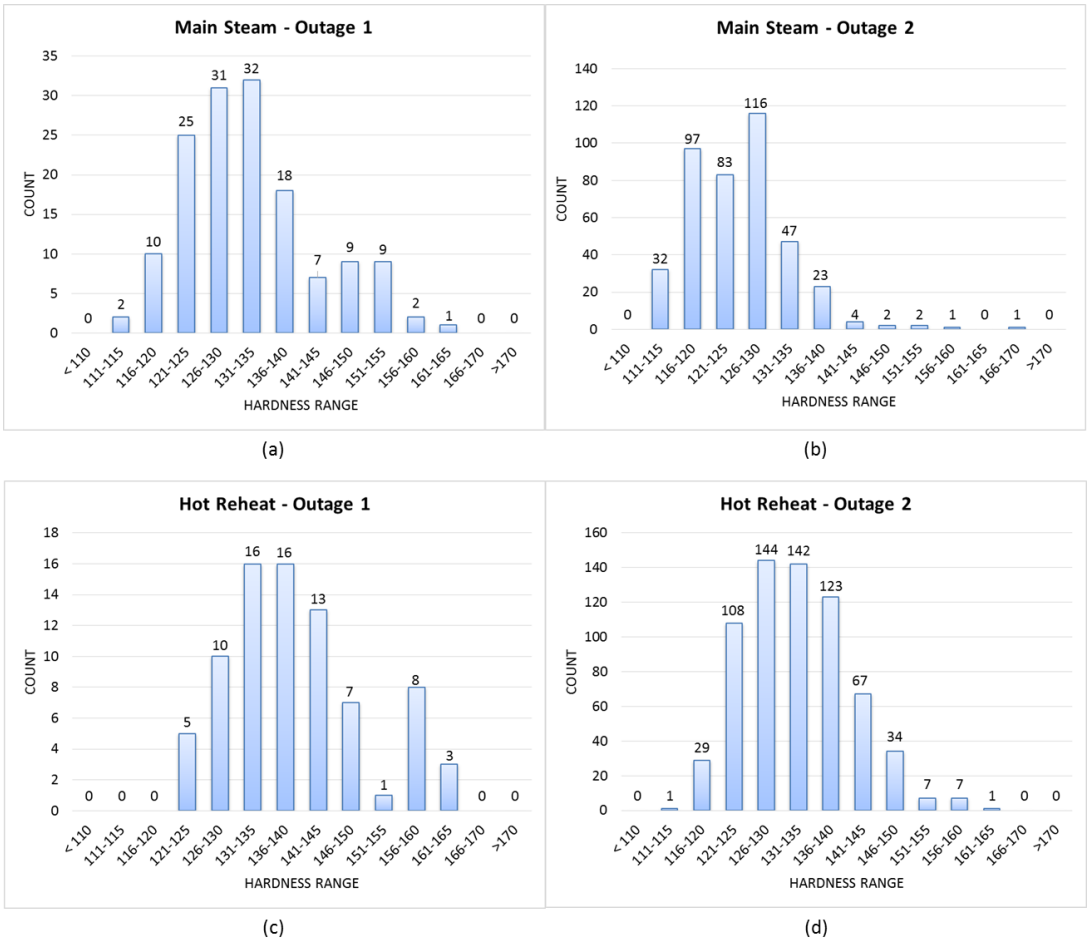


Figure 41. Hardness range for main steam for **(a)** outages 1 and **(b)** outages 2; hardness range for hot reheat pipework for **(c)** outages 1 and **(d)** outages 2.

Figure 42 compares, for each hardness reading, the associated surface creep replica assessment level; in particular Figure 42 (a) and (b) are related to the main steam for outage 1 and 2, respectively, and Figure 42 (c) and (d) to the hot reheat

pipework material for outage 1 and 2, respectively. There is no clear correlation between the respective hardness values and the assessed creep replica level. Unpublished information describing the sectioning of similar ex-service parent pipework and through thickness creep replication studies from sister units of similar age and pedigree have shown that the creep cavitation tends to peak at the outer surface or just below, with a progressive and significant reduction through wall. Importantly, in these data sets, when comparing successive hardness and creep replica data from the same location it is apparent that there is a greater probability of identifying a change in the hardness level as opposed to a change in the creep replica assessment level.

Typically, during such a site assessment, intelligence gleaned from examination of the surface replicas is often used as the leading indicator to determine subsequent re-inspection intervals or replacement and repair options. The hardness data is used primarily as a back-up measurement, which may or may not correlate with a trend of gradual in-service degradation over time. In this particular case study the hardness data is (for the population) showing a general deterioration between the two outages, whereas there is little correlation between the change in hardness level and the assessment of the creep cavity count. This in itself provides the challenge for parent material, especially since the through section studies on retired pipe sections have shown only surface creep damage, with very limited evidence of further creep cavitation through the majority of the remaining pipe section.

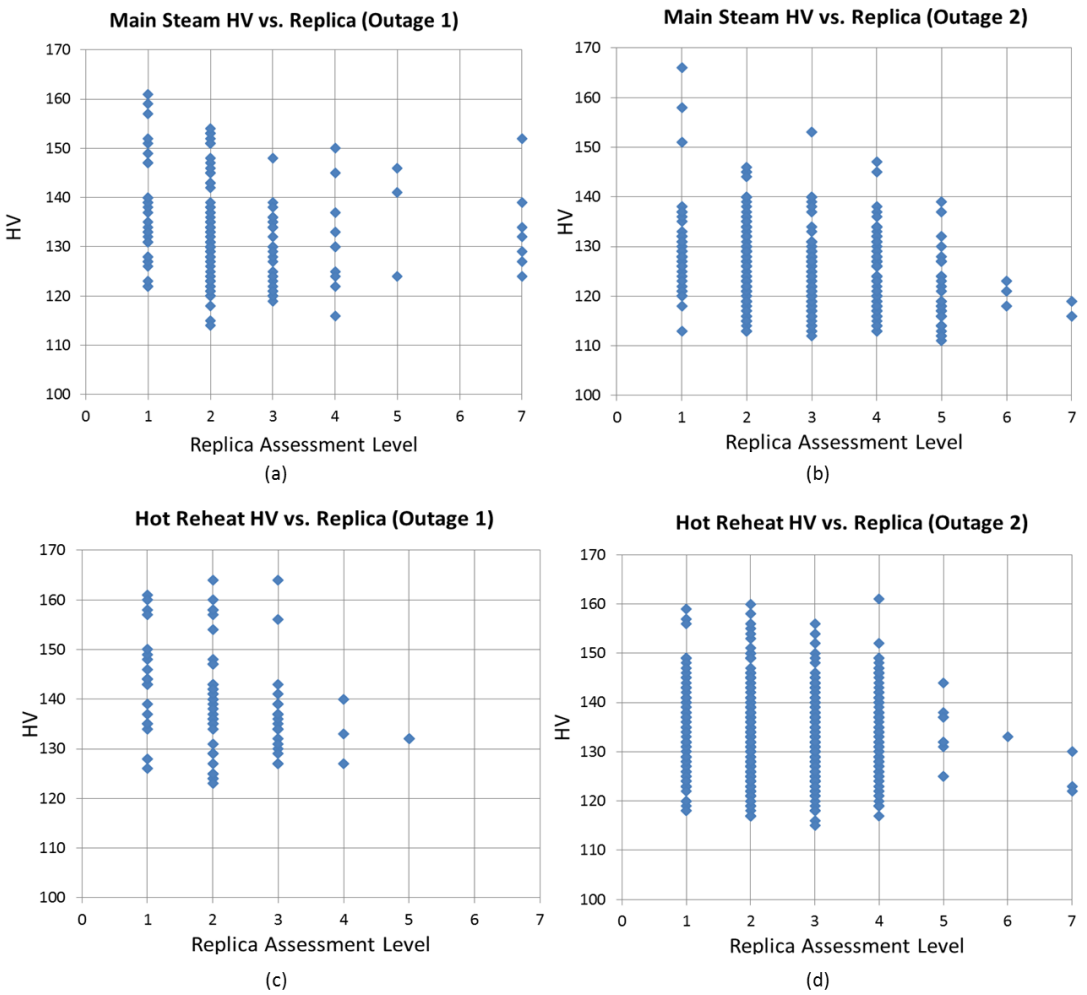


Figure 42. Hardness vs. Creep Replica Assessment Level for **(a)** Outages 1 and **(b)** Outages 2; hardness range for Hot Reheat pipework for **(c)** Outages 1 and **(d)** Outages 2.

It can be seen that the application of a representative hardness based stress model, that could account for the loading applied to an operational steam line and importantly be amenable for update, by use of small specimen sampling and other data such as obtained from pipe hanger adjustments and operational steam temperatures and pressures would be advantageous.

3.3.2.3 Application of data in life assessment

In addition to the physical inspections described in the case study, periodic assessments of operating temperatures are undertaken as well to determine the creep effective temperature. This provides a reference operating temperature, which is subsequently compared against the design specification, which may of course subsequently prompt adjustments to the boiler operating parameters. This creep effective operating temperature assessment however does not take into account the

specific material condition and creep response under load, nor does it take into account the imposed loading as result of how the pipe system is supported and adjusted throughout its operational life. So, when faced with this type of data and findings from periodic outage inspections a number of approaches are considered as the asset approaches end of life. The benefits and challenges associated with these options are outlined in Table 14.

Table 14. End of life options.

Options	Benefits	Challenges
Run (No strategic replacement schemes planned)	Low capital investment	Incur significant increase in outage scope and cost as the plant ages if the operational risk is to be adequately managed.
Repair	Remove perceived higher risk components	Conducting repairs on ageing materials may not be straightforward and will invariably require additional inspection and condition monitoring.
Replace (Complete system)	Replace and effectively eliminate the risk	Very significant costs involved

In the safety case scenario described, the decision was made to replace the complete pipework system, but on the premise that the station had a relatively long remaining life and the market revenue outlook was healthy. Subsequent to this decision, another unit of similar age was faced with the same considerations 12 months later. However, in this case the market conditions had changed significantly, with much lower revenue projections and earlier station closure date. It is no surprise that for this unit the full pipework replacement was deferred and only limited (higher risk) sections of pipework were subsequently replaced. Operation of this unit until station closure will incur increased outage inspection and condition monitoring.

3.3.3 Risk management

Ongoing risk management is heavily reliant on a proactive response to the findings from statutory outage inspections. Ideally and arising problems are dealt with (repaired or replaced) during the outage, hence reducing the risk over the next operational period. However, this is not a cost effective approach and it is notable that as the plant ages there is a very significant increase in the scope and cost of site

inspections during an outage. The described case studies on parent CMV material represents only a small proportion of the inspections that occur on a unit's pressure systems. Because of the potentially serious consequences arising from the failure of a high temperature pressure system, all operating stations take a cautious approach and will, in the absence of more quantitative assessment methods, continue to implement repair-replace options. This approach is commercially tolerable if the revenues are healthy, however recent market forces in the UK has significantly reduced available revenues and stations are having to reassess operating risks and seek opportunities that can reduce the remaining life cost, whilst maintaining adequate risk management.

It is useful to put the current inspection and assessment approach into context. Figure 43 illustrates the increase in the volume of outage metallurgical inspections that arise as a plant approaches its end of life, denoted by 't' in Figure 43 and is based on the actual volume of inspections on plant obtained from a review of outage reports. The preceding statutory outages are specified at points 't-1', 't-2', etc., and each of these operating periods are typically of 4 year duration, equating to circa 20,000 hours operation. The end of life outage 't' represents the position outlined in the case study outage 2. It is not inconceivable to consider a t+1 period of heavily monitored life extension whereby the increase in site metallurgical inspections would significantly exceed the endpoint illustrated in Figure 43.

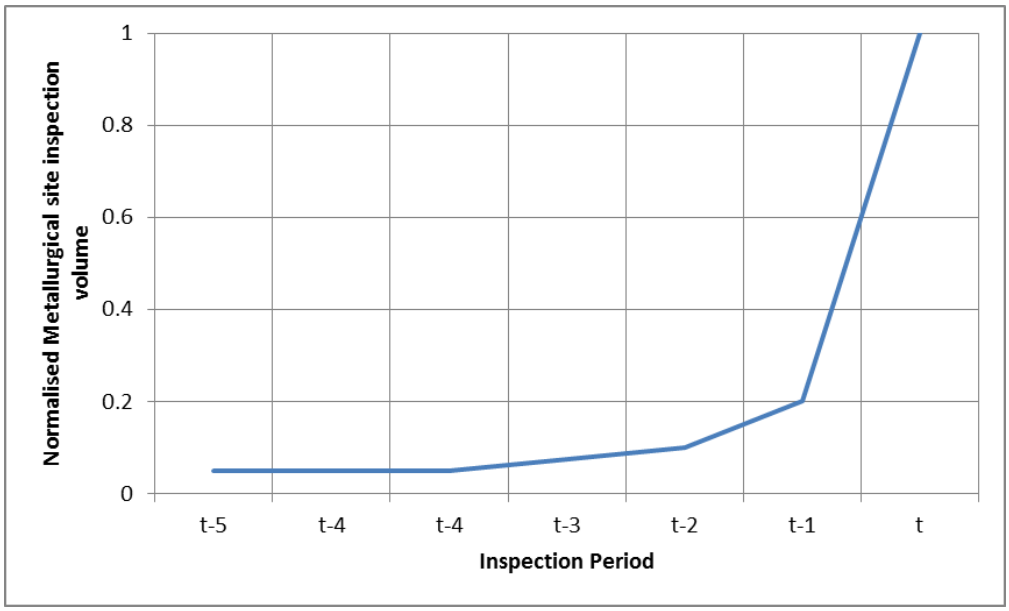


Figure 43. Normalised metallurgical inspection volume against outage period.

From a risk management perspective there is currently a heavy reliance on the intelligence gathered from such invasive metallurgical inspections. Figure 44 provides an overview of how this manifests itself in terms of decision making and informing the asset owner on risk and mitigation options.

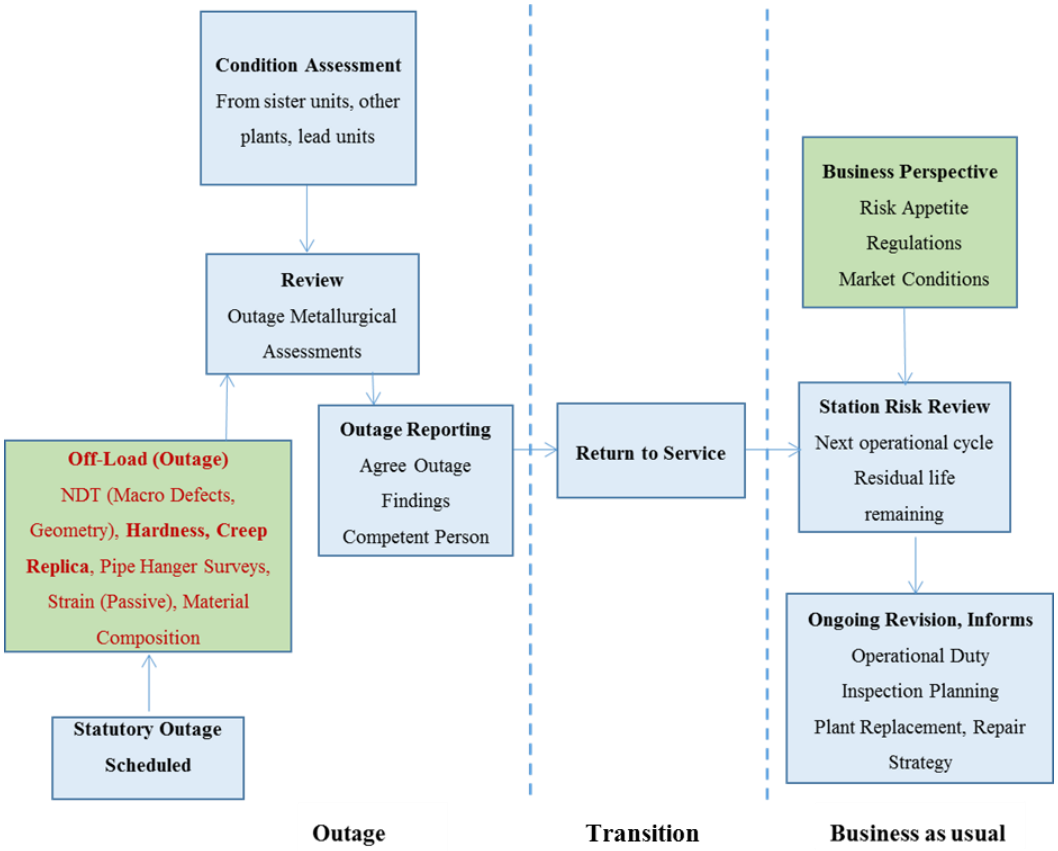


Figure 44. Current risk management process.

3.4 CONCLUSIONS

The framework for applying high temperature plant condition assessment provided in Figure 35 emphasizes the need to correlate the data acquired during off-load monitoring, such as hardness, with creep data, obtained, for instance, by use of miniature creep test specimens, in order to develop a more proactive method for life management. The important point to note is there is an opportunity to deploy targeted hardness testing, supported by an improved life assessment model as described in this Chapter. It is useful to reflect on the graphical illustration in Figure 43, which is based on current practice and the significant increase in the extent of invasive inspections as a plant ages in service. An approach for the implementation of surface hardness in the Liu and Murakami damage model has been illustrated. Currently the only approach in

common use to predict the rate of creep life consumption is via the calculation of the creep effective temperature. However this has been shown (see also Chapter 2, section 2.2.4.2) to have several limitations and can realistically only be considered to provide information complementary to that acquired during the invasive outage inspections, which increase in scope as the plant ages, as illustrated in Figure 43. Use of routinely acquired hardness data in a model such as Liu and Murakami's gives the operator scope to assess the effect of the rate of change in hardness and predict the likely impact of this for future operation and ultimately influencing the scope of future outage inspections.

4 INVESTIGATION ON THE CAPABILITY OF IMPRESSION CREEP TEST

4.1 INTRODUCTION

Chapter 3 highlighted the need of a new holistic assessment approach that integrates normally acquired industry data with that obtained by small specimen creep tests. Therefore, Chapter 5 will focus on demonstrating how those data could be used in a real situation by investigating the creep damage evolution of an ex-service CrMoV pipe section by means of both traditional techniques and impression creep testing method. The objective of this Chapter is therefore to assess the capability of data conversion of impression creep test (ICT).

As mentioned in Chapter 2, the reference stress method is used to convert small specimen creep testing data to the corresponding uniaxial data, in term of minimum creep strain rate, through two conversion parameters, η and β. The present section will investigate some aspects that may influence the accuracy of the data conversion. First, impression creep test data, obtained from P91, P92 and ½CrMoV steels at different stresses and temperatures, will be presented with their correlation with uniaxial data. Then consequences of possible geometry inaccuracies in the position of the indenter will be investigated and, finally, some general comments on the conversion relationships will be provided.

4.2 COMPARISON OF UNIAXIAL CREEP AND IMPRESSION CREEP TEST DATA OUTPUT

Several uniaxial creep and impression creep tests were carried out for a number of power plant materials, i.e. P91, P92 and 1/2CrMoV steels, in the range of temperatures between 575 and 650 °C, with stresses ranging from 90 to 200 MPa. The values of the parameters used to convert the displacement rates obtained by impression creep tests to the corresponding uniaxial minimum creep strain rates are 0.43 and 2.18 for η and β, respectively.

Figure 45 (a) shows impression deformations with time at different reference stresses and at 600 °C obtained for P91 steel and ½CrMoV steel, while Figure 45 (b) presents a comparison between the minimum creep strain data obtained by uniaxial

creep tests and the converted MSR data obtained by impression creep tests for the same materials.

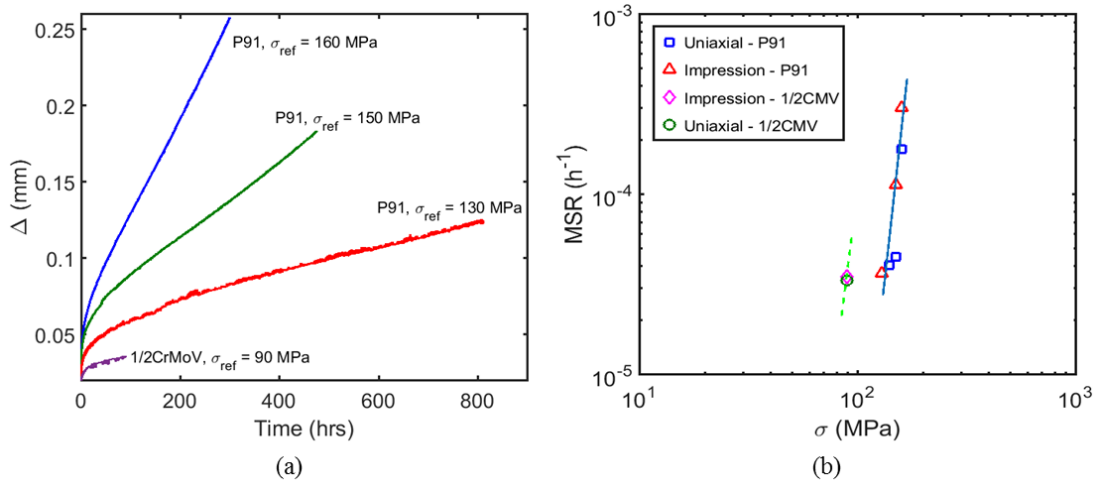


Figure 45. (a) Impression deformations with time at different reference stresses and 600 °C and **(b)** minimum creep strain rate data at 600 °C, obtained for P91 steel and ½CrMoV steel.

Figure 46 (a) shows impression deformations with time at different reference stresses and at 575 °C obtained for a cast ½CrMoV steel, while Figure 46 (b) presents a comparison between the minimum creep strain data obtained by uniaxial creep tests and the converted MSR data obtained by impression creep tests for the same materials.

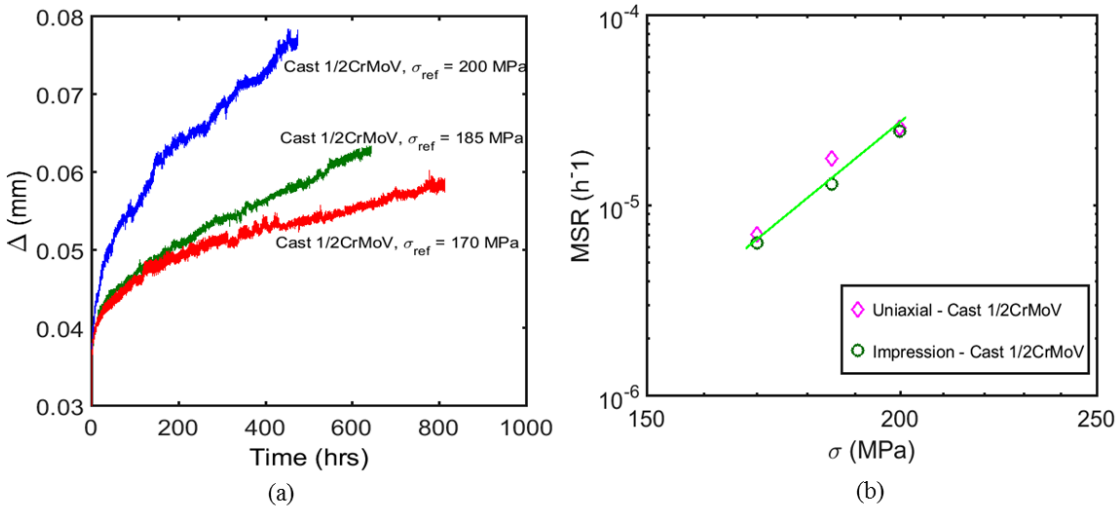


Figure 46. (a) Impression deformations with time at different reference stresses and 575 °C and **(b)** minimum creep strain rate data at 575 °C, obtained for a cast ½CrMoV steel.

Figure 47 (a) shows impression deformations with time at different reference stresses and at 650 °C obtained for P91 Bar257/KA1200 and P92 steels, while Figure 47 (b) compares the minimum creep strain data obtained by uniaxial creep tests with the converted MSR data obtained by impression creep tests for the same materials.

Converted MSRs from impression creep test presented so far show good agreement with the corresponding uniaxial data. The deformation versus time curve related to the specimen of P91 Bar257/KA1200 tested at 70 MPa shows a drastic increment in displacement at about 100 hrs. This behaviour is more likely related to a possible slipping of the extensometer than to temperature variations within the furnace and laboratory because the MSR in the secondary state before 100 hrs is the same as the MSR after 100 hrs.

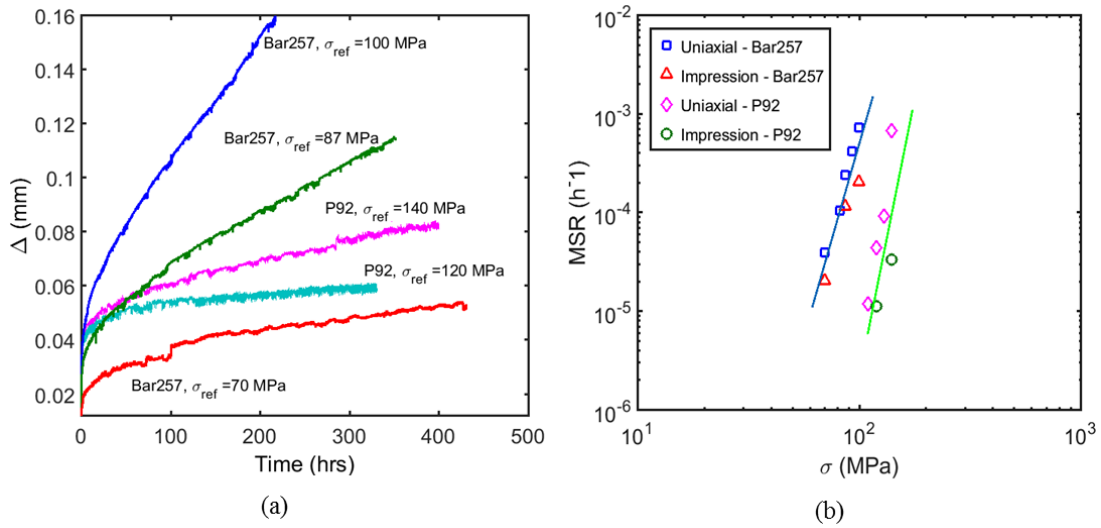


Figure 47. (a) Impression deformations with time at different reference stresses and 650 °C and **(b)** minimum creep strain rate data at 650 °C, obtained for P92 steel and P91 Bar257/KA1200 steel.

4.3 EFFECT OF MISALIGNMENT OF THE ICT INDENTER

During an impression creep test, the indenter should always be perfectly aligned with the specimen. When the tester machine is set up for the test, it may happen that the longitudinal plane of symmetry of the indenter is rotated by an angle, δ, with respect to the xz-plane around the vertical direction, *y*, as shown in Figure 48. In such a case, the contact area, A_c, between the indenter and the specimen will depend on the cosine of the δ angle, and, in particular, will increase with increasing δ. In fact, since the indenter is generally longer than the specimen, when the indenter is rotated of δ, a bigger region of the specimen is in contact with it. The new contact region is no longer that covered by a rectangle of area $A_c = bd$, but by a parallelogram of sides b' and d' and of area $A'_c = b'd$, where the width of the indenter, d, is the height of the parallelogram, as shown in Figure 48. b' and A'_c are given in equations (77) and (78), respectively.

$$b' = \frac{b}{\cos\delta} \tag{77}$$

$$A'_c = \frac{bd}{\cos\delta} \tag{78}$$

By substituting equation (78) in equation (53) and then in equation (57) (both presented in Chapter 2), the rate of the indenter vertical displacement in the steady state region of the test is given by equation (79).

$$\dot{\Delta}^c_{ss}(\delta) = \left(\frac{P\eta}{bd}\right)^n Bd\beta(\cos\delta)^n \tag{79}$$

The ratio between $\dot{\Delta}^c_{ss}(\delta)$ and $\dot{\Delta}^c_{ss}(\delta = 0°)$ is a function, *f(δ,n)*, of δ and *n* and is obtained by equation (80).

$$f(\delta, n) = \frac{\dot{\Delta}^c_{ss}(\delta)}{\dot{\Delta}^c_{ss}(\delta = 0)} = \frac{\left(\frac{P\eta}{bd}\right)^n Bd\beta(\cos\delta)^n}{\left(\frac{P\eta}{bd}\right)^n Bd\beta} = (\cos\delta)^n \tag{80}$$

When δ is small, the ratio between $\dot{\Delta}^c_{ss}(\delta)$ and $\dot{\Delta}^c_{ss}(\delta = 0°)$ becomes close to unity, as shown in Figure 49. From an engineering point of view, it is very unlikely that rotations of the indenter bigger than 3° occur during the test. For a P91 steel at 650 °C, *n* = 8.462 and the percent error in MSRs between the ideal (δ = 0°) and the worst (δ = 3°) situation is 1.2%.

The accuracy of the converted MSR depends on $\dot{\Delta}^c_{ss}$ (see equation (55) of Chapter 2), thus, angles bigger than 0° can lead to converted MSR that cannot be compared to the corresponding uniaxial data because the conversion relationships are based on the ideal hypothesis of δ = 0°. Nonetheless, errors due to indenter misalignment of up to 3° can still be accepted from an engineering point of view.

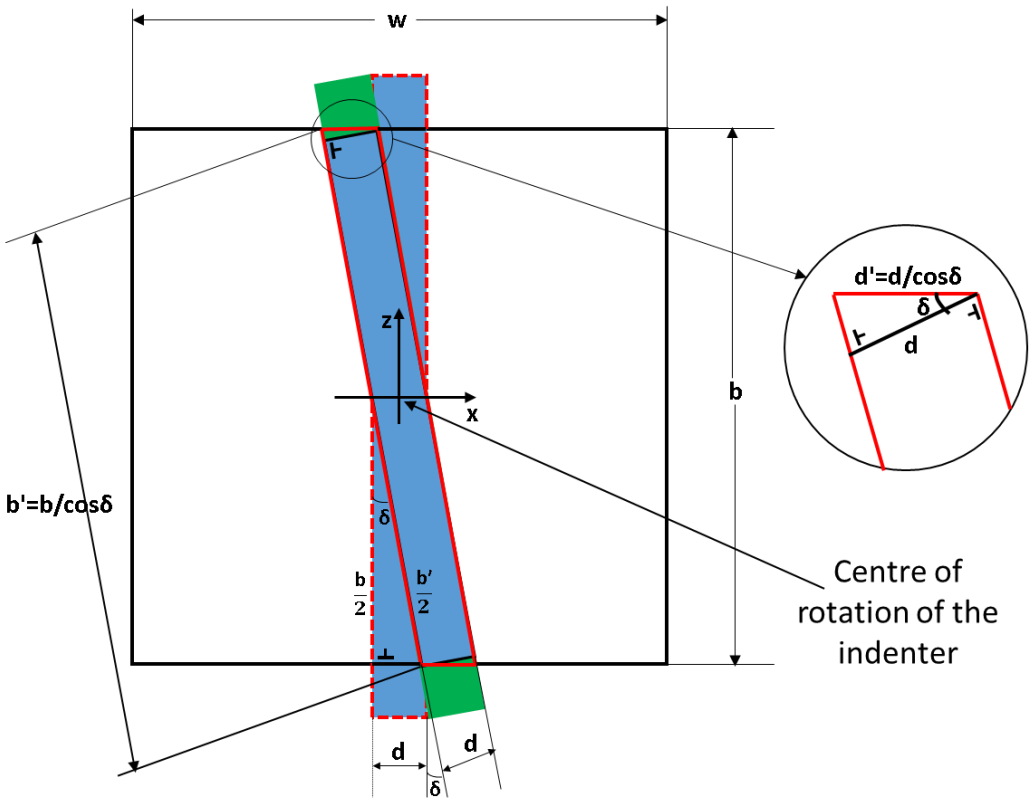


Figure 48. ICT specimen in the xz-plane with the indenter rotated of the δ angle: definition of the contact area.

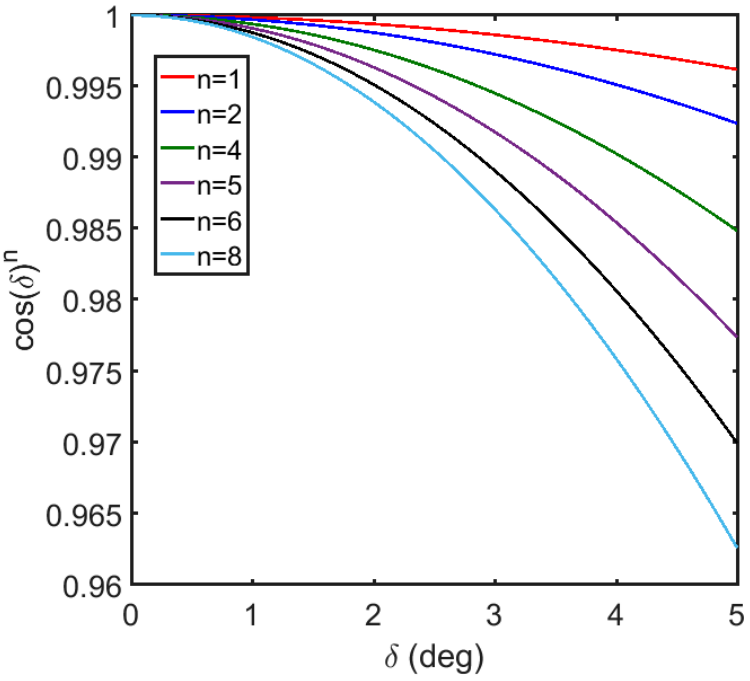


Figure 49. *f(δ,n) = cos(δ)*^{n} vs. δ.

4.4 GENERAL COMMENTS ON ICT CONVERSION PARAMETERS

The accuracy of the reference stress parameters, η and β, plays a critical role in converting creep deformation rates obtained by impression creep tests to the corresponding minimum creep strain rates. η and β are sensitive to the specimen dimension ratios (see Figure 23 (a) and Figure 23 (b) in Chapter 2), thus, care in calculating their values must be taken when "non-standard-sized" samples are used. An important aspect to be noted is that the material constant n depends on the test temperature and stress range. Therefore, since the conversion parameters do not depend on n, they do not depend on the test temperature either. This allows comparison of a large number of creep data of different materials tested at different temperatures by using the same values for η and β.

Data provided in Section 4.2 show that converted minimum creep strain rates are, in general, in good agreement with the corresponding uniaxial creep test data. On occasion, the converted impression MSRs could vary by a factor of up to 10 time different from the corresponding uniaxial minimum creep strain rates. Causes of this are likely to be partly related to the factors beyond the conversion relationships. For example if the indenter is misaligned with respect to the sample, using the reference stress parameters, which are derived from the idealised conditions, can still give accurate results (the maximum estimated error is 1.2%). Experimental evidence of data collected so far, in fact, indicates the reliability of the conversion relationships, even though a standard procedure for impression creep test and further improvements are still needed. In particular, the conversion parameters are determined without considering the geometry changes due to the indentation deformation during the test. Although relatively small deformations may be involved during impression creep test, the indentation depth is not constant and it differs from zero after a certain time. This may have a noticeable effect on the conversion parameters (and therefore on the reference stress) when the impression creep deformation is relatively large, and consequently requires further compensation.

Figure 50 shows the microstructure of a 316LN stainless steel sample near the contact area with the indenter, where three regions can be identified [173]. The grains in the first region, indicated as 1 in Figure 50, that is the closest to the indenter, are not significantly distorted, due to the hydrostatic stress field [7, 173]. On the contrary, the grains in the second zone, indicated as 2 in Figure 50, are stretched by shear

deformation, while the grains in the third region, indicated as 3 in Figure 50, that is the farthest from the indenter, do not show any distortion, meaning that their shape is not affected by the test loading conditions [7, 173]. Although it can be concluded that plastic deformation occurs in the specimen areas only in the vicinity of the indenter [7, 173], elastic-plastic-creep FE analysis could give reasonably accurate results in establishing the conversion parameters with respect to the elastic-creep FE analysis performed so far. In fact, the conversion parameters highly depend on the accuracy of the creep deformation rate in the steady state, especially if the applied load is high enough to induce relatively large deformation in the indentation area.

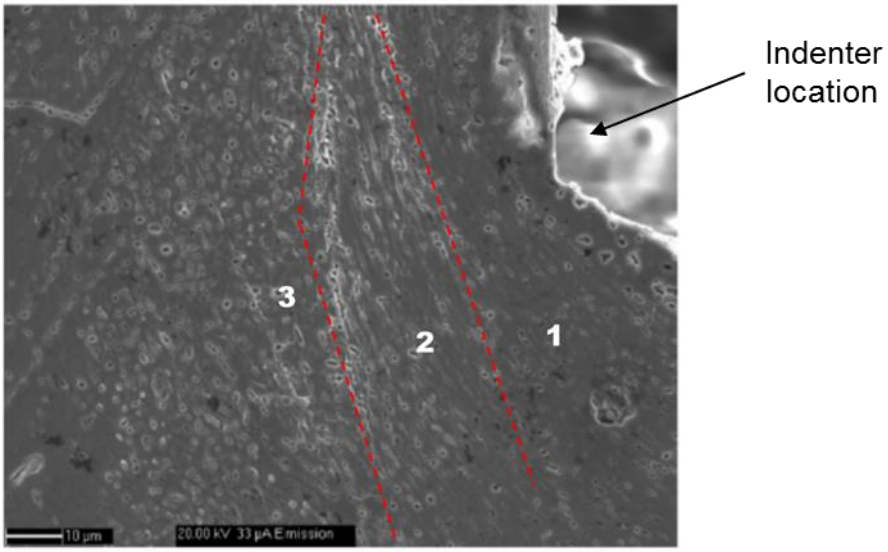


Figure 50. Microstructure of a 316LN stainless steel sample near the contact area with the indenter, adapted from ref. [173].

As an example, Figure 51 shows the contour plot of the shear component of the creep strain tensor in an ICT specimen of P91 steel, obtained by an elastic-plastic-creep FE analysis at 650 °C, where regions 1, 2, and 3 described above can be easily recognised and the rotation of the grains in region 2 can be observed. The plastic properties of the P91 steel used for the analysis were the same used by Cortellino et al. in ref. [114] for the same material; Norton's material constants were taken from ref. [174]. In the 2D FE model, the indenter and the support plane were modelled as rigid bodies, while the specimen was modelled as a deformable body. A frictionless contact formulation was used to model the interaction between the indenter and the specimen and a Lagrangian contact formulation was used for the interaction between the specimen and the support plane. Quadratic plane strain elements (CPE8 [17]) were used for the specimen meshing. A mesh convergence study led to refine the mesh in

the area of the specimen underneath the indenter with elements of 8.33E-3 mm size. The support plane was constrained in rotation and in translation in both vertical and horizontal directions. Since only half of the specimen and of the indenter were modelled, the axis of symmetry was constrained in translation in the horizontal direction. The indenter was also constrained in translation in the vertical direction.

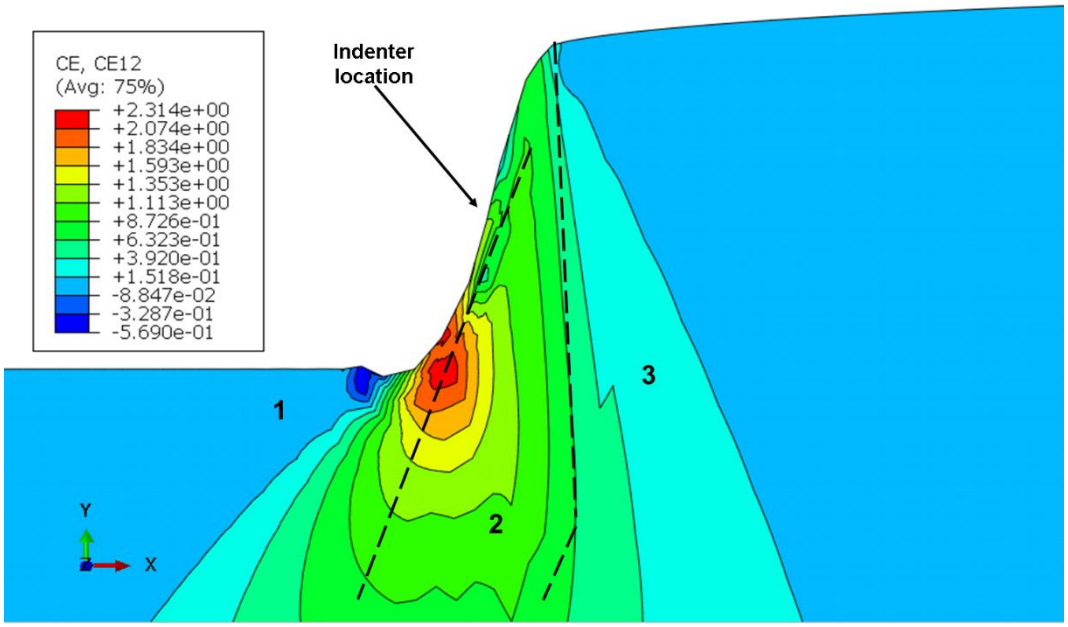


Figure 51. Shear component of the creep strain tensor in an ICT specimen of P91 steel, obtained by an elastic-plastic-creep FE analysis at 650 °C.

4.5 CONCLUSIONS

In conclusion, impression creep testing technique is easy to perform and it has shown to be reliable in providing secondary creep properties, e.g. converted minimum creep strain rate. Creep data acquired by means of impression creep tests could be useful in a life assessment model for power plant components. Collection of these data from the service-aged structures in power plant companies can be a major concern for the utilities that, generally, in order to perform conventional uniaxial creep tests, have to remove a large volume of material from out of service components, which then need to be weld repaired, resulting in potentially large costs for the power plant. Although a standard procedure still does not exist, a way forward to overcome these problems and take away only a small amount of material from in-service components could be considering impression creep testing technique as a valuable candidate to, in part, substitute traditional creep tests.

5 INVESTIGATION ON THE CREEP DAMAGE EVOLUTION OF AN EX-SERVICE CrMoV PIPE SECTION THROUGH IMPRESSION CREEP TEST AND METALLURGICAL INSPECTION DATA

5.1 INTRODUCTION

In order to assess repair ranking and replacement strategies of power plant components, which are commonly operating far beyond their designed life, power plant utilities generally carry out off-load and on-load monitoring. Conventional off-load monitoring can comprise passive strain measurement, material composition checks, surface creep replicas and surface hardness data at room temperature. Pipe hanger movement measurements, which are taken when the system is hot (in-service at full load) and cold, are also required periodically. These are used to remedy potential problems due to imposed mechanical loads when the piping system is returned to service and operating at full load and temperature over the next operational period [20]. However, this information is not used as an input into a predictive creep life assessment of the piping system. Passive strain measurements are regularly recorded during an outage on a limited number of components such as main steam lines and selected steam headers, however they are only used as indicators of accumulated creep strain and creep strain rate due to measurement uncertainty [20]. Surface creep replicas are generally targeted at welds and help in locating possible creep voids per square mm and potentially creep void alignment and evidence of micro-cracking in key locations such as the heat affected zone, but cannot be used in a predictive creep damage model [20]. Surface hardness data obtained at room temperature during an outage overhaul are not specifically used in a predictive life assessment model. Decisions on repair or return to service that use hardness data is typically based on an assessment of the rate of change in hardness and experiential knowledge [20], which is invariably complemented by scrutiny of the results from adjacent surface replicas. When a large amount of material is available (for example if a pipe spool is removed to enable installation of a new weld), uniaxial creep tests can be carried out to collect the material creep properties.

On-load monitoring comprises routinely recording of steam temperature and pressure data at selected key points in the process system, in order to evaluate the Creep Effective Temperature (CET), defined as the average temperature at which all of the creep damage can be equated to [20]. The calculation of the creep rupture life

by means of CET gives a value of creep rupture life that depends on stress and temperature. This method can give the reduction in creep rupture life of the component due to variation in temperature or stress; however the analytical sensitivity to modest increases in operating conditions makes planning the scope of subsequent outages or replacement exercises, based on this information, fraught with uncertainty, which can lead to possible premature replacement of large sections of pipework [20].

It is clear that the current approach for the evaluation of life consumption is based on experiential knowledge and on a limited use of analytical methods. This holistic condition assessment process is based on the described off-load and on-load condition monitoring methods, but does not include the proactive use of predictive life assessments beyond the next major statutory outage, and does not seek to integrate the various disparate data sets obtained from the plant outage and on-load monitoring. Miniature specimen creep testing techniques could be successfully used together with the currently used condition assessment methods in order to provide a more predictive life assessment approach [20]. As opposed to the conventional uniaxial creep tests, miniature creep testing techniques require only a small volume of material to machine the specimen and can be successfully used to collect creep properties of critical regions of power plant components, including, for examples, welds with heat affected zones and around pipe bends. Moreover, miniature creep testing techniques can be treated as quasi-non-invasive methods and do not require weld repair when samples are carefully removed (scooped) from in-service components as long as, for example, the maximum excavation depth does not exceed 10% of the wall thickness of the main steam pipe [83-85]. The location selected for the removal of the material requires careful consideration of past inspection findings and may require some level of re-inspection at subsequent outages.

The aim of this work is to compare the capability of the different techniques by characterising the through thickness behaviour of a 46-year-aged CrMoV pipe section by means of conventional and unconventional testing methods. In particular, among the conventional methods, surface replicas and surface hardness data will be considered. For unconventional testing method a miniature creep testing technique, such as impression creep test, will be used to assess the creep properties of the material through the thickness of the pipe section [104, 116, 136, 175]. Through thickness

hardness data could also be potentially related to minimum creep strain rate data obtained by means of impression creep tests, which is explored in this study. In addition, examinations of other aged ex-service CrMoV pipe material is discussed and conclusions are drawn with reference to the detailed examination of the 46-year-aged CrMoV pipe section.

5.2 EXPERIMENTAL WORK

5.2.1 Tested material

The tested material was removed from service in 2014, after initial installation in 1968. It is a plain, low-alloy steel CrMoV pipe section that also contains a weld, with a site reference designation BW61. The plain pipe material section, containing weld BW61, was removed from main steam leg B1, with the position indicated in Figure 52 and the orientation illustrated in Figure 53, where the dotted lines represent the pipe section upstream the pipe section studied in this research. Hence, the straight piece of material removed is just upstream of a 90° vertical bend.

The material specimen was removed from service in 2014 for examination to help support limited continued operation of other operating units until a full pipework replacement could be undertaken. At the time of removal, the pipe section had undergone 271,770 hours and 2739 unit starts.

Section 5.2.2 provides further details on prior in-service examinations and operating history.

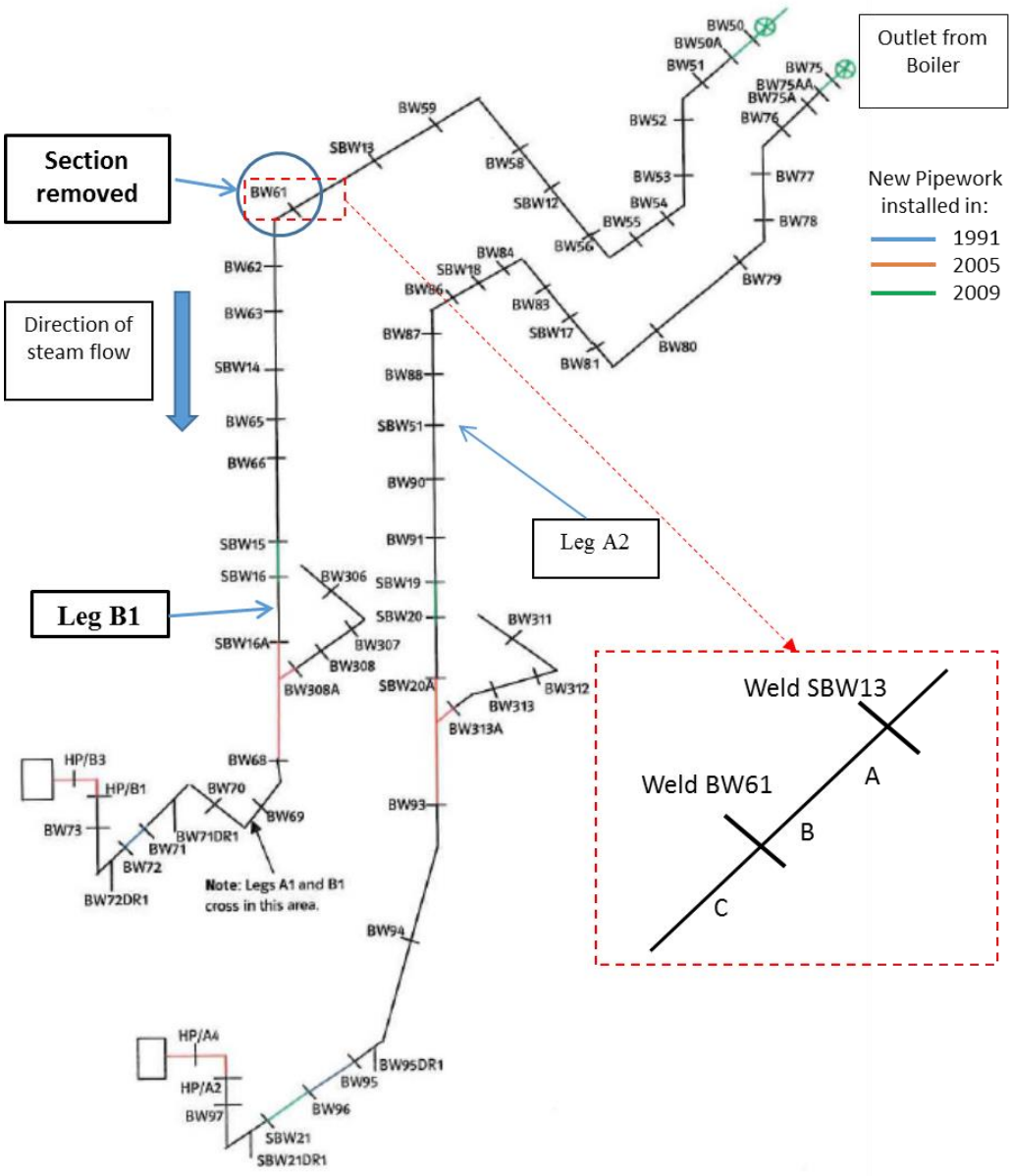


Figure 52. Pipe section position in steam leg B1.

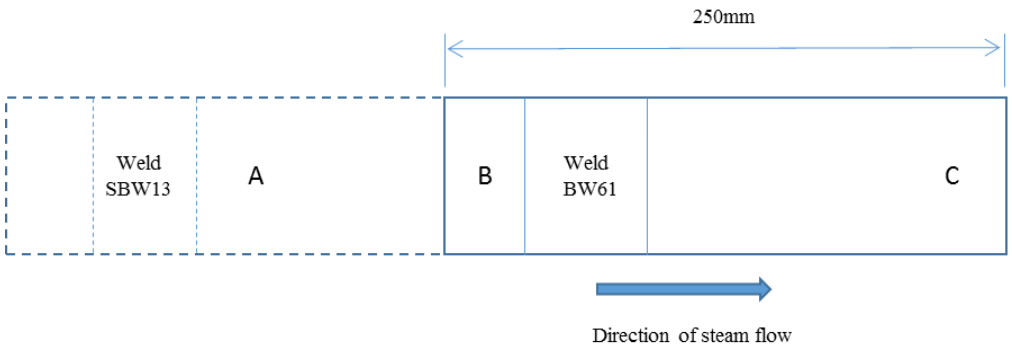


Figure 53. Pipe section orientation. Dotted lines represent the pipe section upstream the pipe section take into account in this work, which is represented by solid lines. Approximate pipe system positions represented by A, B and C.

5.2.2 Operating history and prior examinations

Section 5.2.1 describes the position of the section in main steam leg B1 and age on removal. The last in-service inspection was undertaken in 2009, with a service duty of 242,773 hours and 2522 unit starts. The pipe was subjected to an internal pressure of 168 bar.

Table 15 provides the metallurgical parent material assessments undertaken during the 2009 outage for the material specimen and a selection of adjacent pipe sections both upstream and downstream. In Figure 52 and Figure 53, location SBW13-BW61 adjacent to weld SBW13 is indicated with A, location SBW13-BW61 adjacent to weld BW61 is indicated with B and location BW61-BW62 tangent position, downstream of weld BW61, is indicated with C.

Table 15. Outage parent material metallurgical assessment in 2009.

Pipe section location on leg B1 (Ref Figure X1)	Details of position in relation to the pipe weld	Surface creep replica assessment	Hardness (HV)
BW59-SBW13	Adjacent to weld SBW13	Isolated	135
SBW13-BW61 (Position A in Figure 53)	Adjacent to weld SBW13	Low orientated	139
SBW13-BW61 (Position B in Figure 53)	Adjacent to weld BW61	Isolated	141
BW61-BW62 (Position C in Figure 53)	Tangent position, downstream of weld BW61	Clear	139
BW61-BW62	Bend extrados	Very isolated	131
BW61-BW62	Tangent position, upstream of weld BW62	Clear	143
BW62-BW63	Adjacent to weld BW62	Clear	136
BW62-BW63	Adjacent to weld BW63	Very isolated	133

For convenience the creep cavity count assessment level criteria used in this study is defined in Table 16 [20].

Table 16. Creep replica assessment level.

Replica Assessment Level	Definition	Creep Cavities per mm^2
1	Clear	0
2	Very Isolated	1-10
3	Isolated	10-50
4	Low Orientated	50-250
5	Orientated (Including High Orientated)	250-500
6	Grouped	500-1000
7	Aligned	1000-1500

The notable observations from the weld surface replica examinations for those welds identified in Table 15 is as follows:

- Weld BW58: Low orientated creep damage,
- Weld BW61: High orientated creep damage, and
- Weld BW62: Low orientated creep damage.

Hence, the condition of the parent material adjacent to weld BW61 is of interest, considering the creep replica assessment of the weld that reports high orientated creep damage.

The adjacent straight section immediately upstream of BW61, to include weld SBW13 (see Figure 52), was also removed in 2014 and subjected to a through section creep replica assessment. The parent material condition at a position 100 mm downstream of weld SBW13 (near position A in Figure 53) was obtained from the surface and depths below the outer surface at 1 mm, 5 mm and subsequent intervals of 5 mm. The surface replica revealed a creep cavity count of 50 cavities/mm^2 with all the other depths showing a zero cavity count, apart from a measurement of 7 cavities/mm^2, at a depth of 35 mm.

Periodic assessments of the operating conditions are undertaken at various stages in life, typically this involves obtaining a six-month block of steam temperature and pressure data and computing the creep effective temperature (CET), which is explained in detail in [20]. For leg B1, the design temperature is 568 $^{\circ}$C and the most

recent CET estimates for this leg were 564 ˚C in 2005/2006 (operating duty 215,866 hours and 2295 unit starts) and 559 ˚C in 2010.

Diametral strain measurements are also periodically carried out at various strategic locations on the pipe system, usually targeting circa three locations on the pipe system, towards the top at the boiler outlet, a mid-section position and finally one towards the high pressure steam chests. These measurements, taken with a site micrometer over creep pips installed on the outer diameter, can be prone to inconsistency and error [20]. Various main steam diametral measurements on main steam leg B1 have been taken since first unit operation in 1968; these are reproduced for completeness in Table 17. On this leg there are four creep pips installed at each pipe position, hence measurements are taken using the two pairs of diametrically opposing creep pips.

Table 17. Steam leg B1 historical pipe diametral measurements.

Position on pipe system (Level in feet above ground)	Diametral position	Diameter (mm)				
		1968 (0 hours)	1995 (163,064 hours)	1999 (183,040 hours)	2005 (215,866 hours)	2009 (242,773 hours)
42 ft (Vertical pipe section)	Pair 1		356.44	356.62	356.69	356.22
	Pair 2		358.34	358.42	357.71	358.88
	Average		357.39	357.52	357.20	358.05
104 ft (Vertical pipe section)	Pair 1	360.07	360.25	360.43	360.78	360.34
	Pair 2	360.55	360.71	360.88	360.97	360.74
	Average	360.31	360.48	360.66	360.88	360.54
142 ft (Vertical pipe section)	Pair 1	357.71		361.59		
	Pair 2	357.45		352.76		
	Average	357.58		357.17		
164 ft (Horizontal pipe section)	Pair 1		358.37	356.01	358.44	
	Pair 2		357.00	356.72	356.80	
	Average		357.68	356.36	357.62	
	New Pair 1			356.01		356.89
	New Pair 2			356.72		356.72
	New Pair Average			356.36		356.80

The inconsistencies are evident from inspection of the periodic diametral measurements in Table 17, which in some instances show decreasing strain levels over time. Typically, the approach to confirm the acceptability of measurements is to focus on those which show a successive and plausible increase in diameter. The data in Table 17 are notable for their inconsistency across the four different pipe measurement positions. However, the "new pair" measurements at the 164 foot level show a degree of plausibility and are also relatively close to the position of weld B63. For this data, taking the worst case two successive measurements for "new pair 1", this converts to a strain rate over the period 1999 to 2009 (59,733 hours) of $4.2 \times 10^{-8} hr^{-1}$. This subsequently can be converted to a minimum creep life of ~ 310,000 hours. Other reviews [20] describe case studies with similar diametral measurements, along with the shortfalls.

In summary, sections of parent pipework adjacent to welds showing relatively high levels of creep damage from outage inspections were selected for removal from the operating unit in 2009. The purpose of this was to assess the condition of the parent material by examination of the through thickness distribution of creep cavities and hence underpin operation of other units, until their pipe systems can be replaced. The limited examination of through thickness creep cavity distribution through the parent material, adjacent to weld SBW13 and upstream of the specimen examined in this study, showed only surface cavitation of any note.

The available information on operating conditions and prior inspection history related to the specimen examined in this study indicates an advanced age at 271,770 hours, but with some indicators of adherence to design operating limits due to historical CET studies. It is noted that based on very limited diametral strain measurements that the parent material may be > 85% creep life consumed (based on minimum creep properties).

Hence, the laboratory examination and testing of the selected section (weld BW61 and parent material indicated with B and C in Figure 53) is necessary, which aims to further assess the condition of the material status with a variety of techniques, to seek any realistic correlations, and to make practical recommendations on the use of the techniques on service aged materials.

5.2.3 Test program

The parent material composition, in wt%, is reported in Table 18 and it has been taken from the outer surface of the BW61 pipe section. This study only concerns the pipe section parent material. The test program aims to characterize the material behaviour through the thickness of the pipe and by the collection of room temperature data, such as hardness, surface replicas, and high temperature data from impression creep tests (ICTs). The impression creep tests have been carried out at a temperature of 575 °C, at three reference stresses of 110, 130 and 150 MPa.

Table 18. Material composition in wt% of the tested material.

C	Si	Mn	P	S	Cr	Mo	Ni
0.176	0.330	0.580	0.0186	0.0266	0.388	0.578	0.103
Al	**Co**	**Cu**	**Nb**	**Ti**	**V**	**W**	**Pb**
0.0959	0.012	0.1660	<0.005	0.0059	0.381	0.124	<0.050

Figure 54 (a) shows a schematic representation of the selected pipe section (weld BW61 and parent material indicated with B and C in Figure 53) from which the test samples have been machined and Figure 54 (b) shows the pipe section and the location of weld and ICT specimens (see Figure 53 for the section and steam flow orientation during service).

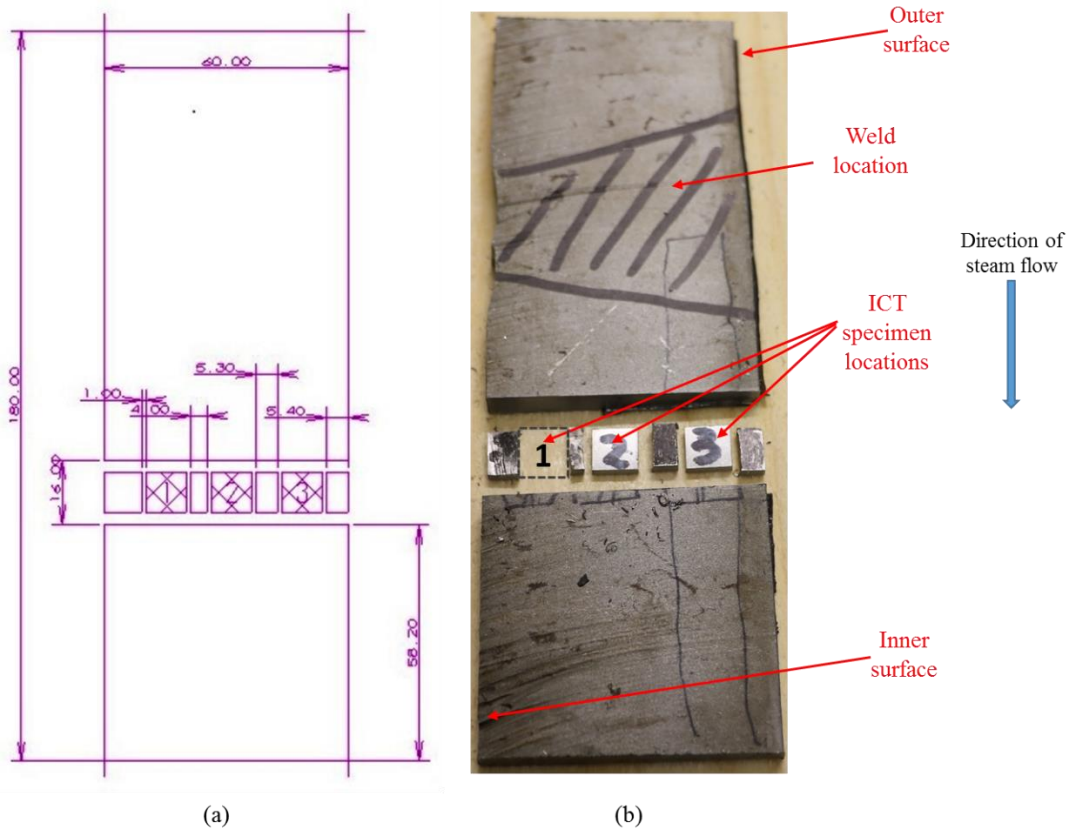


Figure 54. (a) Schematic representation of the pipe section from which the test samples have been machined (dimensions in mm), and (b) the pipe section and location of weld and impression creep test specimens.

5.2.4 Microstructure

For the microstructure investigation of the as received material, four specimens, T1, T2, T3 and T4 (from the outer to inner surface), have been machined through the thickness of the pipe section and away from the weld as far as possible. The samples dimensions are 10x10x2.5 mm. Figure 55 shows the specimens and the

radial, *r*, and axial, *a*, directions of the pipe section. Optical micrographs and SEM images have been taken from the centre of each sample and are showed and descripted in Section 5.3.1.

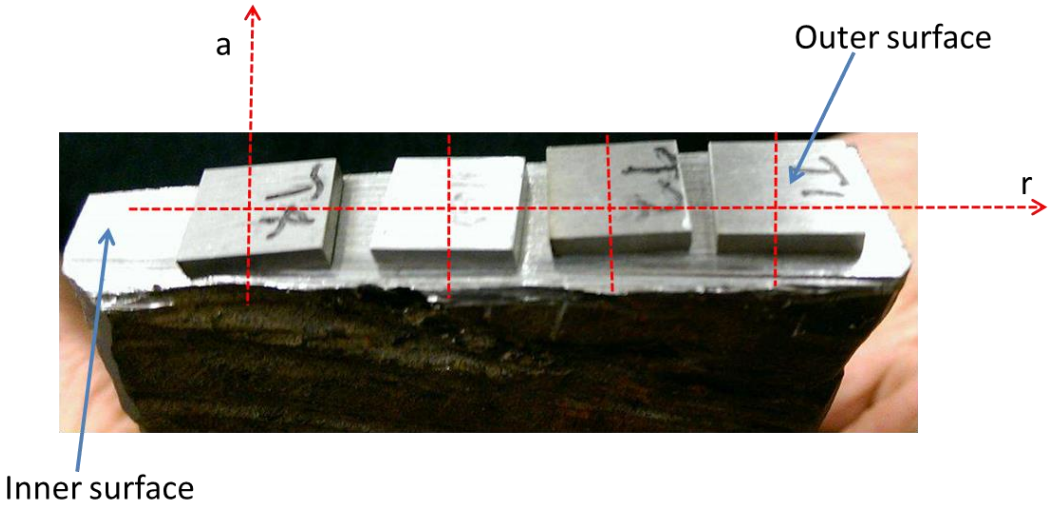


Figure 55. Specimens used for the microstructural investigation and the radial, *r*, and axial, a, directions of the pipe section.

5.2.5 Hardness and replica

5.2.5.1 Hardness tests

Hardness tests were carried out along the length of a slice, similar to that shown in Figure 54 (b), of 200 mm length along both the inner and the outer surfaces in five different positions. As a general rule for obtaining a successful hardness value, every indentation must be carried out at a distance of at least 3 or 4 times the length of the indentation diagonal (in μm) [37, 50]. Therefore, in order to assure enough distance among the indentations and between indentations and borders, only four measurements had to be considered for each position. The tester machine used for the tests was a Vickers-Armstrongs HTM 2000 and the load used was 20 kgf.

Micro-hardness tests have been carried out on the specimens T1 to T4 in order to assess a potential variation in hardness through the thickness of the pipe. In the axial direction 20 measurements were taken, while in the radial direction only 10 measurements were taken as the scatter in data was low (of the order of 10-20 HV). The tester machine used for the tests was a Buehler 1600-6400 and the load used was 0.5 kgf.

5.2.5.2 Surface replica for creep cavity count

The replicas were assessed for cavitation levels using an optical microscope at a magnification of 500x. As shown in Figure 56, where *r* and *a* indicate the radial and the axial directions of the pipe, respectively, assessments were taken at four different positions along the hoop direction on the slice of material: two positions in the parent material (location I and IV in Figure 56), one through the centre of the weld (location II in Figure 56), and one coincident with the Type IV region of the HAZ (location III in Figure 56). Cavity count assessments were carried out starting from the outer surface of the pipe fully through wall in the radial direction at 6-7 mm intervals, resulting in a through wall cavity profile (10 readings in total for each position along the hoop direction). For parent and weld material assessment, two readings were recorded as "Peak", that is the maximum number of cavities observed in one field of view, and "Background", that is the average number of cavities observed over a number of fields. These readings were then converted into a reading of cavities/mm^2. In the Type IV region only peak values were considered.

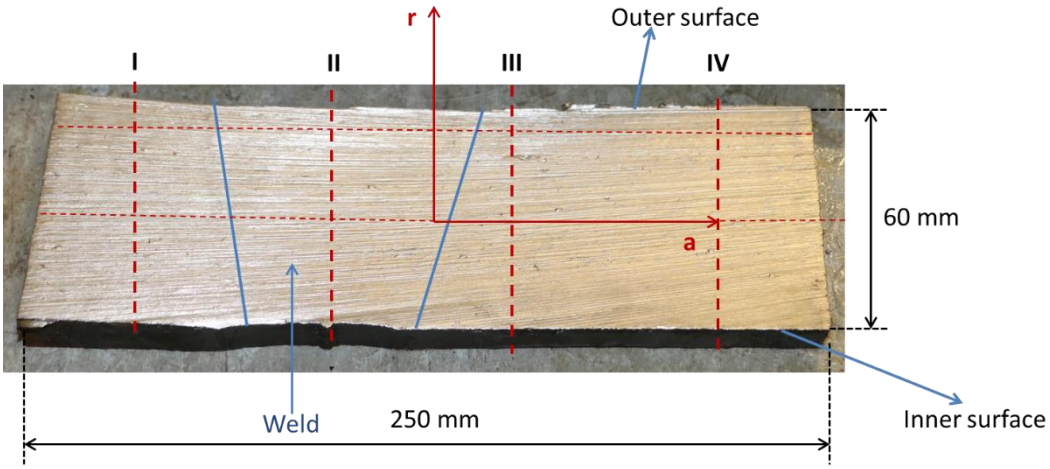


Figure 56. Position of replicas.

5.2.6 Impression creep test

For this work, impression creep test specimens have been machined through the thickness of the pipe section according to Figure 54 (a) and Figure 54 (b). A summary of the test program is collated in Table 19. All of the specimens have been tested at 575 °C.

Table 19. Impression creep test program.

Sample	Position through the thickness (centre of the specimen) from the inner bore	Reference stress in MPa
1	20 mm	110 130 150
2	34.3 mm	110 130
3	49.6 mm	110 130 150

5.3 CHARACTERISATION OF THE PIPE SECTION MATERIAL

5.3.1 Microstructure investigation

The optical micrographs presented in Figure 57 (a) to Figure 57 (d) show the microstructure of the specimens T1 to T4 (Figure 55). From this optical investigation, significant differences in the metallurgy among the samples cannot be revealed, but it is possible to note a progressive increase in the grain size from the outer to the inner surface. This can be due to both manufacturing and in-service creep. The hoop stress varies through the wall of the pipe due to internal pressure loading being maximum in the inner surface, and on some pipe sections, pipe system bending loads may also act to increase this through section stress gradient. SEM images of the specimens T1, T2 and T4 were also taken and they are illustrated in Figure 58 to Figure 60. Grain boundary precipitate has been found in all of the specimens, as shown in Figure 58 (a) to Figure 58 (d) and in Figure 60 (a). A small number of cavities was only observed in the T1 sample (see Figure 59 (a) and Figure 59 (b)), while some inclusions were found in all of the analysed specimens (see Figure 58 (e) and Figure 58 (f)). The detachment of the grain boundary from the matrix, showed in Figure 59 (a) and Figure 59 (b), is mostly due to creep, while the inclusions presented in Figure 58 (e) and Figure 58 (f) are considered due to manufacturing.

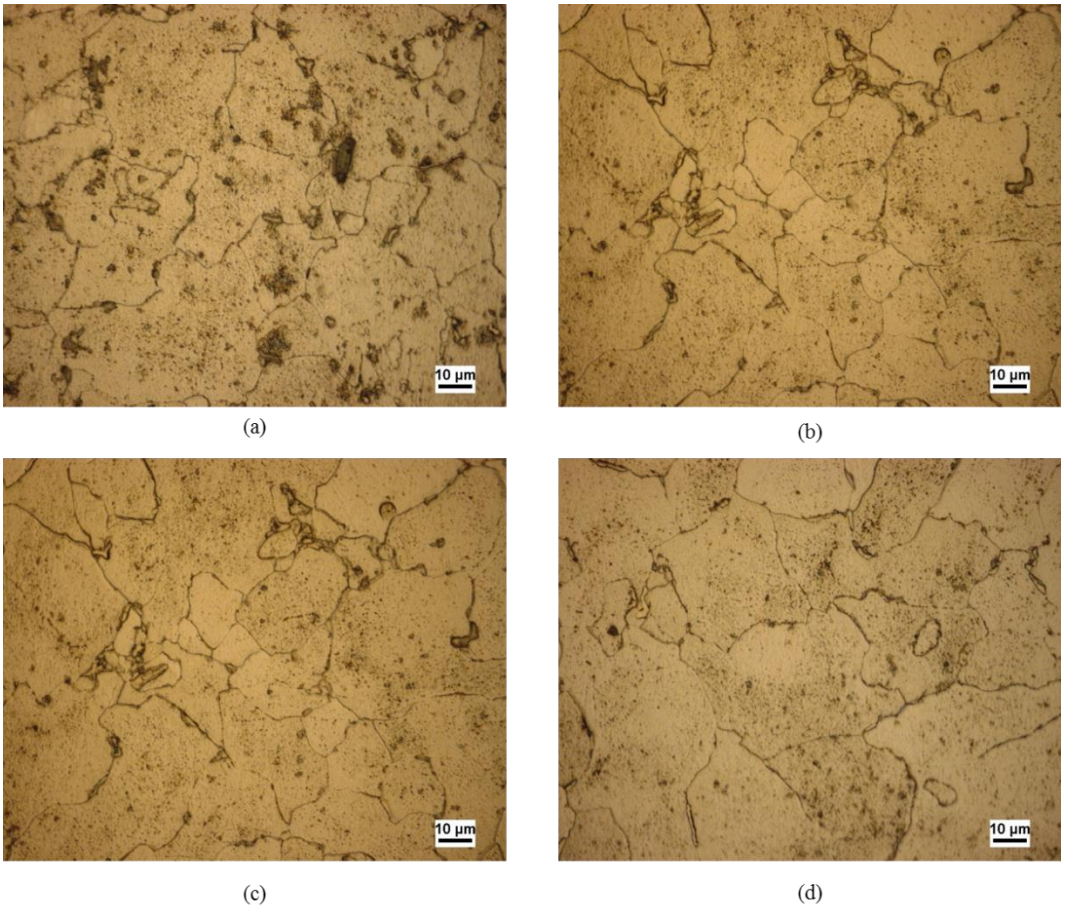


Figure 57. Optical micrographs of specimen **(a)** T1, **(b)** T2, **(c)** T3 and **(d)** T4.

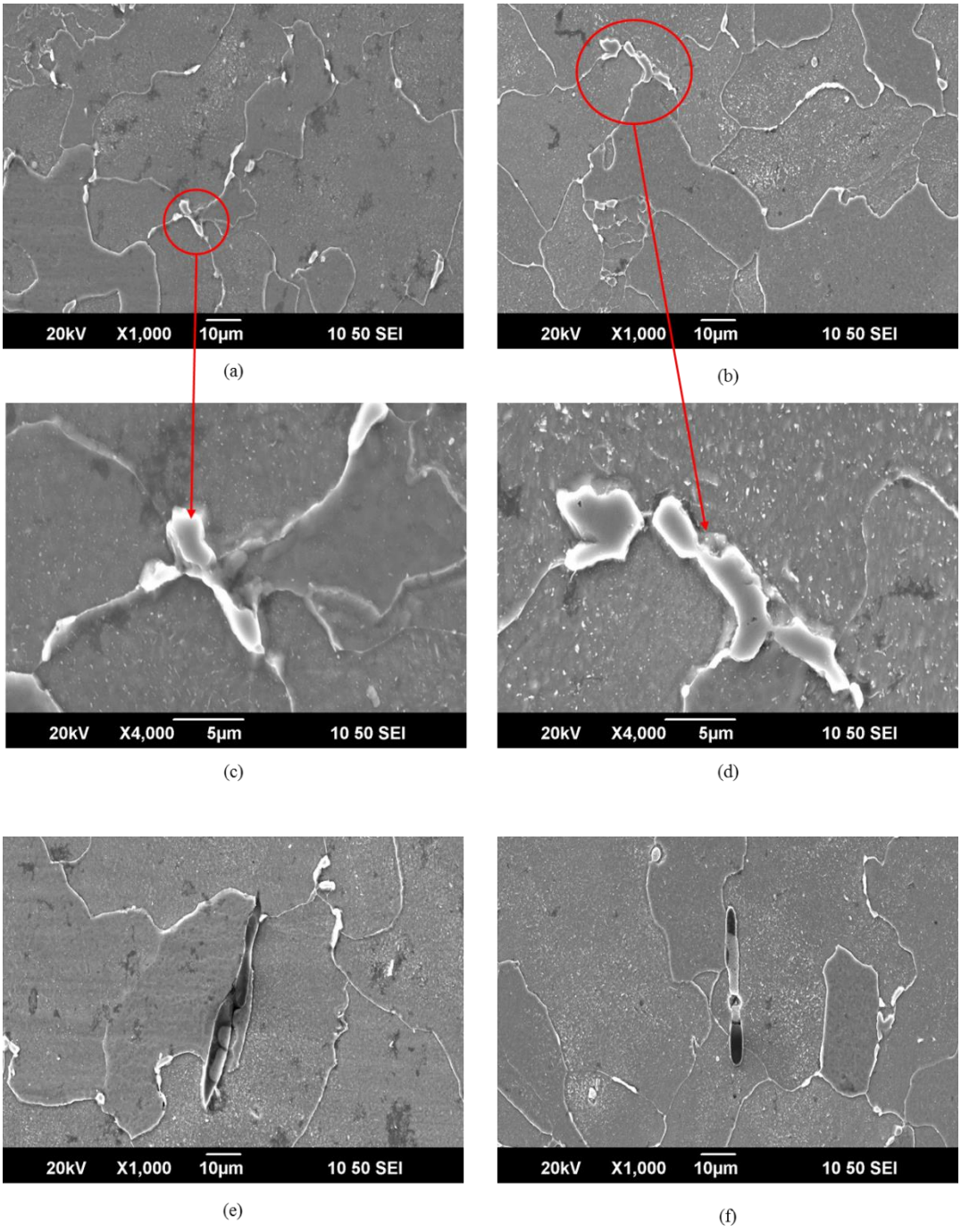


Figure 58. SEM images of specimens **(a)** T1 and **(b)** T4; details of the grain boundary precipitate of specimens **(c)** T1, **(d)** T4; inclusion in specimens **(e)** T1 and **(f)** T4.

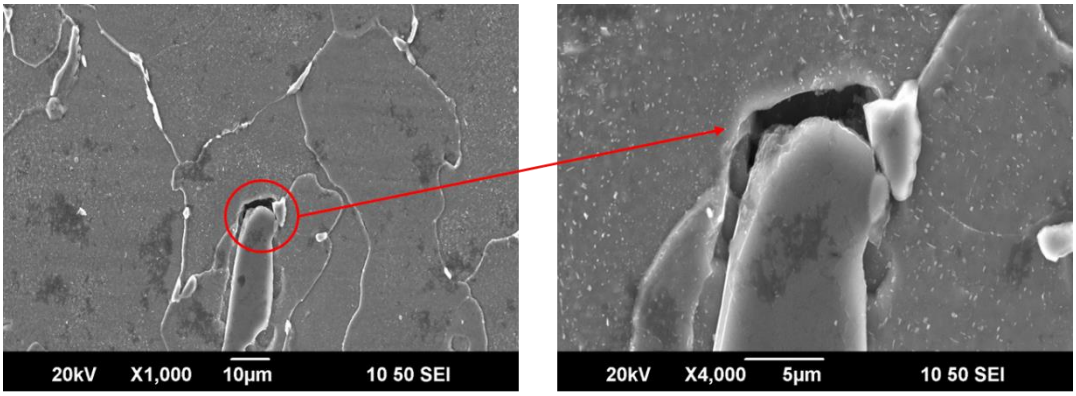


Figure 59. (a) SEM image of a cavity in specimen T1 and **(b)** detail of the cavity.

A sub-micron precipitate phase in the matrix of sample T2 and a rather coarse grain boundary precipitate, which might be an alloy carbide, have also been found, as shown in Figure 60 (a). The spectrum of the chemical composition of such precipitate is shown in Figure 60 (b) and reported in Table 20 for clarity. The concentration of heavy metals, excluding iron, results in 28.75%, which is higher than the 3% precipitates found in the outer surface of the pipe section (see Table 18). This means that the matrix surrounding the grain boundary precipitate is weaker than the matrix in the outer surface as, due to creep, it has lost most of the elements commonly used to strength a 0.5CrMoV material because of their migration to the grain boundary. However, this characteristic grain boundary precipitate was rarely observed in the analysed specimens.

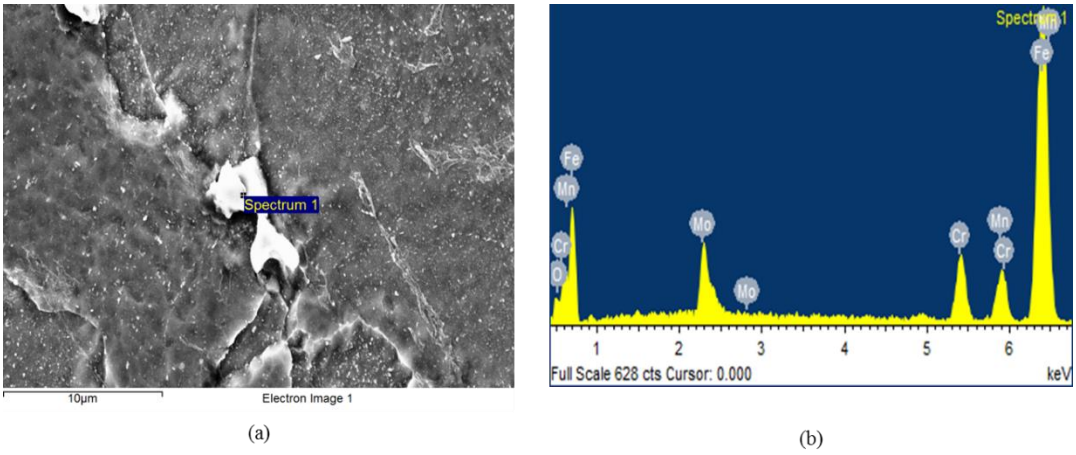


Figure 60. (a) SEM image of precipitate and **(b)** spectrum of the chemical composition of precipitate in specimen T2.

Table 20. Chemical composition of precipitate in specimen T2.

Element	Weight%	Atomic%
O	2.25	7.73
Cr	8.56	9.06
Mn	8.40	8.42
Fe	69.01	68.03
Mo	11.79	6.76
Total	100.00	100.00

The microstructural analysis has not revealed any acute signs of material damage through the section of the pipe. The prior 2009 in-service condition assessment in Table 15 identified surface creep cavitation on this particular pipe section and adjacent downstream and upstream positions, albeit at relatively low levels. Subsequent examination of the creep cavity distribution is discussed in Section 5.4 and reveals this to be a surface effect, with little evidence of creep cavity formation through the pipe thickness.

5.4 HARDNESS AND REPLICA INVESTIGATION

Macro hardness values along the length of the pipe were found to be consistent in both the inner and the outer surfaces and are here plotted in Figure 61 (a) and Figure 61 (b), respectively. Standard deviation, mean, maximum and minimum values of the hardness data for each position are collated in Table 21. Very large scatter in hardness data at the weld position was observed, meaning that those data cannot be used in a predictive lifing model. This very large scatter in the readings in the weld are unusual based on macro hardness sampling of other similar weldments [20].

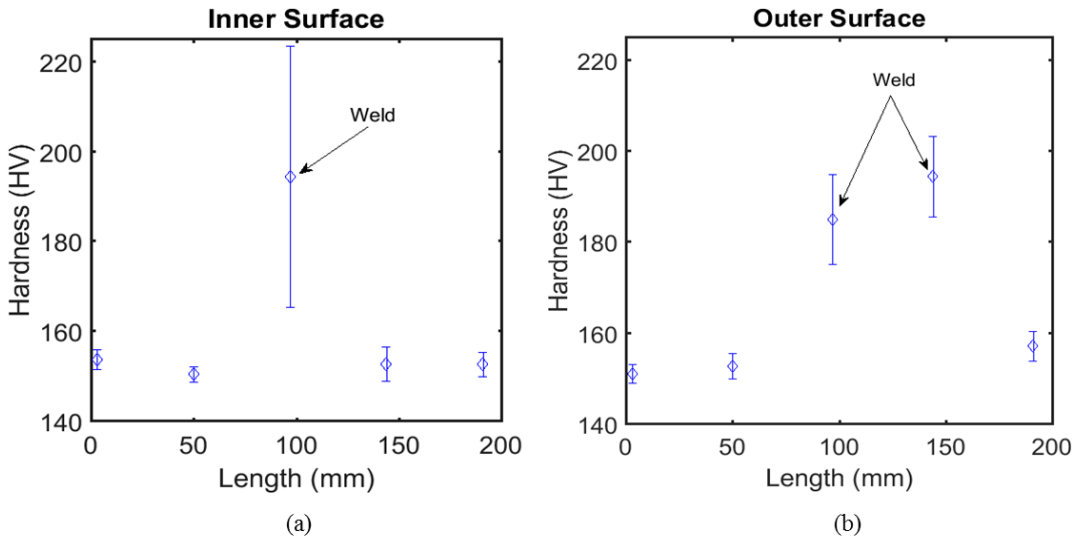


Figure 61. Hardness values along the length of the pipe section on the **(a)** inner and **(b)** outer surfaces.

Table 21. Standard deviation, mean, maximum and minimum values of the hardness data.

	Mean (HV)	Std (HV)	Min (HV)	Max (HV)
Inner Surface				
3 mm	153.75	2.17	150.6	155.4
50 mm	150.43	1.76	148.6	152.3
97 mm	194.45	29.14	168	221.10
144 mm	152.73	3.85	148.20	157.60
191 mm	152.70	2.69	151.10	156.70
Outer Surface				
3 mm	151.08	2.08	149.40	154.10
50 mm	152.73	2.75	150.70	156.70
97 mm	185.05	9.85	177.30	198.30
144 mm	194.45	8.81	182.80	203.50
191 mm	157.18	3.20	154.50	161.70

Table 22 shows the results of the cavitation assessment. The levels of cavitation in the Type IV region peaked at 240 cavs/mm^2 at a distance of 5 mm below the outer surface of the pipe which is typical of that generally seen in service (cavitation usually initiates just below the weld capping bead at a depth of 2-3 mm below the pipe outer surface). A cavitation level of 240 cavs/mm^2 is relatively low and could be managed in service with scheduled inspections before repair would be required.

The mid-weld position showed relatively low levels of cavitation close to the outer surface, in reality it is difficult to distinguish between reheat cavitation and genuine creep cavitation at these levels.

The levels of parent cavitation were much higher at position I when compared to position IV. It is also notable that the levels were consistent throughout the wall of the section, usually it would be expected that the levels would be higher at the outer surface of the pipe.

With reference to Table 16, creep cavity level was assessed as low orientated for replicas I, II, and III, and as isolated for replica IV, based on the maximum cavity count in positions 1 and 2.

Table 22. Creep cavity count (in cavs/mm^2) from the outer to the inner surfaces of the pipe section.

	Replica I	**Replica II**	**Replica III**		**Replica IV**
Through thickness position (mm)	**Parent**	**Weld**	**Type IV**	**Parent (10 mm from Type IV)**	**Parent**
60	75	75	60	45	0
53	75	15	240	60	15
47	75	45	195	75	15
40	60	0	105	60	0
33	75	0	150	30	15
27	75	0	45	45	0
20	30	0	150	75	15
13	30	0	15	30	0
7	45	0	30	15	0
0	75	0	45	60	0

Replica I in Table 22 best correlates with the in-service inspection for location B of Figure 53, with creep cavity level assessed as isolated (10-50 cavities). Replica IV best correlate with the in-service inspection for location C. The in-service creep replica assessments for locations A, B and C were captured in 2009, and in the period until removal in 2014, the service duty accrued was an additional 28,997 hours. Hence, based on the surface replicas obtained in 2009 (Table 15) it is expected that replica position IV will have lower absolute cavity counts than replica position I. It is interesting that the intervening 28,997 hours of service has only increased the creep cavity assessment level at replica position I from isolated to low orientated. This has been summarized in Table 23. The slow rate of parent deterioration observed by replica assessment of the parent material in positions B and C suggests that the removal of parent material could be considered as premature.

Cavities in the HAZ of the weld also resulted low orientated, but with a peak of 240 cavs/mm^2 against a peak of 75 cavs/mm^2 in the parent material. This emphasises

the need to use replicas on HAZ regions as a lead position on the weld (which is already standard practice) and the potential benefits of more monitoring earlier in life in order to prevent premature replacement of the parent material. In order to reduce the rate of damage accumulation and avoid the cost of pipework replacement, earlier monitoring could be carried out by use of targeted miniature specimen testing. The use of replica count is even more critical for other materials in wide use, such as P91 steel, because identifying creep cavities is more difficult and the rate of deterioration is faster.

Table 23. Summary of replica evolution between inspections in 2009 and 2014.

Age (hrs)	Position A	Position B	Position 10 mm from Type IV	Position C
242,773	Low orientated	Isolated	Unknown	Clear
271,770	Unknown	Low orientated	Low orientated	Isolated

5.5 IMPRESSION CREEP TEST RESULTS

Figure 62 presents the displacement versus time curves obtained by impression creep tests carried out through the thickness of the pipe section (positions 1, 2 and 3 are illustrated in Figure 54 (b)) at different stress levels at 575 °C, as summarized in Table 19. Figure 63 shows minimum creep strain rates against stress from the impression creep tests and the linear best fit used to calculate Norton's constants, n = 8.3361 and $B = 1.009 \times 10^{-22}$ (stress in MPa and time in hours), which are in line with those found from uniaxial creep tests of similar material [176].

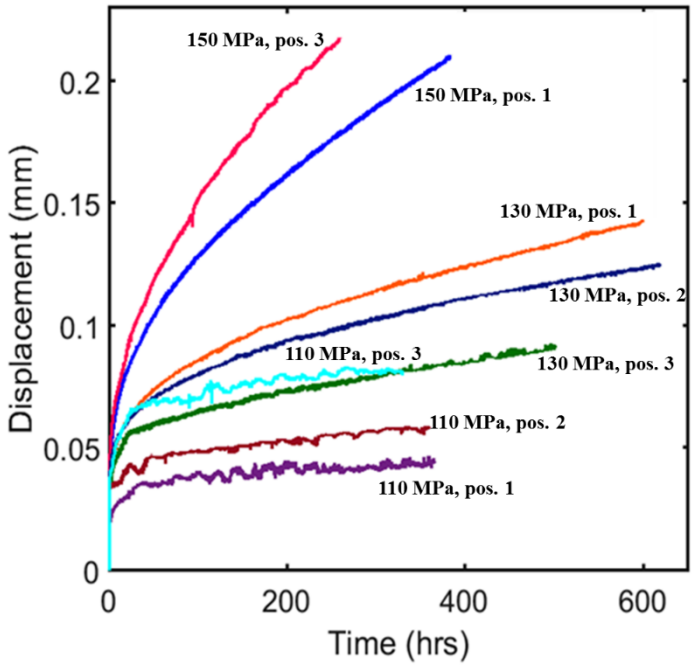


Figure 62. Impression creep tests through the pipe thickness at different stresses and under a temperature of 575 °C.

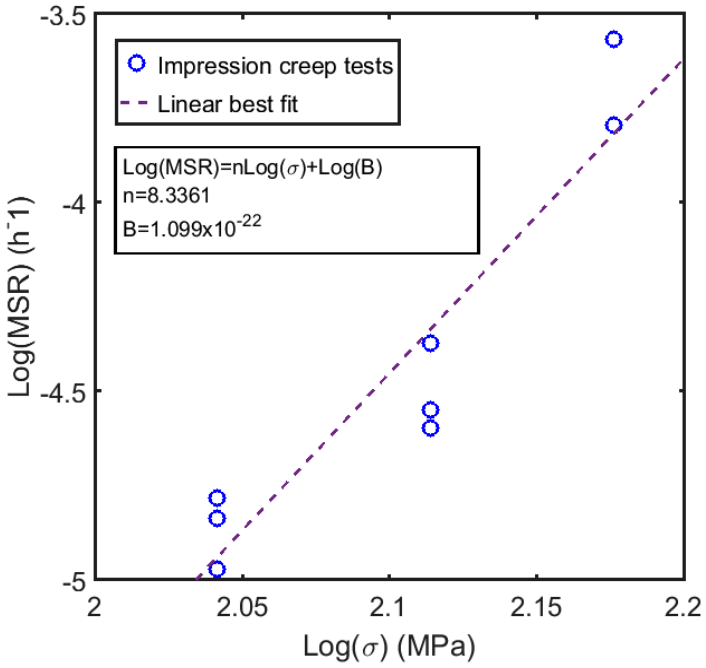


Figure 63. Minimum creep strain rate versus stress from impression creep tests at 575 °C.

5.6 GENERAL COMMENTS ON THE THROUGH THICKNESS BEHAVIOUR

The through thickness behaviour of the pipe section is summarized in Figure 64, where hardness, replica and creep data are plotted against the pipe radius. Only

parent material is considered. The macro-hardness values reported in the figure have been obtained by averaging data along the pipe section from Figure 61 (a) and Figure 61 (b) for the inner (r = 0 mm) and outer (r = 60 mm) surfaces, respectively. As shown in Figure 64, it is not possible to establish a definitive correlation between all of the disparate data collected.

The through section behaviour revels the following:

- Creep cavity distribution at replica positions I and III are broadly similar (and relatively consistent through section), reflect parent material regions relatively close to the main weld and HAZ which accumulates the greatest through section creep cavity distribution. Replica position IV, which is further downstream from the weld, is as expected showing a consistent low or clear response.
- The hardness values through thickness are again relatively consistent, which is reflected in the impression creep MSR values taken at three different positions.
- The impression creep MSR varies as expected in response to the applied stress.

In fact, at r = 0 mm and r = 60 mm and away from the weld, the material is harder and presents no cavities, confirming the theory that the presence of the weld highly affects the creep behaviour of the pipe section. Confirmation of that also arise from the microstructure investigation, carried out far away from the weld, which showed very small creep damage through the thickness of the pipe section. From the present study, there is evidence that the parent material at a distance equal or larger than the weld length, including the heat-affected zone, in the axial direction is not affected anymore by the weld and could have been left in service until the next inspection.

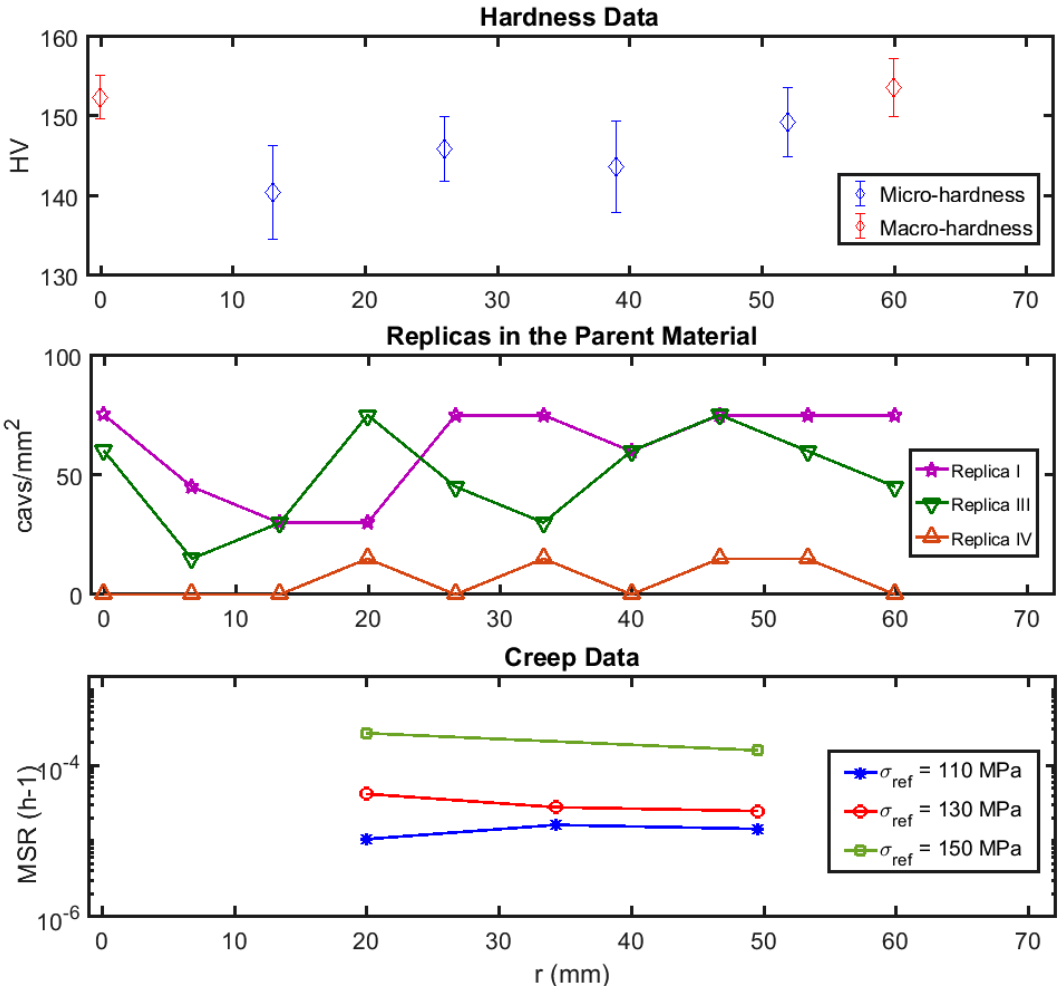


Figure 64. Through thickness behaviour of the pipe section.

5.7 OTHER EX-SERVICE MATERIAL THROUGH SECTION EXAMINATIONS

Other, but more limited studies, on the through thickness extent of creep cavitation on similar age and pedigree parent CrMoV materials has been undertaken. The following summarises these results, with the implications discussed further in Section 5.9. These studies relate to two large conventional power plants (station A and B) in operation in the UK, with original operation commencing in the 1968-1970 period.

5.7.1 Station A: Unit 1: 2014

This refers to main steam CMV specimens removed from steam legs A1 and A2 in 2014 after 268,827 hours and 4133 unit starts. Table 24 shows the through section creep cavity counts obtained for three locations. In this case bend SM23 on leg A1 is in a similar position in the pipe system as the tested material in this study (see

Figure 52). Straight section SM71 on leg A2 is further downstream and located in the main vertical leg.

Table 24. Station A, Unit 1, 2014. Main steam pipe through thickness creep cavity distribution.

Depth below surface (mm)	Creep cavity density (cavities/mm^2)		
	Bend SM23, Extrados	**Bend SM23, Downstream tangent position**	**Straight SM71, Downstream tangent position**
Surface Replica	270	250	150
1	170	150	60
5	190	200	80
10	50	170	70
15	50	200	70
20	50	150	50
25	50	150	50
30	50	150	20
35	30	150	20
40	30	150	20
45	10	150	20
50	0	70	0
55	0	20	0
60	0	0	0

Sections SM23 and SM71 were last inspected in service in 2009 (242,536 hours and 3552 unit starts). Table 25 provides a brief summary of the outage metallurgical inspection results.

Table 25. Station A, Unit 1. Main steam pipe 2009 outage inspection results.

Pipe section location	Surface creep replica assessment	Hardness (HV)
Leg A1:SM23 Bend tangent upstream	Low Orientated	120
Leg A1: SM23 Bend Extrados	Low Orientated	127
Leg A1: SM23 Bend tangent downstream	High Orientated	114
Leg A2: Straight SM70 (immediately upstream from SM71)	Low Orientated	140
Leg A2: Straight SM71	Isolated	Not available
Leg A2: Straight SM72 (immediately downstream from SM71)	Low Orientated	Not available

Main steam line CET assessments have been completed regularly on this unit over a number of years and both legs A1 and A2 have not shown any exceedance of the 568^{o}C design temperature.

5.7.2 Station A: Unit 2: 2015

This refers to main steam CMV specimens removed from steam legs A2 and B1 in 2015 after 283,670 hours and 3875 unit starts. Table 26 shows the through section creep cavity counts obtained for three locations. In this case bend SM155 on steam leg A2 is located close to the high pressure steam chests, with bend SM117 on steam leg B1 in a similar position in the pipe system as the tested material in this study (see Figure 52).

Table 26. Station A, Unit 2, 2015. Main steam pipe through thickness creep cavity distribution**.**

Depth below surface (mm)	Creep cavity density (cavities/mm^2)		
	Bend SM155, Upstream tangent position	**Bend SM155, Downstream tangent position**	**Bend SM117, Extrados**
Surface Replica	0	0	300
1	0	7	118
5	0	0	33
10	7	0	20
15	0	0	20
20	0	0	13
25	0	0	13
30	0	0	20
35	0	0	20
40	0	0	7
45	0	0	13
50	0	0	0
55	0	0	0
60	0	0	0

For these pipe sections the most recent inspections on bend SM155 in 2007 (238,698 hours and 3203 unit starts) was clear, however the bend immediately downstream (SM158) showed aligned creep cavitation on the bend extrados (see Table 16), with a hardness (HV) of 130, and was subsequently replaced.

Bend SM117 was inspected in both 2007 and 2009 (251,936 hours and 3601 unit starts) and revealed very isolated (see Table 16) levels of creep cavitation and a surface hardness (HV) of 127.

5.7.3 Station B: Unit 1: 2015

This refers to main steam CMV specimens removed from steam legs A1 and B2 in 2015 after 261,215 hours and 3300 unit starts. Table 27 shows the through section creep cavity counts obtained for three locations. In this case bend BW6-BW7 on steam leg A1 and two consecutive straight sections on steam leg B2 are all in a similar position in the pipe system as the tested material in this study (see Figure 52).

Table 27. Station B, Unit 1, 2015. Main steam pipe through thickness creep cavity distribution**.**

Depth below surface (mm)	Creep cavity density (cavities/mm^2)		
	Bend BW6-BW7, Extrados	**Straight BW35-SBW7, Adjacent to weld SBW7**	**Straight SBW7-BW37, Adjacent to weld SBW7**
Surface Replica	25	25	25
1	7	20	7
5	0	13	0
10	0	7	0
15	0	0	0
20	0	0	0
25	0	0	0
30	7	0	0
35	0	0	0
40	0	0	0
45	0	0	0
50	0	0	0
55	0	0	0
60	0	0	0

The main steam pipe sections were last inspected in 2010 (232,580 hours and 3046 unit starts), with some further limited inspections in 2012 (245,241 hours and 3208 unit starts). Table 28 provides a brief summary of the outage metallurgical inspection results.

Table 28. Station B, Unit 1. Main steam pipe 2010-2012 outage inspection results**.**

Pipe section location	Year	Surface creep replica assessment	Hardness (HV)
Leg A1: Straight BW5-BW6 (immediately upstream from BW6-BW7)	2010	Very Isolated	120
Leg A1: Bend BW6-BW7	2010	Isolated	129
Leg A1: Straight BW7-SBW1 (immediately downstream from BW6-BW7)	2010	Not inspected	Not inspected
Leg A1: Straight SBW1-BW9 (immediately downstream from BW7-SBW1)	2010	Isolated	139
Leg B2: Straight BW35-SBW7	2010	Isolated	139
	2012	Low Orientated	136
Leg B2: Straight SBW7-BW37	2010	Very Isolated	141
	2012	Low Orientated	139

A limited number of CET surveys on legs A1 and B2 were completed over the period 2007-2011 and these showed a peak value of 574 ºC for leg A1 and 572 ºC for leg B2 compared against a design temperature of 568 ºC.

5.7.4 Station A: Unit 1: 2009

This refers to two main steam straight CMV specimens removed in 2009 (242,536 hours and 3552 unit starts) and believed to be from steam legs B1 and B2. In 2009 a number of straight sections and bends were removed because of high surface creep replica cavity counts, however the precise pedigree of the two straight sections examined is uncertain. A cursory review of the corresponding outage report identifies a number of straight sections removed, with creep replica assessment registered as ‘aligned’, ‘high orientated’ and hardness (HV) levels of ~ 135-145. Some of the bends adjacent to straight sections removed exhibited indications of surface micro-cracking (these bends were replaced).

It is believed that both of these straight sections were removed from steam legs B1 and B2 AT the top section and just downstream of the boiler stop valve; hence

positioned upstream from the tested material in this study (see Figure 52). These specimens are identified as straight A and straight B.

For straight A through section creep cavity counts at three circumferential positions of 90º, 180º and 315º were taken. Table 29 to Table 31 summarise the through section creep replica results, which were taken by two different service providers for comparison purposes.

Table 29. Station A, Unit 1. Straight A, through thickness creep replica results at the 90º position.

Position through wall (% from outer surface)	**Creep cavity density (cavities/mm^2)**	
	Service provider 1	**Service provider 2**
0.00	Not available	Not available
9.23	75	96
18.46	60	48
27.69	45	36
36.92	75	68
46.15	75	48
55.38	90	48
64.62	15	20
73.85	30	12
83.08	0	4
100	0	0

Table 30. Station A, Unit 1. Straight A, through thickness creep replica results at the 180º position**.**

Position through wall (% from outer surface)	**Creep cavity density (cavities/mm^2)**	
	Service provider 1	**Service provider 2**
0.00	Not available	Not available
9.23	180	184
18.46	95	148
27.69	90	128
36.92	75	128
46.15	60	96
55.38	60	104
64.62	60	56
73.85	45	28
83.08	0	12
100	0	0

Table 31. Station A, Unit 1. Straight A, through thickness creep replica results at the 315º position.

Position through wall (% from outer surface)	Creep cavity density (cavities/mm^2)	
	Service provider 1	Service provider 2
0.00	Not available	Not available
9.23	60	145
18.46	45	120
27.69	60	95
36.92	90	145
46.15	60	99
55.38	60	46
64.62	15	20
73.85	15	13
83.08	0	7
100	0	0

For straight B through section creep cavity counts at the following three circumferential positions; 135º, 225º and 315º were taken. Table 32 to Table 34 summarise the through section creep replica results, which were taken by two different service providers for comparison purposes.

Table 32. Station A, Unit 1. Straight B, through thickness creep replica results at the 135° position**.**

Position through wall (% from outer surface)	Creep cavity density (cavities/mm^2)	
	Service provider 1	Service provider 2
0.00	Not available	Not available
9.23	180	135
18.46	120	90
27.69	90	35
36.92	45	68
46.15	45	68
55.38	60	72
64.62	0	18
73.85	30	11
83.08	0	3
100	0	0

Table 33. Station A, Unit 1. Straight B, through thickness creep replica results at the 225° position**.**

Position through wall (% from outer surface)	Creep cavity density (cavities/mm^2)	
	Service provider 1	Service provider 2
0.00	Not available	Not available
9.23	125	216
18.46	90	196
27.69	60	100
36.92	60	20
46.15	45	23
55.38	15	24
64.62	0	9
73.85	0	10
83.08	15	5
100	0	0

Table 34. Station A, Unit 1. Straight B, through thickness creep replica results at the 315° position**.**

Position through wall (% from outer surface)	Creep cavity density (cavities/mm^2)	
	Service provider 1	Service provider 2
0.00	Not available	Not available
9.23	-	115
18.46	-	75
27.69	-	50
36.92	-	60
46.15	-	55
55.38	-	45
64.62	-	25
73.85	-	13
83.08	-	10
100	-	0

5.8 SUMMARY OF THROUGH SECTION CREEP CAVITY COUNTS

It is useful to summarise the extent and magnitude of the observed through section creep cavitation results from the specimen examined in this study and the other samples examined and discussed in Section 3.6. Table 35 provides an overview.

Table 35. Summary of extent of through section creep cavitation**.**

Station[(1)] and Unit	Specimen Identification	At Removal			Cavitation Extent			Peak[(2)]
		Year	Hours	Starts	Within outer 10% of wall (6 mm)	Within first 50% of wall (~ 30mm)	Beyond mid-section	
B: 2	Straight: Examined in this work	2014	271,770	2739			Yes	75
A: 1	Bend SM23	2014	268,827	4133			Yes	200
	Straight SM71						Yes	80
A: 2	Bend SM155	2015	283,670	3875	Yes			7
	Bend SM117						Yes	118
B: 1	Bend BW6-BW7	2015	261,215	3300		Yes		7
	Straight BW35-SBW7				Yes			20
	Straight SBW7-BW37				Yes			7
A: 1	Straight A[(3)]	2009	242,536	3552			Yes	184
	Straight B[(3)]						Yes	216

Notes
[(1)] Station origin defined in section 3.6
[(2)] Represents the peak value at any position, apart from the surface value
[(3)] Adjacent bends showed evidence of greater distress (onset of surface micro-cracking)

In terms of the magnitude and through section extent of creep cavitation, parent material in bends tends to lead straight sections in terms of risk. There is no discernible relationship between the creep cavitation levels observed and the general in-service age (hours and starts) logged for each specimen, which is a simplistic but often used measure of life consumed by the station. The examination described for specimens in 2009 from station A, Unit 1 (Section 3.6.4) illustrate not only the circumferential variation in creep cavity count but also the differences that can be observed from different and reputable service providers. Hence, in practice creep cavity counts are not used to provide a quantitative estimate of the remaining in-service life of components.

5.9 DISCUSSION

The examination of the ex-service CMV specimen has illustrated the difficulty in correlating simple measures of service duty (hours and starts, as used by the station) and the observed level of creep damage obtained from surface replicas. Moreover, other studies [177] that have scrutinised very large outage inspection datasets have shown that, to date, the correlation between creep cavity count and other often used off-load tests, such as surface hardness, is not well defined. The ex-service CMV specimen examined in this dissertation has only shown a relatively modest increase in creep damage (Table 23) between two inspection periods, 2009-2014, equating to 28,997 hours of service. This is not an unexpected finding for CMV parent material. It should be noted that reviews of successive outage inspections and repeat creep replicas show very modest increases in creep cavity counts over a typical 20-25Khr operating period. This implies that the parent material in this instance was prematurely removed from service and it would be expected that at least a further 20-25Khr service could have been achieved. This could be safely managed for example by modestly de-rating the operating temperatures, by circa 5-10 °C.

Table 35 summarises examinations of nine (five straight sections and four bend sections) other ex-service CMV sections, all of a similar age to the section examined for the present research. Pipe bends might be expected to show greater evidence of creep damage; however, the inspections undertaken are quite limited and focussed only on through thickness sections originating from the extrados and with no reference to the acting pipe system loads, which will likely be greater at bend positions. This

emphasises the need to correlate any material examinations with measures or estimates of the active in-service loads, which can be obtained if periodic hot and cold pipe hanger surveys are undertaken in addition to regular surveys of operating temperature and pressure.

The impression creep tests used material at different positions through the pipe thickness (Figure 54) and located between the replica III and replica IV locations identified in Table 22. These show generally consistent creep cavity count and hardness values through the thickness, illustrated in Figure 64. Importantly the impression creep tests reveal a fairly consistent MSR through thickness, and at three different stress levels.

The condition of the parent CMV material examined is such that it could have been retained in service for at least another operating period.

5.9.1 Implications

The examination of the specimen has not identified a notable through section 'damage' gradient (Figure 64) by impression creep test, hardness test or surface replica. The material is in surprisingly good condition considering its long service duty. The comparison with data from prior outage examinations has identified a very gradual change in hardness and the level ascribed for creep cavitation. Other very extensive surveys of periodic surface hardness and creep replica [177] has confirmed a gradual (measurable) change over a typical operating period of ~ 20-25Khr for this material. It is evident from the reported through section creep replica studies summarised in Table 35 that a through section 'damage' gradient can usually be expected for material of this age, for straight sections as well as bends.

The only available in-service data related to the specimen operating conditions and in-service strain rate (Section 5.2.2) indicates that the creep effective operating temperature is slightly less than the design temperature and with a creep strain rate of ~ $4.2 \times 10^{-8} hr^{-1}$. Using this in-service strain rate in the log(MSR) equation determined from the impression creep tests (see Figure 63) reveals an operating stress of 56MPa, which on inspection is judged to be too high for a straight section of pipe in this position in the pipeline and with consideration of pipe system loads, which can be of the order of 10-15% of the mean diameter pressure hoop stress. This estimate of pipe

system loads in CMV is based on examination of in-service creep crack growth through CMV welds [35] and correlation against creep crack growth predictions. The lower operating temperatures will act to further reduce the MSR of the pipe specimen for a given stress level, with the inference being that the measured strain rate of ~ $4.2x10^{-8}hr^{-1}$ is too high.

The above comparison between 'measured' data and 'predicted' using the log(MSR) equation derived from the impression creep test is an example of how small specimen creep test predictions can be used to test the impact and credibility of site operational data and measurements. The requirement to use online measurements in comparison with traditional site inspection data, coupled with targeted small specimen test results has been described in detail within the context of a new holistic life assessment framework [20].

6 INVESTIGATION ON POSSIBLE IMPROVEMENTS OF THE CEN CODE OF PRACTICE

6.1 INTRODUCTION

Chapter 5 has shown how miniature specimen creep testing techniques, in particular the impression creep test, could be successfully used in the new holistic approach presented in Chapter 3 for the evaluation of life consumption of power plant components. However, in the last two decades, several researchers and power plant companies have focused their attention on small punch creep test as a possible technique to use in life assessment approaches of materials used for power generation applications. Unlike other miniaturised specimen techniques, such as the impression creep test [92] and the small ring creep test [27], the SPCT potentially allows to entirely characterise the behaviour of materials up to failure, because the specimen is taken to rupture [127, 133]. The SPCT can also be used to perform focused analyses on critical locations of operating components, e.g. the heat-affected zone of welds, pipe bends or joint sections of steam headers [133]. Despite of these advantages, some concerns about the applicability of SPCT are still open [109, 178]. Indeed, the interaction of several non-linearities, such as large deformations, large strains, non-linear material behaviour and non-linear contact interactions between the specimen and the punch, induces a very complex multi-axial stress field in the specimen which also evolves in time. This affects the SPCT fracture mechanism [109, 127] and introduces several challenges into the identification of a robust correlation to convert SPCT data into respective standard uniaxial creep test data [89, 90, 112, 127]. Another major concern is the non-repeatability of the testing method, since the experimental results depend on the set up geometry [5, 178-180]. One of the major developments in this matter has been achieved by the Code of Practice proposed in 2006 by the European Committee for Standardisation (CEN), where an experimental procedure and a range for the specimen and the test rig components geometry was recommended [5, 112]. Another achievement of the CEN Code of Practice consists of a correlation proposed between the load level to be applied to the small disc specimen and the stress induced in a conventional uniaxial creep test which exhibits the same time to rupture. Various equations have been proposed in the open literature to correlate the quantities involved in the SPCT, i.e. the load-stress ratio [5, 126, 181, 182], but a common problem is faced in determining the angle between the axis of symmetry and the

normal to the specimen's surface at the contact edge, θ_0 [5], as it is an implicit variable in the mentioned relationships.

In order to develop a robust procedure to interpret the experimental output of SPCTs and a reliable correlation technique with conventional uniaxial creep test data, the understanding of the complex behaviour of the specimen during testing is still to be improved.

The research presented in this Chapter is aimed to investigate the applicability of the Chakrabarty solution, which forms the basis for small punch creep data interpretation in the CEN code of practice [5], to the SPCT behaviour, by use of numerical finite elements (FE) calculations and by comparing experimental, numerical and analytical solutions. An improved understanding of the SPCT specimen deformation and failure behaviour is necessary, in order to carry out a step forward for the realization of the improved code of practice based on the existing CWA 15627 [5].

6.2 CHAKRABARTY'S MEMBRANE STRETCHING THEORY

6.2.1 Problem description

Chakrabarty's membrane stretching theory [126] is used by the CEN Code of Practice as it provides a complete set of relations for establishing the correlation between the load level to be applied to the SPCT specimen and the stress induced in a conventional uniaxial creep test which exhibits the same time to rupture [5]. As well as the other equations suggested by the Code of Practice and reported by Liu and Šturm [183] in 2005, and others [181, 182, 184], Chakrabarty's relation between load and stress is derived from equilibrium between load and membrane stresses with bending stresses neglected [126]. As a matter of fact, large deformations (larger than 20% of the maximum structural dimension, according to an engineering judgment) are involved in the SPCT, allowing the bending stresses to be neglected [126].

A representative analytical model of SPCT would be significantly complicated, as it should account for the effects of moving contact edges, nonlinear friction conditions between the test rig components and the tested specimen, and highly localised initial plastic deformation [90, 126, 127, 185]. However, Chakrabarty's theory of membrane stretch forming over a rigid hemispherical punch head, reported in ref. [126], is able to provide an analytical tool for the interpretation

of small punch creep test data [90, 112, 126]. In Chakrabarty's study large plastic deformations are taken into account and the geometry and the loading conditions partly reflect those encountered in the SPCT [7]. Furthermore, the model hypotheses can be very restrictive in comparison with the true material behaviour: an isotropic material is adopted; the punch head is taken to be covered by a film of lubricant, therefore friction between the blank and the punch can be neglected; since large strains are considered, the material is assumed to be rigid-plastic; the thickness of the blank is at least one order of magnitude smaller than the radius of the punch, therefore, the bending rigidity of the blank can be neglected, and, as a consequence, the deformation mode can be assumed to be governed by membrane stretching [126]. Figure 65 is a schematic diagram showing the components Chakrabarty's model comprises of.

6.2.2 Membrane stress solutions

Chakrabarty's model consists of a thin membrane of isotropic material stretched over a static hemispherical punch (Figure 65).

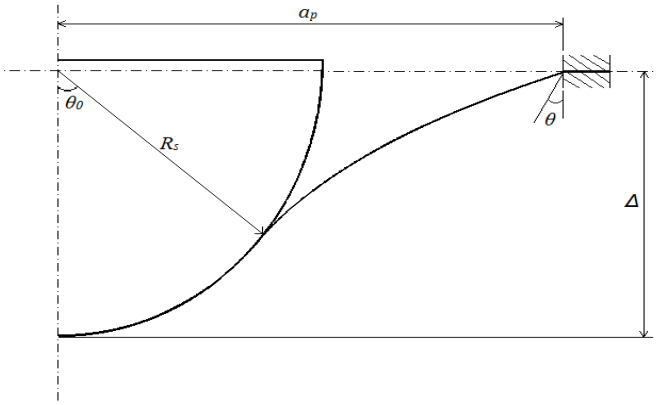


Figure 65. Schematic diagram of the Chakrabarty model of membrane stretching of a circular blank over a rigid punch, adapted from ref. [126].

If p and t_c denote the punch pressure and the current thickness of the specimen, respectively, the normal equilibrium in the contact region is expressed by equation (81).

$$t_c(\sigma_c + \sigma_m) = pR_s \tag{81}$$

where σ_c and σ_m are the circumferential and meridian stresses, respectively, and R_s is the punch radius [126]. In the unsupported region the corresponding relationship is given by equation (82)

$$\frac{\sigma_c}{\rho_c} + \frac{\sigma_m}{\rho_r} = 0 \tag{82}$$

where ρ_c and ρ_r are the circumferential and meridian radii of curvature, respectively, which have opposite signs in the unsupported region, while they are both positive and equal to R_s in the contact region [126]. The central displacement of the punch, Δ, is related to the angle between the surface normal and the axis of rotation, θ, and the normal angle at the contact boundary, θ_0, by equation (83), which can be solved through equation (84), where a_p is the receiving hole radius, by setting θ_0 to vary in the range from 0° to 90° [5, 126].

$$\frac{\Delta}{R_s} = (1 - cos\theta_0) + sin^2\theta_0 ln \frac{\tan(\theta_0/2)}{\tan(\theta/2)} \tag{83}$$

$$sin\theta = \frac{R_s}{a_p} sin^2\theta_0 \tag{84}$$

By assuming an empirical strain-hardening law, as in equation (85), where *C* and *m* are material constants, Chakrabarty also found a correlation between the punch load at any given stage and the stress at the contact boundary, which is expressed by equation (86)

$$\sigma = C\varepsilon^m \tag{85}$$

$$P = 2\pi R_s \sigma^* t^* sin^2\theta_0 \tag{86}$$

where σ^* and t^* are the membrane stress and the thickness, respectively, at the contact boundary and are given by equations (87) and (88), where t_0 is the initial thickness of the specimen [126].

$$\sigma^* = C\left[2ln\left(\frac{1 + cos\theta}{1 + cos\theta_0}\right)\right]^m \tag{87}$$

$$t^* = t_0 \left(\frac{1 + cos\theta_0}{1 + cos\theta} \right)^2 \quad (88)$$

6.2.3 Strain solution and correlation of the contact boundary angle

A relationship between the central deflection of the punch, Δ, and the central equivalent strain, ε, was proposed by Yang and Wang by using Chakrabarty's membrane stress solutions combined with a FE investigation [184]. Li and Šturm identified a correlation between the strain at the contact boundary and the central displacement [112, 125, 183, 186]. Li and Šturm's third order polynomial relation, equation (89), is based on a fitting to Chakrabarty's membrane stretching solution and it is valid for R_s=1.25 mm and a_p=2 mm. The punch radius and the receiving hole radius are consistent with those recommended in the CEN Code of Practice [5].

$$\varepsilon = 0.17959\Delta + 0.09357\Delta^2 + 0.0044\Delta^3 \quad (89)$$

Chakrabarty [126] and, most recently, more researchers [88, 115] reported that the necking of the specimen and the strain distribution are influenced by friction, which causes the maximum thinning of the specimen to occur at a certain distance from the centre of the specimen and near the contact boundary.

6.2.4 Applicability of the Membrane Stretching Theory to the SPCT Specimen Behaviour

Although Chakrabarty's theory was developed for a rigid-plastic membrane (not involving creep deformation) it was used by CEN Code of Practice for SPCT data interpretation [5]. The membrane stretching model is rigorously valid for an exponential hardening law, but it is also applicable to different hardening laws. Furthermore, the specimen is assumed to uniquely experience a membrane stretching deformation, while the strain variation in the through-thickness direction is neglected [112, 126]. During small punch creep test, the specimen deformation is caused by bending prior to membrane stretching, therefore, the work presented in this study is also aimed to investigate the applicability of Chakrabarty's theory to SPCT data interpretation [112, 127, 128, 133]. The study was carried out by investigating the evolution of the contact angle, θ_0, throughout the test.

6.2.5 Finite element model definition

In order to study the evolution of the contact angle, θ_0, with the load magnitude, P, and to find a correlation between the contact angle and the dimensions of the punch and the specimen, a number of finite element analyses were performed. Five punch load levels have been used for the analyses: 90, 110, 130, 150 and 200 N. The receiving hole radius, a_p, has been kept constant and equal to 2 mm. Three different punch radii, R_s, have been adopted: 1.04, 1.25 and 1.50 mm. The initial specimen thickness, t_0, varies among 0.5, 0.4, 0.3 and 0.2 mm. All the geometry parameters are in the respectively ranges suggested by the CEN Code of Practice [5]. The recommended "standard" dimensions in the CEN Code of Practice are t_0=0.5 mm, R_s=1.25 mm and a_p=2 mm.

In the works reported in the open literature, the punch is generally modelled as a rigid body, while displacement boundary conditions, i.e. simply supported constraints, are adopted instead of modelling the holder and the support [89, 131, 187]. In particular Dymáček et al. show that if the punch load is less than 400 N and the upper and lower dies are replaced by corresponding displacement constraints, the time to rupture obtained by the FE analyses is close to the experimental time to failure [89]. However, as also stated by Dymáček et al., the replacement of the contact interaction with pressure, for the punch interaction, and boundary conditions, for the dies, does not lead to an accurate representation of the experimental environment and, despite of the good correlation with experiments, the direct modelling of the interactions of the test rig components and the punch is preferable. Due to the very low stiffness of the specimen in comparison to that of the clamps and the rig, the assumption of the test rig components being rigid would not largely affect the FE results. FE models developed by considering the effects of these contact interactions are reported in ref. [89, 128, 133]. Therefore, in this research, the upper and lower dies and the punch ball were modelled as rigid bodies. However, it is useful to investigate the possible effects of the clamps and the rig stiffness on the small punch response in the future. The horizontal translation and the rotational degrees of freedom of the punch and the holder were constrained, as well as all the rigid body degrees of freedom of the support. The specimen is clamped by a load of 500 N applied to the holder reference point. Since the specimen exhibits large deformations and since its shape significantly changes

during the creep analysis, the non-linear geometry formulation has been adopted [112, 130, 133, 174]. Figure 66 shows the FE model implemented for the calculations. The FE analyses were performed by ABAQUS and a CREEP User Subroutine, available in ABAQUS, was coded and used for the implementation of Liu and Murakami's model [17].

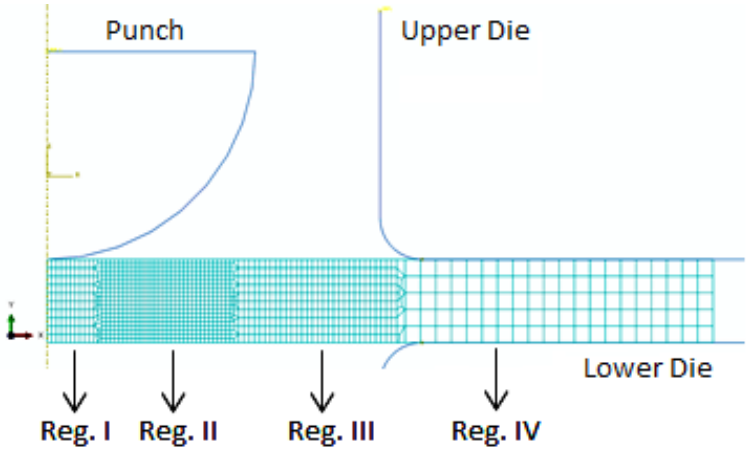


Figure 66. FE model used for the calculations.

6.2.6 Meshing and Contact Modelling

The specimen is the only solid body of the model taken to be deformable. The finite element mesh developed for the calculations consists of 1293 nodes and 1186 axisymmetric CAX4R elements [128] (four-nodded bilinear with a reduced integration scheme) in ABAQUS [17]. Since severe incompressible deformation arises throughout the SPCT analysis, reduced integration elements have been used in order to avoid numerical errors due to shear and volume locking, see also ref. [128]. It should be noted that bending deformation is not negligible during the early stages of the creep deformation [188, 189], at least with the geometry recommended by CEN, therefore, a suitable number of elements was included through the thickness of the specimen in order to accurately calculate the stress field in the specimen. Solid elements would be the most suitable FE element type. The mesh developed for this work has shown to be able to accurately predict bending deformation, as the comparison of FE deformed shapes with those obtained from testing confirms. The layout of the elements was based on the work of Ma et al. [128] and the results obtained by implementing the described model, in terms of damage propagation, are comparable to those found in the literature [7, 109, 127, 128, 180] and high damage locations in the specimens are

compatible with regions where cracking first occurs in the tested specimens. Figure 66 shows the mesh used for the FE analyses, where four regions can be identified. A coarse mesh has been generated in Region IV, because that location is not critical for the numerical results (as it is away from the area of the specimen where necking occurs) and the corresponding deformation is expected to be small [89, 128]. The necking area, Region II in Figure 66, where the most severe deformations are expected, is characterised by the smallest element size. A mesh sensitive study was carried out in order for this region to be centred on the location where necking is expected, which agrees with the findings reported in refs. [89, 128]. Regions I and III are also characterised by a relatively fine discretisation because they are adjacent to the necking area and the contact interaction with the punch has been defined on them as well. A surface to surface contact formulation has been used for the interactions between the specimen (slave contact surface) and the punch (master contact surface) and between the specimen and the dies (master contact surfaces). For the normal behaviour of all of the contact interactions, a hard pressure-overclosure relationship has been used, with a penalty formulation adopted for the tangential behaviour, with a friction coefficient, μ, of 0.8 for the clamps/specimen and 0.3 for the punch/specimen [127]. As reported by Dymáček et al. [135], 0.3 is a realistic value for the friction coefficient between the punch and the specimen for steels at temperatures higher than 600 °C. The coefficient of friction at the contact between the specimen and the test rig components, especially with the punch, is not known and cannot be straightforwardly identified. Therefore, the value 0.3 for the friction coefficient between the punch and the specimen was assumed by Dymáček et al. [135] based on judgement and on small punch creep tests. The values assumed for the present work were based on those reported by Dymáček et al. [135] and Cortellino et al. [127] for the SPCT problem under conditions which are very similar to those of the present study in terms of materials and temperatures adopted. The nodes defined on the contact surfaces between the test rig components (in particular the punch) and the specimen experience relative sliding, therefore, a finite sliding contact tracking approach was used for the frictional formulation [127].

6.2.7 Constitutive material models

Liu and Murakami's creep continuum damage model, in its multiaxial form, was used for this study (see equations from (11) to (14) in Chapter 2, section 2.1.4). A

continuous model for the reduction in load-carrying capability of the damaged material is given in equation (90), where E_0 is the Young's modulus of the undamaged material and E is the Young's modulus of the damaged material. In view of equation (90), the stiffness of the damaged material decreases when the damage variable value increases. Since the specimen rupture occurs when ω approaches 1, in the present work, the maximum damage value has been limited to $\omega_{MAX} = 0.9901$, in order to avoid computational problems. However, the use of equation (90) can also lead to numerical inaccuracies because, in the areas where the specimen is failed, characterised by $\omega = \omega_{MAX}$, the FE model of the specimen can potentially carry some load, while this is not physically realistic. An alternative to equation (90) is proposed in the present work and is reported in equation (91), with $0 \leq \omega < 0.9901$, and in equation (92), with $\omega = 0.9901$.

$$E = E_0(1 - \omega), \quad 0 \leq \omega \leq 1 \tag{90}$$

$$\begin{cases} E = E_0(1 - \omega), & 0 \leq \omega < 0.9901 \quad (91) \\ E = 0.01\ MPa, & \omega = 0.9901 \quad (92) \end{cases}$$

6.2.8 Elastic-Plastic Constitutive Models

In section 6.5.8 attention is paid to the evolution of the contact angle when other material constitutive models are used. In particular, three different material constitutive models have been adopted: two multi-linear isotropic hardening plastic models, characterized by a yielding stress, σ_y, of 280 MPa and a tangential modulus, *E'*, of 175 and 250 MPa, respectively, and an elastic-perfectly plastic constitutive model with $\sigma_y = 280$ MPa. These values for σ_y and *E'* were obtained from the results of uniaxial tensile test carried out for a P91 steel at 600 °C. Figure 67 plots the variation of stress versus strain for the two multi-linear isotropic hardening plastic models and the elastic-perfectly plastic constitutive model.

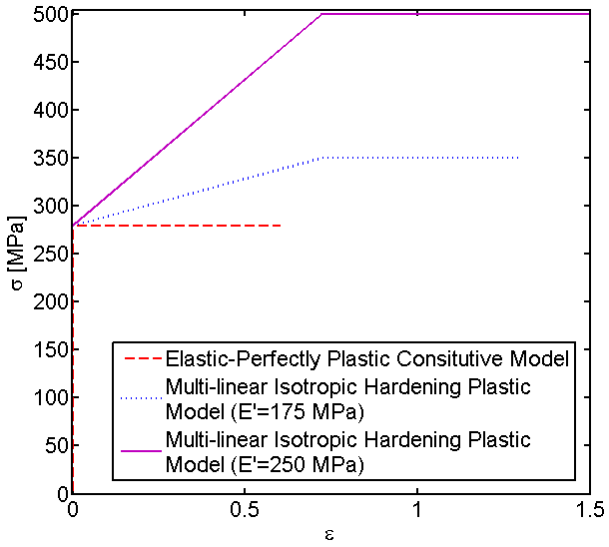


Figure 67. Variation of stress versus strain: two multi-linear isotropic hardening plastic models were used, together with an elastic-perfectly plastic constitutive model.

6.3 TESTED MATERIAL AND TEST RIG

Interrupted small punch creep tests were carried out in order to measure the contact angle at different stages of the creep curve. The test data were compared to those acquired by Cortellino et al. [109] and to the FE results obtained for this research (see section 6.5.7). The tested material and the test rig geometry (see Figure 15 (a), Chapter 2, section 2.4.4 for a schematic cross section), are the same as those used by Cortellino et al. [109], who carried out several interrupted small punch creep tests of a P91 steel with an initial thickness of the specimen of 0.5 mm and a punch radius of 1.04 mm, by applying a load of 25 kgf at a constant temperature of 600 °C. For this research, a P91 steel has been used to machine various small disc specimens with a final thickness of 0.300±0.001 mm from a power plant steam pipe section, sketched in Figure 68, which has an outer diameter and a wall thickness of 298.5 and 55mm, respectively. Table 36 and Table 37 show, respectively, the chemical composition, in wt%, of the P91 steel used for the investigation in ref. [36] and the material constants of the P91 steel at 650 °C for the damage law [25].

A load of 11.5 kg was applied to the dead-weight machine. The temperature was held at 650±1 °C by the single-zone temperature controller of the furnace. A thermocouple was inserted at approximately 10 mm below the specimen for allowing the tracing of potential fluctuations of the temperature by the data acquisition system. The loading mechanism of the machine had centralised slides which allowed the dead

weight load to be applied coaxially with the test assembly. Since the experimental results depend on the set up geometry, the non-repeatability of the small punch testing technique is a major concern [5, 178-180]. Cortellino et al. found that, when eccentricities and misalignments in the punch load occur, both the failure life and the minimum displacement rate can significantly change with respect to a situation in which the punch load is perfectly aligned [133]. This also leads to asymmetry in the maximum principal stress and in the damage variable of the specimen [133].

Table 36. Chemical composition, in wt%, of the P91 steel used for the investigation in ref. [190].

Cr	Mo	C	Si	S	P	Al	V	Nb	N	W
8.60	1.02	0.12	0.34	<0.002	0.017	0.007	0.24	0.070	0.060	0.03

Table 37. Material constants for a P91 steel at 650 °C, with stress (MPa) and time (h) [174].

E_0 [MPa]	ν	B	n	A	χ	q_2	α
1.500×10^5	0.3	1.092×10^{-20}	8.462	2.952×10^{-16}	6.789	3.2	0.215

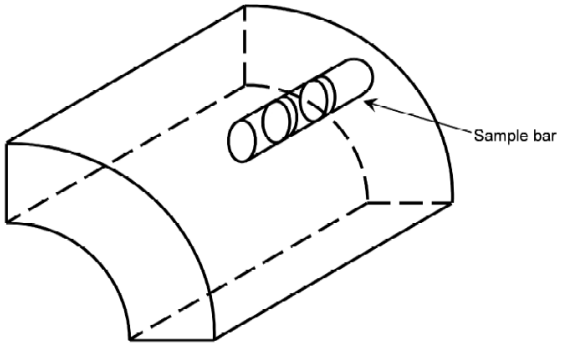


Figure 68. Schematic representation of the specimens manufacturing from the P91 steel pipe, from ref. [109].

6.4 CALCULATION OF THE CONTACT ANGLE

For each time instant, and of the punch displacement, the contact angle, θ_0, has been calculated by equation (93), where $r_{contact}$ is the distance of the contact edge from the axis of symmetry of the specimen, measured on the deformed configuration in the radial direction.

$$\theta_0 = \sin^{-1}\left(\frac{r_{contact}}{R_s}\right) \quad (93)$$

From the FE solution, the contact edge, on the top surface of the specimen (i.e. the slave contact surface), has been identified as the farthest node, from the axis of symmetry, where the contact status is closed, in either slipping or sticking conditions.

6.5 RESULTS AND DISCUSSION

6.5.1 Experimental results

Figure 69 shows the creep test curves, in terms of the variation of the central deformation of the specimen, Δ, versus time, *t*, obtained by small punch creep tests carried out by applying a load of 11.5 kgf to specimens with t_0 =0.3 mm at a constant temperature of 650 °C.

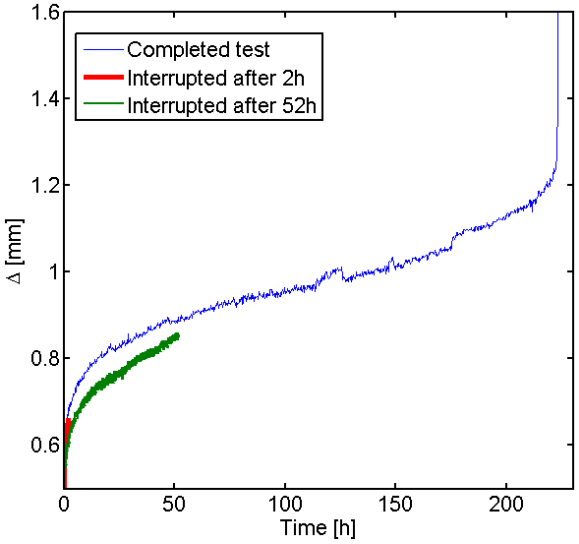


Figure 69. Variation of the central deformation of the specimen versus time for the completed and interrupted tests under a load of 11.35 kgf, with R_s = 1.04 mm and t_0=0.3 mm.

Brucker Interferometer was used to measure the specimen profiles. Figure 70 and Figure 71 show, respectively, 3D and 2D images, respectively, of the profiles of the SPCT specimens from Bruker Interferometer for the tests interrupted after 2 h ($^{t}/_{t_f} \approx 0$, $^{\Delta}/_{\Delta_f} \approx 0.40$) and after 52 h ($^{t}/_{t_f} \approx 0.23$, $^{\Delta}/_{\Delta_f} \approx 0.62$). Figure 72 shows the depth of the 2D profiles, f(y), which was fitted against the distance, y, from the axis of symmetry of the specimen in the radial direction, by use of a Fourier

polynomial function, as shown in equation (18). The fitting constant set, reported in Table 38, consists of a_i, for i=0…5, of b_i, for i=1…5, and of the angular frequency, w.

$$f(y) = a_0 + a_1\cos(wy) + b_1\sin(wy) + a_2\cos(2wy) + b_2\sin(2wy) + a_3\cos(3wy) + b_3\sin(3wy) + a_4\cos(4wy) + b_4\sin(4wy) + a_5\cos(5wy) + b_5\sin(5wy) \quad (94)$$

The contact radii for the two tests, required to obtain the contact angles by equation (93), were identified by the values of *y* that satisfy equation (95), i.e. equating to 0 the second derivative of *f(y)* with respect to *y*. The contact angles, calculated by using the described procedure, are equal to 40° and 45.73° for the test interrupted after 2 and 52 hours, respectively.

$$\frac{d^2(f(y))}{dy^2} = 0 \quad (95)$$

Table 38. Fitting constants for equation (94).

	Test interrupted after 2 h	Test interrupted after 52 h
w	0.0008006	0.0007165
a_0	-0.150200	-0.291300
a_1	-0.321000	-0.460600
a_2	-0.159300	-0.177000
a_3	-0.043120	-0.106900
a_4	-0.033490	-0.019680
a_5	-0.011940	-0.024150
b_1	0.0588100	-0.016370
b_2	-0.024780	0.0227500
b_3	0.0047090	-0.004242
b_4	0.0035520	-0.002899
b_5	-0.003138	0.0005257

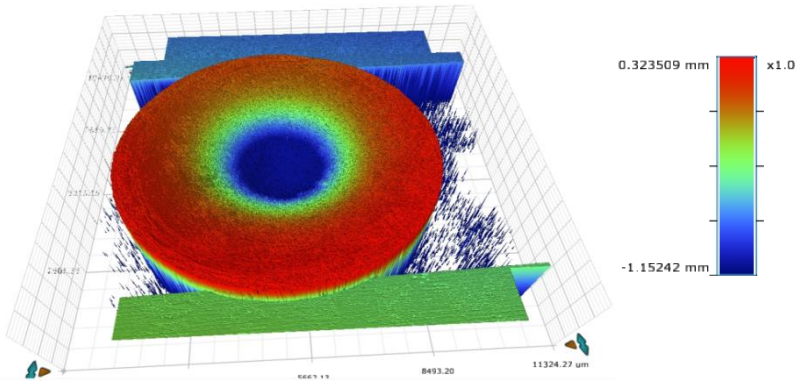
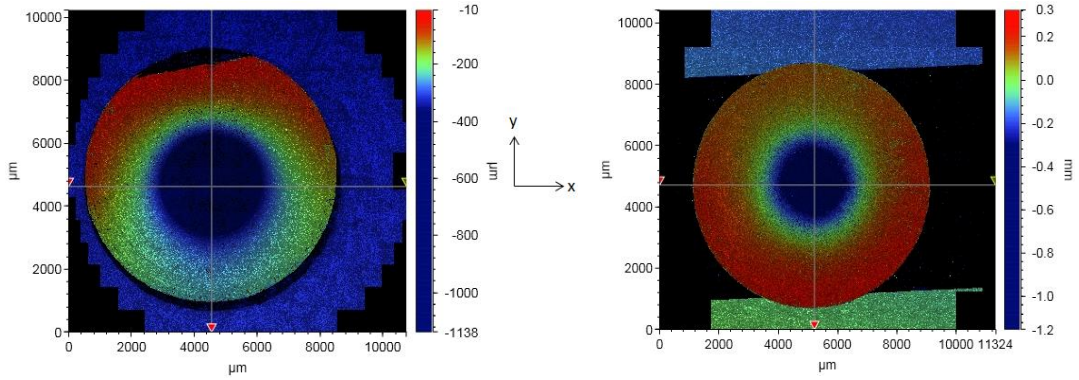


Figure 70. 3D image of the profile of the SPCT specimen from Bruker Interferometer for the test interrupted after 52 hours.



(a) (b)

Figure 71. 2D images, in the xy plane, of the profile of the SPCT specimens from Bruker Interferometer for the tests interrupted after (a) 2 hours and (b) 52 hours.

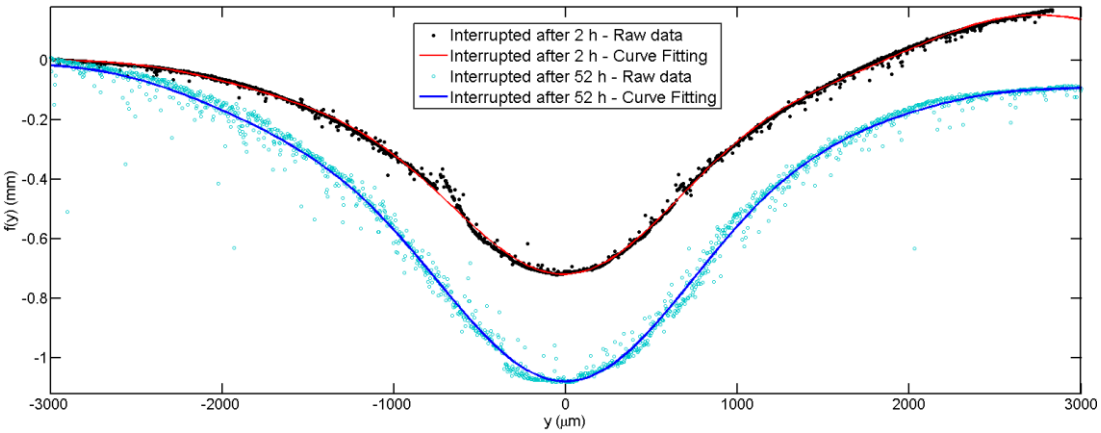


Figure 72. Depth of the SPCT specimen 2D profiles from Bruker Interferometer for the test interrupted after 2 and 52 hours, plotted against the distance from the axis of symmetry of the specimen in the radial direction.

As reported by Cortellino et al., a misalignment of the punch load induces an asymmetry in the specimen deformation [133], therefore, information on punch misalignment can be obtained by analysing the deformed shape of the specimens. The data in Figure 72 representing the top surface of the specimen creep tested up to 52 hours does not exhibit significant asymmetry, therefore the punch load can be taken as centred for this test. On the other hand, the specimen profile obtained from the test interrupted after 2 hours is characterised by a significant degree of asymmetry, indicating that the punch load was not perfectly oriented along the axis of symmetry of the specimen.

Additional small punch creep tests, carried out by Cortellino et al. [109], were considered for a P91 steel, with an initial thickness of the specimen of 0.5 mm and a punch radius of 1.04 mm, by applying a load of 25 kgf at a constant temperature of 600 °C. Figure 73 shows SEM images of those tests interrupted after (a) 2 hours ($^{t}/_{t_f} \approx 0$, $^{\Delta}/_{\Delta_f} \approx 0.40$), (b) 200 hours ($^{t}/_{t_f} \approx 0.20$, $^{\Delta}/_{\Delta_f} \approx 0.62$) and (c) after 669 hours ($^{t}/_{t_f} \approx 0.64$, $^{\Delta}/_{\Delta_f} \approx 0.82$), and FE damage contour plots for a P91 steel at 650 °C under a load of 200 N, with R_s=1.04 mm and t_0=0.5 mm. The FE damage contour plot will be discussed in section 6.5.7. The SEM images were used to calculate the contact angle by equation (93), by considering as contact radius the one at the inflection point of the profile of the inner surface of the specimens, clearly visible from the SEM images in Figure 73. The calculations led to values of the contact angle of 39°, 42.69° and 60.62° for the tests interrupted after 2 h ($^{t}/_{t_f} \approx 0$, $^{\Delta}/_{\Delta_f} \approx 0.40$), 200

h ($^{t}/_{t_f} \approx 0.20$, $^{\Delta}/_{\Delta_f} \approx 0.62$) and 669 h ($^{t}/_{t_f} \approx 0.64$, $^{\Delta}/_{\Delta_f} \approx 0.82$), respectively. These values of θ_0 are similar to those obtained from tests with an initial thickness of the specimen of 0.3 mm.

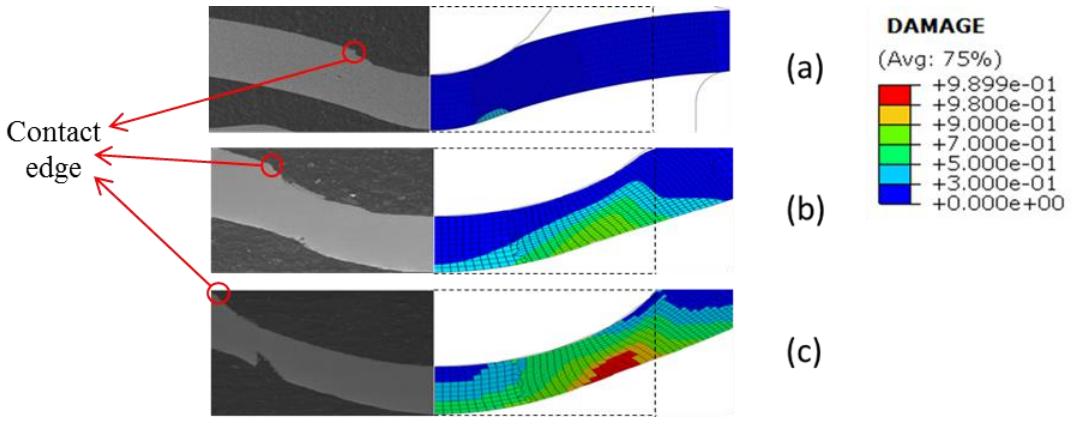


Figure 73. SEM images from ref. [109] for a small punch creep test, for a P91 steel at 600 °C with a load of 25 kgf, interrupted after (a) 2 hours ($^{t}/_{t_f} \approx 0$, $^{\Delta}/_{\Delta_f} \approx 0.40$), (b) 200 hours ($^{t}/_{t_f} \approx 0.20$, $^{\Delta}/_{\Delta_f} \approx 0.62$) and (c) after 669 hours ($^{t}/_{t_f} \approx 0.64$, $^{\Delta}/_{\Delta_f} \approx 0.82$), and FE damage contour plots for a P91 steel at 650 °C under a load of 200 N, with R_s=1.04 mm and t_0=0.5 mm.

6.5.2 Preliminary FE Results

In order to evaluate the accuracy of the coupled equations adopted between creep and elasticity, a set of preliminary analyses was carried out by using equation (90) and equations (91) and (92), respectively. Figure 74 (a) shows the contour plot of the von Mises equivalent stress when the specimen is approaching the failure time, obtained by using equation (90), i.e. the continuous damage model without modification, while Figure 74 (b) shows the contour plot of the von Mises equivalent stress, at the failure time, obtained by using equations (91) and (92). By using the modified continuous damage model, the time to rupture is lower than that obtained by using equation (90). The reduction in the failure time is caused by the complete disappearing of load carrying capability of the material obtained when ω approaches unity and the modified continuous damage model is used, while, when equation (90) is adopted, the material still has a residual strength when $\omega \rightarrow 1$.

When equation (90) is used, the central displacement of the punch continues increasing after the time when the damage variable reaches the upper bound on a path through the whole thickness of the sample. The solver is able to compute an

equilibrium configuration, therefore, the remaining load carrying capability of the specimen, with $\omega=\omega_{MAX}$, shows to be not negligible. When the modified coupling equations are used, the solver cannot calculate a balanced configuration as soon as $\omega=\omega_{MAX}$ through the whole thickness of the specimen. The reason for the more rapid non-convergence of the solution is the faster decrease in the load carrying capability of the specimen, therefore, the modified coupling equations show to be more accurate that equation (90) for the modelling procedure of SPCT. Figure 75 shows the difference in time to failure when using the continuous damage model and the modified version of that.

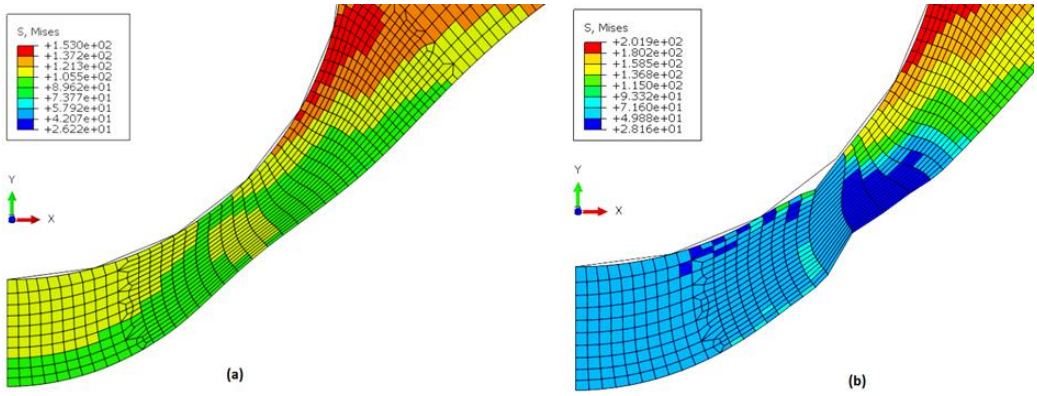


Figure 74. Contour plots of the von Mises equivalent stress obtained with a load of 200 N at (a) t=15.38h, by using a continuous damage model, and at (b) $t=t_f$=13.89h, by using the modified coupling equations.

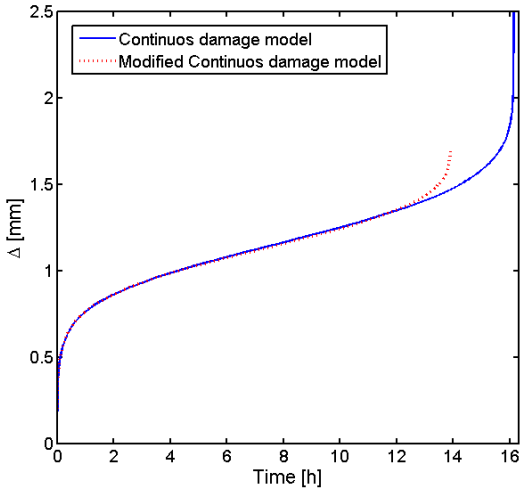


Figure 75. Punch displacement vs. time curves obtained under a load of 200 N, with R_s=1.04 mm, t_0=0.5 mm, by using the continuous damage model and the modified model.

In view of the more accurate description of the decrease in the load carrying capability of the specimen, equations (91) and (92) were used for the calculations discussed hereafter.

6.5.3 Effects of Load Magnitudes

The effects of the punch load magnitude on the evolution of the contact angle were investigated and punch load levels of 90, 110, 130, 150 and 200 N were used for the FE analyses. The punch radius and the specimen initial thickness have been fixed at 1.04 and 0.5 mm, respectively. As shown in Figure 76, the load magnitude does not affect the θ_0 evolution.

However, the load does not influence the variation of θ_0 versus Δ because the model does not include the effects of plasticity, which is governed by the load level, on the creep response of the specimen, which influence the deformation mode of the specimen and, as a consequence, the variation of θ_0 versus Δ [7, 127].

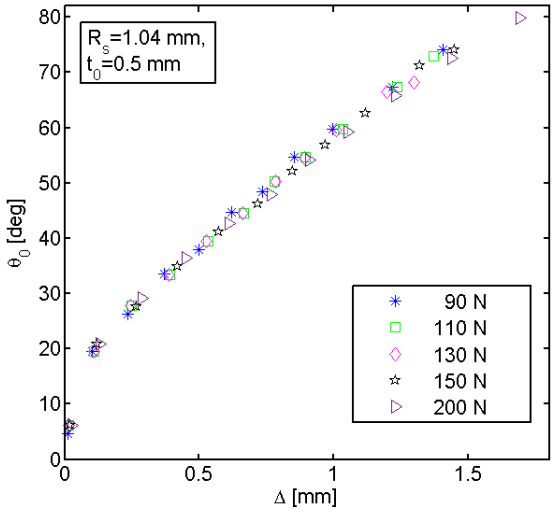


Figure 76. Evolution of the contact angle under five different punch load magnitudes, with R_s=1.04 mm and t_0=0.5 mm.

6.5.4 Effects of Friction Coefficient

The effects of friction between the punch and the specimen on the evolution of the contact angle were investigated and the values of the friction coefficient, μ, of 0, 0.2, 0.3, and 0.5 were used for the FE analyses. The punch radius and the specimen initial thickness were held at 1.04 and 0.5 mm, respectively, while the punch load was held at 90 N. As shown in Figure 77, the friction coefficient does not drastically affect the θ_0 evolution. Figure 78 shows the plot of (a) the creep equivalent strain and (b) the von Mises equivalent stress, evaluated at the integration point of the element 780 in the mid-section of the specimen necking area, against the punch displacement. The

quantities plotted in Figure 78 exhibit similar trends when different friction coefficients between the punch and the specimen are used.

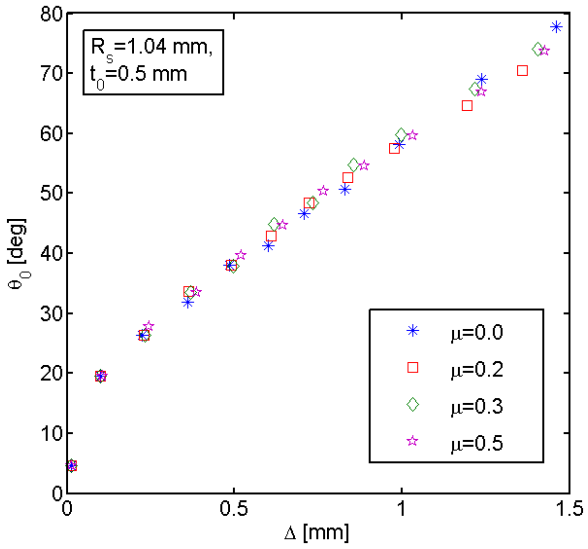


Figure 77. Evolution of the contact angle for different values of the friction coefficient between the punch and the specimen with R_S=1.04 mm and t_0=0.5 mm, under a load of 90 N.

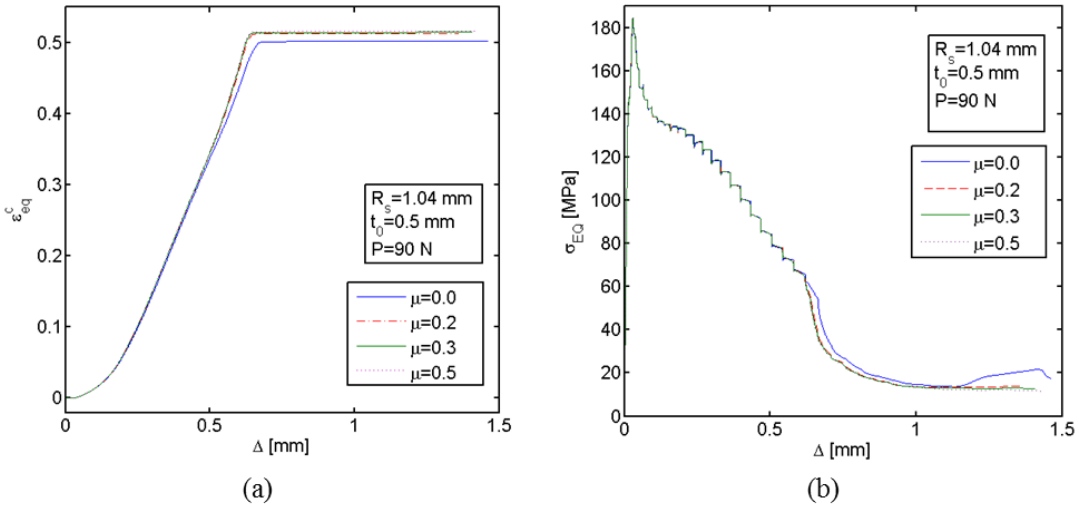


Figure 78. (a) Creep equivalent strain variation and (b) von Mises equivalent stress variation versus punch displacement, evaluated at the integration point of the element 780 in the mid-section of the specimen necking area, for different values of the friction coefficient between the punch and the specimen, with R_S=1.04 mm and t_0=0.5 mm, under a load of 90 N.

6.5.5 Effects of Punch/Specimen Dimensions

In order to investigate the effects of the punch radius and of the initial thickness of the specimen on the evolution of the contact angle, three different punch radii, R_S, (1.04, 1.25 and 1.50 mm) and four different specimen initial thicknesses, t_0, (0.5, 0.4, 0.3 and 0.2 mm) were adopted for the FE analyses. A receiving hole radius, a_p, of 2 mm, and

a punch load of 90 N, were kept constant. The FE results were compared with the Chakrabarty analytical solutions and with the experimental data.

6.5.6 FE and analytical solutions

Figure 79 show that the contact angle evolution, plotted against the central punch displacement, Δ, tends to approach to Chakrabarty's θ_0 distribution when the punch radius increases and the specimen initial thickness decreases. In particular, membrane stretching can be assumed as the governing mechanism for the specimen deformation when

$$\begin{cases} 0.8 < \Delta < 0.95 \text{ mm}, & 1.04 \leq R_s < 1.25 \text{ mm} \\ 0.8 < \Delta < 1.15 \text{ mm}, & 1.25 \leq R_s < 1.50 \text{ mm} \\ \Delta > 0.8 \text{ mm}, & R_s = 1.50 \text{ mm}. \end{cases}$$

In those ranges, the FE results match with the analytical solution when 0.2 mm $\leq t_0 \leq$ 0.3 mm obtained by Chakrabarty's theory, which is valid when the thickness of the blank is small compared to the punch radius. The reason why the SPCT specimen experiences bending as the governing deformation mechanism when Δ is out of the range boundaries determined in this research can be partly related to the boundary conditions applied to the disc. As shown in Figure 65, Chakrabarty's specimen is allowed to rotate of an angle θ where the support is applied, while, in the same position, the SPCT specimen cannot rotate at the support due to the clamping (see Figure 66).

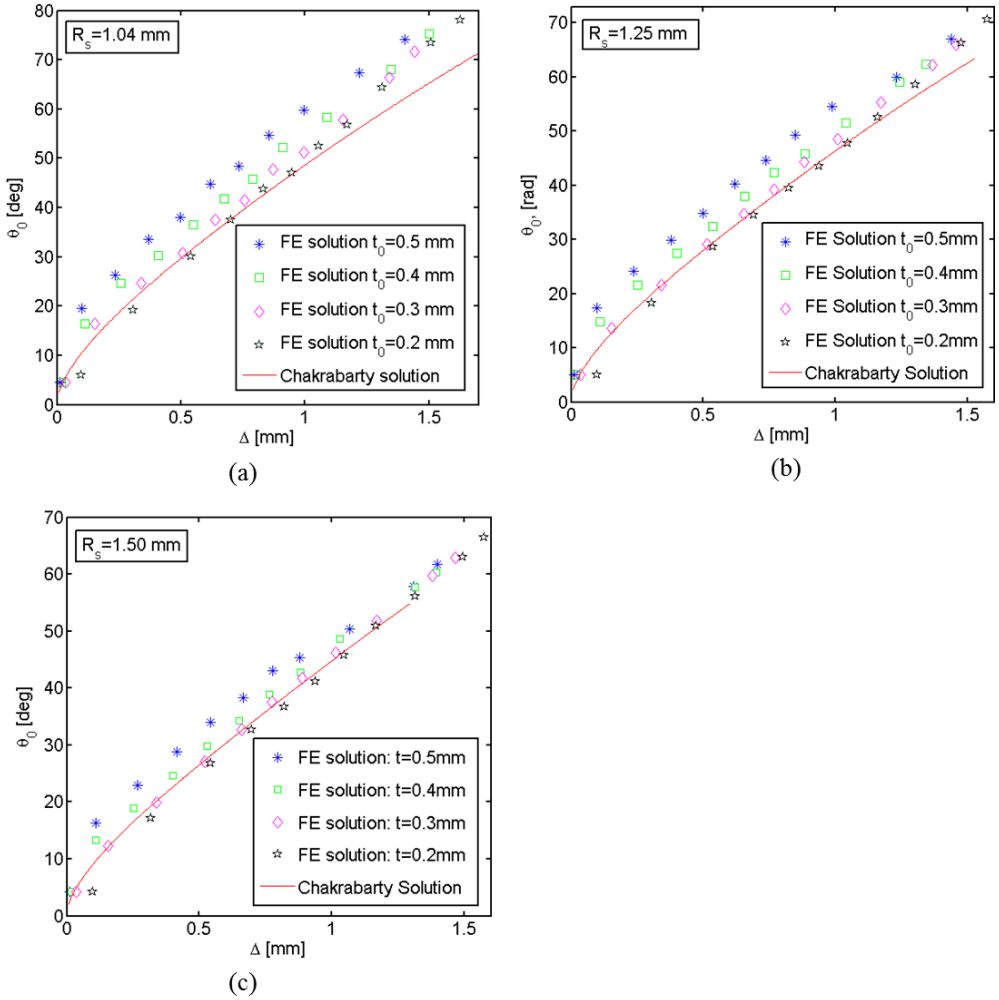


Figure 79. Evolution of the contact angle under a load of 90 N, with different initial thickness of the specimen and with (a) R_s=1.04 mm, (b) R_s=1.25 mm and (c) R_s=1.50 mm. The FE data are compared with Chakrabarty's analytical solution.

Figure 80 shows the variation of the contact angle obtained from FE analyses with the reciprocal initial thickness of the specimen at several fixed Δ values, with R_s equals 1.25 mm. When the specimen initial thickness decreases from 0.2 to 0.1 mm, the contact angle tends to be constant, as assumed in Chakrabarty's theory [126], which is valid when t_0 is small compared to the punch radius.

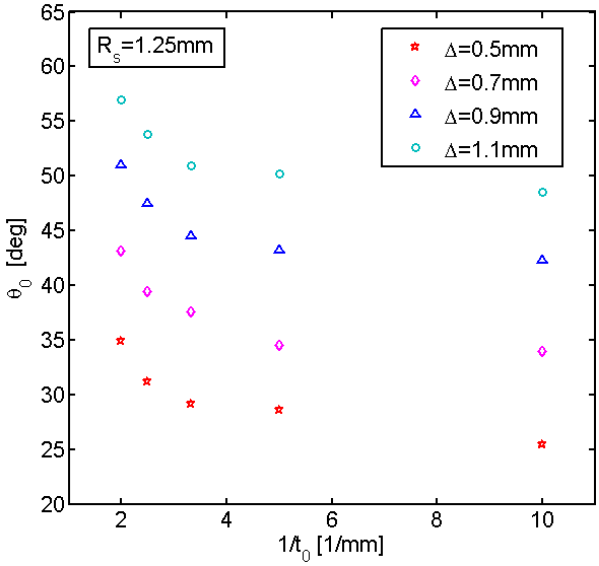


Figure 80. Contact angle vs. thickness reciprocal under a load of 90 N, with R_s=1.25 mm and constant punch displacements.

In Figure 81, the contact angle, obtained by FE calculations, is plotted versus the initial thickness of the specimen and the punch displacement, both normalised by a_p. The FE results of Figure 81 were fitted by a relation of the form of equation (96), where *a*, *b*, *c*, *d*, *e*, *f* and *g* are fitting constants, listed in Table 39. It should be noted that these constants are different for each punch radius.

$$\theta_0 = aln\left(g\frac{t_0}{a_p}\frac{\Delta}{a_p}\right) + \mathrm{b}\frac{\Delta}{a_p} + \mathrm{c}\frac{t_0}{a_p} + \left(\mathrm{d}\frac{t_0}{a_p} + \mathrm{e}\frac{\Delta}{a_p}\right)^f \tag{96}$$

A surface fitting of the form of equation (97) was also found for the evolution of the contact angle at failure, θ_{0f}, versus the specimen thickness and the punch radius, where p_i, for i = 0…8, are fitting constants, listed in Table 40. Figure 82 plots the evolution of θ_{0f} with t_0/a_p and R_s/a_p.

$$\theta_{0f} = p_0 + p_1\frac{t_0}{a_p} + p_2\frac{R_s}{a_p} + p_3\left(\frac{t_0}{a_p}\right)^2 + p_4\frac{t_0}{a_p}\frac{R_s}{a_p} + p_5\left(\frac{R_s}{a_p}\right)^2 + p_6\left(\frac{t_0}{a_p}\right)^3 + p_7\left(\frac{t_0}{a_p}\right)^2\frac{R_s}{a_p} + p_8\frac{t_0}{a_p}\left(\frac{R_s}{a_p}\right)^2 \tag{97}$$

Table 39. Fitting constants for equation (96).

R_s [mm]	a	b	c	d	e	f	g
1.04	0.06195	1.021	-0.875	2.165	0.4317	0.4545	0.5026
1.25	0.04659	0.9759	$0.1492*10^{-3}$	0.4995	0.2288	0.3584	0.2732
1.50	0.03861	0.9509	$0.1369*10^{-3}$	0.4009	0.2258	0.2704	0.006693

Table 40. Fitting constants for equation (97).

p_0	p_1	p_2	p_3	p_4	p_5	p_6	p_7	p_8
2.341	-0.06726	-0.7115	39.3	-27.37	-0.6988	8.217	-45.92	31.15

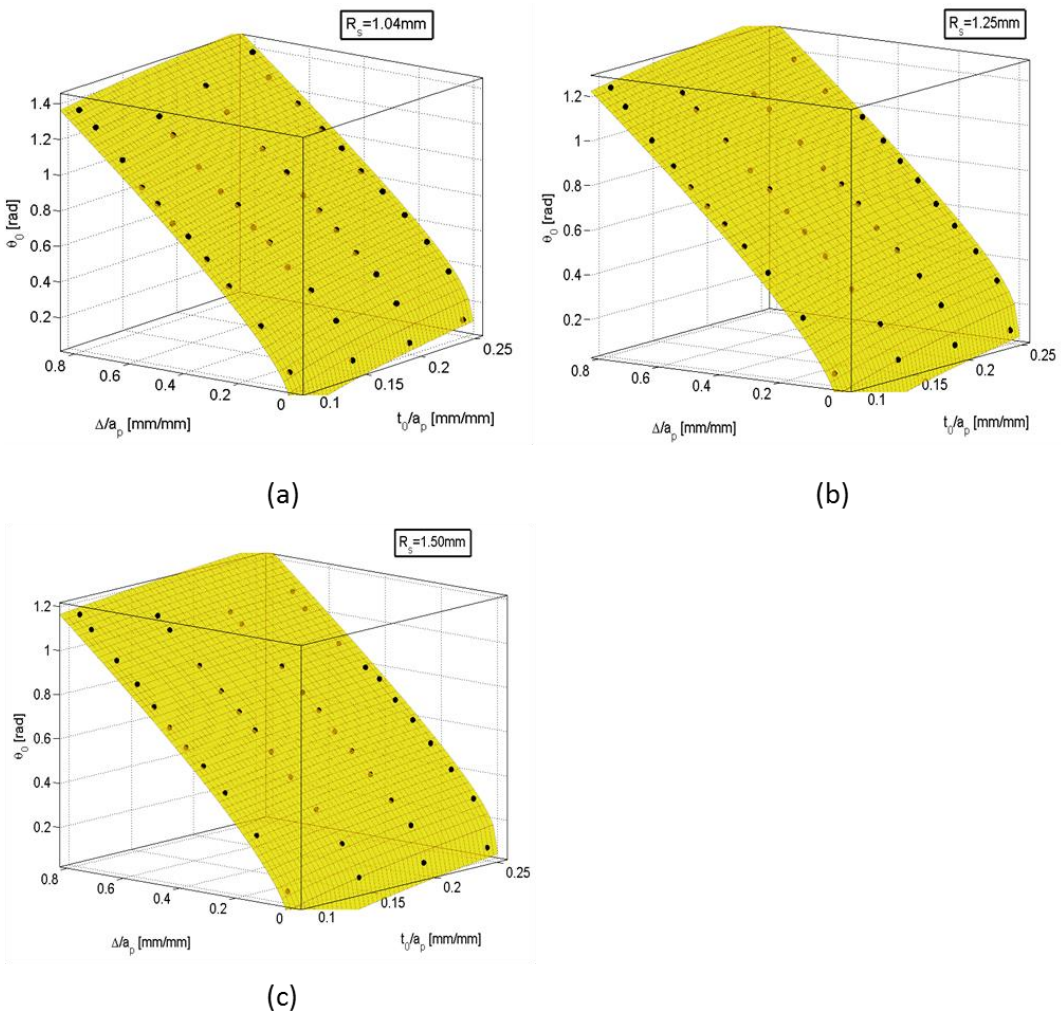


Figure 81. Evolution of the contact angle with the punch displacement and the specimen initial thickness both initialised by a_p, at a constant punch radius, (a) R_s=1.04 mm, (b) R_s=1.25 mm and (c) R_s=1.50 mm, with the fitted surface to the FE data.

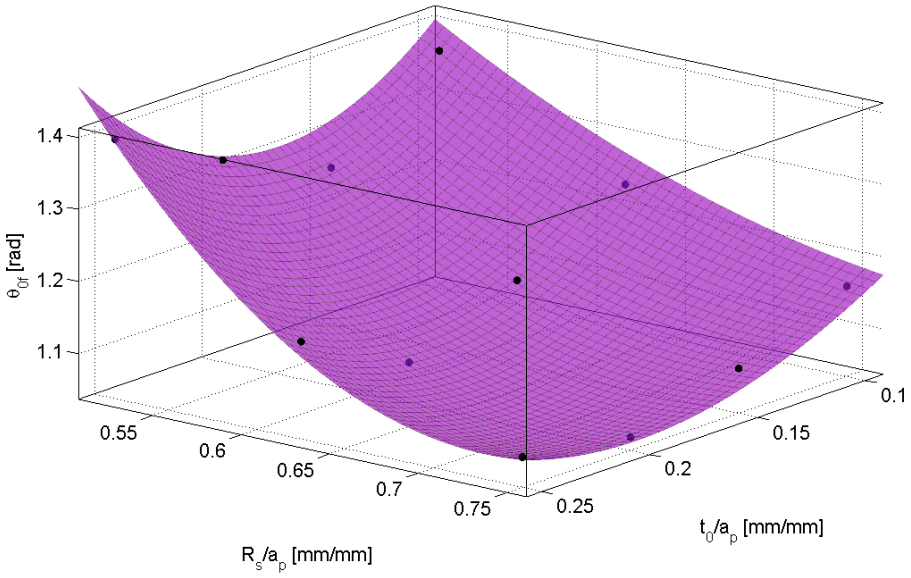


Figure 82. Evolution of the contact angle at failure with the punch radius and the specimen initial thickness, with the fitted surface to the FE data.

6.5.7 Comparison with the Experimental Findings

A comparison of the numerical and analytical results with the measured experimental data of tested SPCT specimens was also carried out. The contact angles found for the two interrupted tests with t_0=0.3 mm match with both Chakrabarty's solution and the FE results.

Also, the experimental results obtained by Cortellino et al. in 2014 [109] with t_0=0.5 mm were compared with FE results in terms of deformation shape and damage propagation. The FE analysis was performed assuming for the specimen and the punch the same geometry as in ref. [109], a punch load of 200 N and a constant temperature of 650 °C. From Figure 73 (a) it is possible to notice that after two hours the deformation of the specimen had already reached the 40% of its final value, due to creep mechanism. The damage of the specimen was found to be very low, around 30%, and localized in the bottom of the specimen in the necking area, close to the axis of symmetry. Figure 73 (b) shows that, after 200 h, the damage in the specimen was around 70%, and it had spread toward the middle of the necking area and through the thickness of the specimen. In Figure 73 (c) the crack in the specimen ($\omega \approx 1$) is visible both in the tested specimen and in the FE contour plot. Cortellino et al. also carried out a microscopic investigation on the tested samples and found that after 669 h the crack had spread along the hoop direction of the bottom surface of the disc as well as through the thickness of the specimen [109]. Figure 83 shows the propagation of

micro-cracks at the tip of the crack for the test interrupted after 669 h [7, 109]. The FE analysis show that the zone affected by the maximum damage spread from the bottom of the specimen through the thickness in the necking area as reported in the open literature [7, 109, 127, 128, 180].

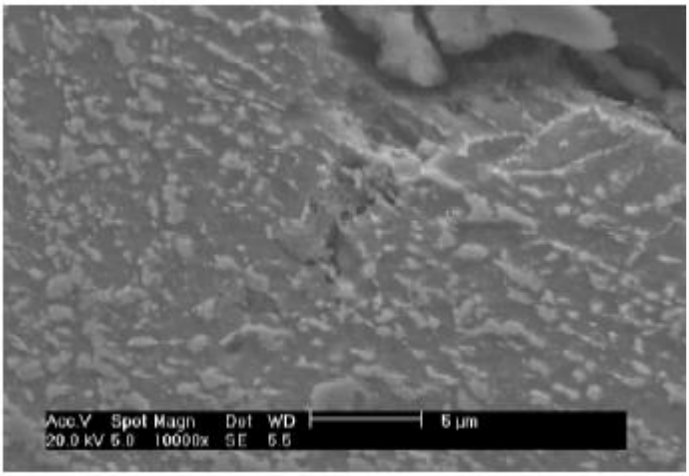


Figure 83. SEM image from ref. [2] for a small punch creep test, for a P91 steel at 600 °C with a load of 25 kg, interrupted after 669 h.

The difference between the test temperature and that assumed for the material properties adopted for the FE analyses does not change the creep mechanism characterising the deformation of the specimen, which is represented by dislocation creep in the secondary creep regime and inter-granular cavitation when the tertiary creep stage is reached [7]. The experimental and FE data in terms of contact angle were also compared with Chakrabarty's solution. Figure 84 plots the contact angle obtained by the numerical, analytical and experimental procedures versus the punch displacement, and shows the consistency between the FE and analytical results with the experimental evidence. The differences between experimental data and FE results can be related to the effects of significant plastic deformation which is experienced by the SPCT specimen during the test [112, 127] and to the approximation of the friction formulation used in the FE analyses for the interactions between the specimens and the testing machine components. In particular, plastic deformation, which differentially takes place in various location of the specimen, affects the creep response of the material in the sub-sequent stages of the test and, in turn, the static response of the structure. Cortellino et al. [114] found that, in a small punch creep test specimen for P91 steel, creep was, in general, accelerated near the punch/specimen contact edge location while it was resisted in other locations of the structure as an

effect of the complex plastic strain field generated upon load application. Cortellino et al. [114] also reported that in the central plane of the specimen, corresponding to the neutral bending plane in the initial stages of the test, no alteration of the creep properties of P91 steel was observed. Such finding relates to classical bending theory which features virtually zero-stress, and no plasticity accumulation, on the neutral bending plane of the specimen [114]. As a result of the balance between creep enhancement and creep resistance effects generated by plasticity accumulation, Cortellino et al. reported an increase of the failure life up to 10 times when initial plastic deformation is included in the model [127].

Furthermore, geometry inaccuracies of the punch load might also occur, as well as specimen elastic recovery [133].

A feature of the test capable of significantly affecting the experimental output is represented by the friction characteristics of the contact interaction between the specimen and the punch. The friction forces developed at such interaction during testing generate a local bending moment which opposes the rotation of the section at the edge of contact that contributes to creep development and failure of the specimen [132]. By applying a classical Coulomb friction formulation in numerical calculations, Cortellino at al. [132] found that an increase in the coefficient of friction led to an increase of the frictional forces and, as a consequence, of the bending moment opposing the specimen deformation. As a result, they reported an increase in creep failure time of the specimen of up to 8 times when the friction coefficient between the specimen and the punch varies from 0 to 0.5. The results of the numerical calculation reported by Cortellino at al. [132] are compatible with detailed experimental work carried out by Kobayashi et al. [134].

Also, misalignments and eccentricity of punch loading was found by Cortellino at al. [133] to affect the static response of the specimen and in turn the experimental output. Both of these two sources of inaccuracy affect the terms of stiffness activated by punch loading in the instantaneous response of the specimen. As a consequence, also the stress field developing in the specimen is modified when the punch load is eccentric and/or at an angle from the vertical direction, as well as the subsequent creep strain field and the test output. In the work reported by Cortellino at al. [133] the failure time was found to increase by up to 1.49 times in the scenario with

the maximum misalignment and eccentricity considered in ref. [133] compared to the nominal configuration.

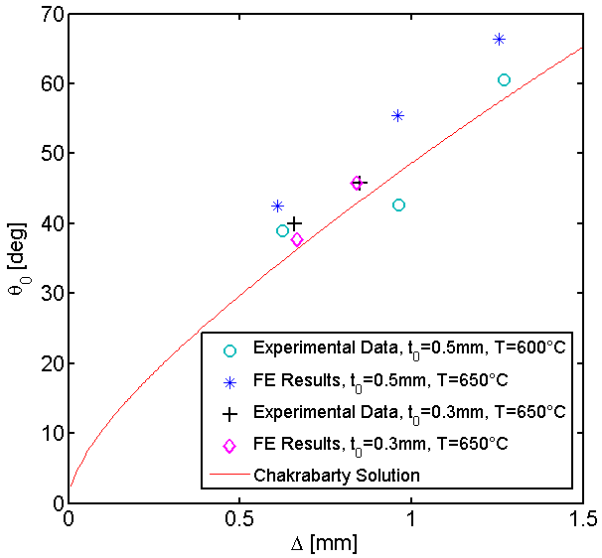


Figure 84. Evolution of the contact angle: comparison among FE results, Chakrabarty's analytical solution and experimental data.

The comparison of the variation of θ_0 versus Δ identified from FE results with material properties at 650 °C with that obtained from the results of tests carried out at 600 °C is possible because, at these two temperatures, the creep mechanism governing the deformation of the specimen is the same, i.e. dislocation creep, therefore the deformation modes are consistent [7].

6.5.8 Evolution of the Contact Angle under Different Material Constitutive Models

The effects of different material constitutive models (such as the multi-linear isotropic hardening plastic models and the elastic-perfectly plastic constitutive model described in section 6.2.8) on the variation of θ_0 versus Δ were investigated and compared to those obtained by Liu and Murakami's damage constitutive model and Norton's model.

The punch radius was held constant to 1.04 mm. The load has been chosen to be 200 N and 90 N for creep analyses, for an initial specimen thickness of 0.5 mm and 0.3 mm, respectively. Figure 85 shows the evolution of the contact angle plotted against the central punch displacement, Δ, for these different constitutive models, also compared with Chakrabarty's solution. The FE results show that the specimen

deformation shape is the same for all models, but, when $\Delta > 0.8$ mm, the instantaneous distortion due to strain hardening is quite different from the viscous distortion due to creep, as the mechanism which governs the stress distribution is different. In fact, during creep, the material is subjected to relaxation (Figure 78) and, even if the stress is redistributed around a failed area, allowing the specimen to continue in carrying some load, this behaviour cannot be described as hardening.

It is to be noted that Norton's model can produce complex θ_0 or numerical errors in θ_0 calculation when $\Delta > 1.6$ mm. This Δ value was found to depend on the initial thickness of the specimen and on the applied load. From the definition of the contact angle in equation (93), this means that Norton's model simulates the penetration of the punch in the specimen. Whereas the specimen volume is constant and this penetration has not been observed during tests (see also ref. [109]) and although Norton's model FE results are close to the Chakrabarty analytical solution, this model can predict the deformation shape, but not the failure mechanism.

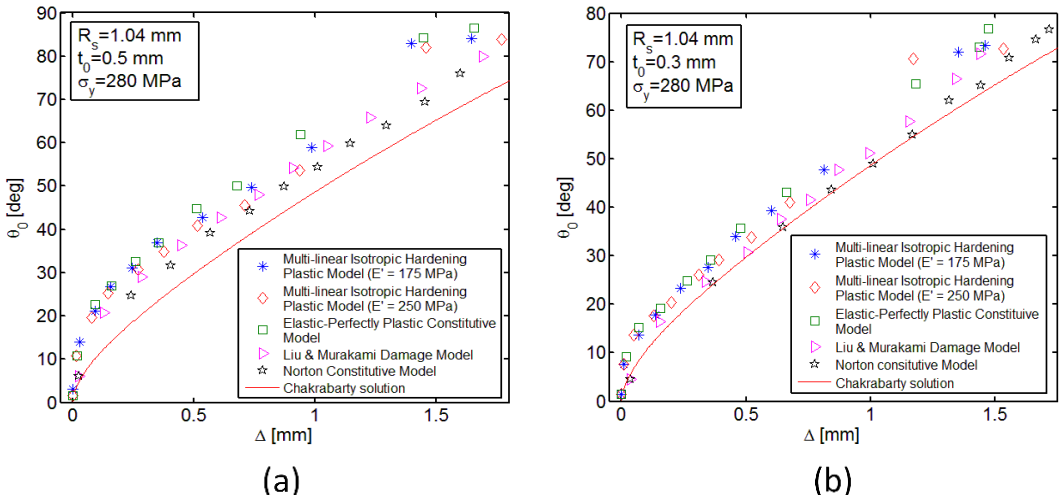


Figure 85. Evolution of the contact angle for different constitutive models, with R_s=1.04 mm and with (a) t_0=0.5 mm, with a load of 200 N, and with (b) t_0=0.3 mm, with a load of 90 N.

7 CONCLUDING DISCUSSION AND FUTURE WORK

7.1 THE ROLE OF SMALL SPECIMENS IN POWER PLANT LIFE MANAGEMENT

This Thesis has focussed on the application of small specimen testing methods with an emphasis on their place in a modified and practical life assessment framework that could be applied to both conventional and nuclear generating assets. Examples have been provided on current practice associated with invasive site inspections and material condition assessment towards the end of economic life on conventional plant pipework systems. The exacting demands associated with the use of small specimen testing methods in nuclear plant applications strongly emphasises the importance of developing agreed codes of practice and standards. The successful development and validation of alloys under consideration for fusion reactors demands the application of standardised small specimen test methods.

In order to reduce the rate of damage accumulation and avoid the cost of pipework replacement, earlier monitoring could be carried out by use of targeted miniature specimen testing. Also, to date, the correlation between creep cavity count and other often used off-load tests, such as surface hardness, is not well defined. Currently run-repair decisions are based on the site inspection data and limited review of operational conditions as described in Section 5.2.2, and in relation to the specimen examined in this study. The use of impression creep tests in this example, and in conjunction with scrutiny of the available information on operating conditions and prior inspections has emphasised the importance of adopting a more rigorous approach to condition assessment. This more rigorous approach can be facilitated by the use of small specimen testing and ideally coupled with more predictive capabilities provided by computational models [20] and use of on-load data from the operating plant.

Importantly, the experiences described in this Thesis on the successful application of both small punch and impression creep techniques to support operational plant gives a clear indication of their potential use in the field. There are of course still a number of challenges to overcome before their use can be more widespread to assist the plant operator. For example, the case study provided in Section 3.3.1 shows how the current methods for assessing the condition of materials via hardness and surface replica surveys have some scope for improvement, ideally

towards a position where more mechanistic material behaviour models can be applied, which would be regularly and seamlessly updated with operational and inspection data. Information from the application of small specimen testing campaigns can support this objective, but only if applied in accordance with a timely and structured approach as described in this Thesis. The development of validated small specimen testing methods will also require complementary innovation of experimental measurement methods, facilities and data interpretation.

Developments to improve measurement methods applied in experimental tests may well result in useful applications on operating plant. The use of laser based measurement systems is now accepted and applied (for measuring component displacements) to assist plant investigations associated with premature failure of welds. High resolution and high temperature optical strain measurement systems have been taken out of the laboratory and engineered for site applications [25]. Features of these high temperature optical strain measurement systems have recently been used to assist the first site application of creep damage sensors [26]. There are also examples of the first trials of non-contact full field strain measurement on high temperature plant using digital image correlation [33] and the site application of thermographic approaches for defect identification and residual stress measurement using infra-red camera systems [191]. The power industry is facing severe challenges as the economy transitions to a low carbon future. This puts much emphasis on conventional and nuclear AGR plant continuing to operate reliably, cost effectively and with a focus on life extension.

The current practice for life management of high temperature and pressure systems, presented in Chapter 3, proposes that small specimen testing methods should ideally be used earlier in the plant lifecycle. The current inspection based approach for life management is unable to provide sufficiently rigorous future life predictions that allow the plant operator to efficiently optimise plant operation and reduce through life inspections costs. It is recognised that developing rigorous predictive life assessment models is not trivial; however, targeted use of small specimen testing methods described in this Thesis and within a new life assessment framework, that also exploits the capabilities offered by modern computational techniques, provides an opportunity to achieve this objective. To support this aim there is a critical need to improve the

exploitation of extensive plant data acquired during outages, along with on-line data routinely captured during operation.

The ultimate aim is to develop ‘point of application’ material models that can seamlessly use in-service metallurgical, inspection and operational data and provide the station operator with a timely and predictive life assessment capability. These aims are applicable to both conventional and nuclear generating stations. Moreover, the arduous operational duty experienced by conventional generating plant provides a useful source of both metallurgical and operational experience to assist the cost-effective life management of existing nuclear AGR plants and could support the approach to life management of materials used in next generation nuclear reactors.

7.1.1 A novel approach based on hardness and impression creep tests for condition monitoring

The case study on CMV parent material presented in Section 3.3.2 has illustrated the general reduction in surface hardness as material ages under operational conditions. A correlation between the change in creep replica assessment level and surface hardness is not evident from the data set studied; moreover, it is important to consider that any change in creep replica assessment level will only be identified during the later stages of operational life. Hence, this is not particularly conducive for through life condition monitoring and future life prediction. The reduction in hardness through life presents an opportunity to use this routinely measured parameter in a predictive assessment model, hence providing a proactive means of identifying adverse rates of change in hardness that may be indicative of the approach to end of life and retirement from service. Currently the hardness data acquired from a site outage is scrutinised to determine any notable and consistent trends that indicate deterioration, often in conjunction with review of surface replicas. Unfortunately, there is no routinely deployed assessment model in use to provide a quantitative prediction of residual life. Typically, indications of consistent hardness reduction (softening) will proactively prompt repairs or component replacements. This approach is clearly sub-optimal and practical improvements can only be achieved by the development and use of a suitable predictive life model, with timely feedback to improve plant operation.

An approach for the implementation of surface hardness in the Liu and Murakami damage model has been illustrated in Section 3.2.2. Currently the only approach in common use to predict the rate of creep life consumption is via the calculation of the creep effective temperature. However this has been shown to have several limitations [20] and can realistically only be considered to provide information complementary to that acquired during the invasive outage inspections, which increase in scope as the plant ages, as illustrated in Figure 43. Use of routinely acquired hardness data in a model such as Liu and Murakami's gives the operator scope to assess the effect of the rate of change in hardness and predict the likely impact of this for future operation and ultimately influencing the scope of future outage inspections.

Practical assessment tools have been developed as part of the Flex-E-Plant consortium [167] that allow the rapid definition of whole pipe system models, which permit the input of pipe support hanger loads, operational conditions and user defined creep damage models such as the modified Liu and Murakami model described in this Thesis. This for the first time allows the station to proactively use this routinely acquired data to determine the current rate of damage accumulation and importantly predict the future rate of damage accumulation. Clearly, as the comparison of the site outage hardness and creep replica results has shown, there is a need to validate any subsequent prediction of life consumption. This is necessarily an iterative process, but one which will not be implemented unless suitable and cost-effective assessment tools are available. Section 3.2.2.1 describes an iterative approach to plant assessment that will guide validation of the model proposed in this work and for that matter any other similarly defined lifing model. The case study presented in Section 3.3 has alluded to more restrictive electricity markets for conventional thermal power plants; this in itself should drive the implementation of these novel predictive life assessment approaches that importantly take advantage of site information currently acquired and enabled by the efficient use of novel computational models. The inconsistency of the CET and the impossibility of a correlation between diametral strain rates and CET show the current difficulty interpreting such measurement data in isolation and the reason why other more invasive methods, such as surface replication, is used to assess material condition. Also, a greater probability of identifying a change in the hardness level as opposed to a change in the creep replica assessment level has been found when comparing successive hardness and creep replica data from the same location. Thus,

the application of a representative hardness based stress model, that could account for the loading applied to an operational steam line and importantly be amenable for update, by use of small specimen sampling and other data such as obtained from pipe hanger adjustments and operational steam temperatures and pressures would be advantageous.

7.1.2 Considerations on impression creep test

In view of the high importance that miniature specimens may have in novel lifing models, Chapter 4 focussed on the reliability of impression creep tests, by presenting several test data and by illustrating the consequences of geometry inaccuracies of the indenter during the test. Impression creep test has been confirmed to be reliable as well as the conversion relationships available so far. In fact, rotations of the indenter of 3° or smaller, do not significantly affect the conversion parameters

Elastic-plastic-creep FE analysis has been shown to be able to replicate the specimen behaviour in terms of shear deformation, which causes the distortion of the grains of the specimen underneath the indenter at a certain distance from the contact edge. Therefore, more accurate conversion parameters may be determined by elastic-plastic-creep FE analyses.

7.1.3 Through thickness examination of an ex-service CrMoV pipe section

The study on the CrMoV section presented in Chapter 5 has emphasised the importance of correlating the operating conditions (temperature and stress) with the results from metallurgical examinations and small specimen creep tests. The specimen parent material is degrading at an unusually slow rate for this service age and can be considered to have been retired from service too early. The use of traditional hardness and creep replica methods has revealed relatively uniform damage throughout the pipe section. Summary results from other studies have also been presented and these show quite different characteristics, some with pronounced through section creep cavity gradients. Impression creep tests have produced results in agreement with uniaxial tests of similar materials [176, 192]. Importantly extrapolation of the MSR to plant stress levels confirm the slow rate of degradation observed from the limited operational data. The thorough examination of this CMV section and inspection of other through section creep replica data obtained from ex-service pipes has confirmed

the importance of also acquiring the fullest understanding of the operational conditions (temperature and stress) as well. Operating stations will not necessarily have the luxury of being able to regularly remove pipe sections for through section examination of the nature described in this Thesis. They will rely on limited small specimen sampling from the component surface at various stages through life, which therefore provides a reference condition or measurement. The subsequent use of analytical models that use operational data as inputs is essential in order to validate this reference measurement and hence modify operating conditions accordingly as required [20].

7.1.4 A step forward for the realization of an improved Code of Practice for small punch creep test

Finally, Chapter 6 presented a study on the evolution of the contact angle of small punch creep test specimen, with the goals to investigate the applicability of both Chakrabarty's membrane stretching theory and of the CEN Code of Practice CWA 15627 on SPCTs, and to enlighten the deformation and failure mechanisms of the SPCT specimen.

Currently, material continuous damage models, based on Liu and Murakami's model, cannot simulate zero-stress in those areas where the specimen was supposed to be failed, therefore a modified continuous damage model was developed and used in this work. The results of FE analyses showed that the variation of the friction coefficient and of the punch load level has no influence on the evolution of the contact angle with the central punch displacement. Further FE analyses were performed for evaluating the effects of different material constitutive models on the variation of θ_0 with Δ. The deformed shape of the specimen was found to be the same for all material models, but the instantaneous distortion was found to be different from the viscous distortion caused by creep.

Changes in the initial thickness of the specimen and in the punch radius have significant effects on the evolution of the contact angle with the central punch displacement, as they determine the values of Δ for which membrane stretching can be assumed as the governing mechanism of the specimen deformation. The numerical results were fitted by equations in two variables and compared to the Chakrabarty analytical solution and to the experimental data, allowing for the evaluation of new

ranges of applicability of the CEN Code of Practice CWA 15627 and of Chakrabarty's theory on the SPCTs.

Some differences were found between the numerical results and the experimental data, and they have been associated to some factors which have not been included in the numerical calculations, but could have been occurred during the tests, i.e. the effects, on the specimen time to failure, of punch load misalignments, of initial plasticity, and of friction coefficient between the punch and the specimen. In the open literature, it has been found that the increment in the failure life is larger when the effects of initial plasticity and of friction coefficient are considered in the FE model.

The results obtained could be useful for the development of an improved data conversion relationship between the SPCT data and the uniaxial creep test data, and in particular for the progression in the upgrade of the CEN Code of Practice CWA 15627.

7.2 CONCLUDING REMARKS

The gaps raised in Section 2.7 were analysed and addressed in this Thesis.

- A new holistic condition assessment that includes miniature specimen creep testing data was discussed (see Chapter 3) and supported by a case study that demonstrates the inefficacy of the current methods in determining the remaining life of power plant components. The presented method defines a more targeted and cost-effective forward inspection plan. In fact, cost reductions would be achieved by:
    - Reduction in the use of diametral strain measurements;
    - Optimisation of outage site creep replica and hardness sampling and analysis campaigns;
    - Optimisation of outage weld inspections.
- A novel lifing method based on a modified Liu and Murakami creep damage model that involves hardness and impression creep testing data was developed (see Chapter 3) and supported by an example of implementation and validation

of the technique. The discussed technique could be very useful in monitoring the residual life of power plant components. The advantages of this approach are as per follow:

- It gives the utility useful information about the current conditions of the component;
- It provides failure time from impression creep test results closer to the corresponding uniaxial creep test data than Monkman-Grant's relationship when HV > 190;
- It does not need an initial hardness value at t = 0 h for the failure life to be established, contrary to other approaches established so far.

- The reliability of impression creep test was assessed through a discussion of test data, of possible geometry inaccuracies of the indenter that may occur during the test, and of the determination and accuracy of the parameters currently used to convert impression creep test data to the corresponding uniaxial creep test data (see Chapter 4).

- A possible correlation between data obtained by well-established methods, e.g. replica creep cavity count, hardness measurements, micrographs, etc., and data obtained by miniature specimen creep testing data was investigated (see Chapter 5). This investigation shows how miniature creep test specimen data could be practically used as part of the new holistic approach described in Chapter 3 for the evaluation of life consumption of power plant components and concludes that the studied parent material could have been retired from service too early.

- A step forward in the understanding of the complex behaviour of small punch specimen was made (see Chapter 6) and new ranges of applicability of Chakrabarty's membrane stretching theory were determined. Updated versions of the CEN Code of Practice should take into account the results of the presented research in order to improve the accuracy of the test data interpretation.

7.3 FUTURE WORK

Impression creep tests have shown to be useful and in line with other test methods, such as hardness and replicas techniques. The current measurement tolerance of the testing machine for ICTs does not allow to obtain accurate material data at stresses similar to those applied to in-service components (~ 40-60MPa) in relatively short duration. The design of a more accurate testing machine would increase the test reliability.

Increasing the accuracy of the conversion parameters for impression creep test could produce great benefits in data comparison. In fact, the conversion relationships available so far are based on the hypothesis that the conversion parameters do not vary in the steady state because the change in specimen geometry is assumed to be small. Further improvements could be achieved by verifying the rightness of this hypothesis, by performing FE analyses that take into account the variation of the indentation depth during the test. Also, the accuracy of η and β could be increased by determining the vertical displacement through elastic-plastic FE analyse.

Other miniature creep test specimen techniques, such as the two-bar and the small punch creep tests, could be very useful to obtain creep data to be compared with industrial data currently acquired, but round robin tests and standards for these tests are still needed.

Further research on the proposed new holistic approach and novel lifing method based on hardness and impression creep testing data is certainly needed. In particular, more studies similar to the investigation presented in Chapter 5, that correlates the disparate site inspection data and small specimen creep testing data, would produce a large database and additional demonstration of the validity of the proposed techniques.

8 REFERENCES

1. Kraus, H., *Creep Analysis*, ed. I. John Wiley & Sons. 1980, New York, NY, (USA).

2. Penny, R.K. and D.L. Marriott, *Design for creep*, ed. 2nd. 1995, London: Chapman and Hall.

3. Viswanathan, R. and J. Stringer, *Failure mechanisms of high temperature components in power plants.* TRANSACTIONS-AMERICAN SOCIETY OF MECHANICAL ENGINEERS JOURNAL OF ENGINEERING MATERIALS AND TECHNOLOGY, 2000. **122**(3): p. 246-255.

4. Abe, F., T.-U. Kern, and R. Viswanathan, *Creep-resistant steels*. 2008: Elsevier.

5. *CEN WORKSHOP AGREEMENT, Small Punch Test Method for Metallic Materials, CWA 15627: 2007, D/E/F*. European Committee for Standardisation, December 2007.

6. Hyde, T.H., W. Sun, and C.J. Hyde, *Applied Creep Mechanics*. 2013: McGraw-Hill Professional.

7. Cortellino, F., *Experimental and Numerical Investigation of Small Punch Creep Test*. 2015, Ph. D Thesis, The Univeristy of Nottingham.

8. Wilshire, B. and M. Willis, *Mechanism of Strain Accumulation and Damage Developmant During Creep of Prestrained 316 Stainless Steel.* Metaallurgical and Materials Transactions A, 2004. **35**(2): p. 563-571.

9. Guglielmino, E., R. Pino, C. Servetto, and A. Sili, *Chapter 4 - Creep damage of high alloyed reformer tubes A2 - Makhlouf, Abdel Salam Hamdy*, in *Handbook of Materials Failure Analysis with Case Studies from the Chemicals, Concrete and Power Industries*, M. Aliofkhazraei, Editor. 2016, Butterworth-Heinemann. p. 69-91.

10. MacKenzie, A.C., *On the use of a Single Uniaxial Test to Estimate Deformation Rates in Some Structures Undergoing Creep.* International Journal of Mechanical Sciences, 1968. **10**(5): p. 441-453.

11. Sklenička, V. and L. Kloc, *5 - Creep in boiler materials: mechanisms, measurement and modelling A2 - Oakey, John E*, in *Power Plant Life Management and Performance Improvement*. 2011, Woodhead Publishing. p. 180-221.

12. Ashby, M., H. Shercliff, and D. Cebon, *Materials Engineering Science, Processing and Design*. 2014, Oxford: Butterorth - Heinemann.

13. Liu, Y. and S. Murakami, *Damage Localization of Conventional Creep Damage Models and Proposition of a New Model for Creep Damage Analysis.* JSME International Journal Series A, 1998. **41**(1): p. 57-65.

14. Rabotnov, Y.N., *Creep problems in structural members.* 1969.

15. Hutchinson, J., *Constitutive behavior and crack tip fields for materials undergoing creep-constrained grain boundary cavitation.* Acta Metallurgica, 1983. **31**(7): p. 1079-1088.

16. Riedel, H., *Fracture at high temperatures*. 2014: Springer.

17. *ABAQUS Theory Manual.* Hibbitt, Karlsson & Sorensen, Inc., 1998. **Version 5.8**.

18. Hyde, T., M. Saber, and W. Sun, *Testing and modelling of creep crack growth in compact tension specimens from a P91 weld at 650 C.* Engineering Fracture Mechanics, 2010. **77**(15): p. 2946-2957.

19. Lin, J., Y. Liu, and T. Dean, *A review on damage mechanisms, models and calibration methods under various deformation conditions.* International Journal of damage mechanics, 2005. **14**(4): p. 299-319.

20. Morris, A., B. Cacciapuoti, and W. Sun, *The Role of Small Specimen Creep Testing within a Life Assessment Framework for High Temperature Power Plant.* International Materials Reviews, 2018. **63**(2): p. 102-137.

21. Abson, D.J., *17 - Power plant welds and joints: materials management and performance improvement A2 - Oakey, John E*, in *Power Plant Life Management and Performance Improvement*. 2011, Woodhead Publishing. p. 635-665.

22. Barker, R., Y. Hua, and A. Neville, *Internal corrosion of carbon steel pipelines for dense-phase CO2 transport in carbon capture and storage (CCS) – a review.* International Materials Reviews, 2017. **62**(1): p. 1-31.

23. Gorman, J.A., *7 - Corrosion problems affecting steam generator tubes in commercial water-cooled nuclear power plants A2 - Riznic, Jovica*, in *Steam Generators for Nuclear Power Plants*. 2017, Woodhead Publishing. p. 155-181.

24. Brear, J. and A. Fleming. *Prediction of P91 Life Plant Operating Conditions*. in *Proc. Int. Conf." High-Temperature Plant Integrity and Life Extention", Cambridge, 14-16 April*. 2004.

25. Morris, A., M. Kourmpetis, I.D. Dear, M. Sjodahl, and J.P. Dear, *Optical Strain Monitoring Techniques for Life Assessment of Components in Power Generation Plant.* Proc. Instn Mech Engrs, Part A, Journal of Power and Energy, 2007. **221 (A8)**: p. 1141-1152.

26. Davies, C.M., P. Nagy, A. Narayanan, and P. Cawley, *Continuous Creep Damage Monitoring Using a Novel Potential Drop Technique*. 2012, AMER SOC MECHANICAL ENGINEERS. p. 35-39.

27. Hyde, T.H. and W. Sun, *A Novel, High Sensitivity, Small Specimen Creep Test.* The Journal of Strain Analysis, 2009. **44**(3): p. 171-185.

28. Hyde, T.H., W. Sun, and J.A. Williams, *Requirements for and Use of Miniature Test Specimens to Provide Mechanical and Creep Properties of Materials: a Review.* Int. Mater. Rev., 2007. **52**(4): p. 213-255.

29. *Pressure Systems Safety Regulations 2000 SI 2000 128.*

30. Thoraval, G., *Creep of High Temperature Steam Piping; EDF Experience With Fossil-Fired Power Plants From 1955 to 1987.* Nuclear Engineering and Design, 1989. **116** p. 389-398

31. Morris, A., C. Maharaj, M. Kourmpetis, I.D. Dear, A. Puri, and J.P. Dear, *Optical Strain Measurement Techniques to Assist in Life Monitoring of Power Plant Components.* Journal of Pressure Vessel Technology. **131**(2): p. 024502-024502-024508.

32. Morris, A., C. Maharaj, I. Palmer, A. Puri, and J.P. Dear, *ARCMAC Optical Strain Measurement for Creep Monitoring: Recent Improvements in Accuracy and Resolution*, in *ASME PVP 2009 Conference - Sustainable Energy for the Third Millenium*. July 2009: Prague, Czech Republic, PVP200977511.

33. Morris, A., C. Maharaj, I. Palmer, A. Puri, and J.P. Dear, *Developments in Combined ARCMAC and Strain Mapping Systems for Creep Measurement*, in *ASME PVP 2008 Conference - Nuclear Power Plant Renaissance Change in Paradigm*, A.A.G. Dermenjian, L. H. eds, Editor. July 2008, PVP200861118: Marriott on Magnificent Mile Hotel, Chicago, Illinois, USA, PVP200861118.

34. Morris, A., C. Maharaj, A. Puri, M. Kourmpetis, and J.P. Dear, *Recent Developments in Methods to study Creep Strain Variations in Power Station Steam Plant*, in *ASME PVP 2008 Conference - Nuclear Power Plant Renaissance Change in Paradigm*, A.A.G. Dermenjian, L. H. eds, Editor. July 2008: Marriott on Magnificent Mile Hotel, Chicago, Illinois, USA, PVP200861119.

35. Fenton, S.T., A. Morris, and P. Mulvihill, *Investigation and analysis of CrMoV Bore Cracking*, in *IOM 2nd International Conference "Integrity of High Temperature Welds"*, I. Communications, Editor. November 2003: London.

36. Hyde, T.H., W. Sun, and B.S.M. Ali. *A Small Creep Test Specimen for Use in Determining Uniaxial Creep Rupture Data*. in *SSTT. Proceedings of the 2nd International Conference SSTT: Determination of Mechanical Properties of Materials by Small Punch and Other Miniature Testing Techniques*. October 2-4, 2012. Ostrava, Czech Rep.

37. Tabor, D., *The hardness of solids.* Review of Physics in Technology, 1970. **1**(3): p. 145.

38. Aristotele, *Meterology*. translated by E. W. Webster, 384-322 BC. **Book IV**.

39. Geach, G.A., *Hardness and Temperature.* International Metallurgical Reviews, 1974. **19**: p. 255-267.

40. Ashby, N.A., *The factor of hardness in metals.* Journal of Nuclear Engineering, 1951. **6**: p. 33.

41. Wyatt, O.H. and D. Dew-Hughes, *Metals, Ceramics, and Polymers: An Introduction to the Structure and Properties of Engineering Materials*. 1974: Cambridge University Press.

42. Brinell, J.A., in *Déuxieme Congres Int. Méthodes d'essai*. 1900: Paris.

43. Smith, R. and G. Sandland, Journal of Iron and Steel Institute, 192. **110**: p. 285.

44. Ludwick, P., *Die Kegelprobe*. 1908, Berlin.

45. Wilson, C.H., *PENETRATOR FOR TESTING PENETRATION HARDNESS.* Patent US 1571310 A, 1926.

46. Knoop, F., C. Peters, and W. Emerson, *A Sensitive Pyramidal-Diamond Tool for Indentation Measurements.* Journal of Research of the National Bureau of Standards, 1939. **23**(1): p. 39-61.

47. Oliver, W.C. and G.M. Pharr, *An Improved Technique for Determining Hardness and Elastic Modulus using Load and Displacement Sensing Indentation Experiments.* Journal of Materials Research, 1992. **7**(06): p. 1564-1583.

48. Smith, R. and G. Sandland, *An Accurate Method of Determining the Hardness of metals, with Particular Reference to Those of a High Degree of Hardness.* Proceedings of the Institution of Mechanical Engineers, 1922. **1**: p. 623-641.

49. Lips, E.M.H. and J. Sack, *A Hardness Tester for Microscopical Objects.* Nature, 1936. **138**: p. 328-329.

50. Vander Voort, G.F. and G.M. Lucas, *Microindentetion Hardness testing.* Advanced Materials and Processes, 2000. **9/98**: p. 21-25.

51. Song, J.-F., S. Low, D. Pitchure, A. Germak, S. DeSogus, T. Polzin, H.-Q. Yang, and H. Ishida, *Establishing a worldwide unified Rockwell hardness scale using standard diamond indenters.* Measurement, 1998. **24**(4): p. 197-205.

52. Hill, R., *The mathematical theory of plasticity*. 1950, Oxford: Clarendon Press.

53. Tabor, D., *The hardness of metals*. 1951, Oxford: Clarendon Press.

54. Tresca, M.H., *On further applications of the flow of solids.* Journal of the Franklin Institute, 1878. **106**(4): p. 263-270.

55. Pavlina, E. and C. Van Tyne, *Correlation of yield strength and tensile strength with hardness for steels.* Journal of Materials Engineering and Performance, 2008. **17**(6): p. 888-893.

56. Shaw, M.C. and G.J. DeSalvo, *A new approach to plasticity and its application to blunt two dimensional indenters.* Journal of Engineering for Industry, 1970. **92**(2): p. 469-479.

57. Shaw, M.C. and G.J. DeSalvo, *The role of elasticity in hardness testing.* Met. Eng. Quart., 1972. **12**: p. 1-7.

58. Westbrook, J.H., *The science of hardness testing and its research applications.* 1973.

59. Cahoon, J., *An Improved Equation Relating Hardness to Ultimate Strength.* Metallurgical and Materials Transactions B, 1972. **3**: p. 3040.

60. Cahoon, J., W. Broughton, and A. Kutzak, *The determination of yield strength from hardness measurements.* Metallurgical and Materials Transactions B, 1971. **2**(7): p. 1979-1983.

61. Hsu, C.-y., *Correlation of hot-microhardness with elevated-temperature tensile properties of low activation ferritic steel.* Journal of Nuclear Materials, 1986. **141**: p. 518-522.

62. Gooch, D.J., *Creep and high-temperature failure*, in *Comprehensive structural integrity (ed. I. Milne et al.)*, A. Saxena, Editor. 2003, Elsevier: Amsterdam. p. 309–359.

63. Masuyama, F., *Creep degradation in welds of Mod.9Cr-1Mo steel.* International Journal of Pressure Vessels and Piping, 2006. **83**(11–12): p. 819-825.

64. Sposito, G., C. Ward, P. Cawley, P.B. Nagy, and C. Scruby, *A Review of Non-Destructive Techniques for the Detection of Creep Damage in Power Plant Steels.* NDT & E International, 2010. **43**(7): p. 555-567.

65. Viswanathan, R., S.R. Paterson, H. Grunloh, and S. Gehl, *Life assessment of superheater reheater tubes in fossil boilers.* Journal of Pressure Vessel Technology, Transactions of the ASME, 1994. **116**(1): p. 1-16.

66. Parker, J., *In-service behavior of creep strength enhanced ferritic steels Grade 91 and Grade 92 – Part 1 parent metal.* International Journal of Pressure Vessels and Piping, 2013. **101**: p. 30-36.

67. *The Use of Portable Hardness Testing in Field Applications for Grade 91 Steel.* EPRI, Palo Alto, CA (2011) 1023199, 2012.

68. *Guidelines and specifications for high-reliability fossil power plants: best practice guideline for manufacturing and construction of Grade 91 steel components.* EPRI, Palo Alto, CA (2011) 1023199, 2015.

69. *An Informed Perspective on the Use of Hardness Testing in an Integrated Approach to the Life Management of Grade 91 Steel Components.* EPRI, Palo Alto, CA (2011) 1023199, 2016.

70. Infante, V., J.M. Silva, M. de Freitas, and L. Reis, *Failures analysis of compressor blades of aeroengines due to service.* Engineering Failure Analysis, 2009. **16**(4): p. 1118-1125.

71. Hollomon, J.H. and L.D. Jaffee, *Time-temperature relations in tempering steel.* Trans. AIME, 1943. **162**: p. 223-249.

72. Kohlhofer, W. and R.K. Penny, *Hardness testing as a means for creep assessment.* International Journal of Pressure Vessels and Piping, 1996. **66**(1–3): p. 333-339.

73. Cane, B.J., P.F. Aplin, and J.M. Brear, *A Mechanistic Approach to Remanent Creep Life Assessment of Low Alloy Ferritic Components Based on Hardness Measurements.* Journal of Pressure Vessel Technology. Transactions of the ASME, 1985. **107**(3): p. 295-300.

74. Kachanov, L.M., *The Theory of Creep*. 1958: Kennedy A.J. (ed., English Translation), National Lending Library, Boston, Spa.

75. Masuyama, F., *Hardness model for creep-life assessment of high-strength martensitic steels.* Materials Science and Engineering: A, 2009. **510–511**: p. 154-157.

76. Larson, F.R. and J. Miller, *A time-temperature relationship for rupture and creep stress.* Transactions ASME, 1952. **74**(5): p. 765–775.

77. Ghassemi Armaki, H., R. Chen, S. Kano, K. Maruyama, Y. Hasegawa, and M. Igarashi, *Microstructural degradation mechanisms during creep in strength enhanced high Cr ferritic steels and their evaluation by hardness measurement.* Journal of Nuclear Materials, 2011. **416**(3): p. 273-279.

78. Mukhopadhyay, S.K., H. Roy, and A. Roy, *Development of hardness-based model for remaining life assessment of thermally loaded components.* International Journal of Pressure Vessels and Piping, 2009. **86**(4): p. 246-251.

79. Furtado, H.C., B.R. Cardoso, F. Santos, C. Matt, and L.H. de Almeida, *Remaining Life Evaluation of Power Plant Based on Strain Deformation Monitoring and Computational Diagnosis*, in *The 12th International Conference of the Slovenian Society for Non-Destructive Testing: Application of Contemporary Non-Destructive Testing in Engineering*. September 4-6, 2013: Portorož, Slovenia.

80. Furtado, H.C., L.H. de Almeida, J. Dille, and I. Le May, *Correlation Between Hardness Measurements and Remaining Life Prediction for 2.25Cr-1Mo Steel Used in Power Plants.* Journal of Materials Engineering and Performance, 2010. **19**(4): p. 558-561.

81. Furtado, H.C., L.H. de Almeida, and I. Le May, *Damage and Remaining Life Estimation in High Temperature Plant with Variable Operating Conditions.* OMMI, Power Plant, 2008. **5**: p. 1-10.

82. Allen, D.J. and S.T. Fenton, *A hardness-based creep rupture model for new and service aged P91 steel*, in *VTT Symposium*. 2007, VTT; 1999. p. 156-170.

83. *Rolls-Royce Power Engineering Plc, Scoop Sampling – Extraction of Material Samples for Examination and Analysis.* 2010.

84. Brett, S.J., *Small Scale Sampling and Impression Creep Testing of Aged ½CrMoV Steam Pipework Systems*, in *Proc. of ECCC Conf. on Creep and Fracture in High Temperature Components - Design and Life Assessment*. April 2009: Dübendorf, Switzerland. p. 1088-1096.

85. Klevtsov, I. and A. Dedov. *Impact of Small Specimens Sampling on Durability of In-Service Power Plant Components*. in *SSTT. Proceedings of the 2nd International Conference SSTT: Determination of Mechanical Properties of Materials by Small Punch and Other Miniature Testing Techniques*. October 2-4, 2012. Ostrava, Czech Rep.

86. *GB/T 29459.1-2012 Small Punch Test Methods of Metallic Materials for In-Service Pressure Equipment-Part 1: General Requirements.* General Administration of Quality Supervision, Inspection and Quarantine of China/ Standardization Administration of China, 2012.

87. *GB/T 29459.1-2012 Small Punch Test Methods of Metallic Materials for In-Service Pressure Equipment-Part 2: Method of Test For Tensile Properties at Room Temperature*. General Administration of Quality Supervision, Inspection and Quarantine of China/ Standardization Administration of China, 2012.

88. Dobeš, F. and K. Milička, *Application of Creep Small Punch Testing in Assessment of Creep Lifetime.* Materials Science and Engineering: A: Properties, Microstructure and Processing, 2009. **510**(11): p. 440-443.

89. Dymáček, P. and K. Milička, *Creep Small-Punch Testing and its Numerical Simulations.* Materials Science and Engineering: A, 2009. **510–511**: p. 444-449.

90. Hyde, T.H., M. Stoyanov, W. Sun, and C.J. Hyde, *On the Interpretation of Results from Small Punch Creep Tests.* The Journal of Strain Analysis for Engineering Design, 2010. **45**(3): p. 141-164.

91. Hyde, C.J., T.H. Hyde, W. Sun, S. Nardone, and E. De Bruycker, *Small Ring Testing of a Creep Resistant Material.* Materials Science and Engineering: A, 2013. **586**(0): p. 358-366.

92. Hyde, T.H., W. Sun, and A.A. Becker, *Analysis of the Impression Creep Test Method Using a Rectangular Indenter for Determining the Creep Properties in Welds.* International Journal of Mechanical Sciences, 1996. **38**: p. 1089-1102.

93. Sun, W., T.H. Hyde, and S.J. Brett, *Application of Impression Creep Data in Life Assessment of Power Plant Materials at High Temperatures.* Proc. Instn

Mech Engrs, Journal of Materials: Design and Applications, 2008. **222**(Part L): p. 175-182.

94. Cacciapuoti, B., W. Sun, and D.G. McCartney, *A study on the evolution of the contact angle of small punch creep test of ductile materials.* International Journal of Pressure Vessels and Piping, 2016. **145**: p. 60-74.

95. *European Technology Development (ETD),* http://www.etd-consulting.com/our-services/engineering-services/advanced-nondestructive-evaluation/.

96. *Data acceptability criteria and data generation: recommendations for creep testing of post exposed (ex-service) materials.* ECCC Recommendations, http://www.ommi.co.uk/etd/eccc/advancedcreep/v3piiii4x.pdf, 18 June 2012. **3**(III).

97. Dedov, A., I. Klevtsov, T. Lausmaa, and D. Neshumayev, *Method of small samples for assessment of properties of power plant components: sampling devices and stress concentration in dimples*, in *Proc. Conference Plant Maintenance for Managing Life & Performance BALTICA VII*. 2007. p. 180-192.

98. Hyde, C.J., T.H. Hyde, and W. Sun. *Small Ring Specimen Creep Testing of a Nickel-Based Superalloy*. in *Determination of Mechanical Properties of Materials by Small Punch and other Miniature Testing Techniques*. 2012. Ostrava, Czech Republic.

99. Brett, S.J., *The creep strength of weak thick section modified 9Cr forgings.* Baltica V: Condition and Life Management for Power Plants, VTT, ESPOO, 2001: p. 35-44.

100. Brett, S.J., *UK Experience with Modified 9Cr (Grade 91) Steel*, in *Baltica VII: International Conference on Life Management & Maintenance for Power Plants*. 2007: Helsinki-Stockholm-Helsinki. p. 48-60.

101. Brett, S.J., *Early Type IV Cracking on Two Retrofit Grade 91 Steel Headers*, in *IIW Int. Conf. on Safety and Reliability of Welded Components in Energy and Processing Industry*. 2008: Graz, Austria.

102. Rouse, J.P., W. Sun, and T.H. Hyde, *The effects of scoop sampling on the creep behaviour of power plant straight pipes.* Journal of Strain Analysis, 2013. **48**(8): p. 494–511.

103. Sun, W., T.H. Hyde, and S.J. Brett, *Small Specimen Creep Testing and Application for Power Plant Component Remainig Life Assessment*, in *IRF2013 - 4th International Conference on Integrity, Reliability and Failure*. 2013: Funchal, Portugal.

104. Hyde, T.H. and W. Sun, *Evaluation of Conversion Relationships for Impression Creep Test at Elevated Temperatures.* International Journal of Pressure Vessels and Piping, 2009. **86**(11): p. 757-763.

105. Sun, W., T.H. Hyde, and S.J. Brett, *Use of the Impression Creep Test Method for Determining Minimum Creep Strain Rate Data*, in *SSTT - Determination of mechanical properties of materials by small punch and other miniature testing techniques* K. Matocha, R. Hurst, and W. Sun, Editors. 2012, OCELOT s.r.o.: Ostrava (CZ).

106. Brett, S., B. Kuhn, J. Rantala, and C. Hyde, *Impression creep testing for material characterization in development and application*, in *10th Liège Conference on Materials for Advanced Power Engineering*. 14th – 17th September 2014: Palais des Congrès Liège, Belgium.

107. Monkman, F.C. and N.J. Grant, *An Empirical Relationship Between Rupture Life and Minimum Creep Rate in Creep-Rupture Tests.* Proc. ASTM, 1956. **56**: p. 593–605.

108. Hyde, T.H., B.S.M. Ali, and W. Sun, *On the Determination of Material Creep Constants Using Miniature Creep Test Specimens.* Journal of Engineering Materials and Technology, 2014. **136**: p. 021006-021001-021010.

109. Cortellino, F., R. Chen, W. Sun, and T.H. Hyde, *A Microscopic Investigation on the Failure Mechanisms of Small Punch Creep Test of a P91 Steel at 873 K*, in *SSTT - Determination of mechanical properties of materials by small punch and other miniature testing techniques* K. Matocha, R. Hurst, and W. Sun, Editors. 2014, OCELOT s.r.o.: Castle Seggau - Graz (Austria). p. 260-269.

110. Hyde, T.H., C.J. Hyde, and W. Sun, *A Basis for Selecting the Most Appropriate Small Specimen Creep Test Type.* Journal of Pressure Vessel Technology, 2014. **136**(2): p. 024502-024501-024506.

111. Milička, K. and F. Dobeš, *Small punch testing of P91 steel.* International Journal of Pressure Vessels and Piping, 2006. **83**(9): p. 625-634.

112. Rouse, J.P., F. Cortellino, W. Sun, T.H. Hyde, and J. Shingledecker, *Small Punch Creep Testing: Review on Modelling And Data Interpretation.* Materials Science and Technology, 2013. **29**(11): p. 1328-1345.

113. Evans, R.W. and M. Evans, *Numerical modelling of small disc creep test.* Materials Science and Technology, 2006. **22**(10): p. 1155-1162.

114. Cortellino, F., J.P. Rouse, B. Cacciapuoti, W. Sun, and T.H. Hyde, *Experimental and Numerical Analysis of Initial Plasticity in P91 Steel Small Punch Creep Samples.* Experimental Mechanics, 2017. **57**: p. 1193–1212.

115. Kobayashi, K.I., I. Kajihara, H. Koyama, and G.C. Stratford, *Deformation and Fracture Mode During Small Punch Creep Tests.* Journal of Solid Mechanics and Materials Engineering, 2010. **4**(1): p. 75-86.

116. Hyde, T.H., B.S.M. Ali, and W. Sun, *Analysis and Design of a Small, Two-Bar Creep Test Specimen.* ASME. Journal of Engineering Materials and Technology, 2013. **135**(4): p. 041006-041006-041009.

117. Sun, W., T.H. Hyde, and B.S.M. Ali, *Small Tensile Bar Specimen Creep Tests for Use in Determining Creep Deformation and Rupture Properties*, in *SSTT - Determination of mechanical properties of materials by small punch and other miniature testing techniques* K. Matocha, R. Hurst, and W. Sun, Editors. 2014, OCELOT s.r.o.: Castle Seggau - Graz (Austria).

118. Hyde, T.H. and W. Sun, *Multi-step Load Impression Creep Tests for a 1/2Cr1/2Mo1/4V Steel at 565°C.* Strain, 2001. **37**(3): p. 99-103.

119. Hyde, T.H., K.A. Yehia, and A.A. Becker, *Interpretation of impression creep data using a reference stress approach.* International Journal of Mechanical Sciences, 1993. **35**(6): p. 451-462.

120. *Standard for Small Punch Creep Test -Estimation of Residual Life for High Temperature Component.* The Committee on High Temperature Strength of Materials. The Society of Materials Science, September, 2012. ISBN 978-4-901381-38-3.

121. *Standard Test Method for Small Punch Testing of Ultra-High Molecular Weight Polyethylene Used in Surgical Implants*. 2008, ASTM International.

122. Hurst, R.C. and K. Matocha, *A Renaissance in the Use of the Small Punch Testing Technique*, in *Proceedings of the ASME 2015 Pressure Vessels and Piping Conference*. 2015: Boston, Massachusetts, USA. p. V01BT01A048-041 - V001BT001A048-016.

123. Kasiviswanathan, K.V., V. Karthik, P. Visweswaran, K. Laha, and T. Jayakumar, *Small Specimen Testing - Research and Development Activities at Igcar, India*, in *SSTT. Proceedings of the 2nd International Conference SSTT: Determination of Mechanical Properties of Materials by Small Punch and Other Miniature Testing Techniques*, K. Matocha, R. Hurst, and W. Sun, Editors. October 2-4, 2012: Ostrava, Czech Rep.

124. Hurst, R.C. and K. Matocha, *Small Punch Testing – the transition from a Code of Practice to a European testing standard*, in *SSTT. Proceedings of the 4th International Conference: Determination of Mechanical Properties of Materials by Small Punch and other Miniature Testing Techniques*, K. Matocha, R. Hurst, and W. Sun, Editors. 12-14 October 2016: Shanghai, China.

125. Li, Y.Z. and R. Šturm, *Determination of Creep Properties from Small Punch Test.* Proceedings of the ASME Pressure Vessels and Piping Conference, 2009. **Vol 3**: p. 741-752.

126. Chakrabarty, J., *A Theory of Stretch Forming Over Hemispherical Punch Heads.* International Journal of Mechanical Sciences, 1970. **12**(4): p. 315–325.

127. Cortellino, F., J.P. Rouse, W. Sun, and T.H. Hyde. *A Study on the Effect of Initial Plasticity on the Small Punch Creep Test for a P91 Steel at 600 ^{o}C* in *SSTT - Determination of mechanical properties of materials by small punch*

and other miniature testing techniques. 2014. Castle Seggau - Graz (Austria): OCELOT s.r.o.

128. Ma, Y.W., S. Shim, and K.B. Yoon, *Assessment of Power Law Creep Constants of Gr91 Steel Using Small Punch Creep Tests.* Fatigue & Fracture of Engineering Materials & Structures, 2009. **32**(12): p. 951-960.

129. Li, Y.Z., R. Šturm, R.C. Hurst, and D.T. Blagoeva, *Derivation of Creep Properties From Small Punch Test Small Punch Test (SPT),* in *International Worshop*. June 27-28 2011: University of Nottingham, United Kingdom.

130. Li, Y. and R. Šturm, *Determination of Creep Properties from Small Punch Test,* in *ASME 2008 pressure vessels and piping conference*, ASME, Editor. 2008: Chicago, Illinois, USA. p. 739-750.

131. Ling, X., Y. Zheng, Y. You, and Y. Chen, *Creep Damage in Small Punch Creep Specimens of Type 304 Stainless Steel.* International Journal of Pressure Vessels and Piping, 2006. **84**(5): p. 304-309.

132. Cortellino, F., W. Sun, and T. Hyde, *On the effects of friction modelling on small punch creep test responses: A numerical investigation.* The Journal of Strain Analysis for Engineering Design, 2016. **51**(7): p. 493-506.

133. Cortellino, F., W. Sun, T.H. Hyde, and J. Shingledecker, *The Effects of Geometrical Inaccuracies of the Experimental Set-Up on Small Punch Creep Test Results.* The Journal of Strain Analysis for Engineering Design, 2014. **49**(8): p. 571-582.

134. Kobayashi, K.I., M. Kaneko, H. Koyama, G.C. Stratford, and M. Tabuchi, *The Influence of Both Testing Environment and Fillet Radius of the Die Holder on the Rupture Life of Small Punch Creep Tests.* Journal of Solid Mechanics and Materials Engineering, 2012. **6**(8): p. 925-934.

135. Dymáček, P., S. Seitl, K. Milička, and F. Dobeš, *Influence of Friction on Stress and Strain Distributions in Small Punch Creep Test Models.* Key Engineering Materials, 2010. **417-418**: p. 561-564.

136. Hyde, T.H. and W. Sun, *Application of Impression Creep Test Data for the Assessment of Service Exposed Power Plant Components.* Metallurgical Journal - Theme 3: Numerical Approach, 2010. **Vol. LXIII**: p. 138-145.

137. Corwin, W.R. and G.E. Lucas, *The use of small scale specimens for testing irradiated materials*. Conference: Symposium on the use of nonstandard subsized specimens for irradiated testing, Albuquerque, NM, USA, 23 Sep 1983; Related Information: ASTM Special Technical Publication 888. 1983: ASTM,Philadelphia, PA; None. Medium: X; Size: Pages: 373.

138. Petzová, J., M. Březina, and L. Kupča. *Evaluation of mechanical properties of the reactor pressure vessel materials changes by small punch test application*. in *Proceedings of the 2013 ASME Pressure Vessels & Piping Conference PVP2013*. July, 14-18, 2013. Paris, France.

139. Březina, M., J. Petzová, L. Kupča, and M. Kapusňák, *Utilization of SPT techniques for evaluation of changes in the properties of the vver-440 reactor pressure vessel steels after their irradiation in the research and power reactors*, in *Proceedings of the 2015 ASME Pressure Vessels & Piping Conference PVP2015*. 2015: Boston, Massachusetts, USA.

140. Katona, T.J., *Long-Term Operation of VVER Power Plants.* Nuclear Power-Deployment, Operation and Sustainability, 2011: p. 152-196.

141. Knaster, J., F. Arbeiter, P. Cara, S. Chel, A. Facco, R. Heidinger, A. Ibarra, A. Kasugai, H. Kondo, and G. Micciche, *IFMIF, the European–Japanese efforts under the Broader Approach agreement towards a Li (d, xn) neutron source: Current status and future options.* Nuclear Materials and Energy, 2016. **9**: p. 46-54.

142. Lucas, G.E., G.R. Odette, H. Matsui, A. Möslang, P. Spätig, J. Rensman, and T. Yamamoto, *The role of small specimen test technology in fusion materials development.* Journal of Nuclear Materials, 2007. **367–370**: p. 1549–1556.

143. Klueh, R., *Reduced-activation bainitic and martensitic steels for nuclear fusion applications.* Current Opinion in Solid State and Materials Science, 2004. **8**(3): p. 239-250.

144. Bruchhausen, M., K. Turba, F. de Haan, P. Hähner, T. Austin, and Y. de Carlan, *Characterization of a 14Cr ODS steel by means of small punch and uniaxial testing with regard to creep and fatigue at elevated temperatures.* Journal of Nuclear Materials, 2014. **444**: p. 283–291.

145. Odette, G.R., M. He, D. Gragg, D. Klingensmith, and G.E. Lucas, *Some recent innovations in small specimen testing.* Journal of Nuclear Materials, 2002. **307–311**: p. 1643–1648.

146. Gilbert, M., S. Dudarev, S. Zheng, L. Packer, and J.-C. Sublet, *An integrated model for materials in a fusion power plant: transmutation, gas production, and helium embrittlement under neutron irradiation.* Nuclear Fusion, 2012. **52**(8): p. 083019.

147. Nakata, T., S.-i. Komazaki, Y. Kohno, and H. Tanigawa, *Development of a small punch testing method to evaluate the creep property of high Cr ferritic steel: Part II – Stress analysis of small punch tests pecimen by finite element method.* Materials Science and Engineering: A, 2016. **666**: p. 80-87.

148. Baik, J.M., J. Kameda, and O. Buck, *Small punch test evaluation of intergranular embrittlement of an alloy steel.* Scripta Metallurgica, 1983. **17**(12): p. 1443-1447.

149. Chi, S.-H., J.-H. Hong, and I.-S. Kim, *Evaluation of irradiation effects of 16 MeV proton-irradiated 12Cr-1MoV steel by small punch (SP) tests.* Scripta Metallurgica et Materialia, 1994. **30**(12): p. 1521-1525.

150. Mao, X. and J. Kameda, *Small-punch technique for measurements of material degradation of irradiated ferritic alloys.* Journal of Materials Science, 1991. **26**: p. 2436-2440.

151. Wakai, E., H. Ohtsuka, S. Matsukawa, K. Furuya, H. Tanigawa, K. Oka, S. Ohnuki, T. Yamamoto, F. Takada, and S. Jitsukawa, *Mechanical properties of small size specimens of F82H steel.* Fusion Engineering and Design, 2006. **81**: p. 1077–1084.

152. Kasada, R., H. Ono, and A. Kimura, *Small specimen test technique for evaluating fracture toughness of blanket structural materials.* Fusion Engineering and Design, 2005. **81**: p. 981-986.

153. *Standard Test Method for Determination of Reference Temperature, T_0, for Ferritic Steels in the Transition Range.* ASTM E 1921-02, Annual Book of ASTM Standards, 2002. **03.01**.

154. Martínez-Pañeda, E., T.E. García, and C. Rodríguez, *Fracture toughness characterization through notched small punch test specimens.* Materials Science and Engineering: A, 2016. **657**: p. 422-430.

155. Mathew, M.D., J. Ganesh Kumar, V. Ganesan, and K. Laha, *Small Punch Creep Studies for Optimization of Nitrogen Content in 316LN SS for Enhanced Creep Resistance.* Metallurgical and Materials Transactions A, 2014. **45**(2): p. 731-737.

156. Bueno, A.H.S., E.D. Moreira, and J.A.C.P. Gomes, *Evaluation of stress corrosion cracking and hydrogen embrittlement in an API grade steel.* Engineering Failure Analysis, 2014. **36**: p. 423-431.

157. Rehrl, J., K. Mraczek, A. Pichler, and E. Werner, *Mechanical properties and fracture behavior of hydrogen charged AHSS/UHSS grades at high- and low strain rate tests.* Materials Science and Engineering: A, 2014. **590**: p. 360-367.

158. Magudeeswaran, G., V. Balasubramanian, and G. Madhusudhan Reddy, *Hydrogen induced cold cracking studies on armour grade high strength, quenched and tempered steel weldments.* International Journal of Hydrogen Energy, 2008. **33**(7): p. 1897-1908.

159. García, T.E., C. Rodríguez, F.J. Belzunce, and I.I. Cuesta, *Effect of hydrogen embrittlement on the tensile properties of CrMoV steels by means of the small punch test.* Materials Science and Engineering: A, 2016. **664**: p. 165-176.

160. Hirose, T., H. Sakasegawa, A. Kohyama, Y. Katoh, and H. Tanigawa, *Effect of specimen size on fatigue properties of reduced activation ferritic/martensitic steels.* Journal of Nuclear Materials, 2000. **283–287, Part 2**: p. 1018-1022.

161. Nogami, S., T. Itoh, H. Sakasegawa, H. Tanigawa, E. Wakai, A. Nishimura, and A. Hasegawa, *Study on fatigue life evaluation usinf small specimens for testing neutron-irradiated materials.* Journal of Nuclear Science and Technology, 2011. **48**(1): p. 60-64.

162. Bao, C., L.X. Cai, and C. Dan, *Estimation of fatigue crack growth behavior for small-sized C-shaped inside edge-notched tension (CIET) specimen using compliance technique.* International Journal of Fatigue, 2015. **81**: p. 202-212.

163. Volak, J., M. Novak, J. Kaiser, and V. Mentl, *Fatigue testing by means of miniature test specimens.* Journal of Achievements in Materials and Manufacturing Engineering, 2012. **55**(2): p. 386-389.

164. Roebuck, B., D.C. Cox, and R.C. Reed, *An innovative device for the mechanical testing of miniature specimens of superalloys* in *Superalloys 2004*, T.M.P. K.A. Green, H. Harada, T.E. Howson, R.C. Reed, J.J. Schirra, and S, Walston, TMS (The Minerals, Metals & Materials Society), Editor. January 2004.

165. Brett, S.J., *The Creep Strength of Weak Thick Section Modified 9Cr Forgings*, in *BALTICA V: Condition and Life Management for Power Plants, VTT Symposium, ESPOO*, V.M.T. Seija Hietanen & Pertti Auerkari, Editor. 2001: Hotel Haikko Manor, Porvoo, Finland. p. 35-44.

166. Petzová, J., M. Březina, M. Kapusňák, and L. Kupča, *Application of small punch testing methods for thermal ageing monitoring at primary circuit components in nuclear power plant*, in *Proceedings of the 2015 ASME Pressure Vessels & Piping Conference PVP2015*. 2015: Boston Park Plaza, USA.

167. Kapadia, P. *Assessment of System Stresses and Creep-Fatigue Damage on Power Plant Pipelines using a Pipeline Modelling Tool*. in *International Conference HIDA-7: Life/Defect Assessment & Failures in High Temperature Industrial Structures* 15 – 17 May 2017. Portsmouth, UK.

168. Rouse, J.P. and C.J. Hyde, *A comparison of simple methods to incorporate material temperature dependency in the Green's function method for estimating transient thermal stresses in thick-walled power plant components.* Materials, 2016. **9**(1): p. 26.

169. *GENSIP Publication, CMV Pipework Management in Conventional UK Power Stations.* GENSIP/GPG/PS001. **Issue 1.2, August 2011**.

170. *VGB-TW 507, Guidelines for the Assessment of Microstructure and Damage Development of Creep Exposed Materials for Pipes and Boiler Components.* VGB Technical Association of Large Power Plant Operators, 1992.

171. Neubauer, B. and U. Wedel, *Restlife Estimation of Creeping Components by Means of Replicas*, in *ASME International Conference on Advances in Life Prediction Methods*, J.R.W. Eds. D.A. Woodford, ASME, Editor. 1983: New York.

172. Concari, S., *Residual Life Assessment and Microstructure.* ECCC Recommendations, 2005. **6**(1).

173. Naveena, V.D. Vijayanand, V. Ganesan, K. Laha, and M.D. Mathew, *Evaluation of the Effect of Nitrogen on Creep Properties of 316LN Stainless*

Steel from Impression Creep Tests. Materials Science and Engineering: A, 2012. **552**: p. 112-118.

174. Li, R., T.H. Hyde, W. Sun, and B. Dogan, *Modelling and Data Interpretation of Small Punch Creep Testing*, in *ASME 2011 pressure vessels and piping conference* 2011: Baltimore, Maryland, USA. p. 1119-1127.

175. Cacciapuoti, B., A. Morris, W. Sun, D.G. McCartney, and J. Hulance, *Correlation and Capability of using Site Inspection Data and Small Specimen Creep Testing for a Service-Exposed CrMoV Pipe Section.* Materials at High Temperatures. Under review., 2017.

176. Hyde, T.H., W. Sun, and J.A. Williams, *Creep behaviour of parent, weld and HAZ materials of new, service-aged and repaired 1/2Cr1/2Mo1/4V: 2 1/4Cr1Mo pipe welds at 640°C.* Materials at High Temperatures, 1999. **16**(3): p. 117-129.

177. Morris, A., B. Cacciapuoti, and W. Sun, *The Role of Hardness on Condition Monitoring and Lifing for High Temperature Power Plant Structural Risk Management.* Measurement, 2017. **Under review**.

178. Hyde, T.H., F. Cortellino, J.P. Rouse, and W. Sun, *Small Punch Creep Testing and Data Analysis of a P91 Steel at 650 ^{o}C*, in *SSTT - Determination of mechanical properties of materials by small punch and other miniature testing techniques*, K. Matocha, R. Hurst, and W. Sun, Editors. 2012, OCELOT s.r.o.: Ostrava (CZ).

179. Evans, M. and D. Wang, *Stochastic Modelling of the Small Disc Creep Test.* Materials Science and Technology, 2007. **23**(8): p. 883-892.

180. Evans, M. and D. Wang, *The Small Punch Creep Test: Some Results from a Numerical Model.* Journal of Materials Science, 2008. **43**(6): p. 1825-1835.

181. Bicego, V., E. Lucon, and R. Crudeli, *Integrated Technologies for Life Assessment of Primary Power Plant Components.* Nuclear and Engineering Design, 1998. **182**(2): p. 113-121.

182. Tettamanti, S. and R. Crudeli. *A Procedure for High Temperature Plant Components Life Evaluation: Small Punch Creep Test Methodology*. in *Case histories on integrity and failures in industry (CHIFI)*. 1999. Milan - Italy.

183. Li, Y. and R. Šturm, *Small Punch Tests for Welded Heat Affected Zones*, in *International Conference on Welds 2005*. 2005: Geesthacht.

184. Yang, Z. and Z.W. Wang, *Relationship Between Strain and Central Deflection in Small Punch Creep Specimens.* International Journal of Pressure Vessels and Piping, 2003. **80**(6): p. 397-404.

185. Hyde, T.H. and W. Sun, *Interpretation of Small Punch Creep Test Data for Ductile Materials.* Hutnické listy (Metallurgical Journal), 2010. **LXIII**: p. 25-33.

186. Li, Y.Z. and R. Šturm, *Small Punch Test for Weld Heat Affected Zones.* Matererials at High Temperatures, 2006. **23**(3-4): p. 225-232.

187. Zhou, Z., Y. Zheng, X. Ling, R. Hu, and J. Zhou, *A Study on Influence Factors of Small Punch Creep Test by Experimental Investigation and Finite Element Analysis.* Materials Science and Engineering: A, 2010. **527**(10–11): p. 2784-2789.

188. Blagoeva, D.T. and R.C. Hurst, *Application of the CEN (European Committee for Standardization) small punch creep testing code of practice to a representative repair welded P91 pipe.* Materials Science and Engineering: A, 2009. **510–511**: p. 219-223.

189. Crocker, L.E., A.T. Fry, and J. Banks, *An Extended Small Punch Test Method for Providing Measured Displacements across a Test Specimen*, in *National Physical Laboratory*. Hampton Road, Teddington, Middlesex, TW11 0LW, UK.

190. Saad, A.A., T.H. Hyde, W. Sun, C.J. Hyde, and D.W.J. Tanner, *Characterization of viscoplasticity behaviour of P91 and P92 power plant steels.* International Journal of Pressure Vessels and Piping, 2013. **111–112**: p. 246-252.

191. Tighe, R., G. Howell, J. Tyler, S. Lormor, and J. Dulieu-Barton, *Stress based non-destructive evaluation using thermographic approaches: From laboratory trials to on-site assessment.* NDT & E International, 2016. **84**: p. 76-88.

192. Cacciapuoti, B., W. Sun, D.G. McCartney, A. Morris, S. Lockyer, N.A. Razak, C.M. Davies, and J. Hulance, *An Evaluation of the Capability of Data Conversion of Impression Creep Test.* Materials at High Temperatures, 2017. **34**(5-6): p. 415–424.